THE GEOLOGY OF THE COASTAL TRACT BETWEEN TARBAT NESS AND ROCKFIELD, CROMARTY DISTRICT, SCOTLAND

By

THOMAS EDWARD FERRARO

Bachelor of Science

Slippery Rock State College

Slippery Rock, Pennsylvania

1976

Submitted to the Faculty of the Graduate College
of the Oklahoma State University
in partial fulfillment of the requirements
for the Degree of
MASTER OF SCIENCE
December, 1983

THE GEOLOGY OF THE COASTAL TRACT BETWEEN TARBAT NESS AND ROCKFIELD, CROMARTY DISTRICT, SCOTLAND

Thesis Approved:

R. N. Donovan
Thesis Adviser

L. Simpson

Zuhair al-Shaieb

Norman N. Durham
Dean of the Graduate College

PREFACE

The author wishes to express his appreciation to his major adviser, Dr. R. Nowell Donovan, for his assistance, advice, and critical evaluation of this manuscript. Throughout the study, Dr. Donovan's superior knowledge of the geology of the Orcadian Basin proved invaluable. Appreciation is also expressed to the author's other committee members, Dr. Zuhair Al-Shaieb for enlightening discussions concerning diagenesis, and to Dr. Carol Simpson for critical advice concerning the structural analysis of the study area.

Mr. Randall Bissell and Mrs. Martha Ferraro are acknowledged for their excellent drafting services. A note of thanks is expressed to Mrs. Grayce Wynd for formatting advice and superior typing of this manuscript.

Dr. David J. Sanderson of Queens University, Belfast, Northern Ireland, provided the Von Mises computer program. Mr. Bradley Huffman, computer analyst for the Department of Geology at Oklahoma State University, adapted the Von Mises program and the Markov analysis program for use on an Apple II computer. Their contributions are gratefully acknowledged.

The citizens of Great Britain are acknowledged for the hospitality which they extended to the author and his spouse during the field study. In particular, Mr. John Gill, the landowner of the region which surrounds the study area, is acknowledged for access to his property.

Finally, the author would like to extend his love and sincere appreciation to his wife, Martha, for her financial assistance, drafting expertise, and loving support.

TABLE OF CONTENTS

LIST OF TABLES

LIST OF FIGURES

CHAPTER I

INTRODUCTION

This study describes Devonian aged fluvial and lacustrine sequences of the Middle and Upper Old Red Sandstone which were deposited along the southeast fringe of the Orcadian Basin, and are located on the coast of Tarbat Peninsula in northeast Scotland (Figures 1, 2, and 3). Specific objectives are 1) classification and interpretation of depositional environments and depositional facies; 2) discrimination between autocyclic and allocyclic controls on sedimentation; 3) petrologic studies of provenance, red bed genesis and paragenesis; 4) description of minor tectonic structures and the determination of their relationship to the Great Glen fault (which is located directly offshore of the field area).

Background

During late Silurian to early Devonian time, the closure of the Iapetus Ocean culminated in a major orogeny. The resulting fold mountains are known in eastern North America as the Appalachians, and in Europe as the Caledonides. Syntectonic and post-tectonic basins were filled with the eroded debris of these mountains. The resulting mollase, which is found throughout much of eastern North America, Greenland and Europe is collectively known as the Old Red Sandstone (Anderton et al., 1979)(Figure 4).

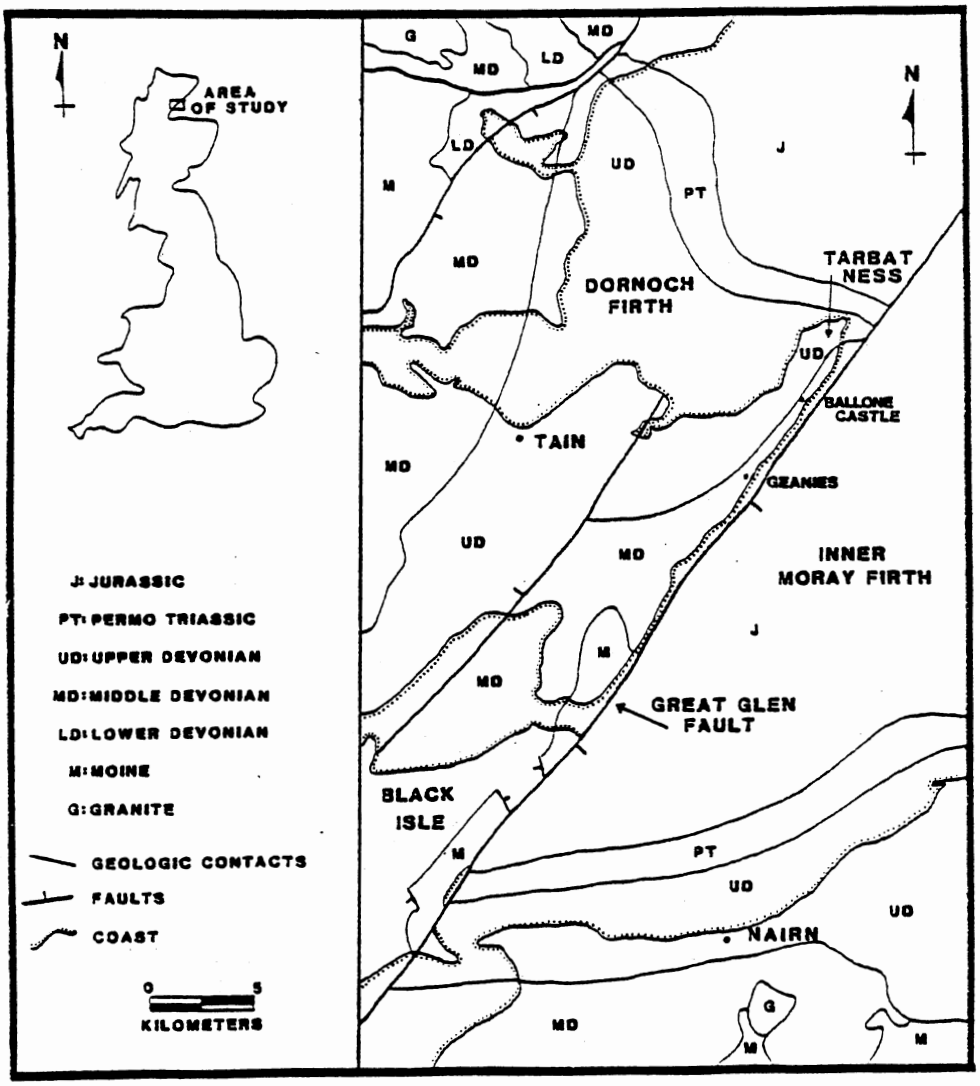

Figure 1. Map of Scotland Enlarged to Show the Geology of the Inner Moray Firth Region. (Note the position of the Tarbat Peninsula with respect to the Great Glen fault.) (After Fettes and Cheshire, 1977.)

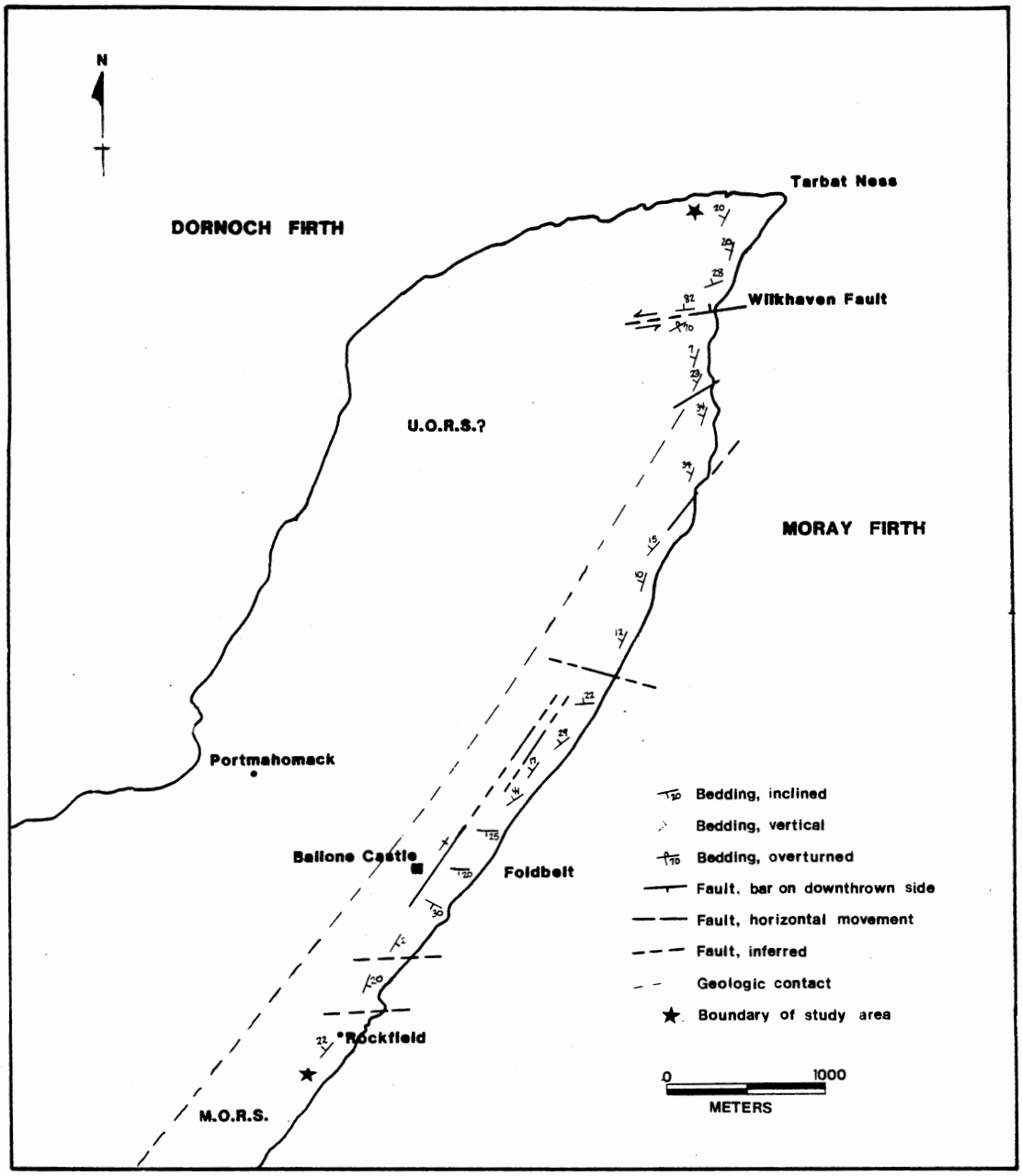

Figure 2. Extent of the Study Area Lies Along the Foreshore of the Eastern Side of the Tarbat Peninsula Between Rockfield and Tarbat Ness. (Note the general structure within the study area and the M.O.R.S-U.O.R.S contact.)

Figure 3. View of Part of Study Area; Northeast Toward Tarbat Ness

Depositional basins that contain Old Red Sandstone (O.R.S.) lithologies were either internal or external in character. External basins were bounded on one side by the orogenic belt and on the other side by the sea. They are characterized by fining upward alluvial plain cycles and shallow marine deposits. Examples of O.R.S. external basins include the Lower and Upper Devonian Anglo-Welsh-Irish Basins of southern England, Ireland, France, Belgium and Poland, and the Catskill Clastic Wedge of eastern North America. Internal basins were self-contained entities within the orogenic belt. Commonly, internal O.R.S. basins were filled by lacustrine facies in the center, and alluvial fan and fluvial sequences around the fringe of the basin (Donovan, 1975). O.R.S. internal basins include the Norwegian, Greenland, Spitsbergen Basins, and the Midland and Orcadian Basins of Scotland (Anderton et al., 1979).

Procedure

The Tarbat Peninsula is bounded to the north by the Dornoch Firth and to the south by the Moray Firth (Figure 2). Field work was conducted during June, July, and August of 1982 on coastal exposures adjacent to the Moray Firth between Rockfield and Tarbat Ness (Figure 2). A total of 520 meters of section was measured (Appendix B). Fifty-one samples were selected at 1-30 meter intervals to be approximately representative of the depositional facies types recognized during the study. These samples were used for megascopic, petrographic x-ray diffraction, and electron microscope analyses.

Megascopic descriptions include textural estimations and color classification according to the Rock Color Chart (Goddard et al.,

1963.) Thin sections were point counted (400 points per sample), and analyzed for textures, textural maturity and paragenesis (Appendix E). Petrographic preparation techniques included blue impregnation for porosity and selective staining of potassium feldspars using a sodium cobaltinitrite solution. Samples suspected to contain ferroean calcite were stained with a potassium ferricyanide solution. Twenty-five samples were chosen for clay extraction and x-ray diffraction analysis, of which five were selected for electron microscopy. X-ray diffraction and electron microscopy were used to determine the authigenic or detrital nature of clay minerals, cement types and perigenesis.

Erosion of the southern side of the Tarbat Peninsula, a remarkably straight coastline oriented at 035, has been controlled by the Great Glen fault which is present directly offshore in the Moray Firth (Figure 1). Consequently, numerous second order structures that were probably generated by stress fields related to the Great Glen fault were encountered during field work. When sufficiently developed, fold, fracture and fault orientations were measured. This data was plotted on rose diagrams and stereonets to determine the sense of movement of the Great Glen fault during post-Devonian time.

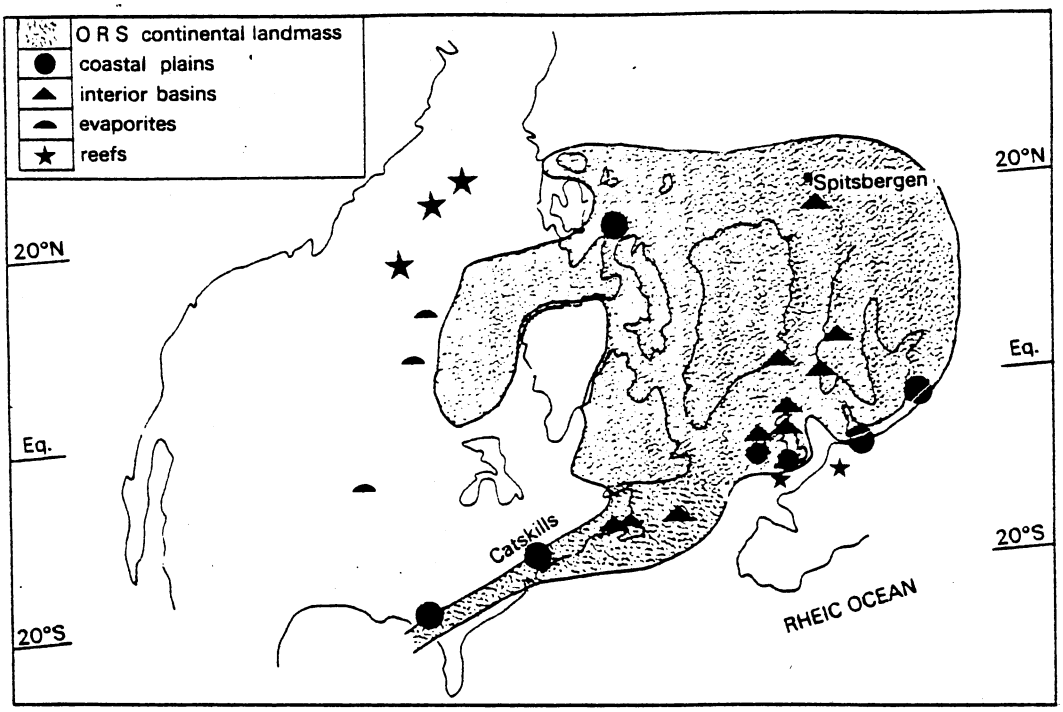

Figure 4. Paleolatitude and Extent of the Former O.R.S. Continental Landmass. (After Anderton et al., 1979, and Woodrow et al., 1973.)

CHAPTER II

HISTORY OF PREVIOUS RESEARCH

Introduction

Coastal exposures of Middle and Upper Devonian O.R.S. present along the Tarbat Peninsula (Figure 2) are located on the fringe of the Orcadian Basin as it is presently exposed. These sequences were first discussed by Sedwick and Murchinson in 1829. Subsequently, Hugh Miller Jr. produced the first geological map of the Cromarty District in 1889. Armstrong and Harris (1973) are responsible for a revised edition of this map. Subsequently, Armstrong (1977) elucidated the stratigraphy of the area; otherwise, no modern work has been published.

Local Stratigraphy

In the Cromarty District the Lower, Middle and Upper O.R.S. are classified as the Struie, Strath Rory, and Balnagowan Groups, respectively (Armstrong, 1977). The Struie Group, of Seigenian-Emsian age (Table I), is up to 2400 meters thick. Typical lithologies (conglomerates, impure limestones, mudstones, siltstones and sandstones) have been identified at Strathpeffer, but are absent along the Tarbat Peninsula 20 miles to the east (Figure 1).

Middle Devonian units, referred to as the Strath Rory Group, comprise 2800 meters of basal conglomerates and sandstones with

TABLE I

STRATIGRAPHIC CORRELATION OF THE LOWER, MIDDLE AND UPPER O.R.S. IN THE ORCADIAN BASIN. (After Westoll, in House et al., 1977.)

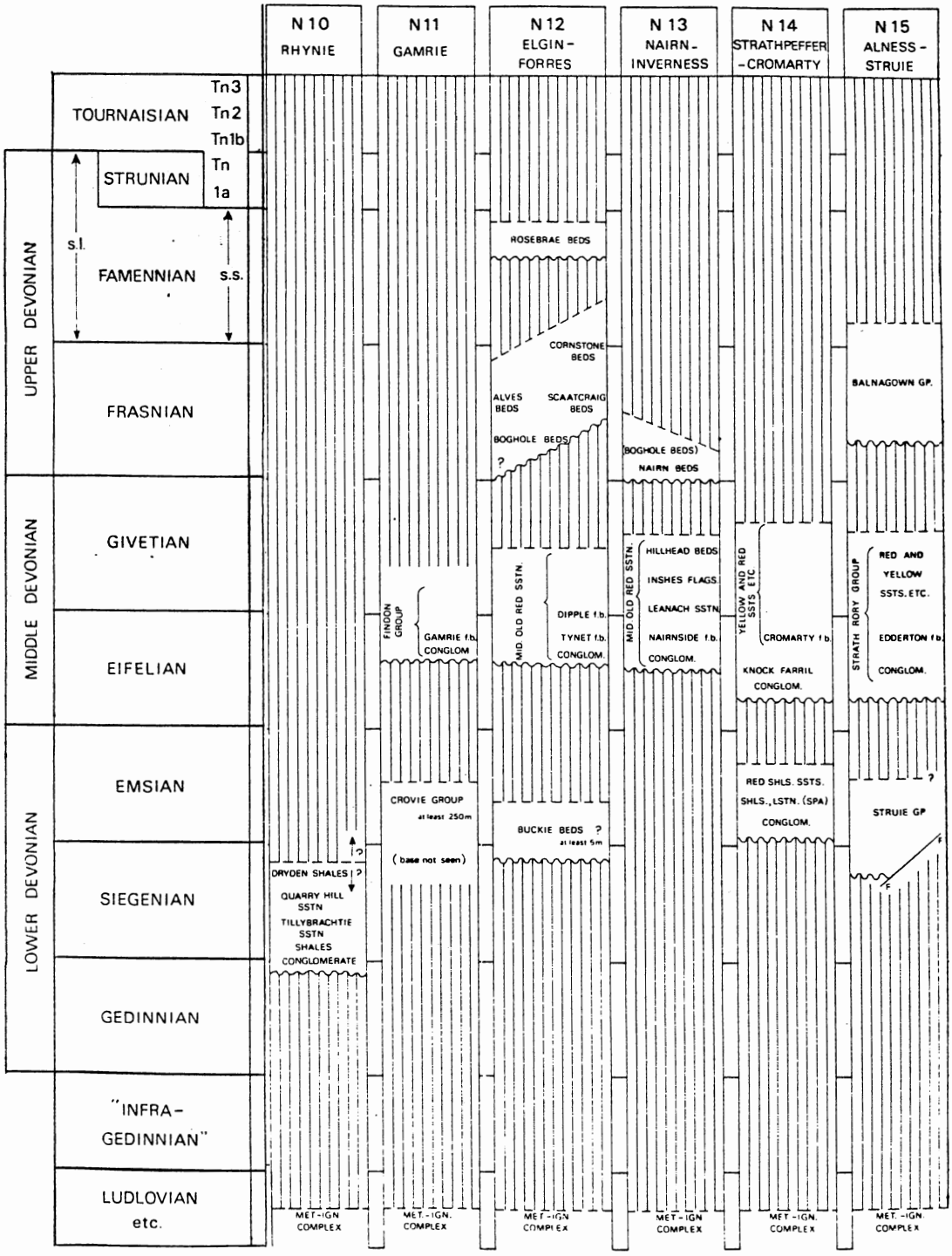

TABLE I (Continued)

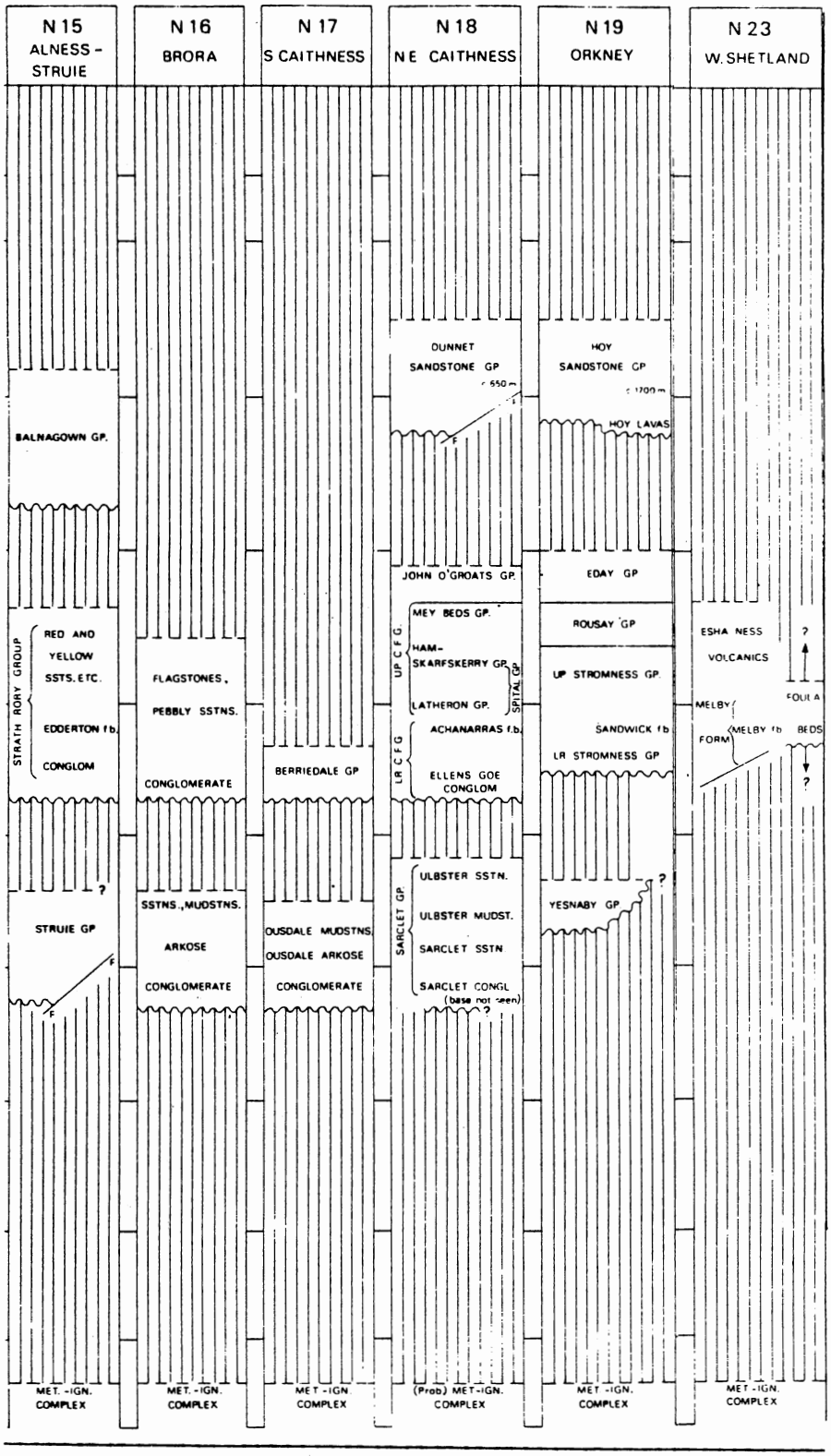

interlaminated calcareous shales. In the Strathpeffer area, these beds rest on the Struie Group but along the Tarbat Peninsula, basal conglomerates rest with profound unconformity upon an irregular surface of Pre-Cambrian Moinian basement.

The Upper Devonian Balnagowan Group, at least 1000 meters thick, comprises mostly sandstones. Fossil fish (Psammosteus, Asterolepis, and Holoptychuis) found near Balnagowan suggest a Frasnian age for lower members. At Tarbat Ness, the contact between the Balnagowan and Strath Rory Groups is obscured by a fault (Armstrong and Harris, 1973). Elsewhere, the Upper-Middle O.R.S. contact is not exposed.

Regional Stratigraphy

Extent of the Orcadian Basin

The geographical extent of the Orcadian Basin includes exposures from Gamrie on the southern coast of the Moray Firth to the Melby District of Shetland (Figure 5). Elswhere in Shetland, O.R.S. deposits in the Walls and East Shetland areas are distinctively different to Orcadian deposits in their stratigraphic and tectonic relationships. Hence, they are considered to have been deposited in distinct basins (Mykura, 1976).

All three O.R.S. divisions, Upper, Middle, and Lower, are present in the Orcadian Basin. Middle Devonian units are most prevalent. The following discussion of the stratigraphy of the Orcadian Basin is adapted chiefly from the Westoll (in House, et al., 1977).

Lower Old Red Sandstone Deposits

Limited exposures of the Lower O.R.S. in the Orcadian Basin suggest

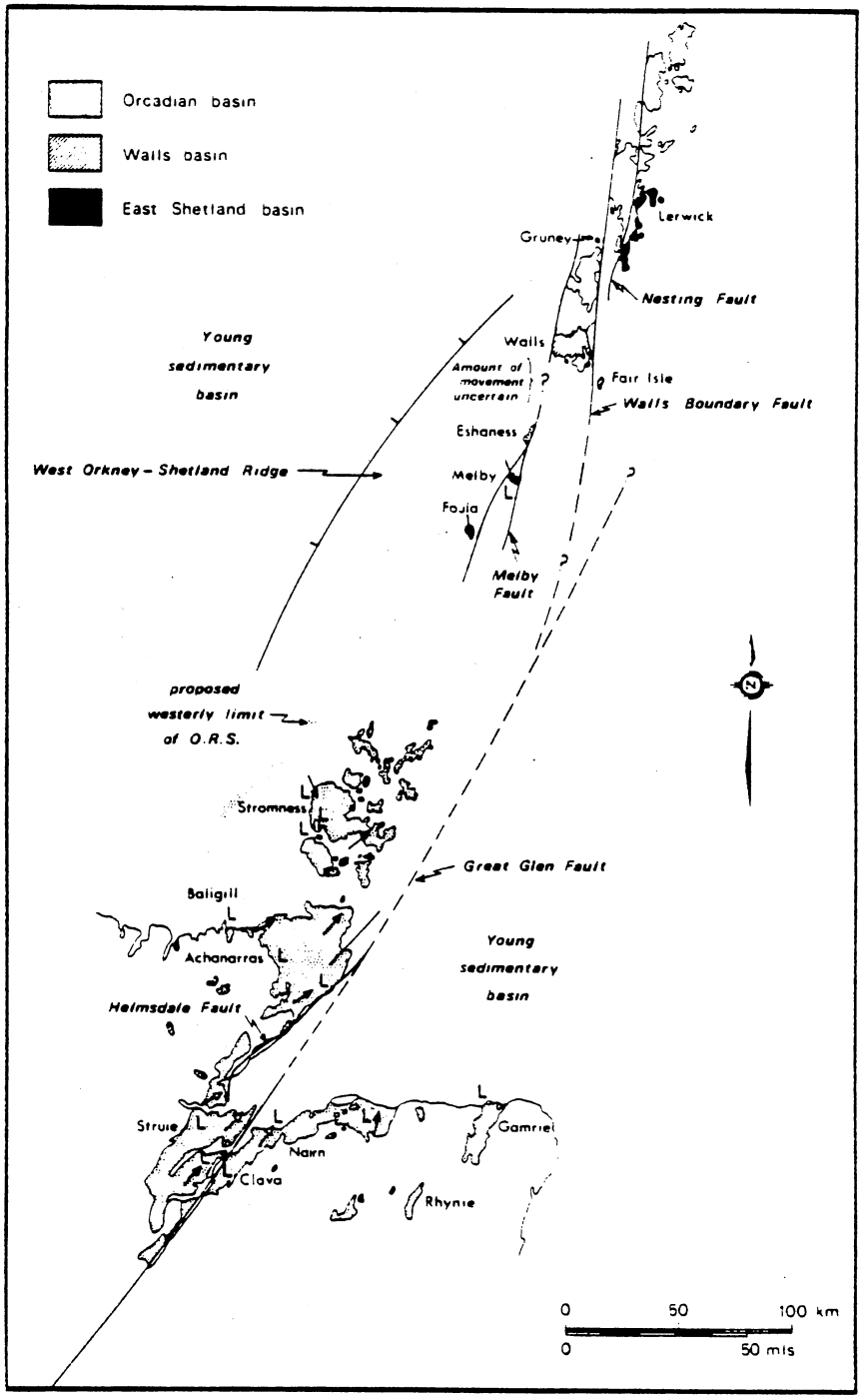

Figure 5. Reconstruction of Devonian Paleogeography in the Orcadian Basin. L is the Achanarras Limestone and Equivalent. (From Donovan et al., 1976.)

that during the Lower Devonian, sedimentation occurred in three distinct sub-basins (Figure 6). Exposures in the easternmost Rhynie-Gardenstown Basin include a basal conglomerate which grades upwards into sandstones, flagstones and marls. Spores found in the marls indicate an age near the Siegenian-Emsian boundary (Table I, N 10-12).

In the Strathpeffer Basin, 200-300 meters of basal conglometates are followed by 400 meters of shales (Figure 6). Eighty meters from the top, the shales become interlaminated with calcareous bands; these units have been named the Spa Beds. Richardson (1965) collected spores from the Spa Beds which yielded an age close to the Siegenian-Emsian boundary (Table I, N-14).

Lower O.R.S. in Caithness include sequences near Ousdale and Sarclet (Figure 6). The succession at Ousdale includes a basal conglomerate which rests unconformably upon the Late Silurian Hemsdale Granite, and is followed by mudstones. Donovan and Collins (1978) described spores, plant fragments (Pacytheca) and fossil fish (Porolepis) that indicate a position near the high Lower Devonian. The Sarclet Group consists of a basal conglomerate or an arkose succeeded thin carbonates, mudstones and sandstones. Spores derived from the topmost mudstones are of mid-Emsian age (Table 1, N 18).

Fannin (1969) and Mykura (1976) identified strata of the Yesnaby Sandstone Group on Orkney, which rests on basement and is overlain unconformably by Middle O.R.S. (Figure 6). Although fossil evidence is lacking, the coarse proximal nature, and the stratigraphic position of the Yesnaby Sandstone are suggestive of a Lower Devonian age.

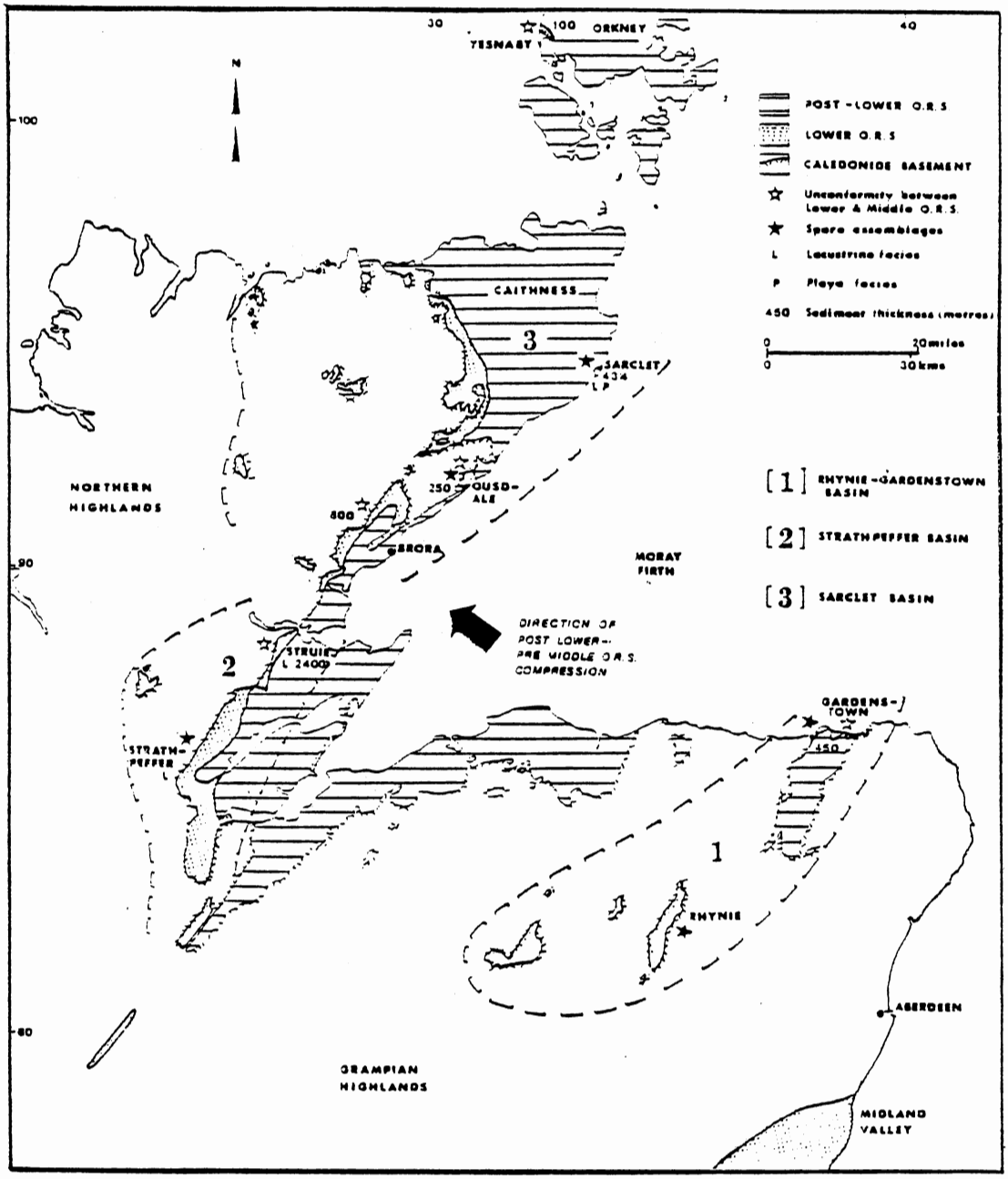

Figure 6. The Lower O.R.S. of the Orcadian Basin.
(From Donovan, 1979.)

Middle Old Red Sandstone Deposits

The extent and the exposure of the Middle O.R.S. preserved indicates that this division constitutes the bulk of Devonian sedimentation in the Orcadian Basin (Figure 7). In general, most sediments in the center of the basin are of lacustrine origin. Mixed fluvial and lacustrine facies are found around the periphery. Paleocurrent orientations and stratigraphic correlations indicate that sediment sourcelands existed to the south, west, and northwest of the basin. In the Moray Firth Area, sediments were derived from the Grampian Highlands to the south. In Sutherland, Caithness and Orkney, sediments were derived from the southwest and west. Shetland M.O.R.S. sediments were shed from sourcelands to the northwest (Donovan et al., 1976).

Around the southern margin of the Moray Firth, over 1000 meters of M.O.R.S. sediments are present (Figure 7). Basal units are unconformable on Lower O.R.S. or overstep onto Moinian or Dalradian basement. Five units have been recognized (Table I, N 13). In ascending order, these are: 1) a basal conglomerate that fines upward into sandstones and rare limestones, 2) sandy flagstones, calcareous flagstones and shales with calcareous lenses. Dipterus and Coccosteus fish derived from this zone indicate a position close to the Eifelian-Givetian boundary, 3) approximately 300 meters of sandy flagstones, and pebbly sandstones and shales (referred to as the Leanach Sandstone), 4) the Inshes Flagstone Group, which includes several hundred meters of arkosic, micaceous and calcareous flagstone, 5) a poorly defined unit, the Hillhead Group, consisting of five meters of micaceous sandstones and laminated dark shales, is the highest sequence exposed.

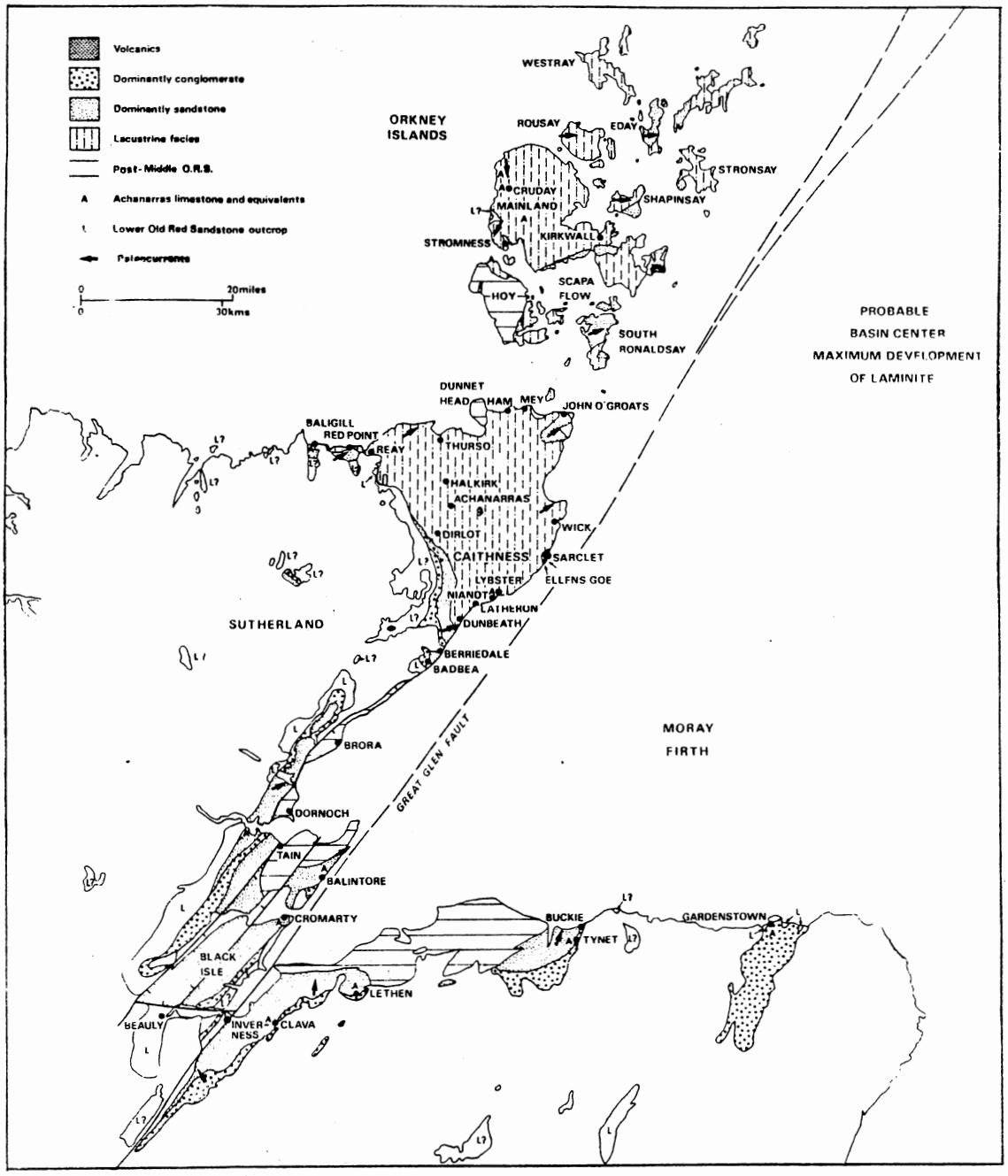

Figure 7. The Middle O.R.S. of the Orcadian Basin. (From Donovan, 1979.)

Middle O.R.S. units are exposed at Strathpeffer, the Black Isle, and the Tarbat Peninsula on the northwest and southeast limbs of the Easter Ross Syncline (Figure 7). At Strathpeffer, the basal Knock Farill Conglomerate passes upwards into the sandstones and shales of the Loch Ussie Group (Table I, N-14). To the northeast, these two units interfinger. On the Black Isle, they are equivalent to the Drunderfit Conglomerate and the Millbuie Sandstone, respectively.

At Cromarty, Hugh Miller's famous fish bed has yielded fauna similar to that of the Achanarras Horizon in Caithness (the principal stratigraphic marker horizon in the basin). At Cromarty, this bed is 100 meters above the local M.O.R.S. base whereas in Caithness the same horizon is 2300 meters above the M.O.R.S. base (Donovan et al., 1974). Observations of this type around the Moray Firth Area support the conclusion that Middle Devonian sedimentation commenced earlier in Caithness than elsewhere in the Orcadian Basin.

In Caithness the Middle O.R.S. may be as much as 4000 meters thick, which is the greatest known thickness in the Orcadian Basin. The majority of these rocks, in particular the finer lithologies, are considered as lacustrine (Crampton and Carruthes, 1914; Donovan, 1975). Crampton and Carruthers (1914) developed the first stratigraphic correlation of this area. However, Miles and Westoll (1963 and 1968) indicated that errors existed in the surveys classification. By adopting new and more conformable type sections, Donovan et al. (1974) further revised this classification in the following manner. The terms "Barren Group," "Wick" and "Thurso Flagstones Groups" were discarded. In their place the Sarclet Group and Upper and Lower Flagstones Groups were defined. The John O'Groats Sandstone was maintained from the original

classification (Table I, N. 18).

Donovan et al. (1974) divided the Lower Flagstone Group into four subgroups. The Clyth Subgroup consists of a basal unit, the Ellens Goe Conglomerate, which fines upward into rhythmic flagstones. Dark calcareous laminites and flagstones are present in the uppermost Robbery Head Subgroup. The topmost member of this subgroup is Achanarras (Niandt) limestone which contains a highly distinctive fossil fish fauna. Elements of this fauna are found in the M.O.R.S. of the Tarbat Peninsula in a position approximately 500 meters below the rocks investigated in this study (personal communication, R. N. Donovan, 1983). This establishes that the M.O.R.S. sediments studied here are equivalent to the uppermost part of the Caithness sequence.

The Upper Caithness Flagstone Group is divided into three subgroups. Typical lithologies include dark gray shales and fine to medium-grained sandstones in the Latheron Subgroup, thinly bedded flagstones and dark gray shales in the Ham-Scarfskerry Subgroup and sandstones with channeling and slumping near the top in the Mey Subgroup.

The overlying John O'Groats Sandstone Group marks the top of the M.O.R.S. in Caithness. A braided fluvial environment of deposition apparently dominated sedimentation although several calcareous laminites of lacustrine origin are present (Donovan et al., 1974).

Middle O.R.S. successions at Orkney are divided into, in ascending order, the Stromness Flagstone, Rousay and Eday Groups (Figure 7). Lower Stromness Flagstone sequences consist of 24 rhythmic units of flagstones, each approximately 11 meters thick. Typical lithologies of these sequences are 1) basal bituminous laminites followed by thinly bedded sandstones and siltstones; 2) sandstones with channeling features;

3) mudstones with abundant desiccation cracks. At the top of the Lower Stromness Flagstone Group, the Sanwick Fish Bed is a correlative to the Achanarras horizon (Table I, N 19). The Upper Stromness Flagstone Group consists of cyclic channeled sandstone sequences.

The overlying Rousay Group is dominated by sequences of lacustrine origin. However, coarse fluvial clastics become prominent near the top. A sharp-to-transitional contact separates the Rousay and Eday Groups. Wilson et al. (1935) and Mykura (1976) have indicated that the absence of lacustrine units defines the base of the Eday Sandstone. Fauna present within the sandstone indicates that it coorelates with the John O'Groats Sandstone of Caithness (Table I, N 18-19).

Upper Old Red Sandstone Deposits

Upper Old Red Sandstone sequences are best exposed along the southern coast of the Moray Firth and the Tarbat Peninsula (Figure 8). At Caithness, they are confined to the Dunnet Head Sandstone while in the Orkneys they are present only on the island of Hoy. The age of the Upper O.R.S. is generally considered as Upper Devonian. It is possible, however, that Lower Carboniferous strata are present.

Upper O.R.S. deposits along the southern coast of the Moray Firth are arenaceous sandstones that were derived from the southwest (Donovan et al., 1976). Estimations of total thickness which varies between 450-1200 meters are tentative. The stratigraphy consists of, in ascending order, the Nairn Beds, Boghole Beds, Alves-Scaat, Craig-Cornstone Beds and the Rosebrae Beds. Upper O.R.S. faunas have been compared with those in the Baltic Region and Western Europe (Westoll, 1977). The Nairn, Boghole and Alves-Scaat Craig Beds are considered to be of

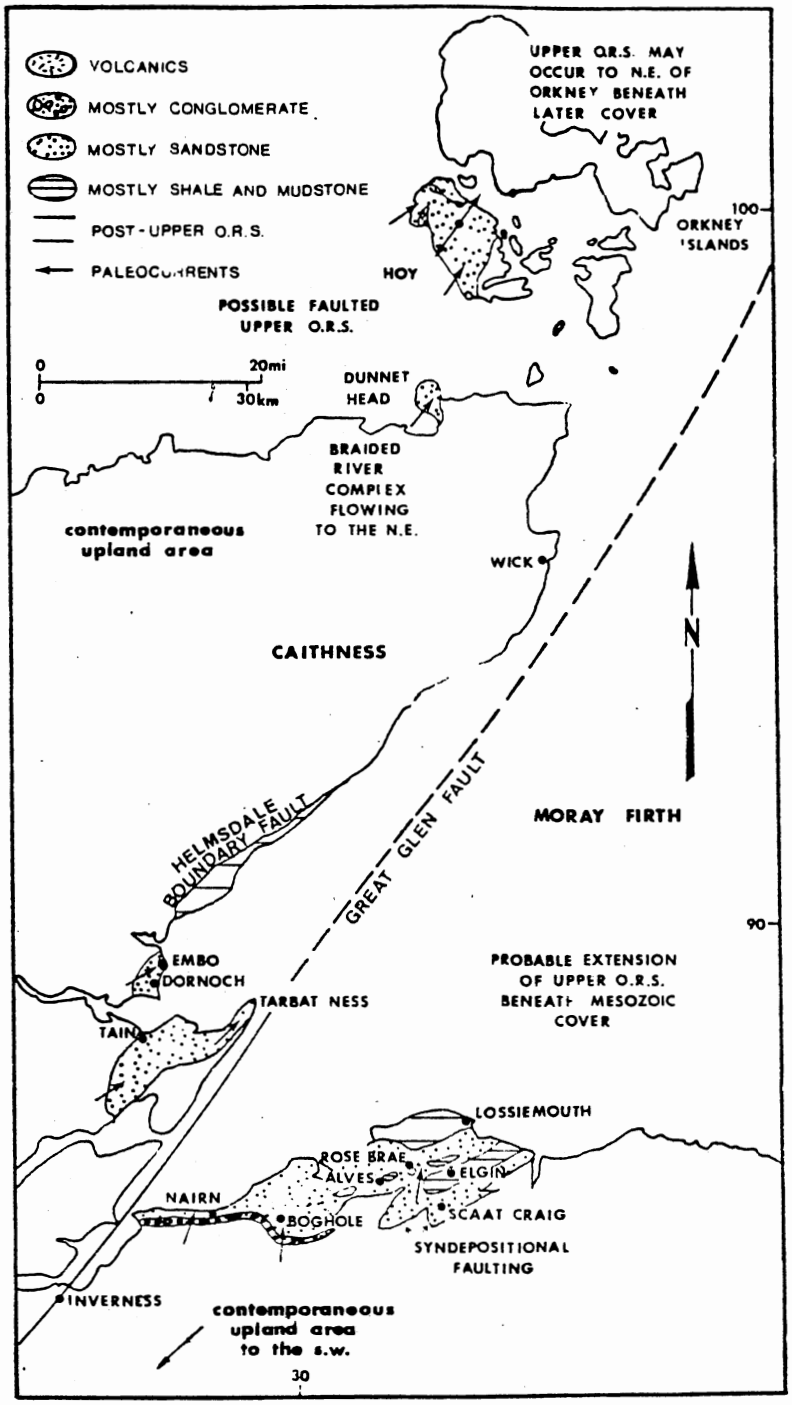

Figure 8. The Upper O.R.S. of the Orcadian Basin. (From Donovan, 1979.)

Frasnian age (Table 1, N 12-13). The Rosebrae Beds have been interpreted to be of Famennian age (Table I, N 12).

Poorly exposed U.O.R.S. deposits are present at Dornoch and in the northwest-central part of the Easter Ross Syncline (Figure 1). Faunal assemblages, including Holoptychuis, suggest that these units, together with the Balnagowan Group of the Tarbat Peninsuala, are correlative with the Boghole and Alves-Scaat Craig Beds.

The Dunnet Head Sandstone (650 meters thick) of Caithness consists of buff to red sands with minor discontinuous clay bands. Orientations of trough cross stratification indicates that these beds were laid down by streams flowing from the southwest. The presence of Holoptychuis suggests a correlation with the Upper O.R.S. of the Moray Firth.

Upper O.R.S. deposits of the Orkneys (1650 meters) are confined to Hoy (Figure 8). These units are unconformable on earlier, deformed Middle O.R.S. units. Basal deposits consist of tuffaceous sandstones which interfinger with olivine basalts. Lithologically, the overlying sandstones resemble other U.O.R.S. units; however, they have not yielded fossils.

Orcadian Basin Middle O.R.S. Sedimentation Model

Primarily as a result of a study of marginal M.O.R.S. lacustrine deposits at various places in Caithness, Donovan (1975, 1980) has developed a sedimentation model of deposition for the Orcadian Basin. The margin of lakes within the basin can be conceptualized either as "coincident" or "non-coincident." Non-coincident margins record circumstances when basin margins were fringed with alluvial deposits. Coincident

margins occurred when the lake level coincided with the basin margin. Recurring facies associations recording coincidence include 1) basal sandstones or breccias of fluvial origin, 2) flagstones of shallow lacustrine origin, 3) carbonate laminites of deep lacustrine origin, 4) thinly bedded siltstones which resulted from lacustrine turbidity currents, 5) an uppermost sandstone of fluvial origin with a markedly erosive base.

These facies developed in response to transgressions and regressions of lakes with resultant variations of base level. The effect of allocyclic processes such as uplift rates, basin subsidence rates, sedimentation rates, and long term climatic variations were critical controls to the development of these facies packages. The most prominent facies variations resulted from long term climatic changes. During cool and wet periods, lake levels and therefore base levels rose, rivers alluviated their valleys, and lacustrine sedimentation was dominant within the basin. Hot and dry periods were characterized desiccation of lakes, regression, and a dominance by fluvial systems eroding to a lower base level.

With the exception of the John O'Groats Sandstone, the dominant Middle O.R.S. sediment type in the center of the Orcadian Basin is lacustrine (Donovan, 1980). Facies packages consist of symmetrical cycles of the following sediment types: 1) non-glacial varves which result from seasonal climatic variations, 2) alternations of thinly bedded (0.5-3 mm) dark gray calcareous rich siltstones with shale laminae, 3) alternations of gray carbon-rich shale and gray coarse siltstones in heterolithic beds averaging 10 mm thick with straight crested symmetrical ripples and subareal shrinkage cracks as characteristic sedimentary

structures, 4) interbedded green shales, siltstones and sandstones with penecontemporaneous deformation, subareal mudcracks, and multi-set rippled cross laminations that originated in shallow and impermanent lacustrine conditions.

Cyclic combinations of these facies packages resulted from lacustrine transgressions and regressions. Examples of transgressive and regressive sequences include (1, 2, 3, 4) and (4, 3, 2, 1), respectively. Transgressions resulted in possible lake overflow from the basin and faunal exchange with other Middle Devonian basins. Regressions resulted in harsher ecological conditions and faunal population reductions (Figure 9).

The Achanarras horizon, present in Caithness, Orkney, Shetland, and the Moray Firth Area records a large fish exchange resulting from a major Orcadian transgression. At Caithness, the Achanarras horizon is 2300 meters above the Middle O.R.S. base. In the Moray Firth Area, the same horizon is approximately 100 meters above basal Middle O.R.S. The difference in the stratigraphic positions of the Achanarras horizon between Caithness and the Moray Firth demonstrates that 1) Caithness was an area of maximum Middle O.R.S. accumulations, 2) regional lacustrine sedimentation in the area surrounding the Moray Firth resulted only when Lake Orcadie transgressed to its maximum extent.

A. Map model illustrating lacustrine transgression and regression during Middle O.R.S. sedimentation in the Orcadian Basin. Upright letters: lake level high. Slanting letters: lake level low. C, coincidence of margins of lake and sedimentation. NC. alluvium accumulating landward of lake margin. d, delta. ssm, shoreline sorting mechanisms. m, mudflats. 1-5 refer to sites illustrated in B.

B. Sedimentation model for cycle development in the Middle O.R.S. Locations 1-5 are keyed to A.

1. Central basin cycle: low sediment supply. Bedding almost entirely laminites (e.g., mostly in Robbery Head Subgroup - time of maximum basin expansion, also in Ham Scarsferry Sub-Group).

2. Central basin cycle: high sediment supply. Symmetrical lacustrine cycles. Both carbonate units (i.e., fish bearing laiminite and dolostones) may be missing (e.g., South Head, Wick; much of exposed Lower Flagstone Group; Ham/ Scarsferry Subgroup (in part).

3. Non coincident lake margin cycle: mixed lacustrine and fluvial (indicated on log by thicker margins)(e.g., Pennyland, Reay; all marginal areas around Moray Firth and in Shetland at Melby).

4. Coincident lake margin (e.g., Baligill, Red Point, Reay, Buckie?).

5. Alluvial cycles: controlled by base-level variation.

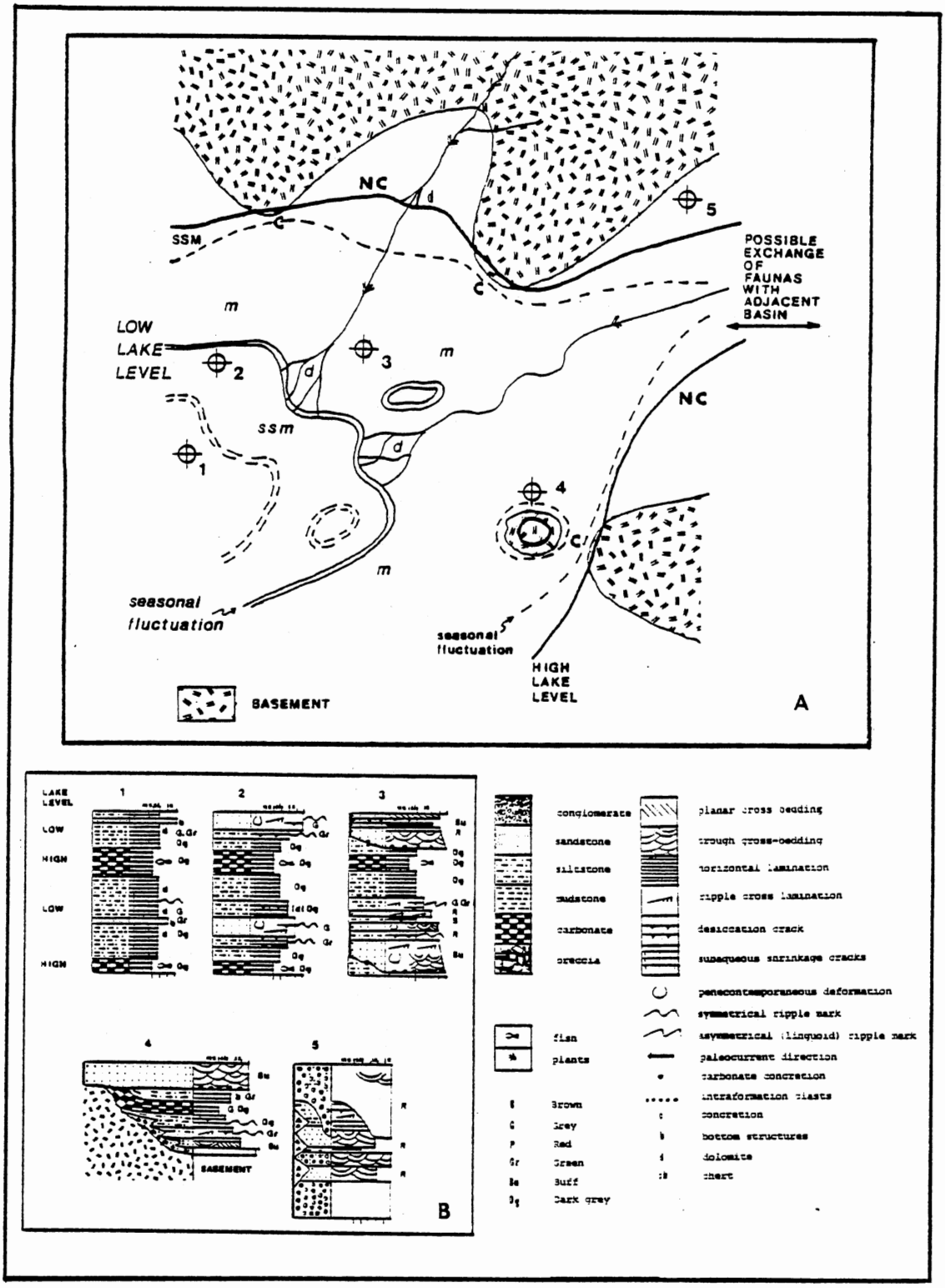

Figure 9. Middle O.R.S. Orcadian Basin Sedimentation Model. (From Donovan, 1975.)

CHAPTER III

STRUCTURAL GEOLOGY

Introduction

Structural evolution of Devonian coastal exposures along the Tarbat Peninsula was dominated by the Great Glen fault; a major transcurrent shear zone that has been active since the early Paleozoic (McQuillin et al., 1982). In Pre-Carboniferous times, the Great Glen fault was positioned as a global small circle that extended from the continental margin north of Ireland, through the Malin Sea, the Great Glen of Scotland and the Moray Firth (McQuillin et al., 1982). North of Scotland, the Great Glen fault is thought to join the Walls Boundary fault in Shetland (Flinn, 1961)(Figure 5).

Numerous arguments have been put forth to explain the nature of offset along the Great Glen fault. These consider both right and left lateral dislocations and tensional and compressional movements. A summary of post-Devonian interpretations, presented by Donovan et al. (1976), is as follows:

1. Sinistral movements of 200-300 kilometers (Storetvedt, (1974) or 500 kilometers (Stortevedt, 1975).

2. Dextral movements of 30 kilometers along the Great Glen fault (Holgate, 1969), approximately 65 to 80 kilometers on the Walls Boundary fault of Shetland (Flinn, 1969; Mykura, 1969, 1972a, 1972b), a considerable movement on the Melby fault in Shetland (Mykura, 1976), approximately 50 kilometers of movement on the Helmsdale fault (Flinn,

1969), and a substantial movement on the Latheron fault in southeastern Caithness (Donovan et al., 1974).

3. Post Jurassic normal movement of the Great Glen fault associated with development of the Moray Firth basin (Bacon and Cheshire, 1976), Post Jurassic movement of the Walls Boundary fault associated with basin development to the southwest of Scotland (Bott and Browitt, 1975).

Other pertinent interpretations subsequent to this summary are 1) a post-Permian seven to eight kilometer dextral displacement and vertical offset of a Permo-Carboniferous dike swarm along the Great Glen fault at Argyll (Speight and Mitchell, 1979), and 2) substantial vertical and minor dextral movements along the Great Glen fault which contributed to the late Paleozoic and Mesozoic crustal extension (McQuillin et al., 1979).

Vertical movements along the Great Glen fault during the late Paleozoic and Mesozoic Eras contributed to local crustal extension and consequent development of the Moray Firth Basin. Controversy arises, however, from interpretations of lateral displacements during the Paleozoic. Because exposures are poor, interpretations of Paleozoic displacements are often based on indirect evidence such as matching of geophysical data, paleomagnetic data and Orcadian Basin facies patterns. One example of the controversy that has arisen over post-Devonian interpretations of lateral displacements is that of Van der Voo and Schotese (1981) and Donovan and Meyerhoff (1982).

Donovan et al. (1976) found a remarkable similarity in the sedimentologic and stratigraphic relationships of Middle Devonian sediments on both sides of the fault. In particular, they noted the occurrence of the distinctive Achanarras fauna in Shetland, Orkney, Caithness, Cromarty, Gamrie and the Nairn-Clava region. East and west of

the Great Glen fault in the Cromarty and the Nairn-Clava regions, respectively, 18 fish species are common to the Achanarras horizon. Consequently, they rejected major lateral movements on the fault and thought that a post-Devonian 30 kilometer dextral offset of the Great Glen fault would provide a reasonable fit of these identical stratigraphic horizons.

In a comparison of paleomagnetic orientations imprinted on hematite in Devonian red beds collected on either side of the Great Glen fault, and Devonian samples collected in eastern North America, Van der Voo and Scotese (1981) found a remarkable similarity between Devonian poles of the Orcadian Basin north of the Great Glen fault and in eastern North America. Allowing for corrections resulting from the breakup of Pangea, mean pole readings for the Orcadian Basin and eastern North America were Lat. 50^{o}N, Long. 112^{o}E and Lat. 50^{o}N and Long. 117^{o}E, respectively. Corrected mean pole readings south of the Great Glen fault were Lat. 30^{o}N, Long. 118^{o}E--a 20^{o} Latitudinal variance from the mean Orcadian-North American poles. To accommodate this 20^{o} variance, they suggested that a 2000 kilometer sinistral offset had occurred along the Great Glen fault during the Carboniferous.

The conclusions presented by Van der Voo and Scotese were based on paleomagnetic variations of hematite in samples collected primarily from the Orcadian Basin. Tarling et al. (1976) had previously noted that the textures of hematite in many of the same Orcadian samples were recrystallized or showed evidence of secondary hematite growth. Examination of the paleomagnetism of hematite from many of these samples indicated that the stable magnetism was Permo-Carboniferous in age. Hence, Tarling and his associates concluded that hematite was subjected

to remagnetism during the arid climatic conditions that persisted in the Permian Period. Lowered groundwater tables resulted in deep penetration of oxygen and enhanced renewed growth or recrystallization of hematite. As the textural and climatic evidence indicates that hematite transformation occurred after the Devonian Period, its use as a meaningful paleomagnetic indicator in the manner proposed by Van der Voo and Scotese is rather dubious.

New Evidence for Dextral Post-Devonian Movement Along the Great Glen Fault[1]

The erosion of the eastern side of the Tarbat Peninsuala, a strike coastline oriented at 035, has been controlled by the Great Glen fault which is present directly offshore in the Moray Firth (Figure 1). Here, the Great Glen fault separates onshore Middle and Upper Devonian O.R.S. from offshore Jurassic units (Armstrong and Harris, 1973). These exposures have been interpreted by Armstrong as the eastern limb of the Easter Ross syncline; a low angle fold whose axis is faulted and is sub-parallel to the Great Flen fault (Figure 1).

Coastal exposures of O.R.S. dip primarily northeast. Near Ballone Castle, however, the regional dip reverses to the southeast (Figure 2). Superimposed on this orientation are 10 small-scale folds that plunge SSW to SSE and two which plunge toward the north (Figure 10). The folds in this Ballone Castle foldbelt are upright structures with limb dips generally less than 45^{o} (Figure 11) that form in a right-handed

---

[1]The information presented in this portion of the current chapter was recently submitted to Nature Magazine by Dr. R. N. Donovan and the author. The title of this manuscript is "Post-Devonian Right Lateral Movement on the Great Glen Fault" (Appendix A).

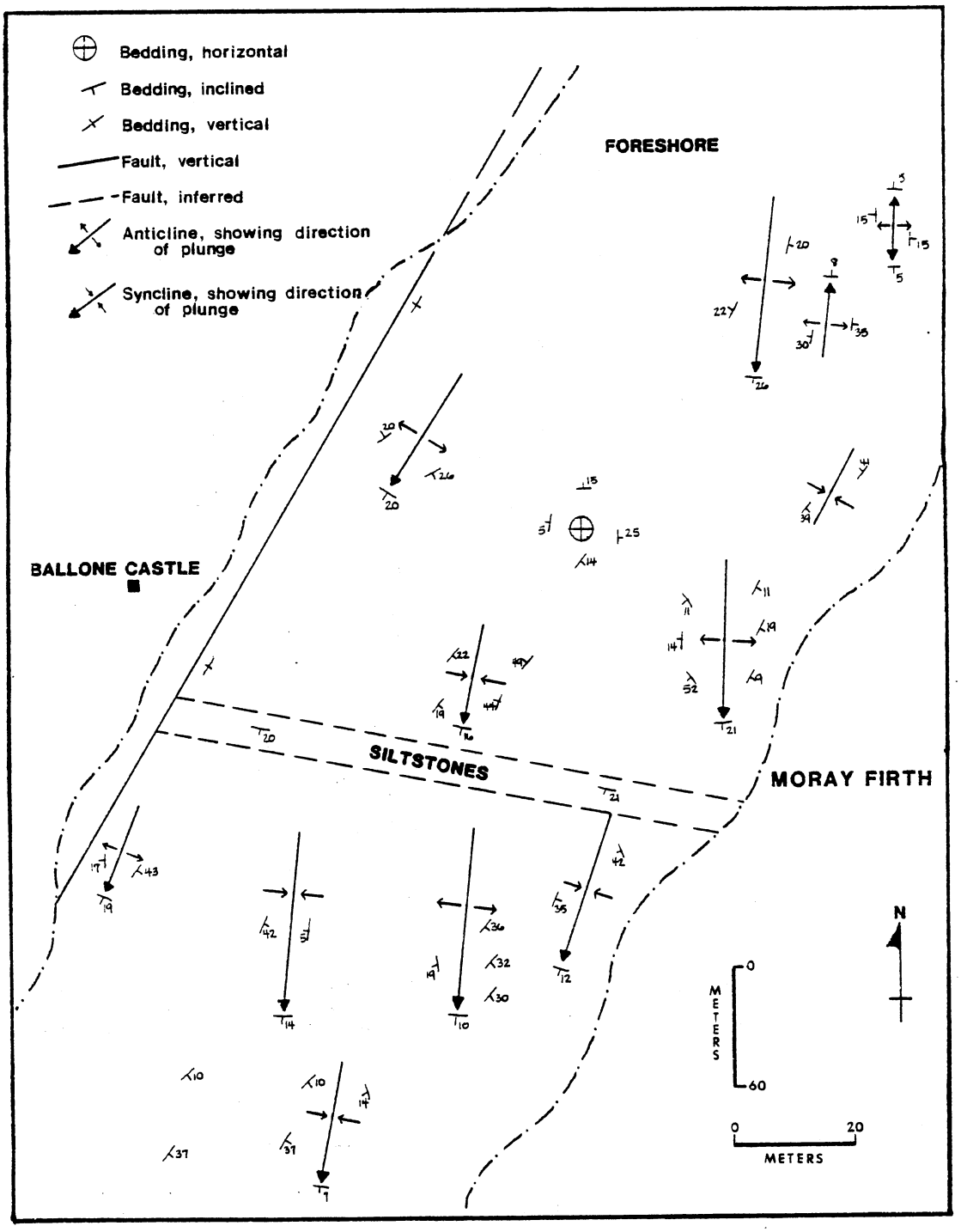

Figure 10. The Ballone Castle Foldbelt

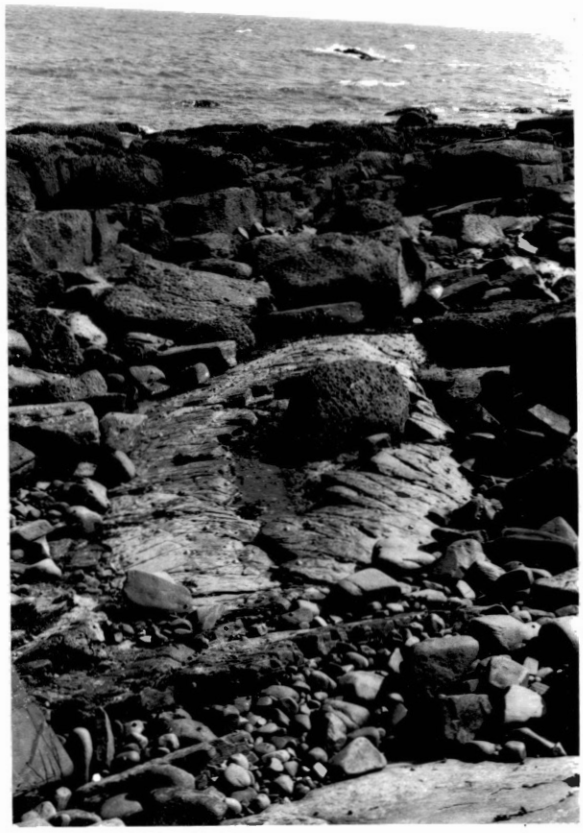

(A)

(B)

Figure 11. Small-scale en echelon Folds, Ballone Castle Foldbelt. [(A) doubly plunging "whaleback fold" at 0° and 180°; (B) another minor structure - plunge 358°.]

en echelon array. The mean orientation of the south plunging structures (185) diverges from the Great Glen fault by about 23° (Figure 12). Their orientation is compatible with generation of en echelon folds by dextral transcurrent displacement during the post-Devonian (Wilcox et al., 1973).

Sporadic but locally intense fracture patterns occur throughout the Ballone Castle foldbelt. A mean orientation of northeast fractures of 047 deviates from the Great Glen fault by about 14° (Figure 13) and is compatible with the development of dextral Reidel fractures (Tchalenko and Ambraseys, 1970). A complementary conjugate Reidel set is poorly developed. Another possible fracture pattern that is present in this region are P fractures which are symmetrical to dextral Reidel fractures (Figure 13).

In the southern portion of the Ballone Castle foldbelt, a fault trending 030 brings steeply dipping buff sandstones striking at 030 into juxtaposition with red siltstones striking at 095 (Figure 10). The siltstones were not encountered on the west side of the fault and, as a consequence, the nature of offset is unknown. To the north, the fault trend encounters covered ground but is then re-exposed approximately one mile north of Ballone Castle. Here a distinctive red-buff mottled sandstone appears to be offset in a dextral manner. However, the exact nature of offset cannot be proven.

Analysis of fracture patterns for the remainder of the field area support the conclusion determined from analysis of the Ballone Castle foldbelt. Both dextral Reidel fractures (mean, 052) and conjugate Reidel fractures (mean 316) are well developed (Figure 14). The orientation of a third fracture pattern (mean, approximately 025) suggests

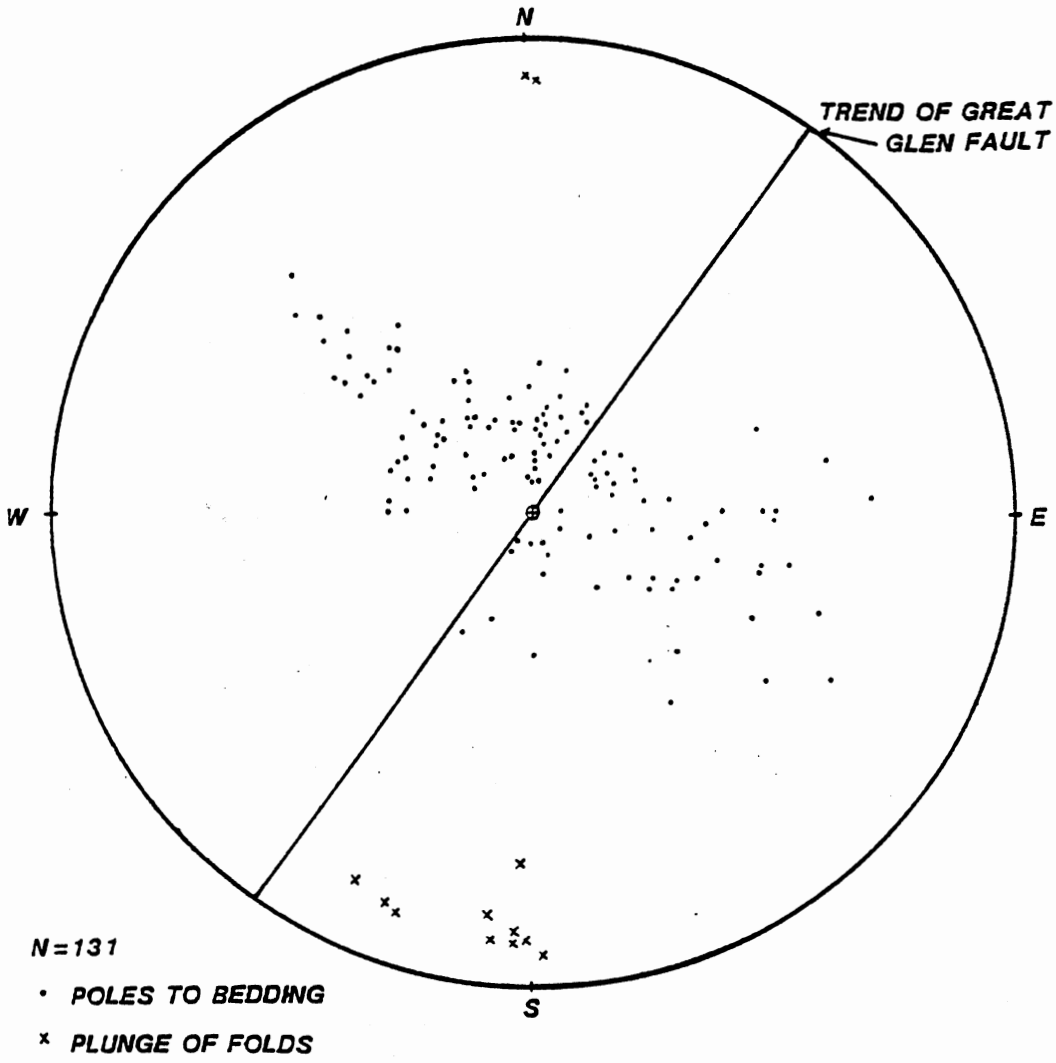

Figure 12. Steronet Showing Relation of Poles to Bedding and Plunge in the Ballone Castle Foldbelt. (From Donovan and Ferraro, recently submitted.)

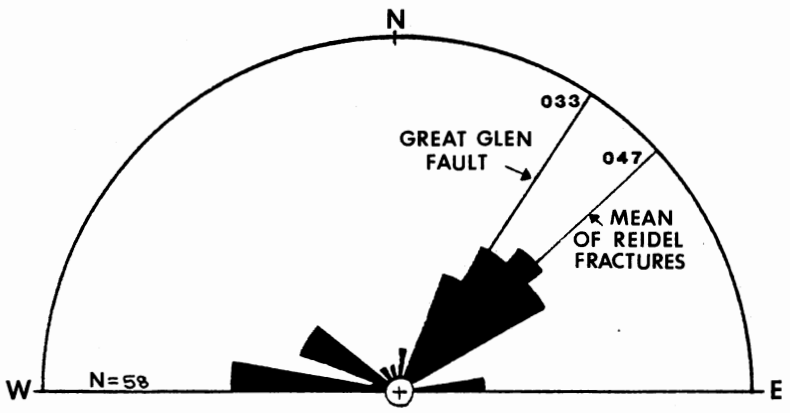

Figure 13. Fracture Pattern, Ballone Castle Fold-belt. (From Donovan and Ferraro, recently submitted.)

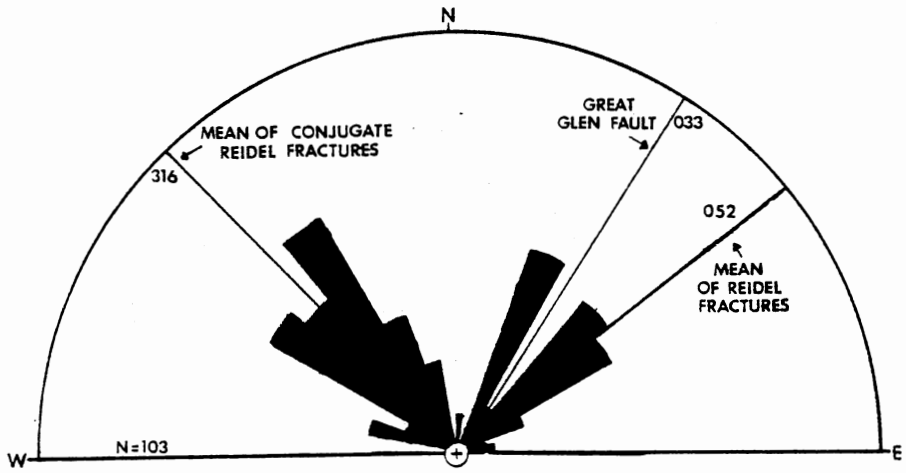

Figure 14. Fracture Pattern, Remainder of Study Area

the presence of P shears (Tchalenko and Ambraseys, 1970). An alternative explanation for this trend is that these fractures are tensional features related to normal movement of the Great Flen fault.

Four well developed fractures have trends that approximate orientations of observed conjugate Reidel or Reidel fractures (Figure 2). Generally, these features have stratigraphic displacements of less than 10 feet. Several fractures which form prominent erosional scarps have orientations which often differ from conjugate Reidel or Reidel fracture correlations. One example of these features is the M.O.R.S.-U.O.R.S. fault contact located approximately .5 kilometers south of Wilkhaven Pier (Figure 2). While the stratigraphic displacement resulting from this fault is unknown, the similarity in lithologies and lack of any second order structures on both sides of the fault suggests that its displacement is very minor.

At Wilkhaven Pier, a high angle reverse fault with a sense of left lateral displacement oriented at 088 (Figure 15) is a conjugate Reidel shear. This fault resulted in emplacement of a minor outlier of the U.O.R.S. south of the pier.

Based on analysis of an en echelon fold system and shear orientations along the Tarbat Peninsula, a post-Devonian dextral offset of the Great Glen fault is postulated. It is possible, however, that a large-scale early fold in the Ballone Castle foldbelt resulted from initial vertical movements (Figure 16). This large-scale fold was then refolded into smaller scale en echelon structures during dextral dislocation. Because the total width of the shear zone is unknown, inferences concerning the amount of lateral displacement are, at best, speculative. However, the size and frequency of occurrence of observed structures suggests that post-Devonian dextral displacements were modest.

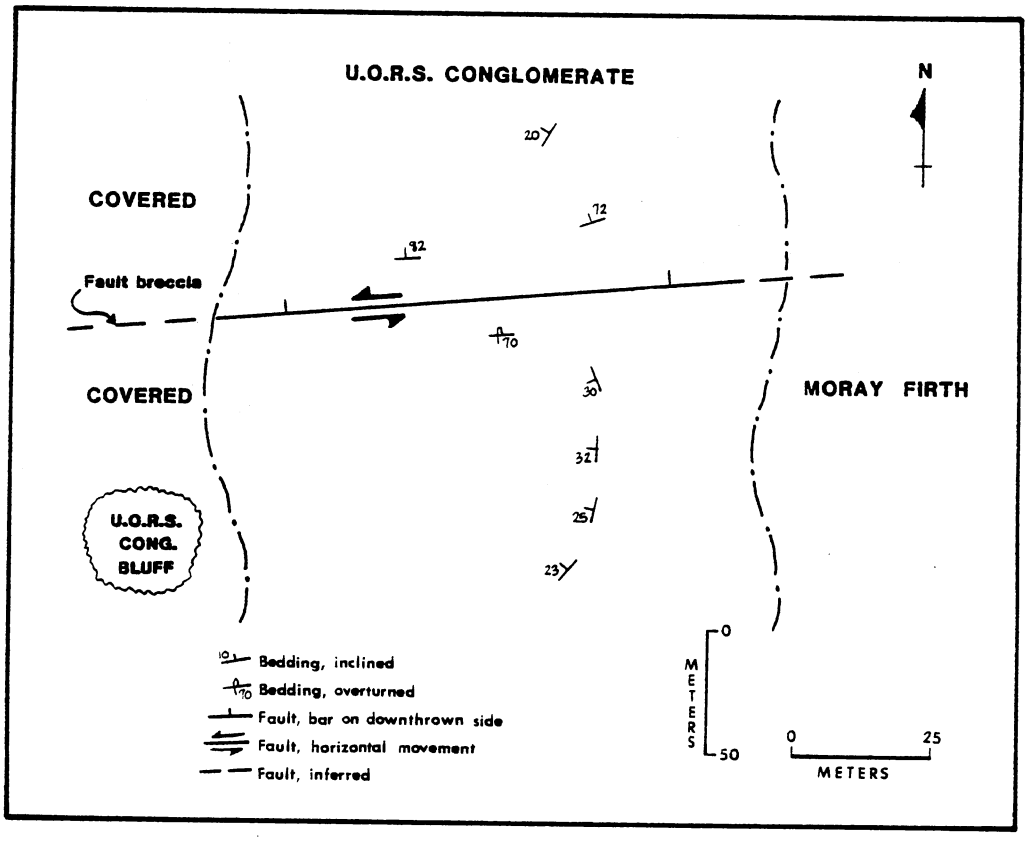

Figure 15. The Wilkhaven Fault is a Well-developed Left Lateral Conjugate Reidel Shear

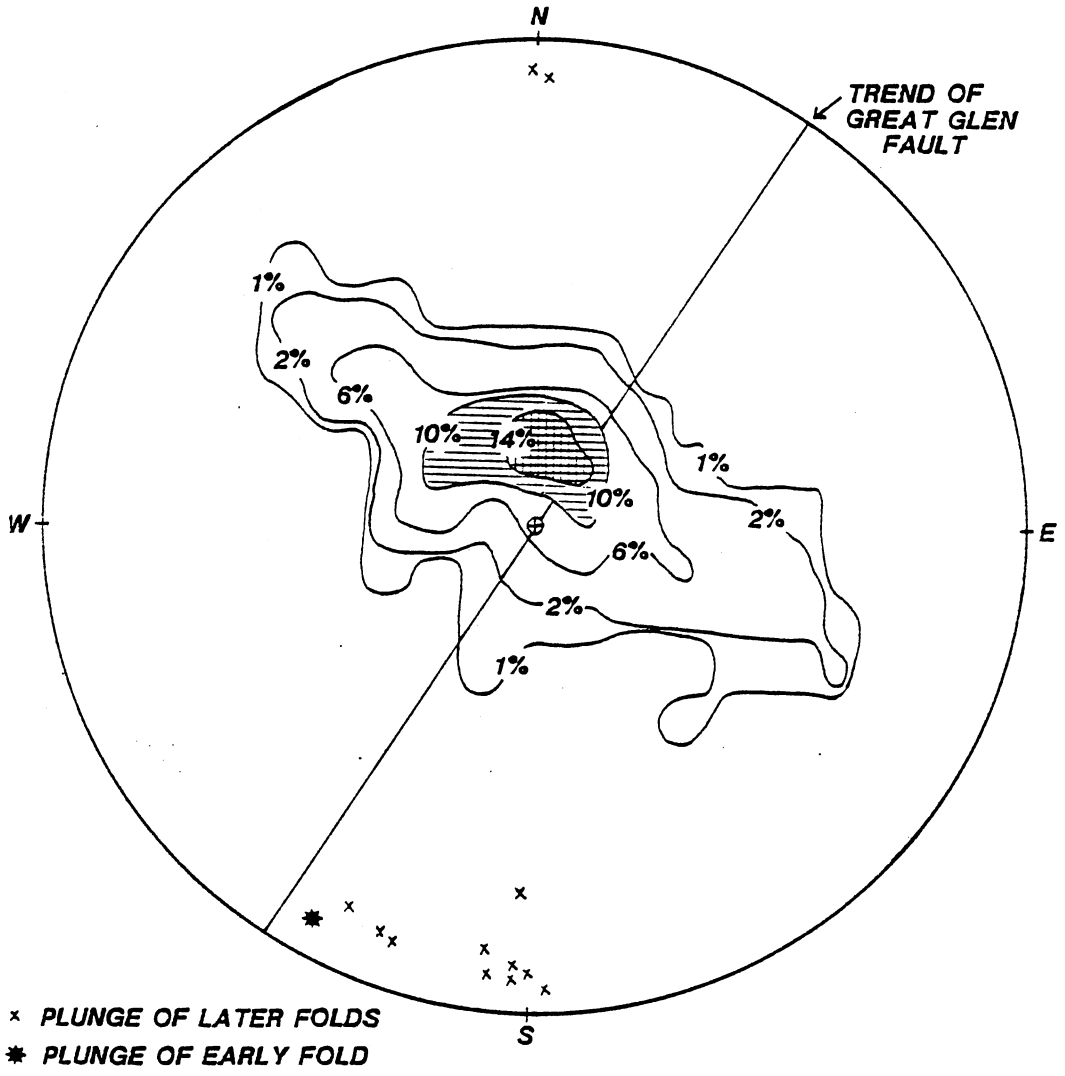

Figure 16. Contoured Stereonet of Poles to Bedding, Ballone Castle Foldbelt. (This noted fold orientation suggests the presence of an early large-scale fold. From Donovan and Ferraro, recently submitted.)

CHAPTER IV

SEDIMENTOLOGY OF BRAIDED ALLUVIUM

Introduction

Reconnaissance work conducted by R. N. Donovan (personal communication, 1982) and by M. Armstrong (1977) indicated that the M.O.R.S.-U.O.R.S. sequence along the Tarbat Peninsula is of a fluvial origin. This conclusion was substantiated by field work conducted during this study. The M.O.R.S. is composed of 92 percent very fine to medium-grained sand, and eight percent silt and mud. Sedimentary structures that characterize sandy lithologies are large-scale cross-bedded units with scoured surfaces and intraclast lags, medium-scale cross-bedded units, horizontal laminations and some convolute bedding. Horizontal laminations are predominant in the fine lithologies. Small-scale cross-bedding, small-scale ripples and climbing ripples are also present. Although the position of sedimentary structures with respect to each other is variable, the M.O.R.S. contains numerous cyclic sequences.

The U.O.R.S. along the Tarbat Peninsula is much coarser than the M.O.R.S. Eighty-two percent of the section is coarse sand; 18 percent of the section is mixed sand and gravel. Characteristic sedimentary structures include large-scale trough cross-bedding with scoured surfaces and pebble lags, and subordinate amounts of medium-scale trough cross-bedding and horizontal laminations. An U.O.R.S. silt and mud facies is lacking.

Paleocurrent orientations in both the U.O.R.S. and the M.O.R.S. are predominately unimodal.

The poorly developed cyclic character of sequences in both the Middle and Upper O.R.S. precludes their deposition in a meandering belt system as proposed by Allen (1964, 1965c, 1970a), or Harms et al. (1963). Rather, a braided river model for their sedimentation is favored.

The Braided River Depositional System

Much of the current understanding concerning the braided river depositional system has resulted from studies of recent braided fluvial systems. Observations of the plan view of braided rivers and their associated lithotypes are distinct advantages of this type of study. Models developed from these studies have been applied to ancient braided alluvial sequences.

In pre-Carboniferous times, the lack of terrestrial vegetation enhanced the development of braided river systems (Rust, 1978b). As Devonian meandering fluvial systems (in O.R.S. external basins) have been reported by Allen (1964, 1965c, 1970a), and by Walker and Harms (1971), this generalization must be approached cautiously.

Channel Morphology

Channel morphology is the dominant control that effects the development of a fluvial system. While various channel classifications exist, Miall (1977, 1982) has adopted a simplified system based on previous work by Leopold and Wolman (1957) and Schumm (1963a, 1968a).

Miall recognizes four channel types: straight, braided, meandering, and anastomosing (Figure 17; Table II), whose identification is defined

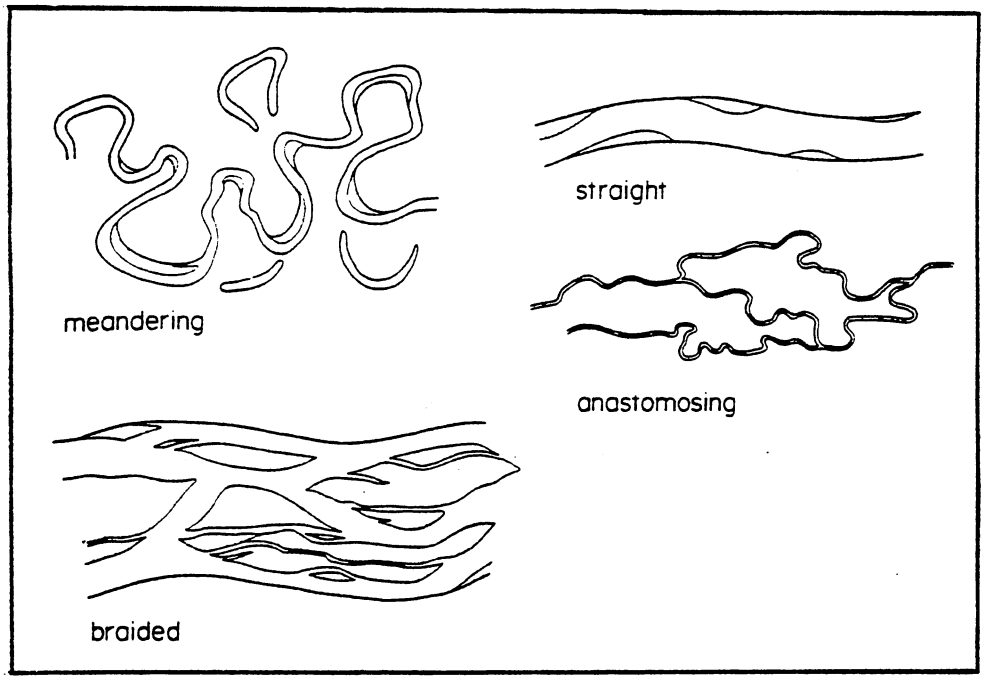

Figure 17. Common River Types. (From Miall, 1977.)

TABLE II

CHANNEL CLASSIFICATION
(From Miall, 1977)

Sinuosity	Single Channel (B.P <1)	Multichannel (B.P.>1)
low	straight	braided
high	meandering	anastomosing

by their sinuosity and braiding parameter. Sinuosity is the ratio of thalweg length to valley length. The braiding parameter is the total number of bars or islands that occur in a channel.

Both meandering and anastomosing rivers have sinuosities that are greater than 1.5. Straight and braided rivers have sinuosities of less than 1.5. Straight and meandering rivers are characterized by braiding parameters of less than one. Braided and anastomosing rivers have braiding parameters that are greater than one and hence, are multi-channel systems.

Depositional Environments of Braided Alluvium

Rust (1978b) has defined three depositional environments that are characteristic of braided alluvium: alluvial fans, braided rivers, and alluvial plains. The dominant lithotypes of these three environments are gravel, sand, and silt, respectively. These environments, along with their associated lithotypes are intergradational; isolated environments, however, are possible. The proximal or distal nature of braided alluvium is inferred from the relation of sequences with respect to the sourceland and their depositional environment.

Alluvial fans form in direct response to erosion of sourcelands with high relief. Their plan is two-dimensional, and they are characterized by rapid proximal to distal variations. Hooke (1967) has divided alluvial fans into upper and lower fan segments (Figure 18). Braid channels incise into the upper fan surface. On the lower fan, braid channels are present on the surface. The intersection point defines the junction between the upper and lower fan and hence, the change from incised to surface braid patterns.

Common facies of alluvial fans are debris flows, sheet floods, stream

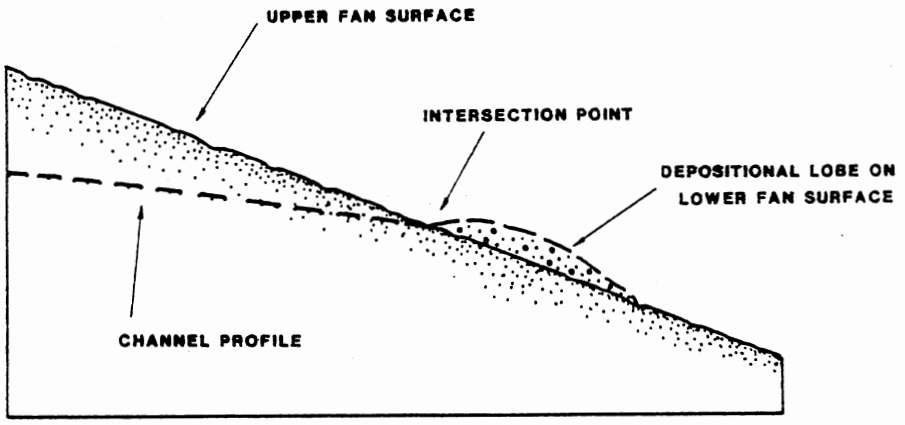

Figure 18. Morphology of an Alluvian Fan. (After Hooke, 1967 and Collinson, 1980.)

channels and sieve deposits (Bull, 1972). Proximal (upper fan) deposits are massive to poorly bedded, unsorted, matrix-supported gravels. While debris flows are the most common facies, stream channel and sheetflood deposits are also prominent.

Distal (lower fan) deposits are characterized by a greater degree of organization than proximal fan deposits. Framework supported gravels are often infilled by sieve deposits. Coarse and fine sediments may grade into one another in crude, fining upward sequences. Sheetfloods and braided streams are the principal sediment dispersal mechanisms.

Braided river deposits result from sediment dispersal of distal alluvial fans or direct erosion of the sourceland. As a result of valley confinement, they are one-dimensional in plan. Proximal braided streams are typically gravelly. However, sandy deposits of a proximal nature have been reported (McKee et al., 1967). Criteria for their recognition include the absence of silt and mud deposits, scoured channel surfaces with siltstone intraclast lags and evidence of a semi-arid environment. The transition from proximal to distal braided river deposits results from a reduction in stream competency. The increase of silt to sand ratios and stabilization of river processes in distal deposits causes the development of fining upward cycles.

Alluvial plains are broad features with low slopes that are characterized by fine-grained fluvial systems whose channels have high lateral aggradation rates. Post-Devonian to recent alluvial plain rivers are dominantly meandering systems. Most lower Paleozoic rivers are interpreted to have a braided type (Miall, 1977). Although rare, some recent alluvial plain river systems have braided characters. These include the Yellow River of China and the Donjek River of the Yukon. High amounts of silt

which are present in the Yellow River result from erosion of massive loess deposits (Chein, 1951). Gravel deposits in the distal portion of the Donjek River result from erosion of a glacial source (Rust, 1972). Braiding in both rivers is caused by stream incompetence.

Physical Controls of Braided River Sedimentation

Miall (1977) provided an excellent summary of the braided river depositional environment. The following discussion of the physical controls on braided alluvium is adapted chiefly from this study.

Braided rivers occur when they are not competent to carry their entire sediment load (Leopold and Wolman, 1957). Common physical controls of braided river incompetency are source areas and alluvial fans of high relief, rapidly fluctuating discharge rates and climate. The predominance of any one of these factors can cause braiding. However, braided systems resulting from two or more physical controls are more common.

Streams that are located in arctic, arid and alpine environments are often braided. The lack of vegetation in these climates (Schumm, 1968a) plus their ephemeral discharge rates (alpine, arid) and high seasonal runoffs (arctic, alpine) enhance braiding. In alpine and arctic environments, braiding is further influenced by erosion of glacial debris.

Braided systems are also recognized in humid-tropical and temperate climates. Fluctuating discharge rates in the Himalayan Mountains, which result from periods of high precipitation during monsoonal seasons, have generated a predominance of braiding in the Mekong, Ganges, and Brahmaputra Rivers. Examples of braided-meandering rivers in temperate climates include the Amite River in Louisiana and the Endrick River in Scotland. Braiding in both rivers results from high bed to suspended load ratios.

Both rivers, however, have sinuosities that are typical of meandering rivers. Vegetation enhances bank stabilization and hence favors meandering.

Braided River Morphology

In studies of recent braided alluvium, several distinct topographic levels can be recognized. Channels comprise the lowest topographic levels. Bars are intermediate structures, and floodplains and vegetated islands which are typically in the abandoned river tract are at the highest topographic levels. Marked topographic differentiation resulting from a high rate of degradation is common in braided streams that are in close proximity to mountain fronts. However, as distance from the sourceland increases, stream degradation and hence topographic differentiation increases (Miall, 1977).

The stability of morphological elements of braided rivers is a function of their topographic level and lateral position with respect to the active braid tract (Williams and Rust, 1969). However, all elements of braided rivers are temporal. Their preservation potential is a function of lateral migration of the active braid tract and the ubiquity of any particular morphological element.

The most stable morphological elements, floodplains and vegetated islands, are present in inactive areas of the braid system. Submergence of these features occurs only during periods of flooding. Because avulsion in braided streams is a common process, channels are the least stable morphological element. Bar stability is directly related to the lateral migration of the active braid tract. Bars present in the active braid tract will continually aggrade and degrade. As the lateral distance between bars and the active braid increases, fine-grained vertical accretion and evolution

of bars into vegetated islands will be enhanced (Smith, 1970; Miall, 1977).

Description of Morphological Elements

Bars. Bar types that are recognized in braided river deposits include longitudinal, transverse, linguoid, point and side bars (Figure 19). Point and side bars are characteristic of meandering channels within the active braided tract. Because of their complexity, these bar types are difficult to recognize in ancient braided alluvium deposits (Miall, 1977).

Longitudinal and transverse bars are common in proximal (gravelly) and distal (sandy) braided rivers, respectively (Smith, 1970). Transverse bars have also been recognized in gravelly braided rivers by Smith (1974) and Rust (1975). As exemplified by Smith's (1970) work on the South Platte River in Colorado and Nebraska, the relative proportion of longitudinal to transverse bars decreases gradationally with increasing distance from the sourceland.

Longitudinal bars are lozenge shaped in outline (Figure 19). Their generation results from the initial transport of bedload in the channel thalweg. Trapping of finer grains as matrix material occurs as stream competency decreases. Internal structures are massive or crudely laminated. In areas of high thalweg sinuosity or at river junctions, distorted flow patterns result in the generation of asymetric longitudinal bars (Miall, 1977).

Transverse bars occur principally in sandy portions of braided rivers, and are generated by dune migration during high water stages in channels of active braided tracts (Reading, 1980; Smith, 1970)(Figure 19). Size ranges include lengths which vary from several meters up to 300 meters and heights from several centimeters up to two meters (Maill, 1977). Coleman

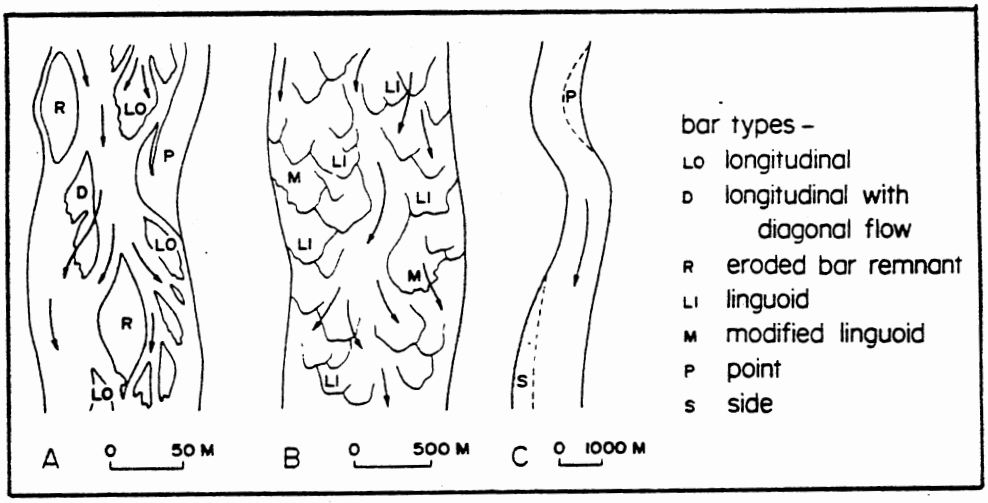

Figure 19. Bar Types of Braided Alluvium.
(From Miall, 1977.)

(1969) has reported flood generated bedforms in sandy braided alluvium of the Brahmaputra River that attain lengths and heights of 640 and 16 meters, respectively. These bedforms are internally comprised of large-scale sets of planar-tabular and trough cross-beds. However, their identity as transverse bars is speculative.

Internally, transverse bars consist of planar-tabular cross beds. Migration is accomplished by avalanche progradation on the lee side of the bar. The direction of progradation is generally transverse to the mean stream orientation (Miall, 1977; Cant and Walker, 1976, 1978). With waning flow, bars often become emergent, small-scale structures migrate over the bar tops and dissection and degradation are initiated by minor channels (Smith, 1970).

Linguoid bars are genetically similar to transverse bars. The major geometric difference is that linguoid bars are lobate in plan whereas transverse bars have straighter crests. Miall (1977) indicates that the differentiation of these bar types in recent and ancient sequences is arbitrary.

In studies of the South Saskatchewan River, Cant and Walker (1978) report that the coalescence of transverse bars, channel dunes, and minor small-scale structures form cross channel bars. Continued aggradation of these bars results in the generation of sand flats.

Channels. Major and minor channels are recognized in recent and ancient braided rivers (Smith, 1970; Cant and Walker, 1976, 1978; Miall, 1977). Major channels occur adjacent to bars, although bar initiation generally develops within them. Lateral migration of major channels is accomplished by avulsion during high water stage or by dissection during waning flow. Minor channels develop during periods of waning flow as bars

become emergent. Both channel types are characterized by scoured surfaces, siltstone intraclast, or pebble lags in trough cross-beds. The magnitude of these features is proportional to the size of the channel in which they occur.

Floodplains and Vegetated Islands. The percentage of fine-grained deposits (very fine-grained sand or smaller) present in braided rivers is significantly less than its coarser counterparts (Cant and Walker, 1976; Miall, 1977; Rust, 1978b). Common sedimentary structures in these facies include horizontal laminations, small-scale cross-bedding of various types, ripples, climbing ripples, mudcracks, and bioturbated horizons. These facies result from deposition of fine sediments under low flow regime conditions during periods of waning flow. Observations of recent braided river systems demonstrate that these deposits are best preserved in non-active areas.

Common Facies of Braided River Deposits

From studies of recent braided rivers, Miall (1977, 1978a) has developed a code of the common lithotypes and associated sedimentary structures of braided alluvium (Table III). The symbols G, S, F, stand for gravel, sand, and fines (very fine sand, silt or mud), respectively. Lower case symbols describe the most prominent feature of the lithofacies; i.e., m-massive, p-planar-tabular cross-beds, h-horizontal laminations, etc. A description of each lithofacies is beyond the scope of this discussion. However, a summary of the major lithotypes is as follows: 1) Characteristic sedimentary structures of gravel deposits are massive or crudely laminated beds and planar-tabular and trough cross-bedding. These deposits,

TABLE III

COMMON FACIES OF BRAIDED ALLUVIUM
(From Miall, 1977, 1978a.)

Facies Code	Lithofacies	Sedimentary structures	Interpretation
Gms	massive, matrix supported gravel	none	debris flow deposits
Gm	massive or crudely bedded gravel	horizontal bedding, imbrication	longitudinal bars, lag deposits, sieve deposits
Gt	gravel, stratified	trough crossbeds	minor channel fills
Gp	gravel, stratified	planar crossbeds	linguoid bars or deltaic growths from older bar remnants
St	sand, medium to v. coarse, may be pebbly	solitary (theta) or grouped (pi) trough crossbeds	dunes (lower flow regime)
Sp	sand, medium to v. coarse, may be pebbly	solitary (alpha) or grouped (omikron) planar crossbeds	linguoid, transverse bars, sand waves (lower flow regime)
Sr	sand, very fine to coarse	ripple marks of all types	ripples (lower flow regime)
Sh	sand, very fine to very coarse, may be pebbly	horizontal lamination, parting or streaming lineation	planar bed flow (l. and u. flow regime)
Sl	sand, fine	low angle (<10°) crossbeds	scour fills, crevasse splays, antidunes
Se	erosional scours with intraclasts	crude crossbedding	scour fills
Ss	sand, fine to coarse, may be pebbly	broad, shallow scours including eta cross-stratification	scour fills
Sse, She, Spe	sand	analogous to *Ss, Sh, Sp*	eolian deposits
Fl	sand, silt, mud	fine lamination, very small ripples	overbank or waning flood deposits
Fsc	silt, mud	laminated to massive	backswamp deposits
Fcf	mud	massive, with freshwater molluscs	backswamp pond deposits
Fm	mud, silt	massive, desiccation cracks	overbank or drape deposits
Fr	silt, mud	rootlets	seatearth
C	coal, carbonaceous mud	plants, mud films	swamp deposits
P	carbonate	pedogenic features	soil

which are principally proximal, result from debris flows, sheet floods, channel fills, and longitudinal bars. 2) Sedimentary structures associated with the sandy facies are planar-tabular and trough cross bedding erosional scours, rippled horizons, and horizontal laminations. Trough and planar-tabular cross bedding are most characteristic of channel dunes and transverse bars. Horizontal laminations result from floods or bar and sand flat accretion. 3) Very fine-grained sand, silt, and mud are most commonly organized into fine laminations and rippled horizons. Other associated features include massive deposits, coal, rootlets, desiccation cracks, and caliche horizons.

Vertical Facies Models

Miall (1977) describes four cycles that are characteristic of braided rivers:

> 1) A flood cycle: a superimposition of beds formed at progressively decreasing energy levels. 2) A cycle due to lateral accretion: a cycle generated by point or side bar generation is possible, as in a meandering river environment. 3) A cycle due to channel aggradation: this cycle would represent the fill of a channel or a local channel system. Waning energy levels would occur during sedimentation, followed by channel abandonment as a result of avulsion. 4) A cycle due to channel re-occupation: an abandoned, partially filled channel may be re-occupied by avulsion.

Because of the variability of these cycles and the possibility of more than one cycle influencing a fluvial succession, one idealized vertical sequence for all braided rivers is inadequate.

As a result of studies of recent braided rivers, Miall (1977, 1978a) has produced six generalized vertical profiles that characterize the spectrum of braided river sedimentation. They include the Trollheim, Scott, Donjek, South Saskatchewan, Platte, and Bijou Creek types

(Figure 20)(Table IV). A discussion of the salient features of each succession follows.

Trollheim Type. This model is based mainly on work carried out by Hooke (1967), Wasson (1977), and Rust (1978b). The Trollheim is a proximal semi-arid alluvial fan that is located in California. Important features include debris flows, incised channels, sheet floods, and crude fining upward cycles.

Scott Type. The Scott type results mainly from work conducted by Boothroyd and Ashley (1975) on glacial outwash fans of the Scott glacier in Alaska. It is characterized by proximal gravel deposits that consist of bars, debris flows, and minor channels. Fining upward cycles are crudely developed.

Donjek Type. The Donjek type is characteristic of distal gravelly river deposits. It was developed primarily from studies conducted by Williams and Rust (1969), and Rust (1972) on the Donjek River located in the Yukon. The succession consists of fining upward sequences of various magnitudes. Individual sequences are comprised of gravelly channels and longitudinal bars, sandy transverse bars, and sand-silty vertical accretion deposits.

South-Saskatchewan Type. This model, developed from work by Cant and Walker (1976) on the South Saskatchewan River, is designed to represent cyclic sedimentation in sandy braided rivers. Fining upward cycles consist of major and minor channels, compound bars, sand flats, and vertical accretion deposits.

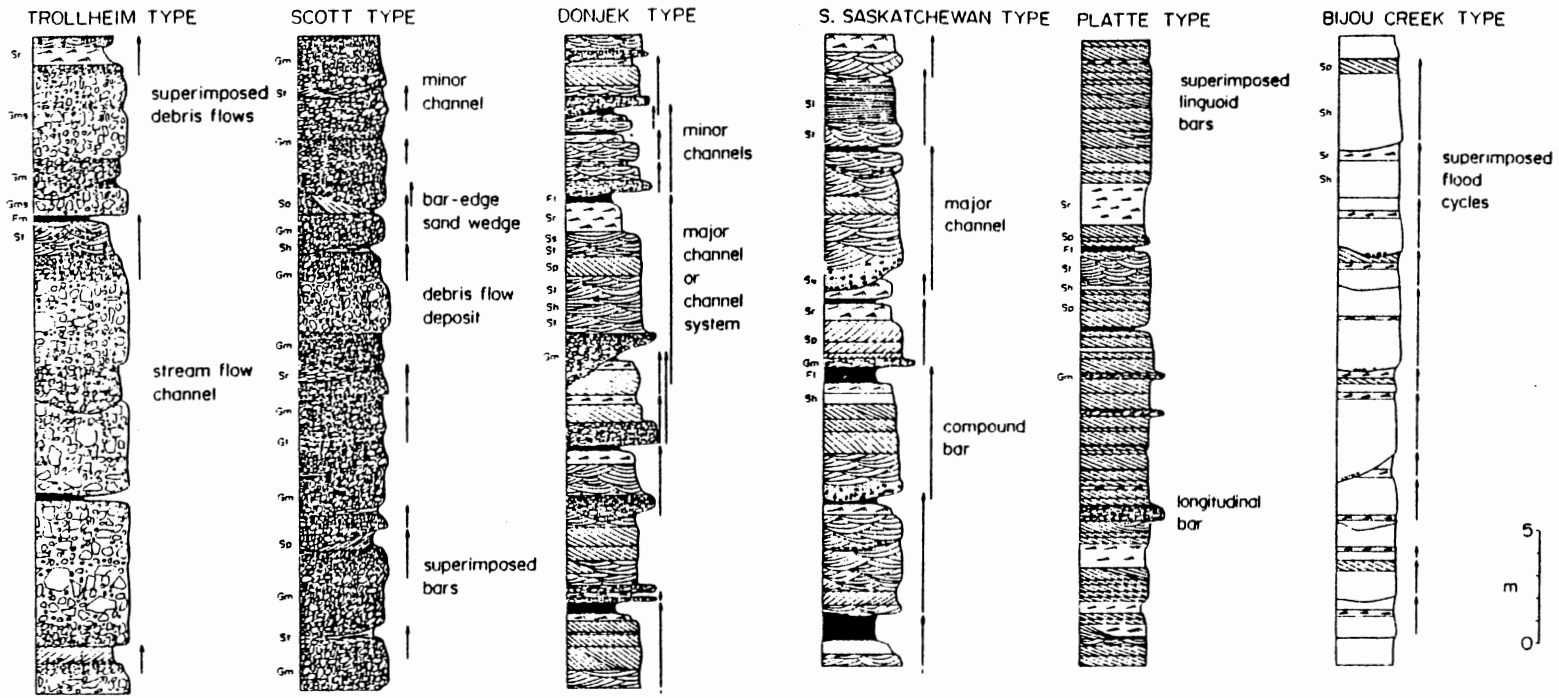

Figure 20. Generalized Vertical Profile for Six Recent Models of Braided Alluvium. (From Miall, 1977, 1978a.)

TABLE IV

SUMMARY OF GENERALIZED VERTICAL PROFILES (Figure 20) WHICH CONSTITUTE THE SPECTRUM OF RECENT BRAIDED ALLUVIUM. (From Miall, 1978a.)

Name	Environmental setting	Main facies	Minor facies
Trollheim type (G_i)	proximal rivers (predominantly alluvial fans) subject to debris flows	*Gms, Gm*	*St, Sp, Fl, Fm*
Scott type (G_{ii})	proximal rivers (including alluvial fans) with stream flows	*Gm*	*Gp, Gt, Sp, St, Sr, Fl, Fm*
Donjek type (G_{iii})	distal gravelly rivers (cyclic deposits)	*Gm, Gt, St*	*Gp, Sh, Sr, Sp, Fl, Fm*
South Saskatchewan type (S_{ii})	sandy braided rivers (cyclic deposits)	*St*	*Sp, Se, Sr, Sh, Ss, Sl, Gm, Fl, Fm*
Platte type (S_{ii})	sandy braided rivers (virtually non cyclic)	*St, Sp*	*Sh, Sr, Ss, Gm, Fl, Fm*
Bijou Creek type (S_i)	Ephemeral or perennial rivers subject to flash floods	*Sh, Sl*	*Sp, Sr*

Platte Type. The Platte type, adapted from work by Smith (1970, 1971a, 1972) is characterized by non-cyclic sedimentation in shallow sandy braided rivers that are subject to semi-arid conditions. Channels are poorly developed. Bars, both longitudinal and linguoid (transverse) are the dominant morphological feature).

Bijou Creek Type. This model results from work by McKee et al. (1967) along with the Bijou Creek in Colorado. It represents flood deposits of ephemeral streams that are located in arid environments with adjacent high relief sourcelands. The most common facies are parallel laminated sands that are transported under upper flow regime conditions during floods.

CHAPTER V

FACIES DESCRIPTIONS

Introduction

Reading (1980) defined the term facies with respect to sedimentary environments in four senses:

> 1) in a strictly observational sense of a rock product, i.e., sandstone facies; 2) in a genetic sense for the products of a process by which a rock is thought to have formed, i.e., turbidite facies; 3) in an environmental sense for the environment in which a suite of mixed rocks is thought to have formed, i.e., fluvial facies or shallow marine facies; 4) as a tectonic facies, i.e., post-orogenic facies or mollasse facies.

Within the context of this study, the term facies will be used in an observational sense to describe the lithologies and their associated sedimentary structures, and in a genetic sense to interpret their origin.

The lithofacies that comprise the M.O.R.S. section include medium to fine-grained sandstones, very fine-grained sandstones, siltstones, and minor amounts of mudstones and sandy limestones. Ninety percent of the section consists of sand whose grain size averages about 0.2 millimeters. The lithofacies that are present in the U.O.R.S. section are medium to coarse-grained sandstones, coarse-grained sandstones with varying amounts of gravel and matrix supported conglomerates.

Sedimentary structures that are present in both sections include

horizontal laminations, convolute bedding, and cross bedding of various types and magnitudes. Small-scale ripples are well developed in silty intervals of the M.O.R.S. To facilitate clear interpretations, the complex classification scheme for cross-bedding that was developed by Allen (1963) was avoided. Rather, cross-bedding is divided into trough or planar-tabular types; a method adopted in the majority of modern braided alluvium studies.

With respect to set thickness, two subdivisions of cross-bedding are recognized. Small-scale cross-bedding consists of set thicknesses of five centimeters or less. Large-scale cross-bedding consists of set thicknesses that are greater than five centimeters (Reinick and Singh, 1975). Three distinct sizes of cross-bedding are present in the Tarbat Peninsula section (Table V). A set of thickness of five centimeters or less is maintained for small-scale cross-bedding. Medium-scale cross-bedding is defined by a set thickness that ranges from five to 50 centimeters and a width that is greater than 1.5 meters. Large-scale cross-bedding is defined by a set of thickness that is greater than 50 centimeters and a width that is greater than 1.5 meters (Table V).

When identifying a cross-bed as planar-tabular or trough shaped, three dimensional views are most definitive (Potter and Pettyjohn, 1977). However, in practice, two dimensional views are commonly encountered. If the observed orientation is parallel to bc (Figure 21), the type of cross-bed can be identified with ease. Identification of cross bedding parallel to the ac direction is more difficult. Ideally, beds with concave foreset laminae are trough shaped, and beds with angular foreset laminae are planar-tabular shaped. This conclusion is substantiated by Coleman (1969), who reported that cross-beds in the

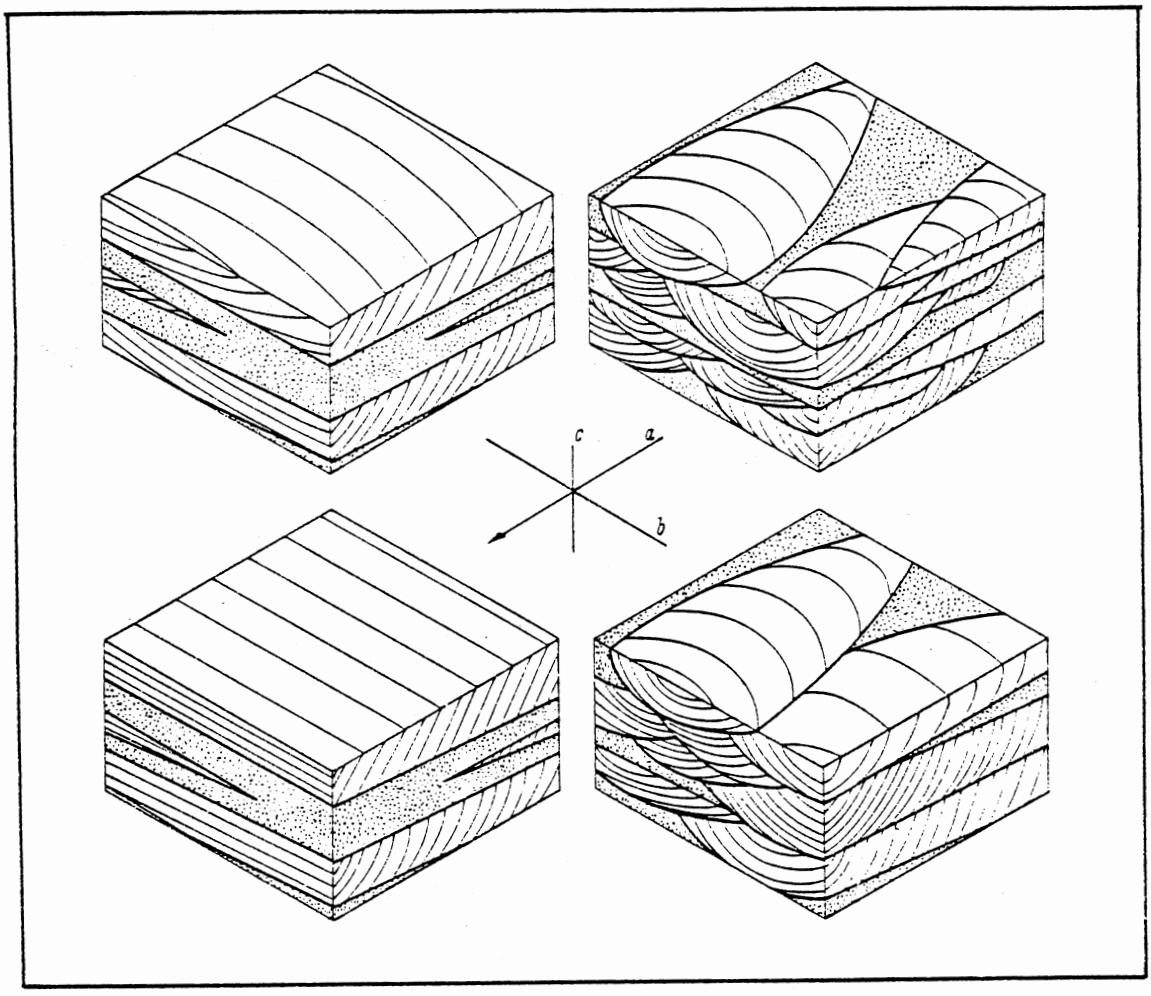

Figure 21. End members of Cross-bedding; Planar-Tabular (left) Trough (right). (From Potter and Pettyjohn, 1977.)

Brahmaputra River with concave foreset laminae in the ac direction were trough shaped in the bc direction.

TABLE V

CLASSIFICATION OF CROSS-BEDDED SETS, TARBAT PENINSULA SECTION

Type	Thickness	Width
small	$\leq$ 5 cm	-
medium	6-50 cm	$\leq$ 1.5 m
large	> 50 cm	> 1.5 m

Two-dimensional views of cross-bedding are common in the Tarbat Peninsula section. When views parallel to the ac direction were encountered, cross-bed shape was identified by the method elucidated in the former paragraph.

Discussion

Various authors have adopted the use of codes to describe the facies which are characteristic of braided alluvium. Examples include work conducted by Cant and Walker (1976), Miall (1977, 1978a), and Rust (1978b). The following facies code symbols for the Tarbat Peninsula section are adapted partially from work by Miall (1977, 1978a).

M.O.R.S. Facies Descriptions

Facies descriptions for the M.O.R.S. appear in Table VI. Statistical data are presented in Table VII.

Erosional Scour Facies (es)

The erosional scour facies (Figure 22) consists of erosional surfaces which are, in most instances, overlain by mudstone intraclast lags. The maximum thickness of intraclast accumulation is 30 centimeters. Thin beds of intraclasts with abrupt basal contacts are interpreted as separate depositional events (Turnbridge, 1981). Typically, intraclasts are unarmored and ellopsoidal in shape. Smith (1972a) reports that the abrasion and rounding of unarmored intraclasts in flumes occurs rapidly. This indicates that intraclasts present in the M.O.R.S. were locally derived.

The maximum depth of erosion of an erosional scour is one meter. Erosional scours are followed by facies Slt (49 instances), facies Slp (21 instances), and facies Smt (20 instances). The association of erosional scours with facies Slt and Smt reflects deposition in major and minor channels, respectively (Miall, 1977). Erosional scours that are followed by facies Slp possibly resulted from deposition in major channels during periods of waning flow.

Sandy Large-scale Trough Cross-Bedded Facies (Slt)

This facies rests upon erosional scours (es) in 49 instances, and precedes facies es and facies Sh in 23 and 29 instances, respectively. They occur as isolated sets or cosets which repeat in a multi-storied

TABLE VI

FACIES DESCRIPTIONS OF THE M.O.R.S.; TARBAT PENINSULA

Facies Code	Lithofacies	Sedimentary Structures	Interpretation	Occurrences
es	mudstone intraclast lags	erosional scours, primarily large-scale trough cross beds	major and minor channel initiation	91
Slt	sand, fine to medium	large-scale trough cross beds	dunes, in and adjacent to channels	94
Slp	sand, fine to medium	large-scale planar-tabular cross beds	transverse bars	58
Smt	sand, fine to medium	medium-scale trough cross beds	megaripple migration minor channel fills	82
Smp	sand, fine to medium	medium-scale planar-tabular cross beds	small-scale bars, possibly transverse	33
Sh	sand, fine to medium	horizontal laminations, parting lineations	stream floods	155
Scv	sand, fine to medium	convoluted large-scale cross beds and horizontal laminations	rapid sedimentation rates sediment liquidization	45
Fl	very fine sand, silt, mud	fine horizontal laminations	vertical accretion deposits on flood-plains; fluvial or lacustrine	76
Fr	very fine sand, silt	small-scale straight crested, lingoid or climbing ripples	vertical accretion deposits on flood-plains; fluvial or lacustrine	15
Fx	very fine sand, silt	small-scale trough or planar-tabular cross beds	vertical accretion deposits or flood-plains; primarily fluvial	28

TABLE VII

STATISTICAL DATA OF THE M.O.R.S.; TARBAT PENINSULA

Facies Code	Number of Occurrences	Total Thickness	Average Bed Thickness	Standard Deviation of Bed Thickness	Percent of M.O.R.S. Section
Slt	94	89.4 m	1.1 m	0.6 m	25.4
Slp	58	39.5 m	0.7 m	0.4 m	11.2
Smt	82	41.1 m	0.5 m	0.2 m	11.7
Smp	33	16.4 m	0.5 m	0.3 m	4.7
Sh	155	104.5 m	0.7 m	0.4 m	29.6
Scv	45	20.8 m	0.45 m	0.2 m	5.9
Fl	76	22.8 m	0.4 m	0.3 m	9.3
Fr	15	2.7 m	0.2 m	0.1 m	.8
Fx	28	5.3 m	0.2 m	0.1 m	1.4

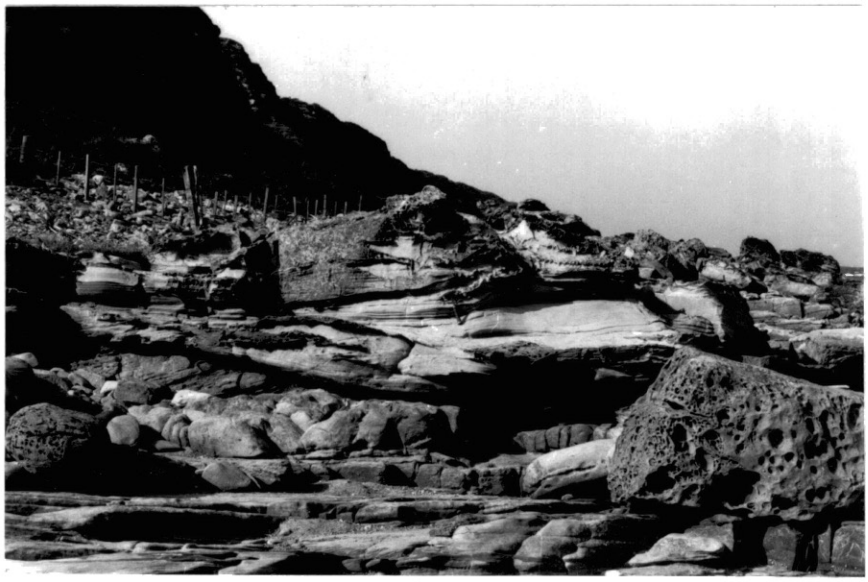

(A)

(B)

Figure 22. M.O.R.S. Sandy Large-scale Trough Cross-bedded Facies. (A) Erosive Channel Base With Large-scale Troughs. (Note facies Sh in foreground.) (B) Detail of Erosive Base. (Note facies Slp below erosive base. Photo at 69-73 m, M.O.R.S. section. Hammer length is 32 cm.)

fashion (Figures 22 and 23). The maximum coset thickness is about two meters. The maximum width of an individual set is about 10 meters. Extremely large units are flat based in the center and curved only at their ends (Figure 22). Facies Slt resulted from bedform migration of dunes (Harms et al., 1975). Their pronounced association with erosional scours indicates that they were predominately in channel bedforms (Cant and Walker, 1976).

Sandy Large-scale Planar-Tabular Cross-bedded Facies (Slp)

Large-scale planar-tabular cross beds comprise 11.2 percent of the M.O.R.S. section and average 0.7 meters in thickness (Figure 24). They generally occur as isolated sets; however, cosets of up to four sets were recorded. The dip of foreset laminae decreases with increasing set thickness. Sets thicker than one meter commonly have foreset dips of less than 20 degrees. With respect to braided rivers, large scale planar-tabular cross beds comprise the internal structure of transverse bars (Smith, 1970; Asquith and Cramer, 1975; Cant and Walker, 1976; Miall, 1977). However, the number of instances in which facies Slp rests on erosional scours in the M.O.R.S. section is atypical. Perhaps this relationship resulted from in-channel transverse bar initiation during periods of reduced stream competency.

Sandy Medium-scale Trough Cross-bedded Facies (Smt)

This facies comprises 11.7 percent of the M.O.R.S. section. In some instances, sets are isolated; however, multi-storied cosets (average 0.5 meters) are predominate. Troughs are generally arcuate in

(A)

(B)

Figure 23. M.O.R.S. Facies Slt. (Note variation in magnitude from Figure 21.) (A) Multi-storied Coset at Meter 145, M.O.R.S.$_1$ Section. (B) Low Angle Trough Cross-beds With Erosive Scour. (Photo at 4-9 m, M.O.R.S.$_1$ section. Hammer length is 32 cm.)

Figure 24. From Bottom of Photo Sequence is Facies F (a), Facies Sh (b), Facies Slp (c), and Facies Sh (d). (Photo at 8-11 m M.O.R.S.$_1$ section. Staff length is 5 ft.)

plan. Foreset laminae dip angles range from 10 to 30 degrees. Eighty-two occurrences of facies Smt were recorded, of which 17 were preceded by an erosive scour (Figure 25). Mudstone intraclasts are often present in sets with erosive bases in bedded or lag positions. The association of facies Smt with erosive bases records the presence of minor channels which developed during river desiccation or floodplain accretion (Miall, 1977). Multi-storied units with abrupt basal contacts (Figure 26) resulted from the migration of megaripples (Harms et al., 1975).

Sandy Medium-scale Planar-Tabular Cross-bedded Facies (Smp)

Medium-scale planar-tabular cross-bedding is a minor facies (4.7 percent) in the M.O.R.S. section. Facies Smp commonly precedes or occurs above finely laminated siltstones and mudstones. This indicates that they were generated during periods of vertical accretion at topographically higher levels of the river system. They are interpreted to be the result of the migration of small-scale bedforms (Cant and Walker, 1976).

Sandy Horizontal-laminated Facies (Sh)

Sandy horizonatal laminations, whose average thickness is 0.7 meters, comprise 29.6 percent of the M.O.R.S. section (Figures 22, 23, 24, 25, 27, 28). Eighty beds out of a total of 155 are greater than or equal to 0.6 meters in thickness. The thickness of individual laminations typically ranges between one and five millimeters; however, laminae thicknesses of up to one centimeter were recorded. Parting

Figure 25. M.O.R.S. Medium-scale Trough Cross-bedded Facies (Smt). (Note erosive scour into facies Sh and bedded intraclasts. Photo at 12 m, M.O.R.S.$_1$ section; lens cap width is 5 cm.)

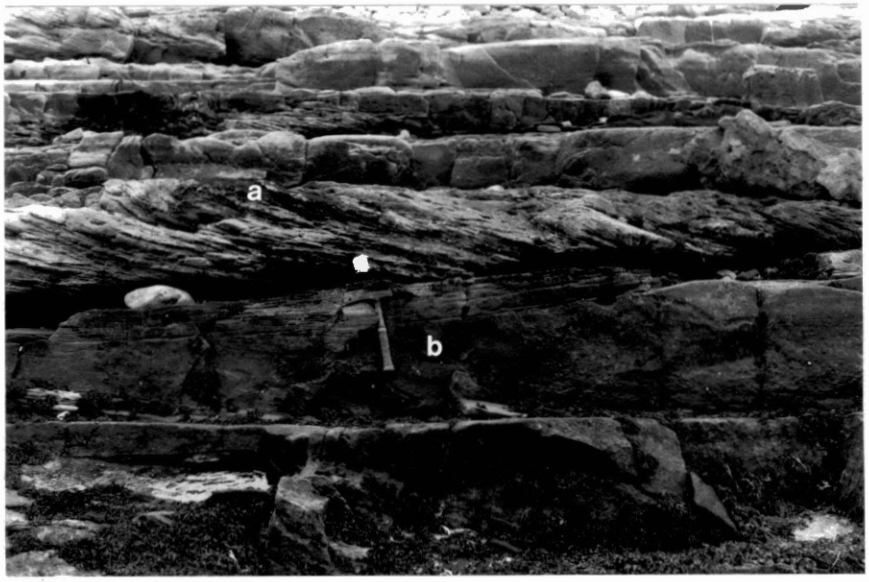

Figure 26. M.O.R.S. Facies Smt Appear as Megaripples. (a) Migrating Over the Lee Side of a Dune (b). (Photo at 10 m, M.O.R.S.$_3$ section. Hammer length is 32 cm.)

(A)

(B)

Figure 27. (A) Sandy Horizontal Laminations (Facies Sh). (B) Parting Lineations on the Surface of Facies Sh Indicate Upper Flow Regime Conditions. (Photo at 160 m, M.O.R.S.$_1$ section. Coin width is 2 cm.)

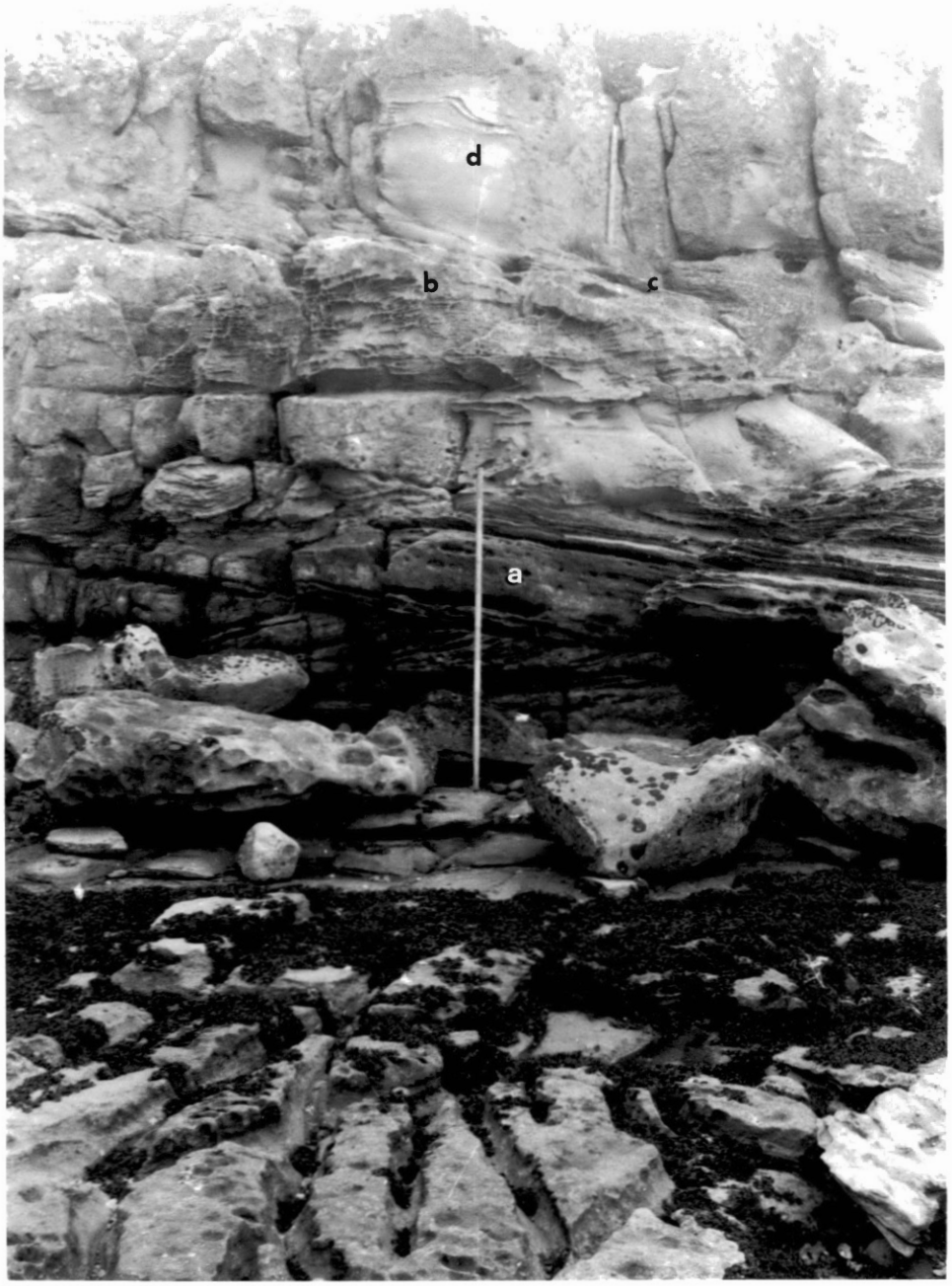

Figure 28. From Bottom of Photo Sequence is Facies Slt (a), Facies Sh (b), Erosional Scour (c) and Facies Slt (d). (Horizon d overturns laterally Figure 28. Photo at 122-127 m, M.O.R.S.$_1$ section. Staff length is 5 ft.)

lineations are common on Sh surfaces throughout the M.O.R.S. section (Figure 27).

The occurrence of horizontal laminations that are associated with sandy lithotypes has been recognized in meandering rivers by Allen (1970a) and in perennial braided rivers by Smith (1971b). However, in both fluvial systems they are of a minor nature. Horizontal laminations are often the predominate component of river systems that are dominated by flood events. Examples include the ephermal Bijou Creek of eastern Colorado (McKee et al., 1973) and the Middle Devonian Trentishoe Formation of southwest England (Turnbridge, 1981). Horizontal laminations, typically with bed thicknesses of two feet or greater, are the predominant sedimentary structure in both sequences. Parting lineations and convolute bedding are also common.

The horizontal laminations that are present in the M.O.R.S. section resulted from high velocity discharge rates that were generated by flood events. This conclusion is supported by 1) the predominance of horizontal laminations; 2) an average bed thickness of facies Sh that is equal to or exceeds two feet; 3) the ubiquity of parting lineations on the surfaces of facies Sh; and 4) an average sand size of 0.2 millimeters whose internal structure assumes a plane bed configuration only during upper flow regime conditions (Harms et al., 1975).

Sandy Convolute-bedded Facies (Scv)

Convolute bedding comprises 5.9 percent of the M.O.R.S. section. With only one exception they occur in the sandy lithofacies. Convolute bedding is present directly above or within large-scale cross bedding in 28 instances and above or within horizontal laminations in 17 instances.

In cross-bedded units, convolutions are predominately overturned (Figure 29). Buttock folds are also present in moderate amounts. Convolutions in facies Sh are upright and tightly folded structures. Pillow and ball deformation was observed in facies Sh in only one instance.

Deformed cross-bedding that is overturned in style is recognized in braided alluvial deposits by Dzulynski and Smith (1963), Rust (1968), Selley (1969), and Hendry and Stauffer (1975). All authors cite the frictional drag produced by heavy sediment laden currents as the major mechanism of deformation. In the M.O.R.S. section, fold axes of overturned cross-bedding are often perpendicular to the regional paleocurrent direction. This orientation suggests that frictional drag was the primary mechanism of cross bedding deformation.

In facies Sh, convolutions were produced by rapid depositional rates which enhanced the development of unstable liquidized zones and negative gravity gradients (Allen, 1977). A similar style of soft sediment deformation found in the flood dominated Trentishoe Formation of southwest England lends credence to this conclusion (Turnbridge, 1981).

Earthquake shocks could also produce convolute bedding (personal communication, R. N. Donovan, 1983). The proximity of the Tarbat Peninsula to the Great Glen fault, which was probably sporadically active throughout the Devonian, enhances the viability of this mechanism. If earthquake shocks were a predominant mechanism, then the distribution of disturbed bedding should be random. However, the association of convolute bedding with large-scale sedimentary structures indicates that soft sediment deformation was not random. Hence, fluvial processes characterized by rapid sedimentation rates are the favored mechanism to produce convolute bedding in the M.O.R.S.

Figure 29. M.O.R.S. Convolute Facies. Facies Slt is Deformed Into Overturned Folds. (Fold Axis Orientation is 120-300. Cross-beds are overturned to the northeast, the regional paleocurrent direction. Photo at 126 m, M.O.R.S.$_1$ section. Staff length is 5 ft.)

Fine Facies (Fl), (Fr), (Fx)

Lithotypes of the fine facies, 11.5 percent of the M.O.R.S. section consist of very fine-grained sand, silt, and mud. Common sedimentary structures include horizontal laminations (laminae thickness of 1-2 millimeters), ripples, and various types of small-scale cross bedding. Their origin resulted from vertical accretion, primarily on floodplains (Miall, 1977).

Two sequences of the fine facies are recognized in the M.O.R.S.: 1) a vertical accretion sequence related to fluvial processes (Figures 30 and 31), and 2) a vertical accretion sequence resulting from lacustrine conditions with indirect fluvial effects (Figures 32 and 33). In one instance, the two sequences are laterally intergradational (Figure 30).

Diagnostic criteria for recognition of lake sequences include 1) a gray-to-green pigmentation of all lithotypes which reflects reducing conditions; 2) the presence of a sandy limestone; 3) the development of small-scale ripples which reflect near shore conditions (personal communication, R. N. Donovan, 1983). Vertical accretion sequences which result from fluvial conditions are primarily red pigmented. Siltstones and very fine-grained sandstones are the predominant lithotypes. Sandy limestones and mudstones are absent. Most commonly, the sequence is finely laminated. Small-scale trough cross beds and climbing ripples are often prevalent near the top of these sequences.

Four well developed lake sequences are present in the M.O.R.S. section. The thickness of these sequences ranges from one to two meters. Two smaller fine sequences with a predominately green color might

(A)

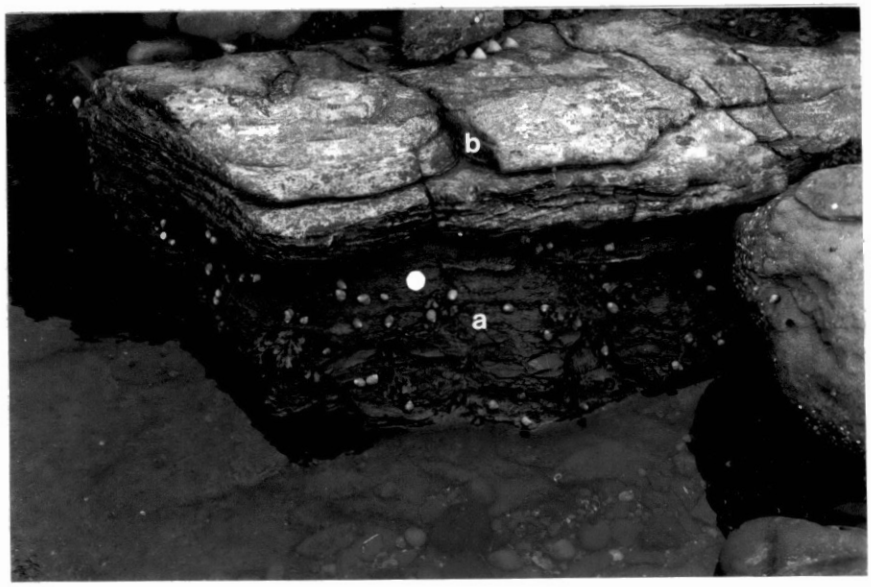

(B)

Figure 30. (A) Lacustrine Sequence; (a) Green Laminated Siltstones; (b) Inlaminated Green Siltstones and Gray Sandy Limestones, and (c) Convoluted Siltstones. (B) Fluvial Vertical Accretion Sequence; (a) Red Laminated Siltstones; and (b) Sandy Horizontal Laminations. (Photo at 8 m, M.O.R.S.$_1$ section.)

(A)

(B)

Figure 31. Fluvial Vertical Accretion Sequence. (A) Interlaminated Silts and Very Fine Sands; (b) Mudcrack Near top of Sequence. (Photo at 167-168 m, M.O.R.S.$_1$ section; hammer length 32 cm; coin width 3 cm.)

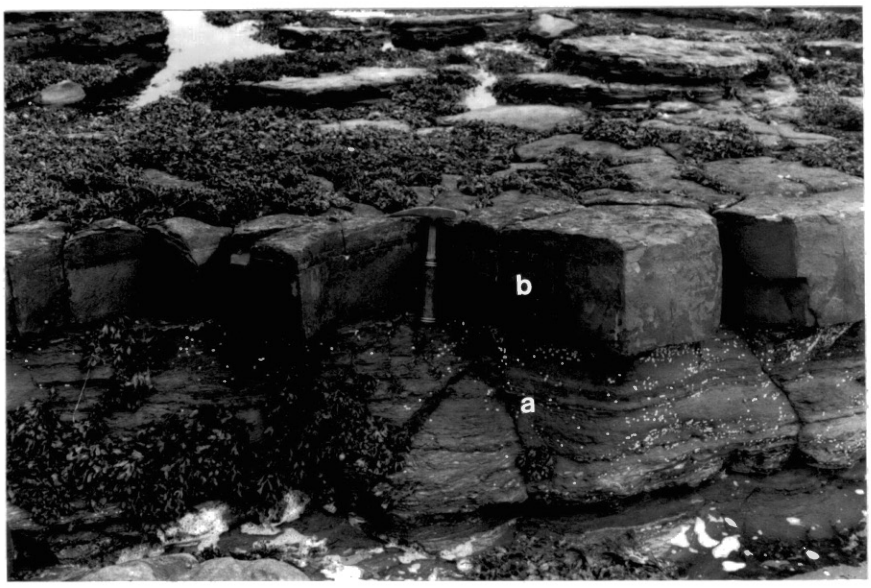

(A)

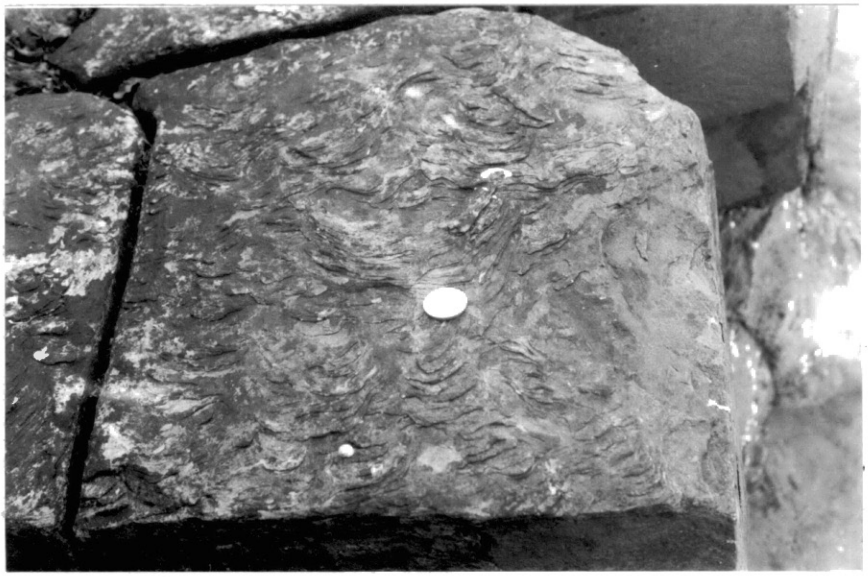

(B)

Figure 32. M.O.R.S. Fine Facies. (A) Green Pigmented Fine Laminations in Silt and Mud (a), pass Upward Into Sandy Limestone with Fine Laminations (b). (Hammer length is 32 cm.) (B) Lingoid Small-scale Ripples on Surface of Sandy Limestone. (Coin is 3 cm wide.) Sequence Resulted From Lacustrine Conditions. (Photo at 14 m, M.O.R.S.$_1$ section.)

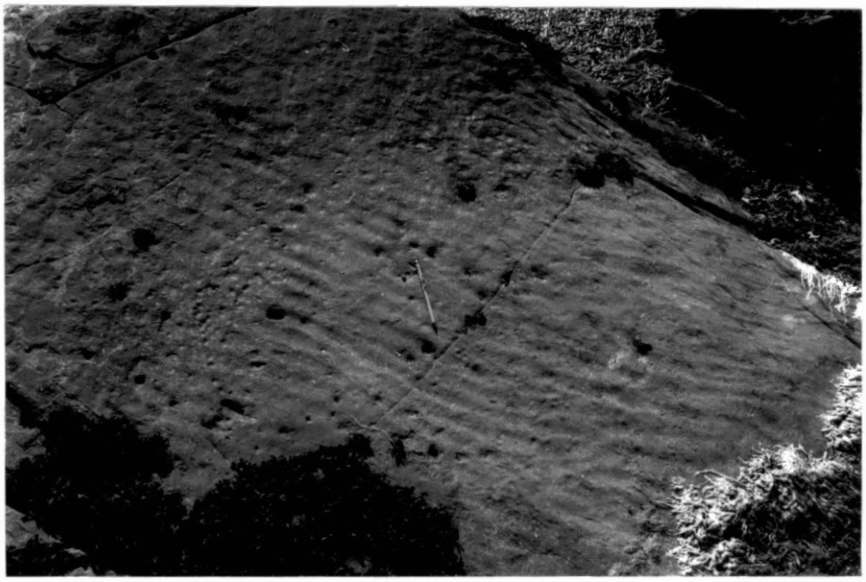

Figure 33. Small-scale Oscillation Ripples (Fr) Resulted From Nearshore Conditions of M.O.R.S. Lakes. (Photo at 47 m, $M.O.R.S._1$ section. Pen length is 15 cm.)

reflect periods of minor lacustrine conditions or secondary reduction of fluvial floodplain deposits.

U.O.R.S. Facies Descriptions

In comparison to the M.O.R.S., the U.O.R.S. of the Tarbat Peninsula reflects fluvial conditions of a greater proportion. Grain size is predominately coarse. Beds with mixed sand and gravel or medium sand occur in moderate amounts. A summary of facies descriptions and statistical data is presented in Tables VIII and IX, respectively.

Erosional Scour Facies (es). Forty-five occurrences of erosional scours were recorded in the U.O.R.S. section. They were predominately associated with facies Gsm, Sglt, and Slt (Figures 34-38). The maximum depth of erosion is three meters (Figure 34).

Pebble lags are often associated with erosional scours (Figure 35). Lag deposits are typically massive; pebble imbrication is poorly developed. Grain size averages for pebble lags range from 2.2-4.0 centimeters.

The erosional scour facies resulted from channel initiation or in channel deposition (Cant and Walker, 1976).

Gravelly-Sandy Massive Facies (Gsm). This facies is massive to poorly laminated (Figures 34 and 35). It occurs in seven instances and comprises 3.7 percent of the U.O.R.S. section. Typical bed thicknesses are about 0.4 meters. However, one deposit which extends laterally for 100 meters is about three meters thick. The thinner beds commonly occur as isolated lenses. Basal contacts within individual deposits are both abrupt and erosive. Pebbles often tend to fine upward; however, random pebble arrangements are also common. The internal geometry of

TABLE VIII

FACIES DESCRIPTIONS OF THE U.O.R.S., TARBAT PENINSULA

Facies Code	Lithofacies	Sedimentary Structures	Interpretation	Occurrences
es	pebble, mudstone intracast lags	erosional scours, associated with Gsm, Sglt, and Slt	channel initiation	45
Gsm	matrix (coarse sand) supported gravels	massive, crudely laminated, poorly developed cross beds	channel lags and longitudinal bars	7
Sglt	coarse sand, minor to moderate bedded and lag gravels	large-scale trough cross beds	dunes, in and adjacent to channels	17
Slt	coarse sand, minor bedded and lag gravel	large-scale trough cross beds	dunes, in and adjacent to channels	53
Slp	medium to coarse sand, minor gravel	large-scale planar-tabular cross beds	transverse bars	4
Sh	medium to coarse sand	horizontal laminations	stream floods, upper flow regime; bar aggradation, lower flow regime	28
Smt	medium to coarse sand, minor bedded gravel	medium-scale trough cross beds	megaripple migration	20
Smp	medium to coarse sand	medium-scale planar-tabular cross beds	small, isolated transverse bars	2
Cv	sand or gravel	convoluted large-scale cross beds and horizontal laminations	rapid sedimentation rates; sediment liquidization	17

pebbles is predominately matrix (coarse sand) supported.

TABLE IX

STATISTICAL DATA OF THE U.O.R.S.; TARBAT PENINSULA

Facies Code	Number of Occurrences	Total Thickness	Average Bed Thickness	Standard Deviation of Bed Thickness	Percent of U.O.R.S. Section
Gsm	7	4.9 m	0.8 m	0.9	3.7
Sglt	17	18.0 m	1.2 m	0.5 m	13.7
Slt	53	60.0 m	1.1 m	0.9 m	45.7
Slp	4	4.6 m	1.1 m	0.2 m	3.5
Smt	20	12.9 m	0.6 m	0.3 m	9.8
Smp	2	0.4 m	0.2 m	-	0.3
Sh	28	20.0 m	0.7 m	0.4 m	15.2
Cv	17	9.7 m	0.6 m	0.3 m	7.4

The massive-to-poorly laminated nature of facies Gsm suggests that they are longitudinal bar deposits (Miall, 1977; Smith, 1970). As reflected by lateral variations in their basal contacts, the deposition of facies Gsm occurred in and adjacent to channels.

Sandy-Gravelly Large-scale Trough Cross-bedded Facies (Sglt). Facies Sglt comprises 13.7 percent of the U.O.R.S. section (Figures 34 and 36. In a total of 17 occurrences, the average bed thickness is 2.1 meters. Lateral variations of the facies are extensive. Isolated deposits thin rapidly. Multi-storied units commonly have

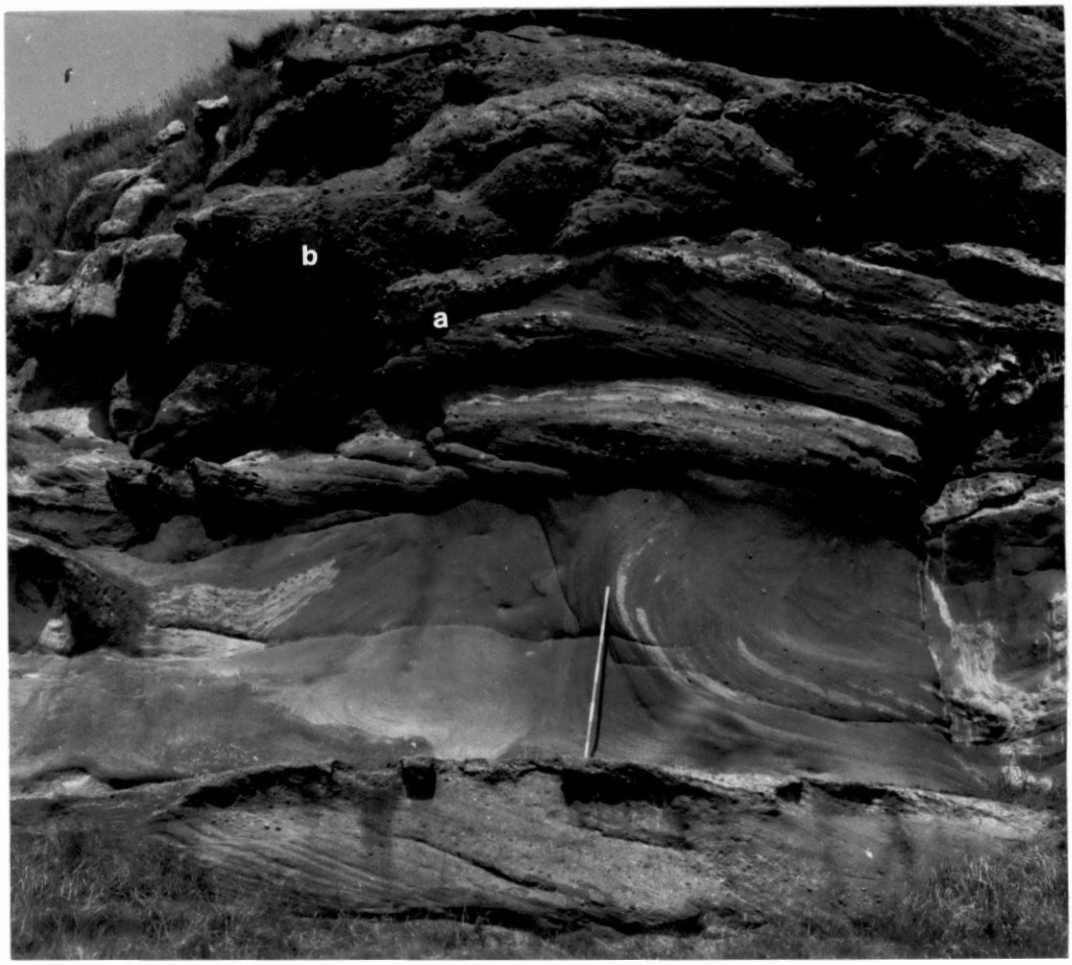

Figure 34. Erosional Scour (a) Cutting Down About Three Meters. Above Scour is Facies Gsm (b). Below Scour are Three Sets of Facies Sglt. (Photo at 280-288 m, U.O.R.S. section. Staff length is 5 ft.)

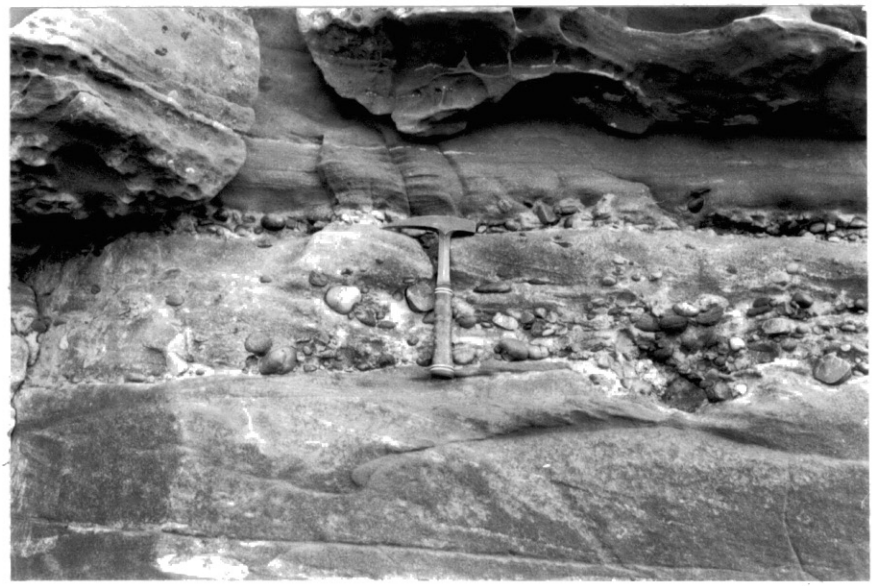

(A)

(B)

Figure 35. U.O.R.S. Facies Gsm. (A) Crude Trough Cross-beds with an Erosive Base. Pebbles are Laterally Continuous for at Least 100 Meters. (Photo at 331 m; hammer length 32 cm.) (B) Three Sets of Facies Gsm (a). (Photo at 285-289 m; staff length 5 ft.)

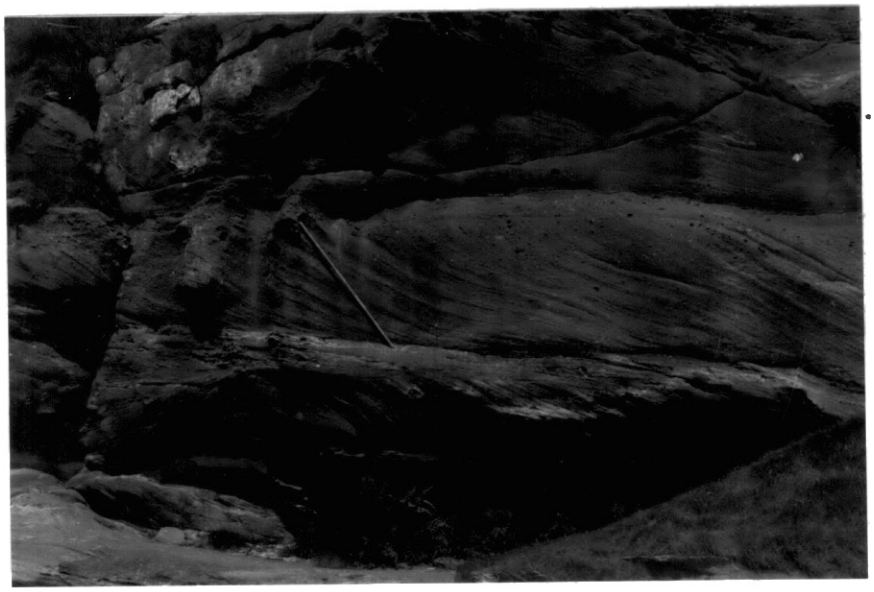

(A)

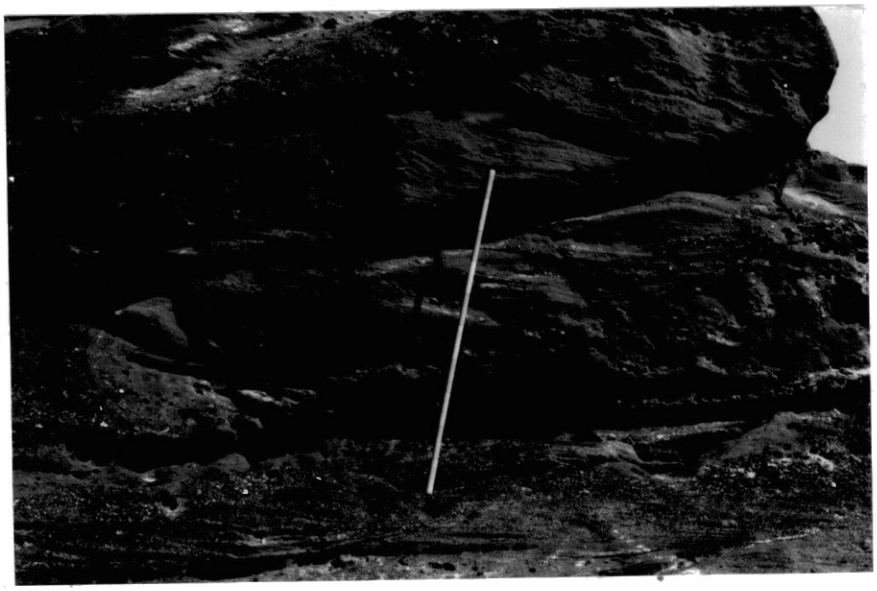

(B)

Figure 36. U.O.R.S. Facies Sglt. (A) Basal Contact Becomes Erosive Laterally (Figure 37). (Photo at 280-281 m.) (B) Four Vertically Stacked Dunes. (Photo at 263-265 m; staff length 5 ft.)

(A)

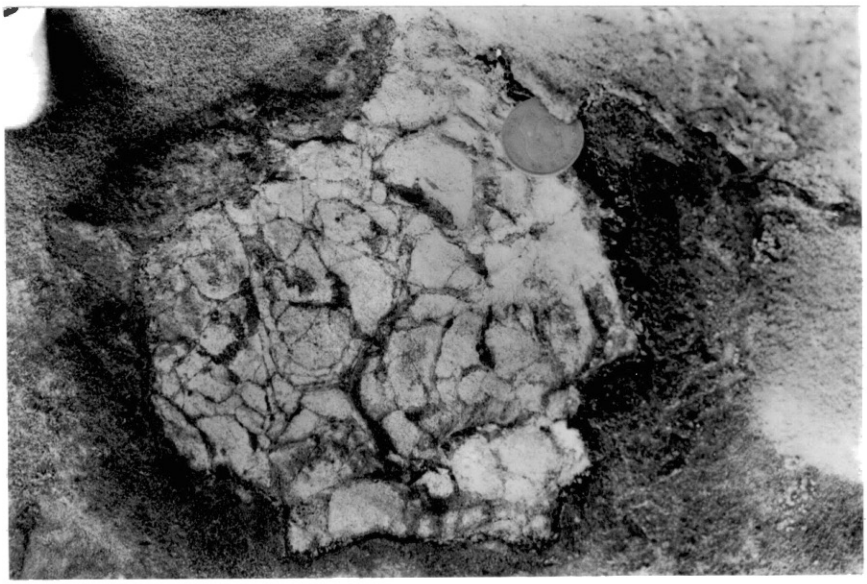

(B)

Figure 37. (A) Pebble and Calcrete Lag at Base of Facies Sglt (Figure 36). (B) Detail of Calcrete. (Photo at 280 m, U.O.R.S. section; coin width 3 cm.)

Figure 38. U.O.R.S. Facies Slt. Erosional Scour at Base Grades Laterally to Abrupt Contact. (Note facies Sh below. Photo at 290-292 m; hammer length 32 cm.)

extensive lateral continuity. Basal contacts are both erosive and abrupt (Figures 36 and 37). Both types of contacts are present in the laterally extensive units. Pebbles occur in both lag and bedded positions.

Facies Sglt resulted from dune migration in and adjacent to channel floors. As evidenced by their multi-storied nature, they commonly repeated in a climbing fashion, oriented downstream (Figure 36).

Sandy Large-scale Trough Cross-bedded Facies (Slt). Facies Slt (Figure 38) is dominated by coarse sands with moderate amounts of medium sand and minor amounts of bedded or lag gravels. It comprises 45.7 percent of the U.O.R.S. section. Abrupt and erosive basal contacts occur in approximately equal proportions. Pebble or mudstone intraclast lags are moderately developed or absent from erosional scours. Both multi-storied units and isolated sets are recognized; multi-storied units, however, are most common. Facies Slt resulted from dune migration in in and adjacent to channels.

Lateral observations in various portions of the U.O.R.S. section indicate that facies Gsm, facies Sglt and facies Slt may be intergradational. Facies Gsm and facies Slt are regarded as end members in this system. This relationship is particularly well developed in meter 285-290. Four cosets of facies Sglt in this interval were observed to grade into and out of facies Gsm. Above meter 290, a similar relationship is often developed between facies Sglt and facies Slt.

Sandy Large-scale Planar-Tabular Cross-bedded Facies (Slp). Facies Slp comprises a minor portion (3.5 percent) of the Tarbat Peninsula section (Figure 39). They are present as isolated structures in medium

to coarse-grained sands. The internal structure of one bed grades laterally from foresets with abrupt planar contacts to foresets with concave basal contacts. This suggests that facies Slp and facies Slt are also intergradational (Potter and Pettijohn, 1977). The minor occurrence of facies Slp suggests that transverse bars were not a predominant feature in the U.O.R.S. fluvial system.

Sandy Horizontal-laminated Facies (Sh). Horizontal laminations comprise 15.2 percent of the U.O.R.S. section (Figure 39). In 15 out of 28 deposits, thicknesses exceed or equal 0.6 meters. The maximum bed thickness is two meters. Bedded mudstone intraclasts are prevalent in two beds. The average bed thickness and the presence of 15 beds whose thickness exceeded 0.6 meters suggests that facies Sh may have resulted from deposition during upper flow regime conditions (McKee et al., 1967; Turnbridge, 1981). However, coarse-grained horizontal laminations could have also developed during low flow regime conditions (Harris et al., 1975). Perhaps horizontal laminations originated during varying flow regime conditions. Assuming this model, beds which are less than 0.6 meters, might have resulted from lower flow regime conditions.

Sandy, Medium-scale Trough Cross-bedded Facies (Smt). This facies (Figure 40) which comprises 9.8 percent of the U.O.R.S. section, consists predominately of coarse to medium-grained sands with minor amounts of bedded gravel. The majority of deposits are arranged in multi-storied cosets whose average thickness is 0.6 meters. Isolated units are poorly developed. Most basal contacts are abrupt; erosive bases occur in only three instances. Typically, the lateral continuity

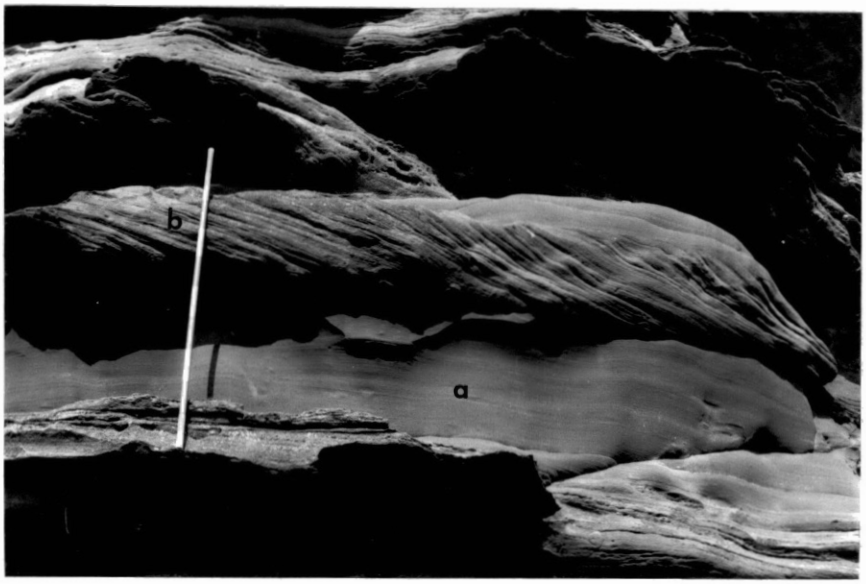

Figure 39. U.O.R.S. Facies Sh (a) and Facies Slp (b). (Foreset beds of facies Slp become concave laterally, suggesting a gradation to facies Slt. Photo at 295-296 m; staff length 5 ft.)

Figure 40. U.O.R.S. Facies Smt. (Photo at 262 m; hammer length 32 cm.)

of facies Smt is poor. This facies resulted from megaripple migration, often over larger bedforms.

Sandy Medium-scale Planar-Tabular Cross-bedded Facies (Smp). Only two occurrences of facies Smp were present in the U.O.R.S. section. It comprises 0.3 percent of the U.O.R.S., and is interpreted to result from small and isolated transverse bars (Cant and Walker, 1976).

Convolute-Bedded Facies (Cv). The convolute-bedded facies is usually associated with facies Sglt or facies Slt (Figure 34). Convolute bedding occurs 17 times and comprises 7.4 percent of the U.O.R.S. section. The maximum thickness of a single deformed bed is two meters. Deformation styles include buttock folds and upright to overturned folds (Figure 41). Upright folding, however, is predominant. Hence, distortions were primarily the result of sediment liquidization and development of negative gravity gradients produced by periods of rapid sedimentation (Allen, 1977).

Figure 41. U.O.R.S. Facies Cv. (Note well developed buttock folds (a) and intensely folded zone (b). (Photo at 283-284 m; staff length 5 ft.)

CHAPTER VI

DEPOSITIONAL HISTORY

Introduction

The Upper and Middle O.R.S. of the Cromarty District has been classified by Armstrong (1977) as the Balnagowan and Strath Rory Groups, respectively. Estimations of their total thicknesses are 1000 meters (Balnagowan Group) and 2800 meters (Strath Rory Group). In the study area, the U.O.R.S. is 139 meters thick and the M.O.R.S. is 378 meters thick. Armstrong (1977) indicates that the M.O.R.S.-U.O.R.S. contact is obscured by a fault. Elsewhere in the Orcadian Basin, this contact is either faulted or characterized by a pronounced unconformity (personal communication, R. N. Donovan, 1983). Numerous other minor faults are present throughout the study area. In all cases, the identification of similar stratigraphic horizons provides for a reasonably continuous section.

About 0.75 kilometers north of Ballone Castle, the regional dip reverses from northwest to southeast (Figure 2) and results in 137 meters of repeated section in the Ballone Castle region. At Rockfield, the M.O.R.S. section resumes its northwest dip orientation and again repeats 21 meters of section. For clarity, the M.O.R.S which is situated in the Ballone Castle and Rockfield areas, will be identified as the $M.O.R.S._2$ and $M.O.R.S._3$ sections, respectively. The symbol $M.O.R.S._1$

will be used to indicate the continuous section which begins 0.75 kilometers north of Ballone Castle.

The exposure throughout the study area is generally excellent. One exception is the M.O.R.S.$_2$ section, which is situated in the Ballone Castle foldbelt. Here the section was subjected to tectonic disturbances which, in places, seriously hampered observations. The M.O.R.S.$_3$ section is too small to develop meaningful facies relations. Hence, the primary M.O.R.S. interpretation will result from the M.O.R.S.$_1$ section. Subsequently, the M.O.R.S.$_2$ and M.O.R.S.$_3$ sections will be used for lateral facies comparisons.

Analysis and Interpretation

To examine a 519-meter thick section as one unit would severely limit the accuracy of the resulting interpretation. Hence, both the M.O.R.S. and U.O.R.S. are treated separately. Within each division, vertical sequences with similar facies elements are identified, described and interpreted. Markov analysis was used to help quantify these interpretations. A complete description of Markov analysis, the computer program used in this portion of the study, and the Markov tests which were conducted appears in Appendix C. A brief summary is as follows:

The first step in a Markov analysis is the generation of a frequency matrix; a two-dimensional array which records the number of facies transitions of each transition couplet in a stratigraphic sequence (Miall, 1973). The frequency matrix is then subjected to equations which result in observed and predicted probability matrices. A difference matrix results from the difference between the observed

and predicted probability matrices. Positive entries in the difference matrix indicate non-random transitions in the tested sequence. Negative entries or entries whose values are zero indicate random transitions in the tested sequence. Finally, each sequence is subjected to a chi-square test which indicates the presence or absence of the Markov property. All sequences tested within the Tarbat Peninsula section are Markovian to a 0.95 confidence level.

It is customary to generate facies relationship diagrams and idealized vertical profiles from principal non-random transitions. Notable examples which involved braided alluvium include work by Miall (1973) and Cant and Walker (1976). Interpretations are based on the accuracy of field observations and the subjective analysis of the difference matrix. Another complexity results from unexpected positive or negative values in the difference matrix; i.e., transitions with low frequencies could result in high non-random values. Because of these inconsistencies, interpretations resulting from Markov analysis must be approached cautiously. In this study, they were synthesized with subjective interpretations from which generalized vertical profiles were generated.

M.O.R.S. Depositional History

A facies relationship diagram for the total M.O.R.S. section appears in Figure 42. Facies code symbols used in this and other facies relationship diagrams result primarily from the symbols established in Chapter V. One exception is that medium-scale trough and planar-tabular cross bedding are combined and appear as facies Smx. Also, convolute bedding (Scv) was excluded from facies relationship diagrams

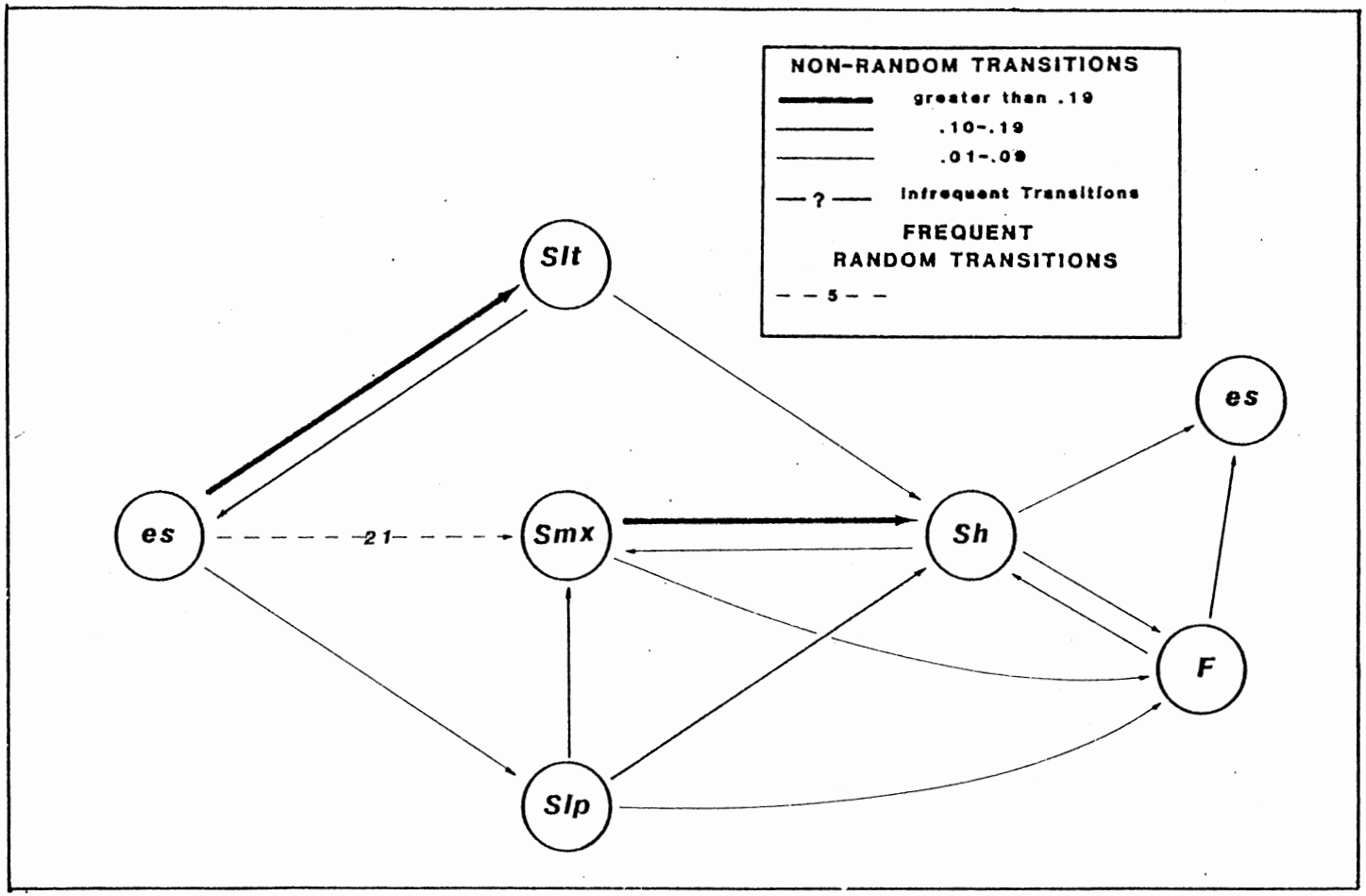

Figure 42. Facies Relationship Diagram, Total M.O.R.S. Section

and generalized vertical profiles because it is not a primary sedimentary structure.

The strongest transitions which appear in Figure 42 include facies es to Slt and Smx to Sh. Both transitions reflect high energy fluvial conditions. Other transitions include the ubiquity of associations with facies Sh and F. These resulted from stream flooding and various styles of vertical accretion. Two other notable transitions, facies es to facies Slp and Smx, record channel initiation during periods of reduced stream discharge. Because of the complexity and variability of individual M.O.R.S. sequences, the use of Figure 42 as a meaningful interpretative tool is imprecise. Certain sequences contain facies relationships which reflect strong fluvial conditions. Other sequences are characterized by facies relations which indicate reduced fluvial conditions. Hence, the M.O.R.S. section must be divided into sequences that are typlified by common facies relationships. Only then can a coherent interpretation for the entire M.O.R.S. section be elucidated.

The $M.O.R.S._1$ section was subjected to four separate Markov analyses which include the following sequences: meter 0-70, meter 70-153, meter 153-180, and meter 180-220. The nature of any one of these sequences formed in direct response to the magnitude and type of processes which acted upon them.

Processes. The processes which control the ultimate character of any stratigraphic succession are of an autocyclic or allocyclic nature. Autocyclic processes occur within the local depositional environment; i.e., the lateral migration of meander belts. Allocyclic controls are external to the local depositional environment; i.e., a regional

transgression inundating a lobate delta.

The primary autocyclic processes that affected the M.O.R.S. section were channel aggradation, channel re-occupation, vertical accretion on floodplains and stream floods. Common facies associated that are characteristic of channel aggradation are dunes (Slt) which are proceeded by erosional scours (es) on channel floors and followed by subordinate structures such as transverse bars (Slp) or megaripples (Smt). After aggradation, channels may have been dissected or avulsed to a new location. Eventually the channel may have been re-occupied, resulting from another period of avulsion.

Another process, vertical accretion on floodplains, was often intimately related to avulsion. Floodplain deposits are dominated by finely laminated very fine-grained sands and silts, and were most prominent laterally adjacent to the active braid tract. As channels avulsed, floodplain deposits migrated laterally over formerly active channels. However, this process was not consistently cyclic.

A minor autocyclic process might have been lateral accretion. In distal braided rivers, lateral accretion could be accomplished by systematic avulsion in one direction. Evidence to suggest that it was a significan process is lacking.

Horizontal laminations in medium to fine-grained sands comprise about 30 percent of the M.O.R.S. section. Out of 155 occurrences, 80 are equal to or exceed a thickness of two feet. The thickness and ubiquity of these deposits, the common presence of parting lineations on their surfaces and their associated sand grain sizes are all indicative of upper flow regime conditions (McKee et al., 1967); Harms et al., 1975). Hence, they document a pronounced flood effect in the M.O.R.S.

section.

In the study area, thick deposits of horizontal laminations are equally well developed during periods that were characterized by wet and dry climates. Turnbridge (1981) suggests that flood deposits that are dominated by horizontal laminations should be common in ancient and modern rivers which are affected by semi-arid conditions. The principal reason for flooding in recent semi-arid climates results from sparse vegetation, which enhances rapid runoff rates.

During the Devonian period, terrestrial vegetation was limited to coastal plains; upland areas were barren (Schumm, 1968a). Stream floods could have resulted from wet or dry climatic conditions. This interpretation is consistent with the ubiquity of flood deposits throughout the M.O.R.S. section. It also suggests that the principle of uniformity is not applicable throughout the geologic realm.

The two allocyclic controls which had a prominent effect on the M.O.R.S. section are 1) fluctuations in Orcadian Basin lake level, and 2) tectonic conditions which existed in the Caledonian sourceland during the Middle Devonian.

Large-scale fluctuations in water level are recognized in both ancient and modern lacustrine environments. During this century, Lake Chad has ranged from 10,000 to 25,000 square kilometers and reached sizes up to 300,000 square kilometers during the Pleistocene (Reading, 1980). The Orcadian Basin was subjected to the same type of water level fluctuations in the Middle Devonian. Lake levels reached a maximum extent of up to 50,000 square kilometers (Donovan, 1980). Paleomagnetic orientations reported by Habicht (1979) indicate that the Orcadian Basin was located in a low latitude geographic position during the

Devonian Period (Figure 43).

Donovan (1980) has developed a regional model for the Orcadian Basin which documents that stratigraphic, sedimentological, and faunal variations resulted from large-scale lake level fluctuations. The following discussion is partially adapted from this study.

The large-scale lake level fluctuations in the Orcadian Basin are thought to have commenced in response to climatic changes. Characteristic of wet periods were transgressing lakes and an eventual predominance of lacustrine conditions throughout much of the basin. The extent of lake level was reduced drastically during dry periods; hence, fluvial conditions became more pronounced.

The M.O.R.S. section within the study area resulted primarily from a fluvial system which flowed northward into Orcadian lakes. Its magnitude, at any instance, formed in direct response to the position of lake level. Discharge rates were reduced significantly during periods of low lake level. However, the lower base level which was characteristic of dry periods enhanced the erosive power of this fluvial system. High river velocities favored channels with markedly erosive bases which were associated with large-scale bedforms and poorly developed fine sequences.

As the climate became wetter, lake level began to rise. Initially, the effect of higher lake level was offset by increased river discharge rates. Hence, the erosive power of this fluvial system was maintained.

As lake level continued to rise, the power generated by increased discharge rates was offset by a significantly higher base level.

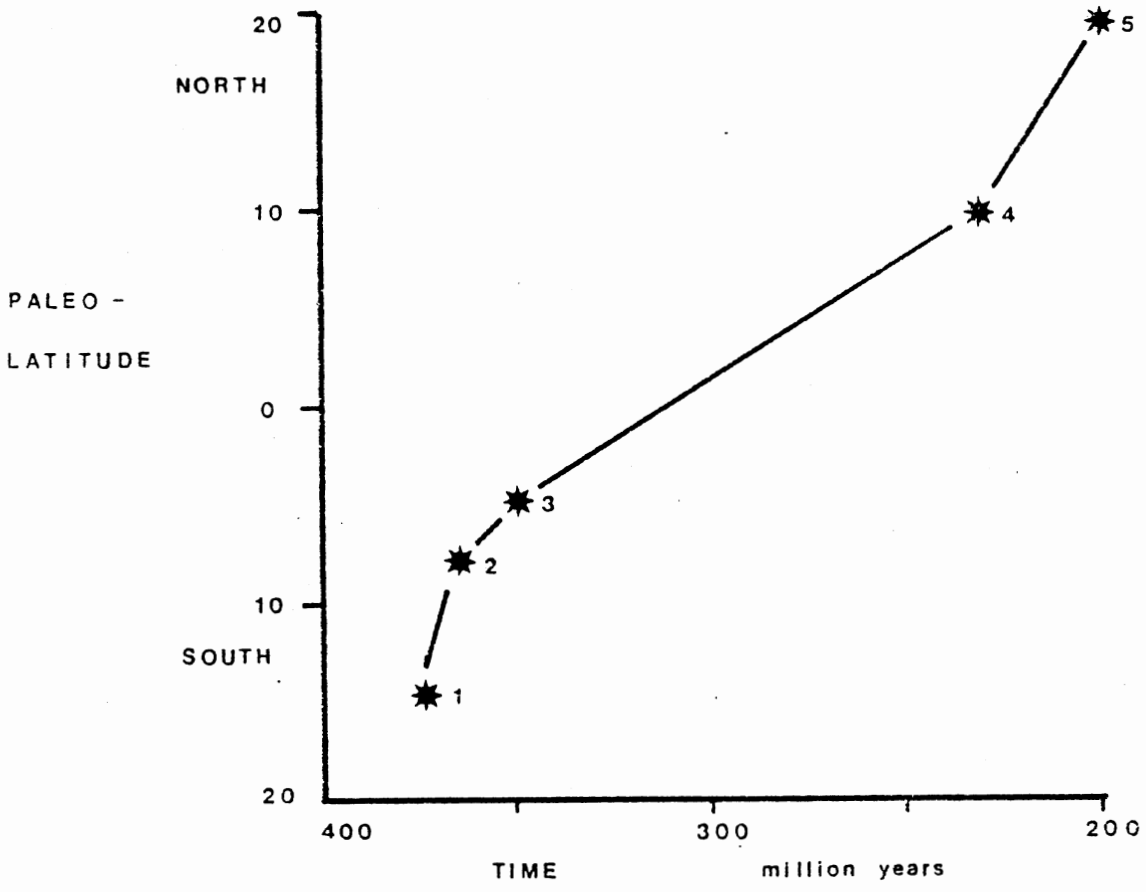

Figure 43. Probable Paleolatitude of the Moray Firth Area in Devonian to Triassic Times (data from Habicht, 1980). [1) Lower O.R.S.; 2) Middle O.R.S.; 3) Upper O.R.S.; 4) Lower Triassic; 5) Upper Triassic. From Donovan and Ferraro, 1982.]

Consequently, the river began to alluviate its valley. The development of channels and large-scale cross bedding became increasingly subordinate to floodplain and lacustrine sequences.

Lacustrine sequences in the study area rarely exceed one meter in thickness. This indicates that the main body of Orcadian lakes probably never reached the position of the Tarbat Peninsula during this period (Figure 44). The presence of small lakes was enhanced by high ground water tables, ample precipitation, and stream floods. Earlier in the Middle Devonian, large Orcadian lakes probably transgressed over the Moray Firth Area. This conclusion is substantiated by well developed Middle Devonian lake sequences which are present in the Moray Firth Area at stratigraphically inferior positons to deposits in the study area.

Isolated periods of Caledonian uplift during the Middle Devonian may have also affected the position of lake level in the Orcadian Basin. Depending on the erosional rate of the Caledonian sourceland and the subsidence rate in the Orcadian Basin, lake level could have risen, fallen, or maintained its position. If the rate of erosion exceeded the rate of subsidence, base level would have fallen in the area of maximum sediment progradation. Subsidence rates that were greater than erosion rates would have favored a fall in lake levels. Equal rates of erosion and subsidence would have resulted in maintenance of lake level.

The consistency of grain size of the M.O.R.S. within the study area suggests that the period was tectonically stable. Locally, a maintenance system characterized by equal rates of erosion and subsidence is postulated.

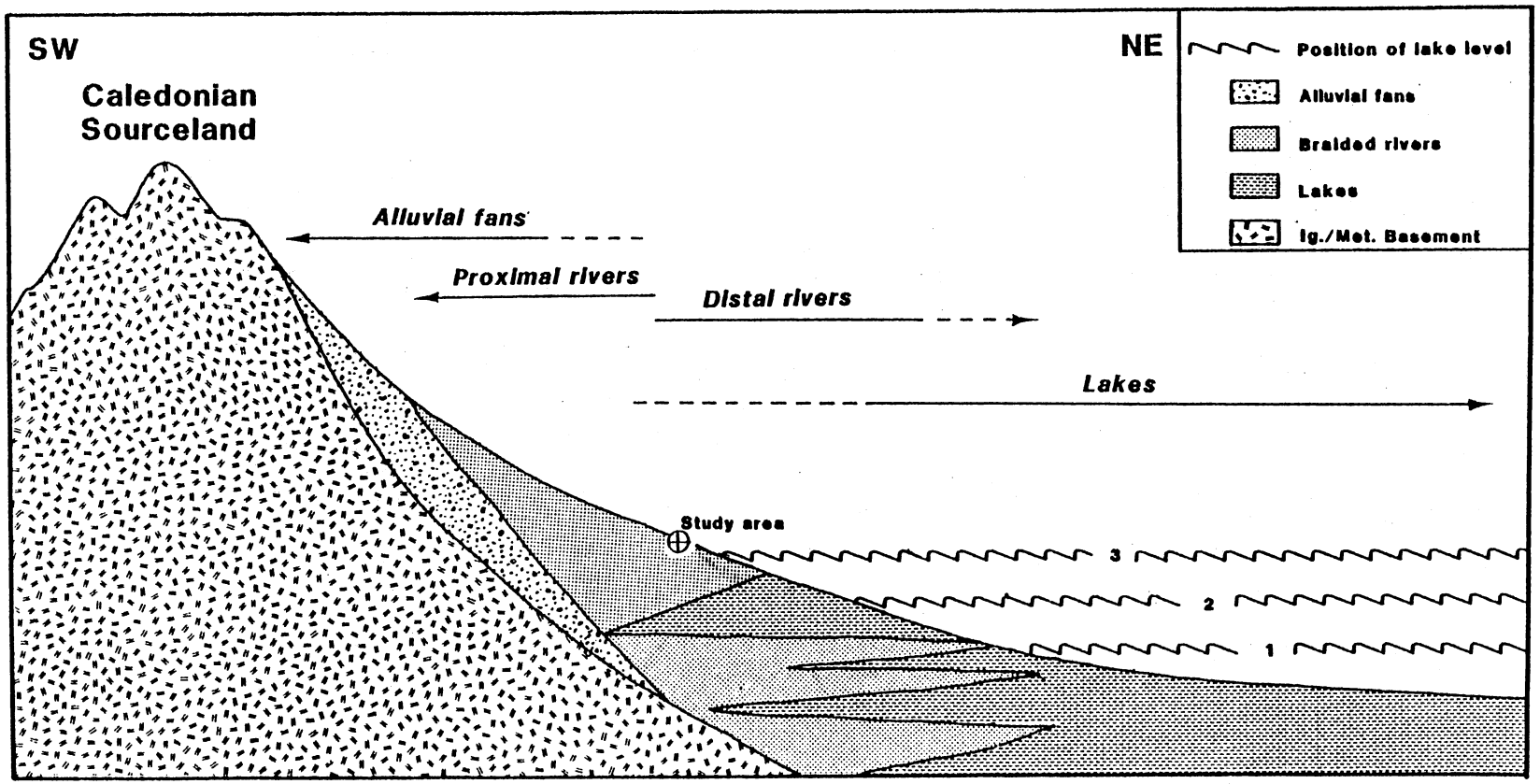

Figure 44. Schematic Diagram of the Principal Depositional Systems of the Middle Devonian Orcadian Basin. [Lateral Relations are approximate and are based partially on work by Donovan (1975, 1980) and Stephenson (1977). Position of lake level (1, 2, 3) may reflect water level variations during M.O.R.S. deposition in the study area.]

Process Application. The interaction of the allocyclic and autocyclic processes that affected the M.O.R.S. section produced complex sedimentological relationships. Most likely, allocyclic processes dominated autocyclic processes; i.e., lake transgressions resulted in reduced fluvial processes whereas lake regressions resulted in enhanced fluvial processes. It is evident that this fluvial system was in a constant state of disequilibrium. Abrupt, short-term changes in stream character resulted from flood events. Long-term changes were predominated by lake level fluctuations in the Orcadian Basin.

Even though the section is complex, certain pronounced relationships are obvious. Generalized vertical profiles (Figures 45-48) result from the subjective interpretation of the Markov analyses that were completed on the M.O.R.S.$_1$ section. These profiles record the most obvious facies relations in the portion of the M.O.R.S.$_1$ section from which they originated. They include the following intervals: meter 0-70, meter 70-153, meter 153-180, meter 180-220.

Heward (1978) defined a sequence as a series of related beds on the order of tens of meters thick, and a megasequence as a series of related sequences which are tens to hundreds of meters thick. These definitions will be maintained for this study. The term cycle will denote a series of facies packages that repeat within sequences.

With respect to the M.O.R.S., a megasequence is thought to record the passage from highest to lowest lake level; i.e., a lake regression. Two megasequences are identified in the M.O.R.S.$_1$ section. Cyclic processes were best developed during periods of moderate to low lake level. As lake level rose, the magnitude of stream processes and

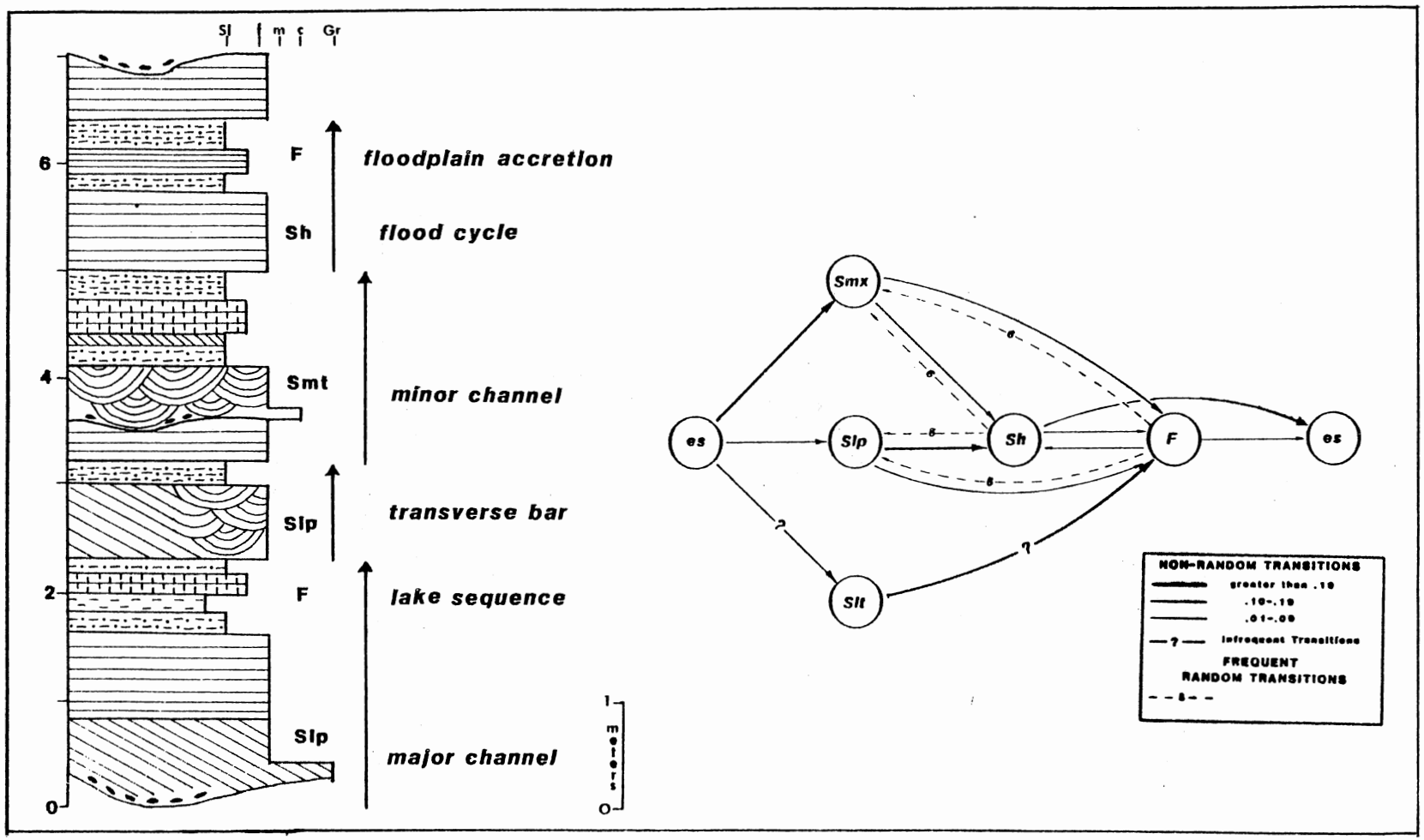

Figure 45. Generalized Vertical Profile and Facies Relationship Diagram, M.O.R.S.$_1$ Section, 0-70 m

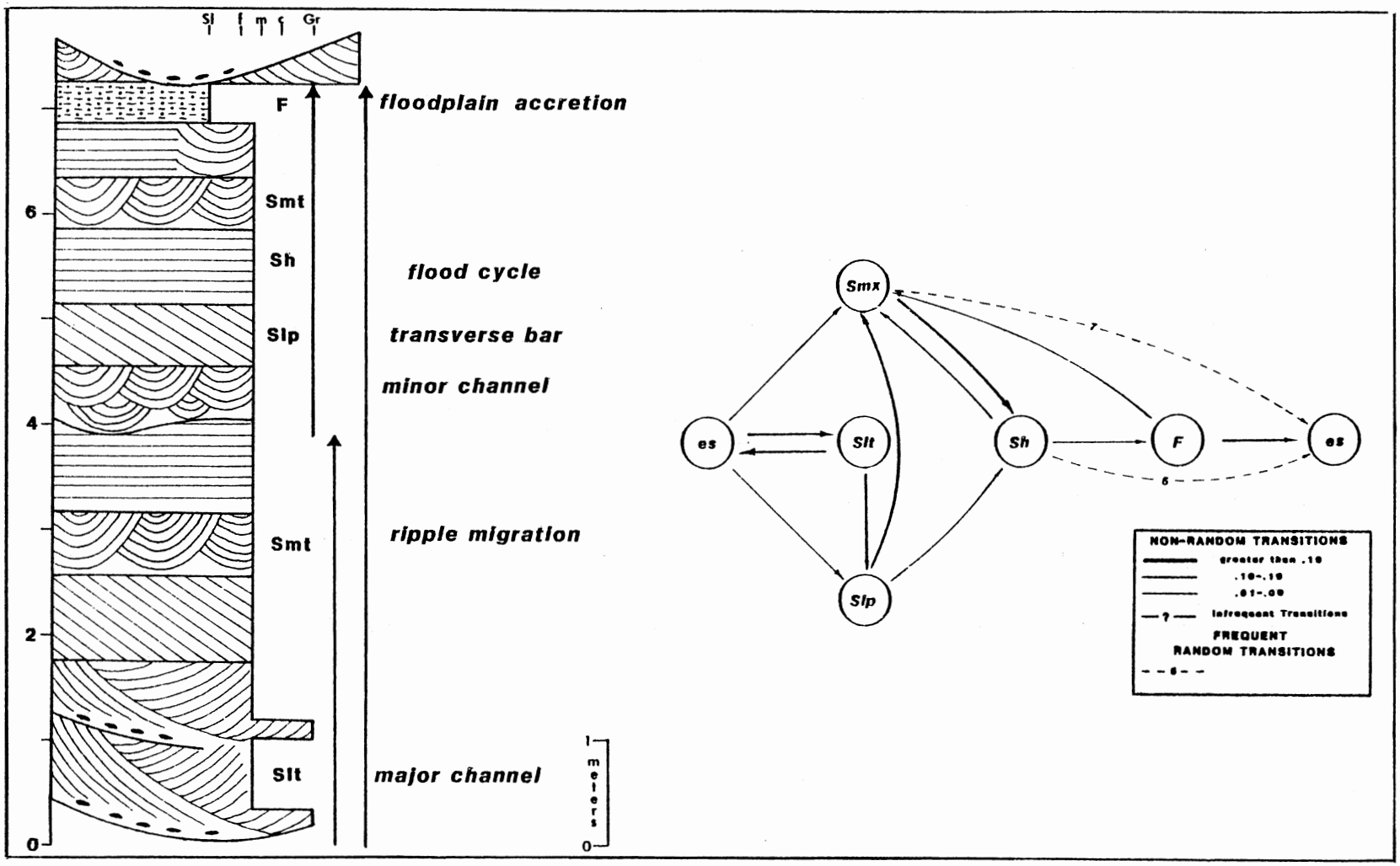

Figure 46. Generalized Vertical Profile and Facies Relationship Diagram, M.O.R.S.$_1$ 70-153 m

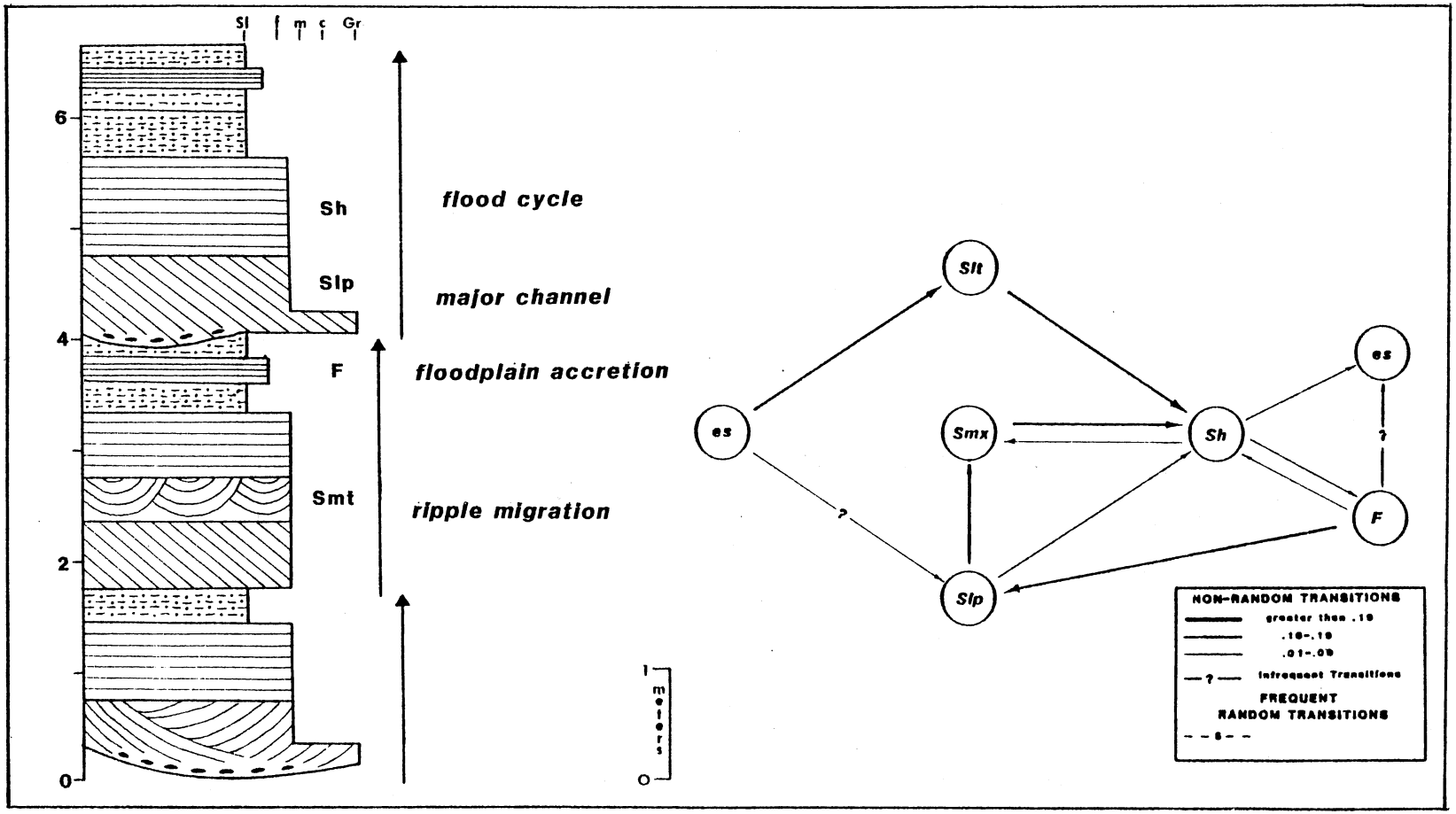

Figure 47. Gneralized Vertical Profile and Facies Relationship Diagram, M.O.R.S$_1$ Section, 153-180 m

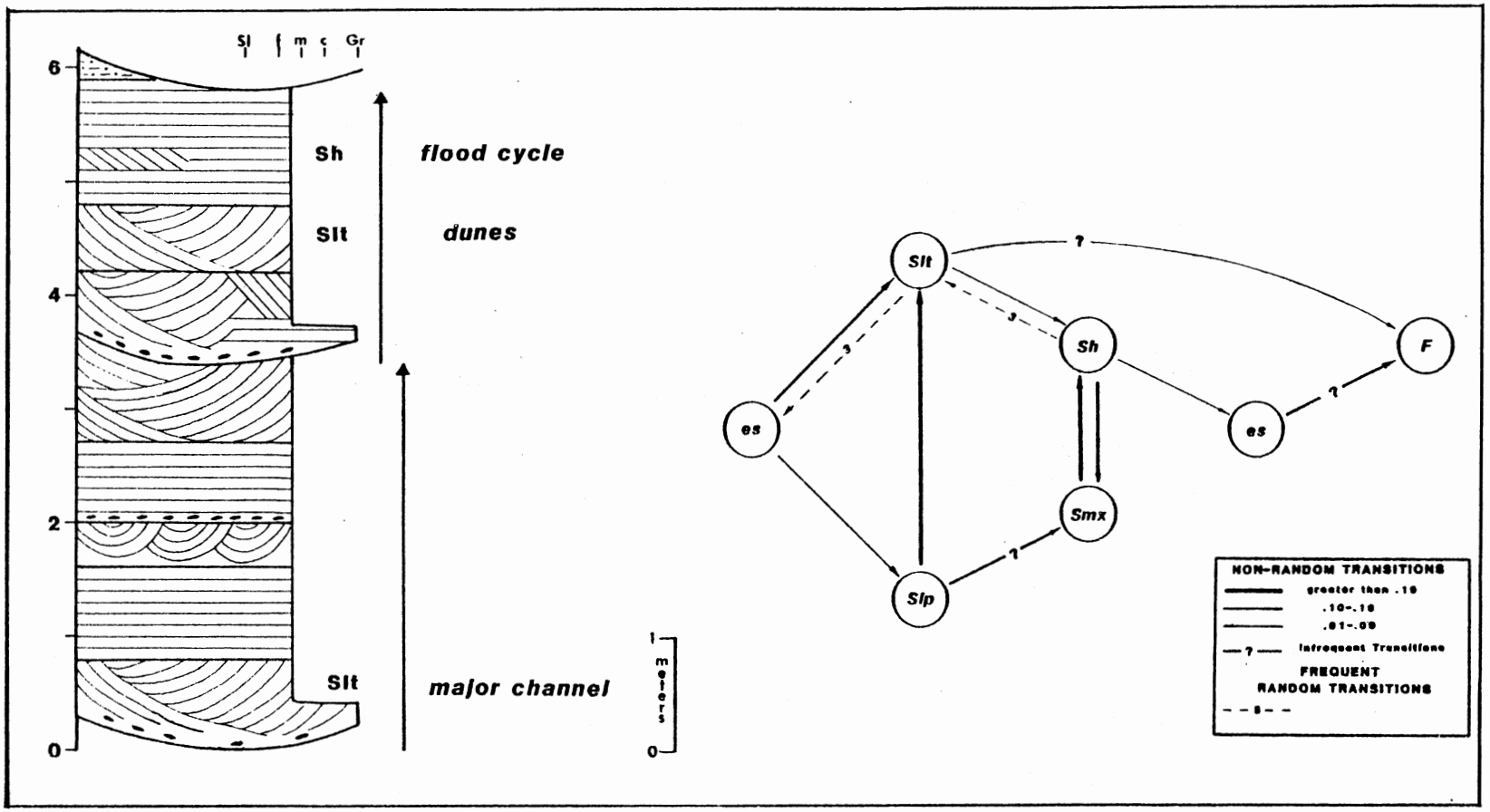

Figure 48. Generalized Vertical Profile and Facies Relationship Diagram, M.O.R.S.$_1$ Section, 180–220 m

cyclicity were reduced significantly.

Megasequences that are recognized in the M.O.R.S.$_1$ section are meter 0-153 and meter 153-220. Sequences which resulted from pronounced fluvial effects occur between meter 70-153 and meter 180-220. Sequences that were dominated by reduced fluvial effects occur between meter 0-70 and meter 153-180.

The fine facies comprise 19 percent of the meter 0-70 sequence. Lake sequences, whose thickness ranges from one to two meters, occur in three instances. Floodplain sequences are thinner but more numerous (23 occurrences) than lacustrine sequences. While the sandy lithotype remains prominent, its association with lower magnitude sedimentary structures (Slp, Smt, Smp) documents a period of reduced river competency. This fact is best exemplified by the association of erosive scours (es), whose depth of erosion is always less than one meter, with large-scale trough cross beds (Slt) in only two instances. Other erosive bases pass into large-scale planar-tabular cross beds (Slp) or medium-scale trough beds (Smt)(Figure 45).

Cycles, the passage of a sandy facies into a fine facies, are comprised of randomly arranged sedimentary structures and are usually no more than three meters thick. Common cycles include random arrangements of facies Slp, Smt, and Sh, which are possibly proceeded by erosional scours (es), and are consistently followed by lactustrine or floodplain deposits (Figure 45). These facies relationships record the movement of a sluggish fluvial system in which transverse bars (Slp) and megaripples (Smt) were constantly capped by fine deposits.

The relationship of stream flood deposits (Sh) to major floodplain deposits (F) is particularly notable. In one instance, a flood event

passed into well developed floodplain deposits. The nature of fine sequences which resulted from floods might have been controlled by their topographic location on the floodplain. Floods which inundated higher levels resulted in floodplain deposits. Floods inundating lower levels produced small lakes. The presence of lake limestones in thicker lake sequences suggests that their life span was at least seasonal (Donovan, 1975). Perhaps elevated water tables, which were characteristic of wet periods, provided additional water. Higher water tables might have also produced lake sequences which were not preceded by floods.

The poorly defined cyclicity throughout meter 0-70 and the predominance of lake and floodplain deposits with respect to other portions of the M.O.R.S. section record a long period of high Orcadian Basin lake level stance.

The sequence between meter 70-153 is characterized by eight cycles which were initiated by channels (Figure 46). Near the base of the sequence, cycles are capped by thin, laterally impersistent floodplain deposits which comprise only seven percent of this sequence. Between meter 90-120, fine deposits are absent. Evidence for lacustrine conditions is lacking throughout the sequence.

Major channel bases are larger in lateral and vertical extent than previously noted in meter 0-70. Three large-scale channels, whose thicknesses average about two meters, are preceded by erosional scours that downcut at least one meter. Facies Slt is commonly multi-storied above channel bases. Erosive scours (es), present above the channel floor, are also common within this facies.

As vertical aggradation continued, the discharge within channels began to decrease. At this point, transverse bars (Slp) which were

often followed by megaripples (Smt) became more prominent (Figure 46). As aggradation continued, channels either dissected or avulsed to a new position within the active braid tract. Perhaps the continuing persistence of flooding favored avulsion. Eventually, another period of avulsion resulted in channel re-occupation.

This sequence records an initial fall in Orcadian Basin lake level. However, the presence of another sequence that documents a period of high lake level (meter 153-180) indicates that the climate again became moist. During the early period of this wet interlude, the strong cyclic nature of meter 70-153 was maintained.

Beginning at meter 153, thin siltstone deposits again became prominent. Initially, their occurrence is random. However, between meter 165-180, they comprise about 50 percent of this sequence. With the exception of the absence of lacustrine deposits, meter 153-180 is similar to meter 0-70 (Figure 47).

Short discontinuous cycles are characteristic of this sequence. Dunes (Slt) are completely absent between meter 166-180. As previously noted, in meter 0-70 flood events (Sh) often pass into floodplain deposits. In one instance, horizontally laminated beds are separated from a floodplain deposit by large-scale planar-tabular cross beds. Perhaps the relationship resulted from progressively decreasing energy conditions. A similar cycle has been reported by McKee et al. (1967) in the flood dominated Bijou Creek of eastern Colorado.

This sequence records the second maximum rise of Orcadian Basin lake level. In comparison to meter 0-70, the absence of lacustrine units and thinness of this sequence reflect a short-lived transgression or a transgression which did not reach the extent of the first rise in lake

level. Perhaps both factors influenced the character of this sequence.

Only one instance of finely laminated siltstones occurs in the final 40 meters (180-220) of the M.O.R.S. section. Erosive channel bases (es) in association with large-scale trough cross beds (Slt) are once again prominent. As previously noted in meter 70-153, these units are commonly multi-storied (Figure 48). Cycles between meter 180-220 are thinner and not nearly as consistent as in meter 70-153.

This sequence records the final fall in Orcadian Basin lake level during the Middle Devonian and perhaps heralds the semi-arid conditions that persisted throughout the Upper Devonian. However, the faulted nature of the M.O.R.S.-U.O.R.S. contact prevents documentation of this conclusion.

Lateral Facies Relations. Comparison of the M.O.R.S.$_1$ section to its lateral equivalents, the M.O.R.S$_2$ section (Ballone Castle area) documents the complexity of facies relations of Middle Devonian units within the study area. While similarities do exist, these sections are not entirely correlatable.

The prominence of facies Slt and Sh (21 and 23 percent of the section, respectively) in the first 70 meters of the M.O.R.S$_2$ section are suggestive of stronger fluvial processes than those of the same interval in the M.O.R.S.$_1$ section. However, cyclicity in this portion of the section remains poorly developed. Cycles commonly contain facies of the sandy lithotype which are randomly arranged and capped by thin siltstone deposits. Lacustrine units are absent. It is suggested that this sequence was more proximal to the active braid tract than the same interval in the M.O.R.S.$_1$ section.

Fluvial processes were strong during the remaining period of deposition of the M.O.R.S.$_2$ section. This conclusion is substantiated by a predominance of multi-storied accumulations of facies Slt, numerous erosive scours which often precede facies Slt, and thick accumulations of facies Sh which resulted from flood events. The domination of similar facies associations in the laterally equivalent M.O.R.S.$_3$ section lends further credence to this conclusion. However, the presence of lacustrine and floodplain deposits which comprise 10 percent of the remaining portion of the M.O.R.S.$_2$ section is unusual. Particularly thick accumulations of these fine deposits are often preceded by sandy horizontal laminations with thicknesses of up to two meters. It is suggested that the relatively high percentage of fine deposits resulted from flood events that enhanced rapid lateral facies variations.

The irregularities of the lateral facies variations in the M.O.R.S.$_2$ and M.O.R.S$_3$ sections do not preclude the interpretations developed from the M.O.R.S.$_1$ section. Rather, such complexities should be expected from braided river deposits that were affected by two or more processes (Miall, 1977).

U.O.R.S. Depositional History

Prior to the beginning of U.O.R.S. deposition, a period of tectonism is recognized throughout much of Great Britain (Waterson, 1970). This is best exemplified in the Midland Valley of central Scotland, where large accumulations of U.O.R.S. fluvial deposits resulted from vertical offsets of up to 10,000 feet along the Highland Boundary fault (Allan, 1940; Simon and Bluck, 1982).

To the north in the Orcadian Basin, the relation between uplift

and the initiation of U.O.R.S. deposition is unclear. With the exception of the island of Hoy where basal U.O.R.S. tuffaceous sandstones interdigitate with volcanic tuffs, a pre-Upper Devonian disturbance has not been recognized (House et al., 1977). Throughout the Orcadian Basin, the U.O.R.S.-M.O.R.S. contact is faulted or lies on covered ground (personal communication R. N. Donovan, 1983).

Upper Devonian sedimentation in the Orcadian Basin is entirely fluvial. In part, this reflects the breakdown of the Orcadian Basin as a lacustrine-dominated entity which resulted from the semi-arid conditions that persisted throughout this area during the Upper Devonian (Donovan and Ferraro, 1982). However, the indirect effect of a pre-Upper Devonian disturbance remains plausable.

Along the Tarbat Peninsula, the U.O.R.S. is comprised of coarse-grained sands with moderate amounts of medium-grained sand and gravel. The thickness of individual beds averages about one meter. Isolated bed thicknesses of up to two meters are not atypical. The U.O.R.S. is dominated by large-scale trough cross bedding (60 percent); i.e., facies Slt and Sglt. All major facies elements, grain size, bed thickness, and sedimentary structures, indicate that U.O.R.S. deposits were more proximal than M.O.R.S. deposits.

The U.O.R.S. section is divided into three sequences, meter 220-261, meter 261-290, and meter 290-359. Generalized vertical profiles (Figures 50-52) document cyclic variations which occur, upsection, in each sequence. Between meter 220-261, the sequence is dominated by medium-grained sand. The sequence between meter 261-290 coarsens upward from coarse sands at the base to matrix supported gravels near the top. While isolated gravel deposits occur between meter 290-359,

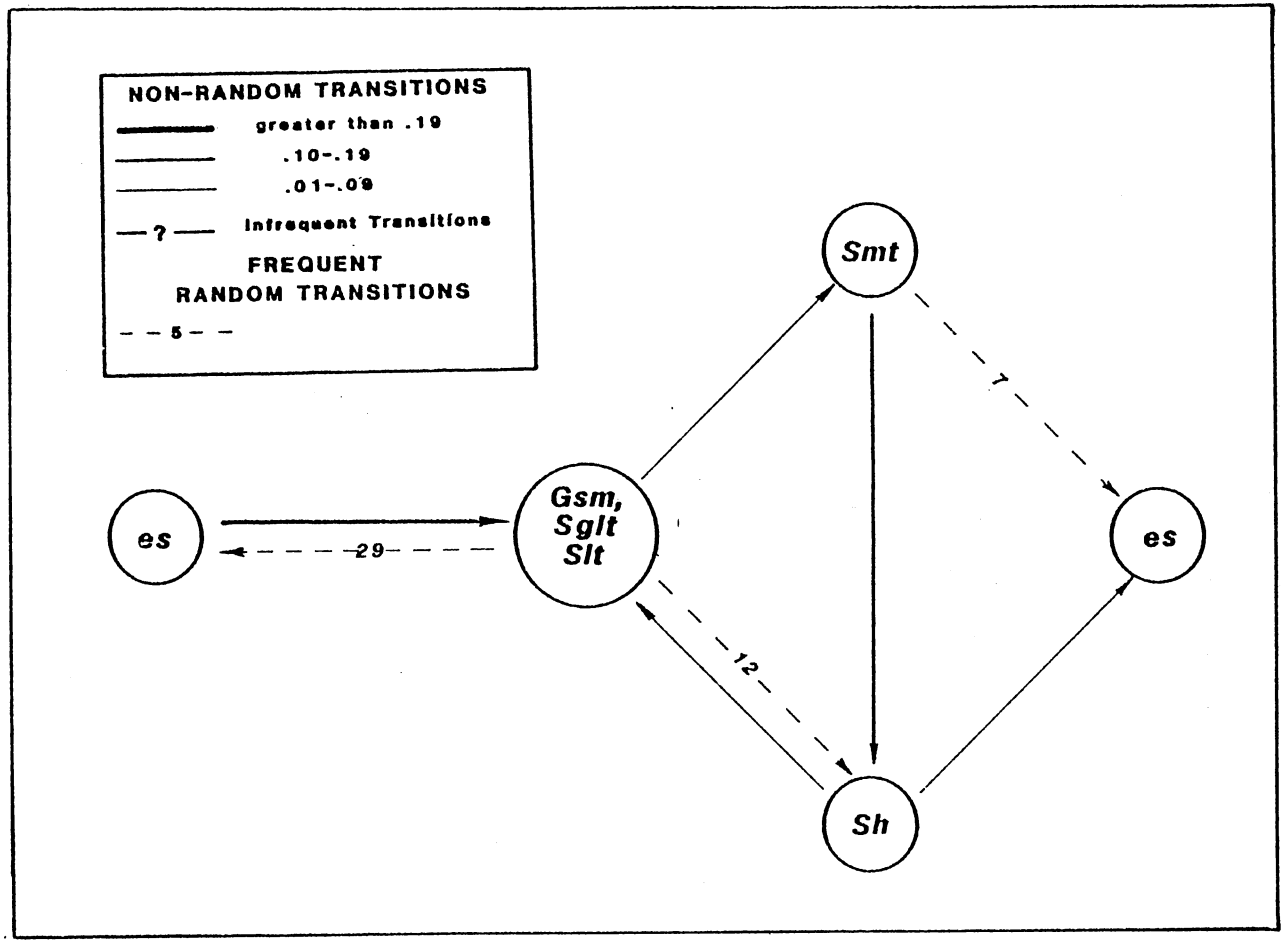

Figure 49. Facies Relationship Diagram, U.O.R.S. Section

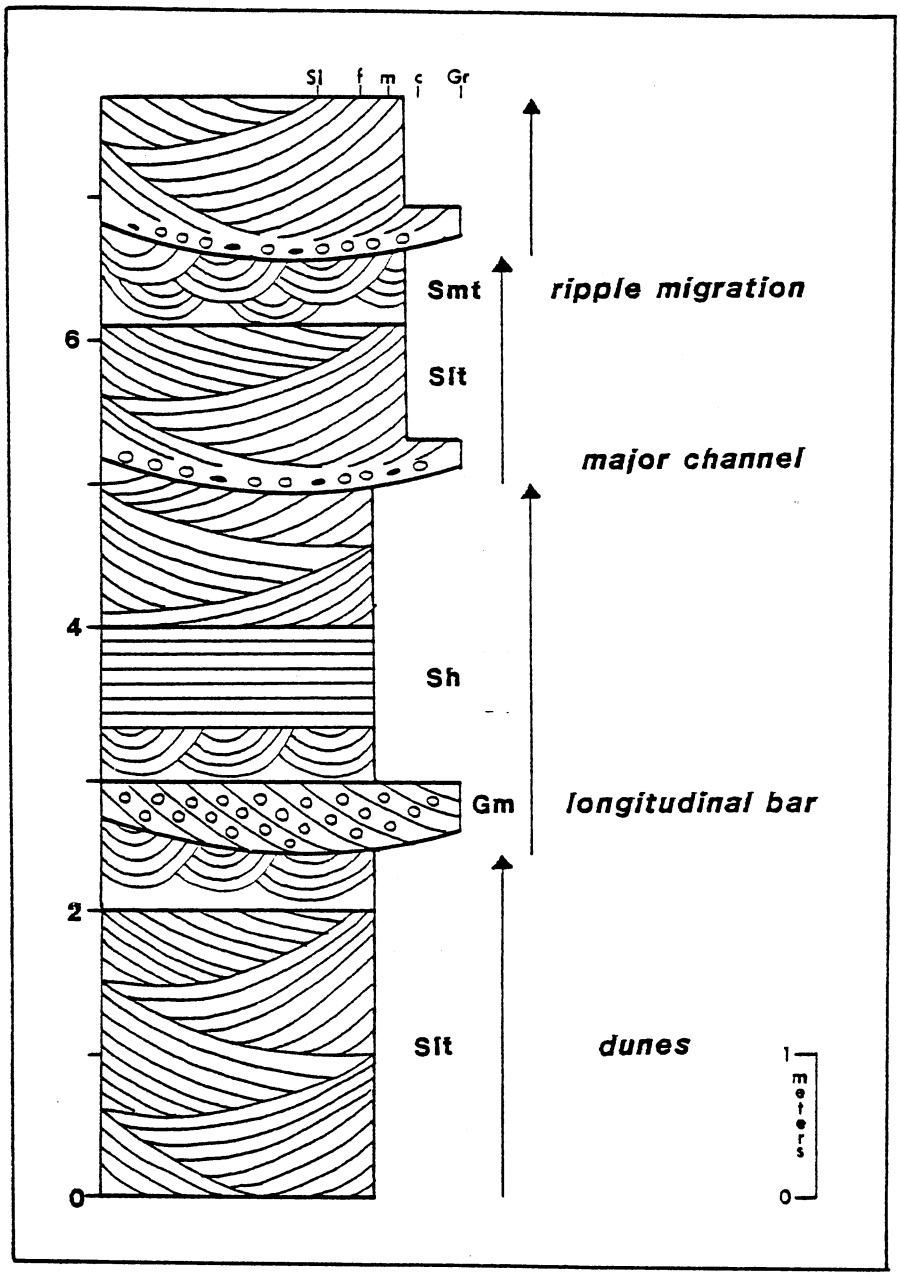

Figure 50. Generalized Vertical Profile, U.O.R.S. Section, 220-261 m

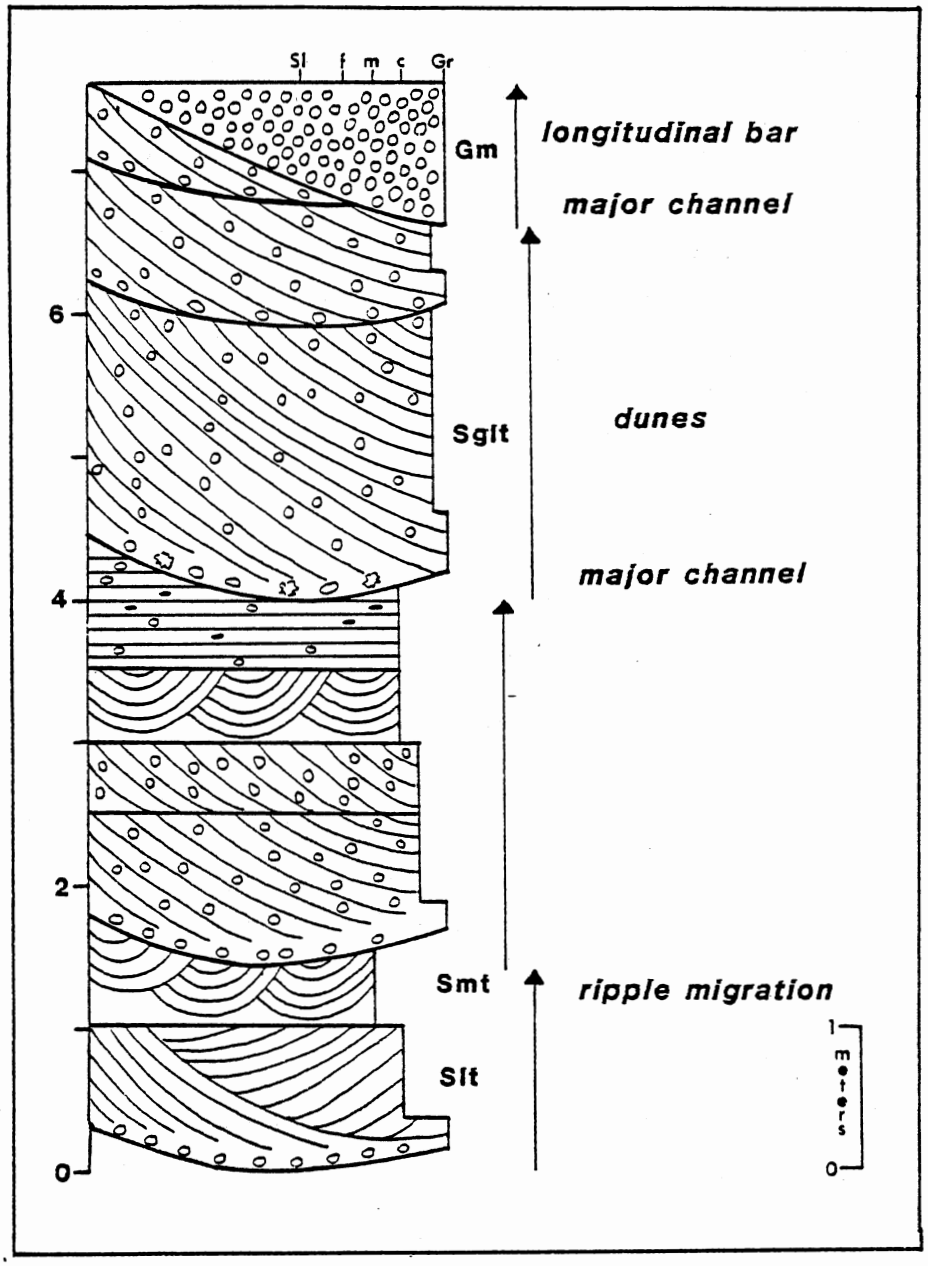

Figure 51. Generalized Vertical Profile, U.O.R.S. Section, 261-290 m

a coarsening upward sequence is not recognized.

Crude fining upward cycles are present throughout the section. However, these cycles are not associated with a decrease in the hierarchy of sedimentary structures upsection. Commonly, gravel deposits at the base of cycles and coarse sand deposits at the top of cycles both contain large-scale trough cross beds. The crude nature of these cycles further documents a braided fluvial origin for the U.O.R.S. section.

One Markov analysis (Figure 49) on the whole U.O.R.S. section was sufficient to develop an accurate interpretation. Medium and large-scale planar-tabular cross bedding was eliminated from this analysis on the grounds that they are insignificant, and therefore not representative of the section. As in the M.O.R.S. section, convolute bedding was not considered. Facies Slt, Sglt and Gsm appear as one transition. However, these facies are treated separately, according to their ubiquity in any portion of the section.

The base of the U.O.R.S. section, following the M.O.R.S.-U.O.R.S. faulted contact begins at meter 261. As previously noted, the sequence is dominated by medium-grained sands; however, minor bedded and lag gravels become more prominent near the top of the sequence. Multi-storied units of large-scale trough cross beds are predominant throughout the section. The first incoming of gravel at meter 231 is comprised of two thin beds with markedly erosive scours that continue laterally for about 100 meters. Other isolated gravel deposits are impersistent laterally.

Cycles within this sequence are comprised of facies Slt, which is most commonly preceded by erosive scours and followed by facies Smt

(Figure 50). This relationship resulted from the migration of in-channel dunes (Slt) which often passed into megaripples (Smt) as channel aggradation continued. The presence of two thin but laterally persistent gravel deposits records the first appearance of longitudinal bars. The lack of large-scale planar-tabular cross beds in this and other portions of the U.O.R.S. section suggests that large-scale bedforms were typically sub-areal in this fluvial system. Hence, the U.O.R.S. fluvial system must have been of a deeper and wider extent than the M.O.R.S. fluvial system.

Initially, the sequence between meter 261-290 is dominated by large-scale trough cross beds (Slt) in coarse sands with minor amounts of gravel (Figure 51). Beds generally are thin and merge into other cross-stratified units within ten meters. Vertical stacking of facies Slt is also common within this interval. These relationships suggest that the fluvial system was dominated by large-scale bedforms, probably dunes, which migrated in wide and stable channels.

Gravels, supported in coarse sand matrices, increase in prominence between meter 280-290. Initially, deposits are comprised of 10-15 percent gravels. Deposits near the top of this interval contain up to 50 percent gravel. Bed thicknesses usually exceed one meter. Well developed convolute zones with buttock or upright folds are common. One such unit, about two meters thick, shows strong lateral persistence.

Unlike the first part of this sequence (meter 280-290), beds may persist up to 100 meters laterally. In four units, facies Slgt grades into and out of facies Gsm. Basal contacts within any unit are both erosive and abrupt. Only one deposit, a massive gravelly bed up to three meters thick, is consistently erosional.

All facies relationships indicate that the U.O.R.S. fluvial system reached its greatest proportions during deposition of meter 280-290. The lateral persistence of beds within this interval is indicative of rapid sedimentation rates. In particular, the changing nature of basal contacts suggests that the fluvial system was subject to sediment pulses which were not localized to channels but rather spread in a sheet-like fashion within the active braid tract. Perhaps this event records the maximum lowering of Orcadian Basin base level or a localized response to a tectonic disturbance in the Caledonian sourceland.

Coarse-grained sands predominate the final U.O.R.S. sequence, meter 290-359. Medium-grained sands occur in minor to moderate amounts. Gravelly deposits are most common between meter 306-330. Within this interval, four fining upward cycles whose thicknesses range between two and six meters are recognized. Thin fining upward cycles (one to two meters in thickness) dominate the last 20 meters of the U.O.R.S. section.

Initially, the sequence is characterized by the presence of facies Sh and Slt with minor amounts of facies Smt (Figure 52). Sandy horizontal laminations occur in deposits which range between one to two meters in thickness. Also, this facies commonly contains bedded mudstone intraclasts. These relationships indicate that stream processes remained strong during their period of deposition and that a return to stream flooding might have again become prominent.

The fining upward cycles between meter 306-330 are floored by erosive scours followed by facies Sglt. Multi-storied units of facies Slt are most common above the former units. However, facies Sglt and Slt may be separated by randomized occurrences of facies Sh (Figure 52).

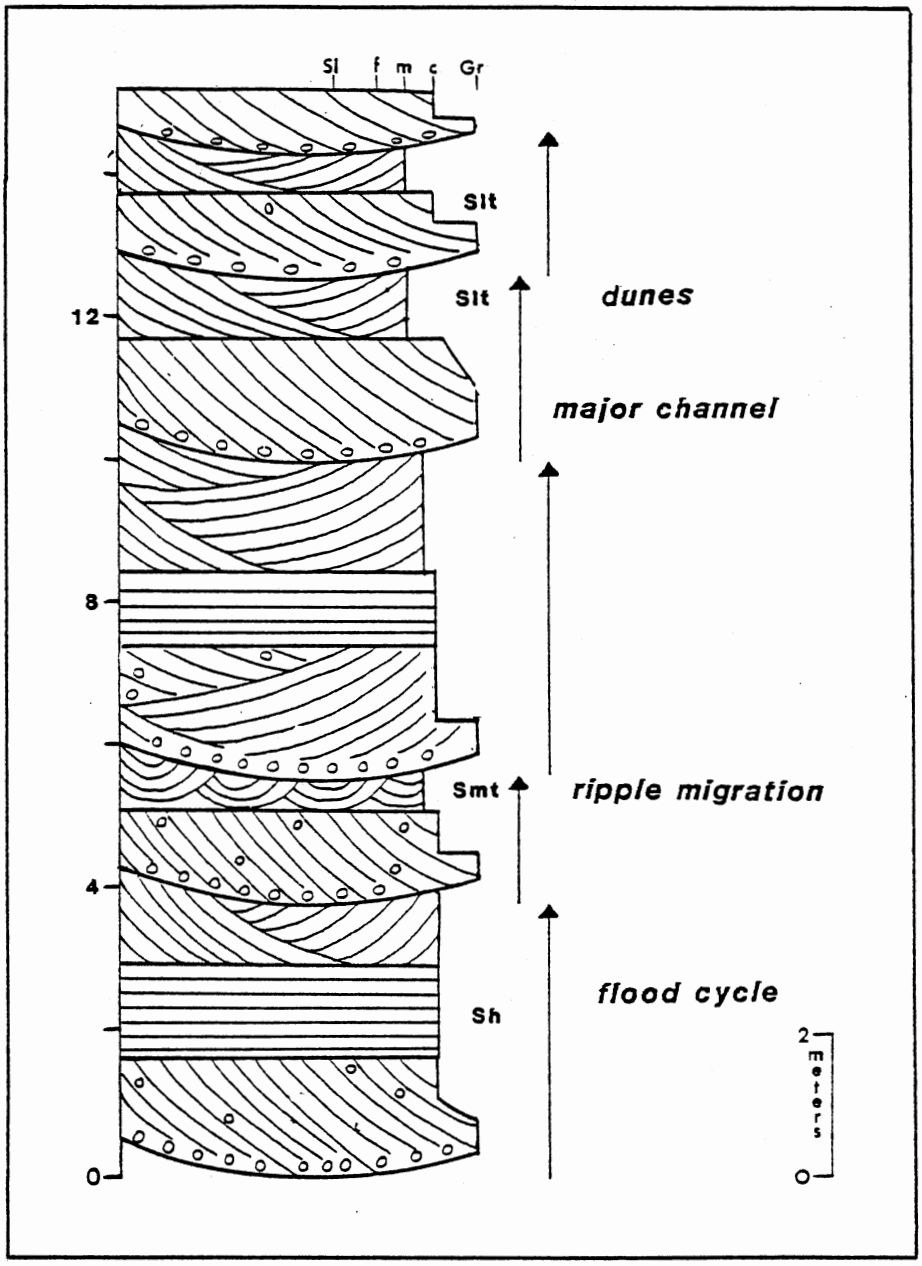

Figure 52. Generalized Vertical Profile, U.O.R.S. Section, 290-359 m

The observed facies relationships in this portion of the section resulted from vertical accretion within channels which were, on occasion, affected by stream floods.

The final portion of the U.O.R.S. section (meter 340-359) is comprised completely of facies Slt. Vertically, the sequence is characterized by coarse-grained and slightly gravelly beds which are typically preceded by erosive scours and followed by medium-grained beds. Both coarse and medium-grained deposits show little lateral persistence. The vertical and lateral consistency of these deposits documents the stability of the fluvial system throughout the period of their deposition. Reconnaissance work conducted above meter 359 indicates that this facies relationship is prominent for at least 140 meters above the end of the section.

CHAPTER VII

PALEOCURRENTS

Introduction

Sorby (1859) was the first to recognize the value of sedimentary structures as meaningful paleocurrent indicators. However, sedimentology studies which integrate paleocurrent data have become prominent only within the last 20 years (Potter and Pettijohn, 1977).

Sedimentary structures that are useful in paleocurrent studies are classified as "directionals" or "vectors." A directional structure does not indicate the sense of flow; e.g., parting lineations, glacial striations, etc. A vector indicates both the sense and direction of flow; e.g., trough cross-bedding axes, flute marks.

The size of sedimentary structures is an important factor in paleocurrent analysis. Large bedforms originate in areas of higher river discharge, and hence are indicative of the mean direction of paleoflow. Smaller bedforms result in areas of reduced discharge and are consequently less representative of the mean direction of paleoflow (Allen, 1966; Miall, 1974).

Cross-bedding is the most commonly used bedform in paleocurrent studies of fluvial systems. Of the two major types, planar and trough cross-beds, the latter have yielded the most consistently accurate data (Dott, 1973; Miall, 1977). In braided rivers, planar-tabular cross-beds

result from the migration of transverse bars, commonly oblique to the mean flow direction (Smith, 1970; Asquith and Cramer, 1975). Thus their orientation may differ markedly from the mean flow direction.

Discussion

The Von Mises distribution, originated by Von Mises (1918), was used for the paleocurrent analysis in this study. The computer program employed in this analysis was written by D. J. Sanderson. This program, together with individual paleocurrent tests, is given in Appendix D.

The Von Mises distribution is a circular normal distribution which computes the vector mean, resultant vector, and the dispersion parameter (Sanderson, 1973). The vector mean is given by the equation

$$\bar{\Theta} = \tan^{-1}\left(\frac{\sum_{i=1}^{N} \sin \Theta_1}{\sum_{i=1}^{N} \cos \Theta_1}\right) \tag{7.1}$$

To properly evaluate the accuracy of the vector mean as a meaningful indicator of paleoflow, the dispersion of individual readings must be considered. The dispersion parameter

$$\frac{R}{N} = \frac{\left[\left(\sum_{i=1}^{N} \cos \Theta_i\right)^2 + \left(\sum_{i=1}^{N} \sin \Theta_i\right)^2\right]^{\frac{1}{2}}}{N} \tag{7.2}$$

where R is the resultant vector and N is the number of readings, provides a useful check for uniformity. The vector mean is considered uniform if the dispersion parameter exceeds the critical value of the Rayleigh test as given by Mardia (1972; Appendix 2.5). In all

paleocurrent tests considered in this study, the dispersion parameter exceeded the critical value to a 0.95 confidence level.

Trough cross-beds, which are prominent throughout the study area, provided a superior method of determining the direction of paleoflow. Most trough axes readings were derived from medium-scale troughs because they are more completely preserved than large-scale troughs. However, in all instances, readings from both sizes of cross-bedding are compatible in their vector means and dispersion.

When structural dip exceeded 20 degrees, paleocurrent readings were rotated to horizontal using a Lambert equal area stereonet. Commonly this rotation resulted in only a 4-5 degree change in azimuth. However, in certain instances azimuths were completely reversed during rotations. This reversal resulted because trough axes were measured on the subhorizontal surface of climbing bed forms of various proportions, whose depositional dip was oriented upstream (personal communication, R. N. Donovan, 1983). Thus, when stereonet rotations resulted in azimuth reversals of this type, the non-corrected paleocurrent azimuth was used.

Middle Devonian river systems in the Moray Firth area flowed northeastward into the Orcadian Basin (Donovan, 1983) (Figure 53). This conclusion is supported by cumulative paleocurrent data obtained from the M.O.R.S. in the study area (Figure 54). Vector means of the medium and large-scale troughs (044), parting lineations (051-231), and small-scale troughs (077), all document a northeastward flowing river system. A similar trend (vector mean 052) has been established from trough readings collected in M.O.R.S. strata several kilometers south of Rockfield (Figure 55).

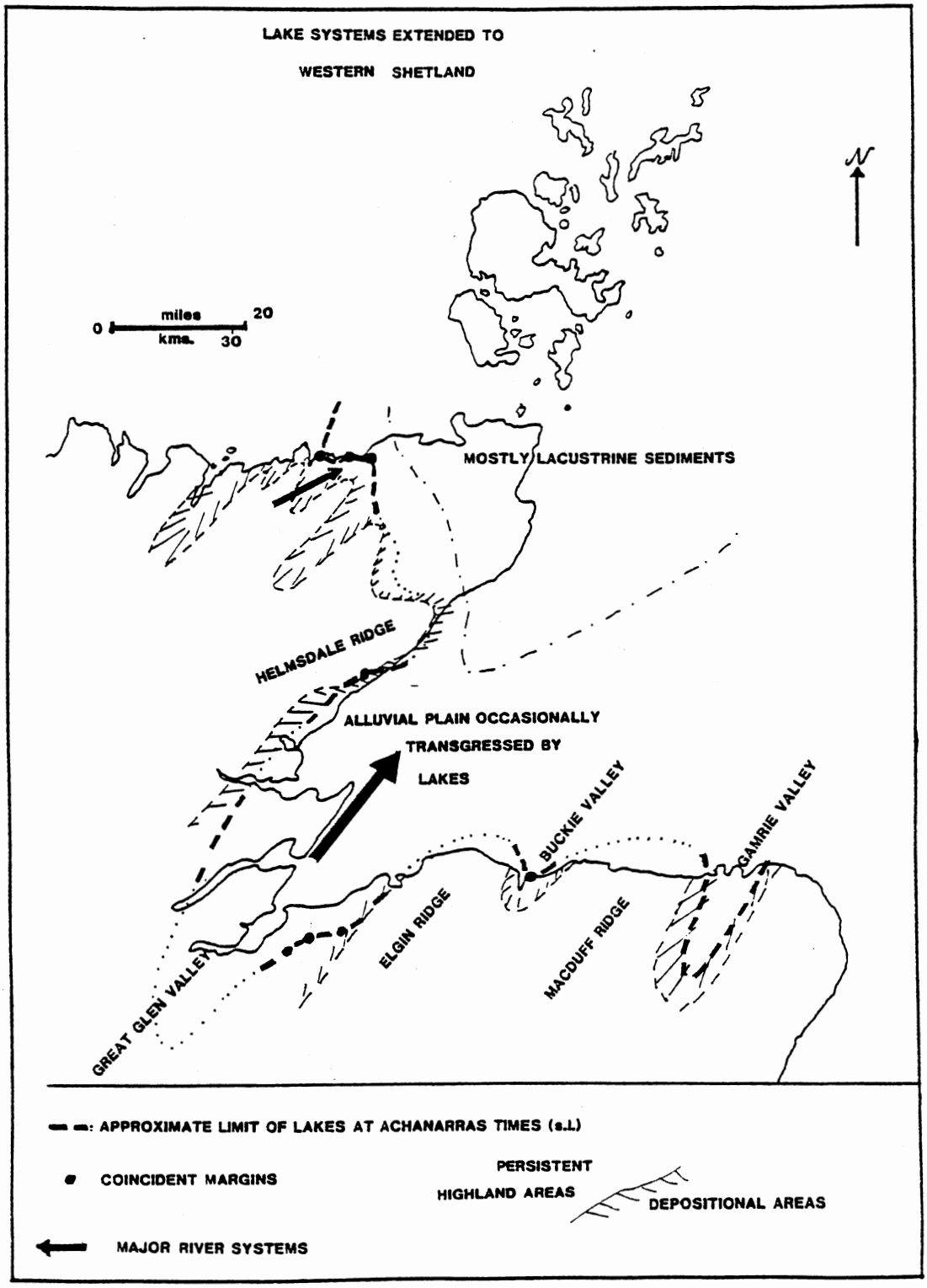

Figure 53. Paleogeography and Facies Variation in Middle O.R.S. Deposits (from Donovan, 1983)

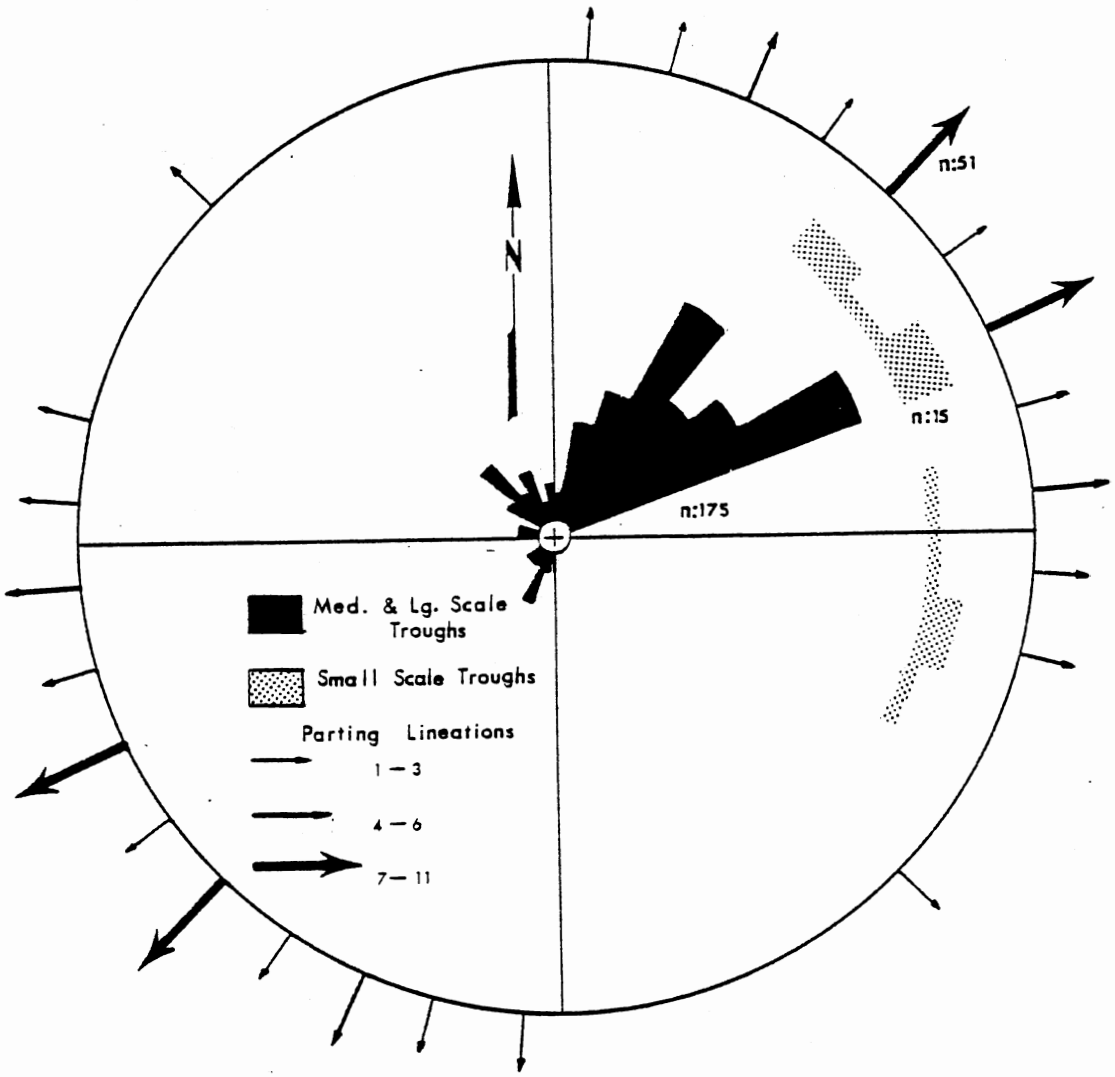

Figure 54. Cumulative Paleocurrent Data of the M.O.R.S. in the Study Area. (Data collected by R. N. Donovan and the author.)

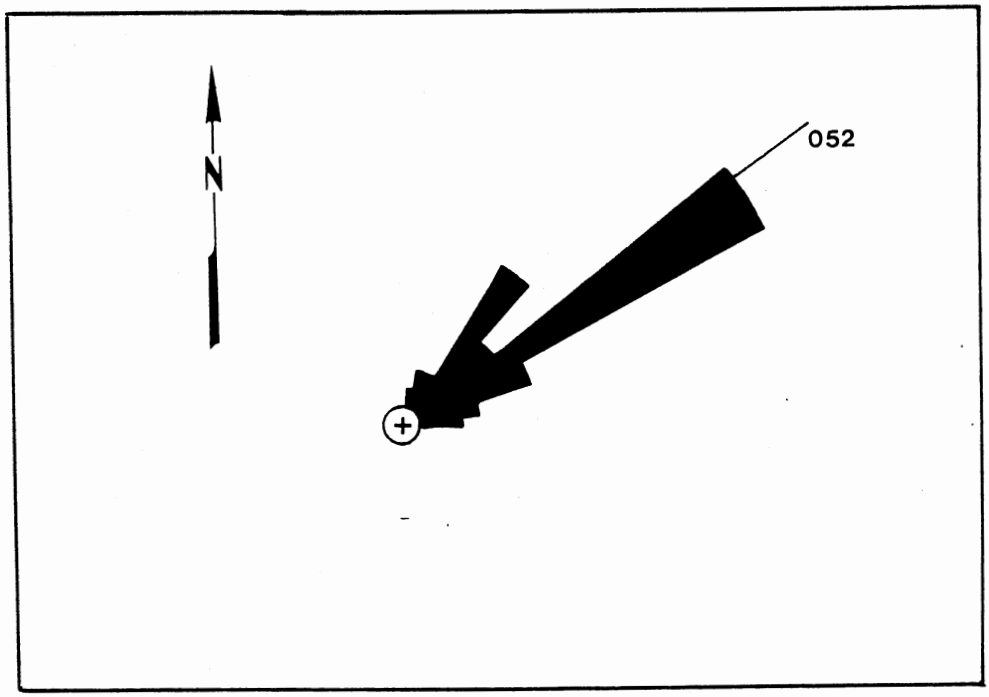

Figure 55. M.O.R.S. Trough Axes, 3 km South of Rockfield. ($\bar{\theta}$ = 052, R = 67.66, N = 69, R/N = 0.97; data collected by R. N. Donovan). (This section is stratigraphically lower than that analyzed in the study area.)

The northeast to southwest orientation of the Orcadian Basin originated from a Caledonian structural inheritance (Leeder, 1982). The principal M.O.R.S. Caledonian sourceland for the study area was probably located in the Grampian Highlands to the southwest. The braided fluvial system which flowed through the present day Tarbat Peninsula area was situated in a valley controlled by the Great Glen fault (Mykura, 1983; Donovan, 1983). The present day topographic character of the Great Glen is in part an exhumed inheritance from Middle Devonian times.

The presence of a strong northwestern paleoflow component in the upper portion of the M.O.R.S. section, however, suggests that northwesterly flowing rivers became prominent during the later stage of the Middle Devonian (Figure 56). In addition, trough axes orientations for the U.O.R.S. (vector mean, 342) indicate that the Upper Devonian fluvial system also flowed to the northwest (Figure 57). This change in paleoflow directions in latest Middle to Upper Devonian times may reflect renewed uplift of the Grampian Highland massif, an event which has been related to left lateral transpressive movements of the Highland Boundary fault (Simon and Bluck, 1982).

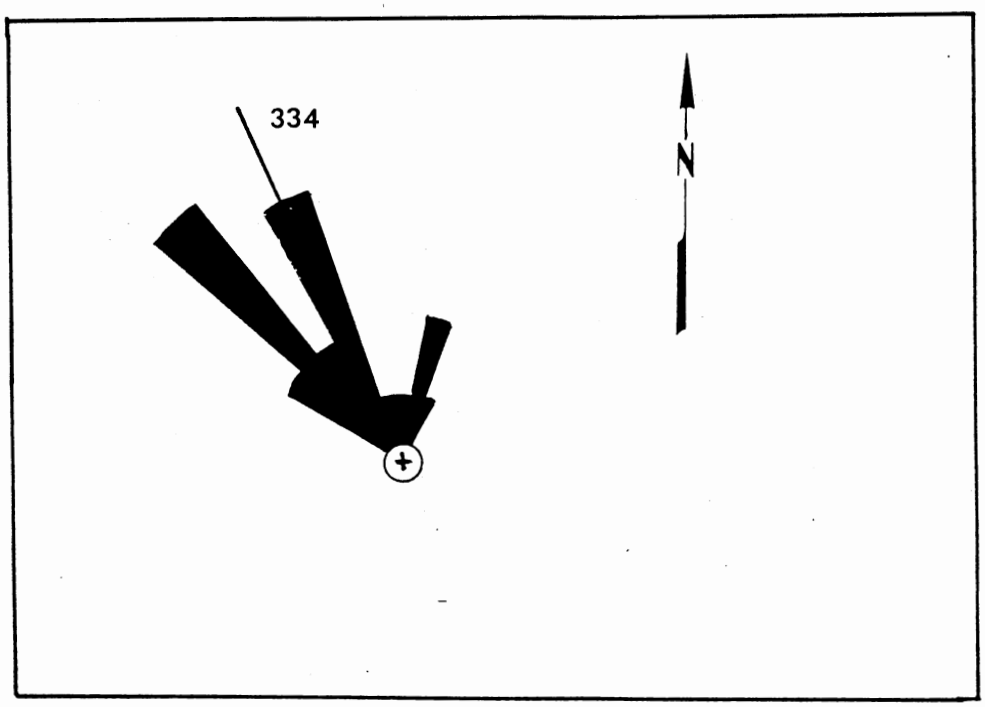

Figure 56. M.O.R.S. Trough Axes, M.O.R.S.$_1$ Section (140-220 m). ($\bar{\theta}$ = 334, R = 23.35, N = 27, R/N = 0.86; data collected by author.)

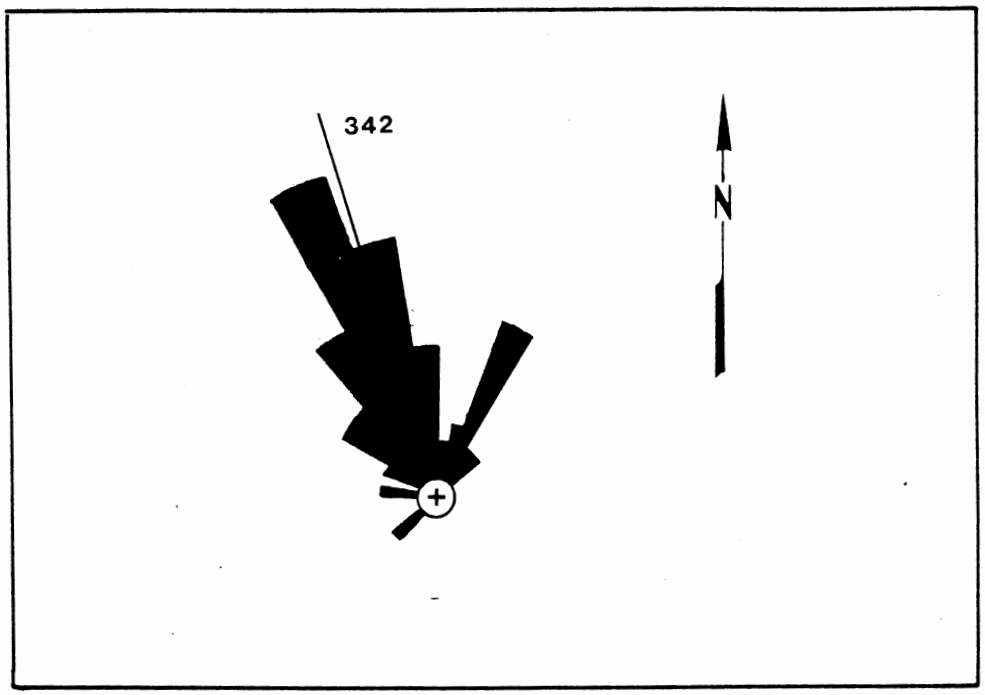

Figure 57. U.O.R.S. Trough Axes, Within Study Area. ($\bar{\theta}$ = 342, R = 38.72, N = 45, R/N = 0.84; data collected by author.)

CHAPTER VIII

SEDIMENTARY PETROLOGY

Introduction

Fifty-one samples were collected from the study area to determine provenance and diagenesis. A summary of textural and mineralogical properties is given in Appendix E. Sample locations are listed in the M.O.R.S.-U.O.R.S. section in Appendix B.

Textures

The majority of samples are texturally submature (Folk, 1974). M.O.R.S. sandstones are generally better sorted than those of U.O.R.S. The grain size throughout the M.O.R.S. section is very consistent. Ninety-percent of the section is comprised of medium-grained sandstone. The remainder of the section is comprised of fine and very fine-grained sandstone, siltstone, and minor amounts (less than one percent) of mudstone and mudstone intraclasts. Only three sand-sized samples, all of which occur in association with climbing ripples, contain an obviously detrital mud matrix.

A greater degree of grain size variance is evident in the U.O.R.S. section. Framework grains range from cobbles to medium sand. In five samples, a detrital mud matrix is evident.

Most detrital grains in both the M.O.R.S. and the U.O.R.S. are

subrounded with moderate sphericities. Those grains which are angular to subangular show evidence of diagenetic corrosion. It is possible that detrital matrices, which have commonly been subjected to dissolution, may have initially been more extensive.

Mineralogy

M.O.R.S. and U.O.R.S. lithologies are classified primarily as subarkoses and feldspathic litharenites, respectively (Figures 58, 59). The detrital mineralogy examined in samples throughout the section indicate a metamorphic and igneous sourceland.

Quartz

In both M.O.R.S. and U.O.R.S. sandstones approximately 50 percent of the grains are detrital quartz. Monocrystalline quartz grains, many of which contain bubble trains and mineral inclusions, are the predominant quartz type throughout the section. Polycrystalline grains (three subrains or less) are a more significant contributant in the U.O.R.S. (9.5 percent) than in the M.O.R.S. (4.3 percent) (Figure 60). The relative paucity of polycrystalline grains in the M.O.R.S. probably reflects an enhanced degree of mechanical breakdown which possibly resulted from a greater distance of transport (Blatt, 1967).

Non-undulose to undulose plus polycrystalline quartz ratios are significantly higher in the M.O.R.S. (average, 2,2) than in the U.O.R.S. (average, 0.63). Silty intervals in the M.O.R.S. contain ratios of up to four. Hence, the tendency toward decreasing undulosity and polycrystalline quartz is consistent with the smaller sand sizes, which are typical in the M.O.R.S. section (Blatt, 1967).

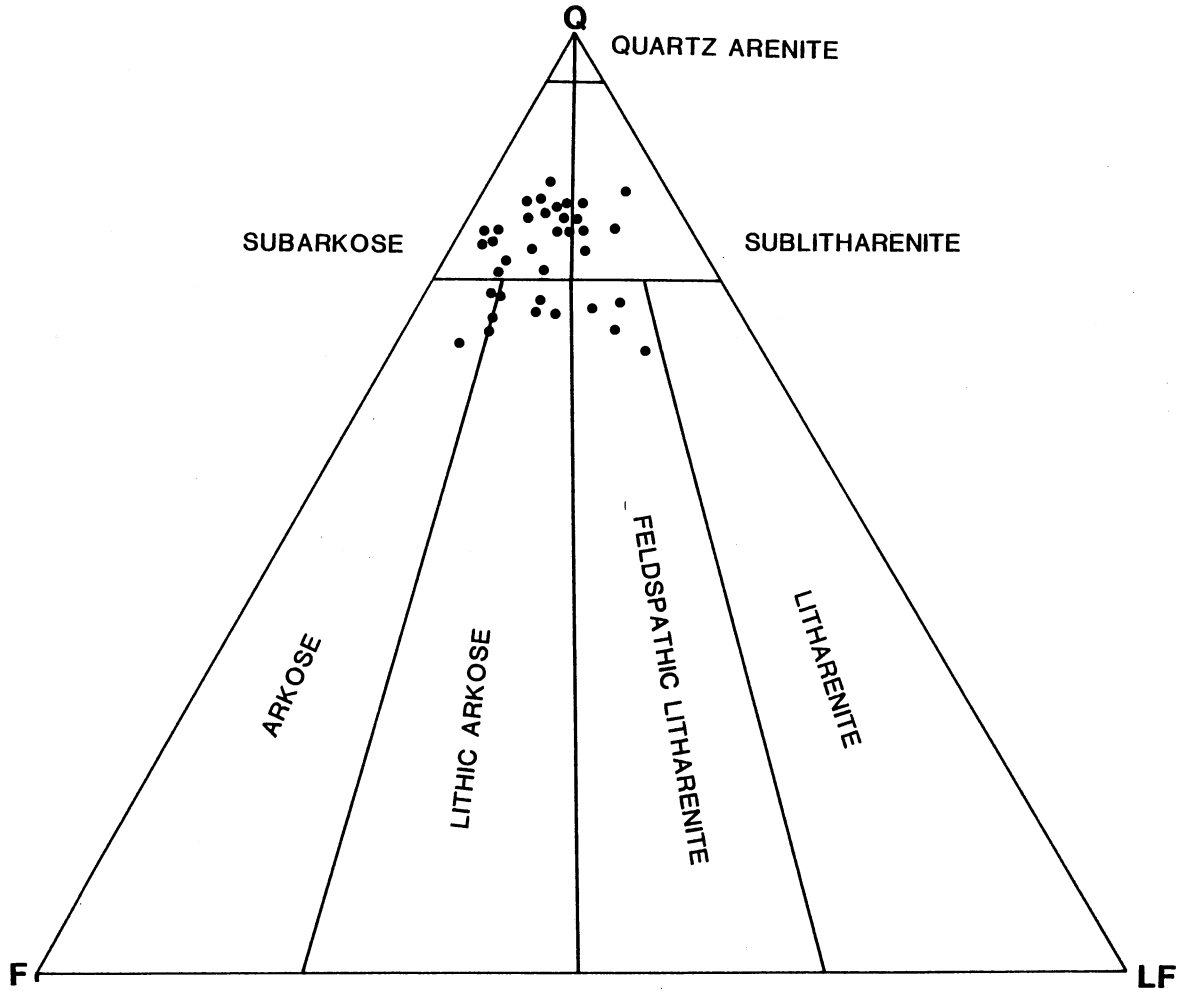

Figure 58. Triangular Diagram of M.O.R.S. Samples from the Study Area. (Q = quartz; F = feldspar, granite and gneissic lithic fragments; L = other lithic fragments. Diagram after Folk, 1974.)

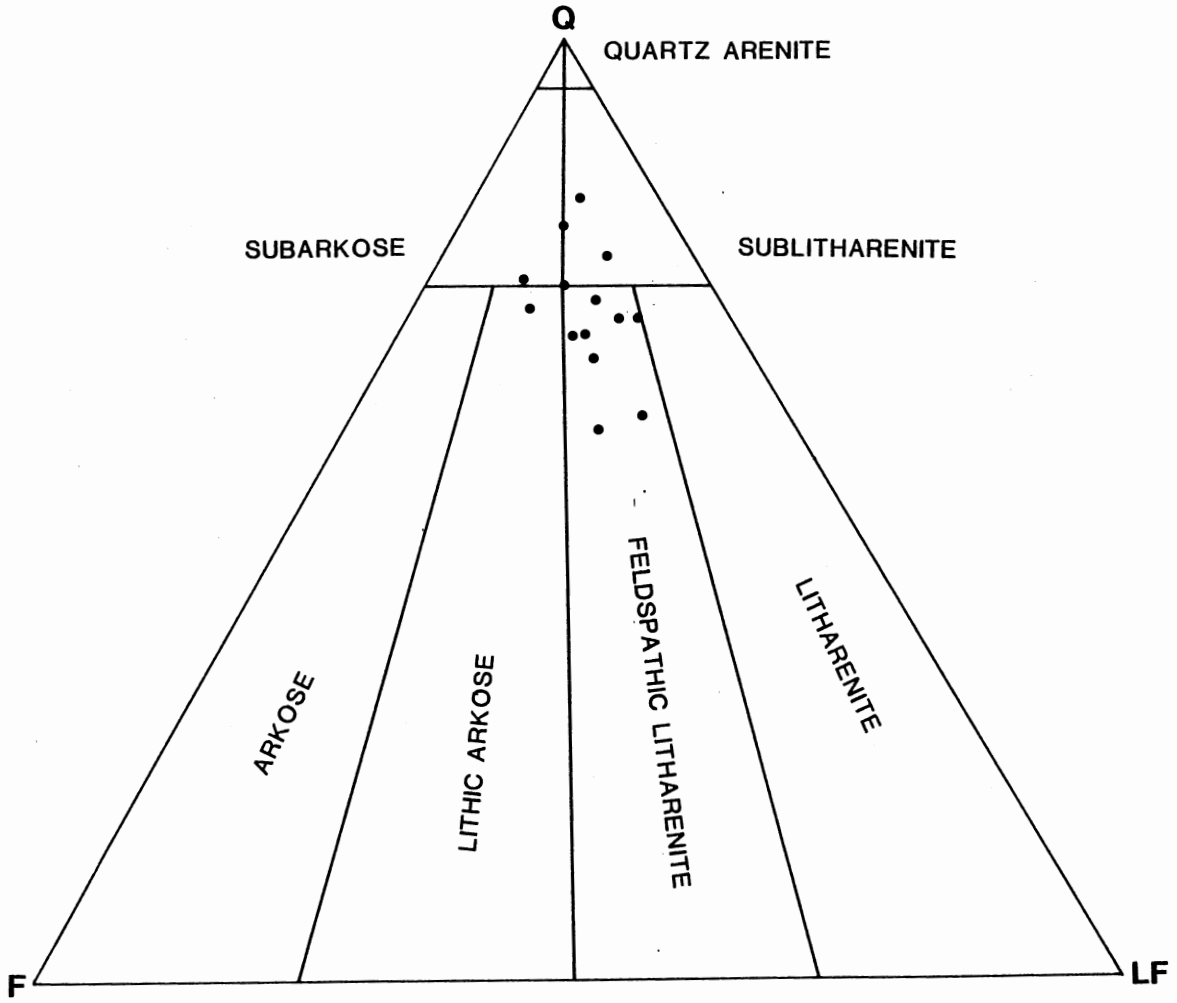

Figure 59. Triangular Diagram of U.O.R.S. Samples Within the Study Area. (Symbols as in Figure 58.)

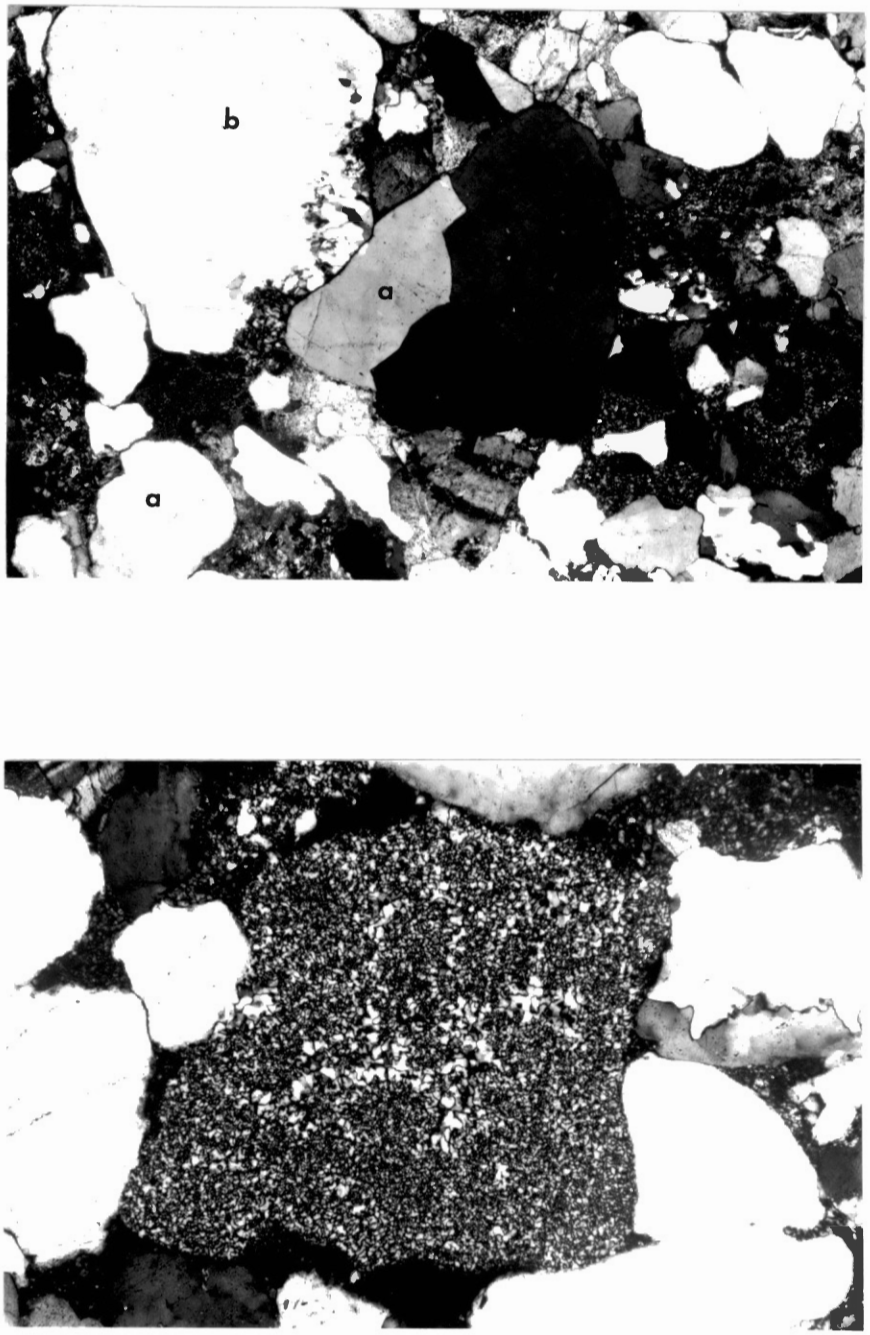

Figure 60. Photomicrographs of (A) Polycrystalline Quartz (a) and Metamorphic Lithic Fragments (b) (x 40); (B) Detrital Chert Fragment (x 100)

Feldspar

Samples from the M.O.R.S. and the U.O.R.S. average eight percent feldspar. Feldspar types are principally orthoclase and microcline (average, 6-7 percent) with lesser amounts of plagioclase (average, 1.5-2.0 percent) (Figure 61). Perthite commonly comprises less than one percent (Figure 62). The presence of numerous partially dissolved plagioclase grains in the M.O.R.S. indicates that this feldspar type was originally more common.

Lithic Fragments

Average percentages of sedimentary, metamorphic, and igneous lithic fragments appear in Tables X, XI, and XII, respectively. Lithic fragments in the U.O.R.S. (average, 11.5 percent) are more prominent than in the M.O.R.S. (average, 7.3 percent). In particular, sedimentary and metamorphic lithic fragments in the U.O.R.S. are about twice as common as in the M.O.R.S. Igneous lithic fragments, principally granite and rhyolite, average less than one percent in both the Middle and Upper O.R.S.

Sedimentary lithic fragments include mudstone, limestone (Figure 63), sandstone, siltstone, and chert (Figure 60). Metamorphic lithic fragments are principally metaquartzite (Figures 60, 64); gneissic and schistose lithic fragments (Figure 64) are less common. The higher percentage of lithic fragments in the U.O.R.S., particularly those of a metamorphic genesis, may reflect a more proximal sourceland during the Upper Devonian.

TABLE X

AVERAGE SEDIMENTARY LITHIC FRAGMENT PERCENTAGES OF SAMPLES FROM THE STUDY AREA

	Mudstone	Siltstone	Sandstone	Chert	Limestone	Total
M.O.R.S.	1.8	0.17	-	0.29	0.39	2.62
U.O.R.S.	2.2	0.64	0.19	0.85	0.37	4.25

TABLE XI

AVERAGE METAMORPHIC LITHIC FRAGMENT PERCENTAGES OF SAMPLES FROM THE STUDY AREA

	Quartzite	Gneiss	Schist	Total
M.O.R.S.	3.2	0.69	-	3.9
U.O.R.S.	6.2	0.25	.02	6.47

TABLE XII

AVERAGE IGNEOUS LITHIC FRAGMENT PERCENTAGES OF SAMPLES FROM THE STUDY AREA

	Granite	Rhyolite	Total
M.O.R.S.	0.32	.02	0.75
U.O.R.S.	0.75	.03	0.78

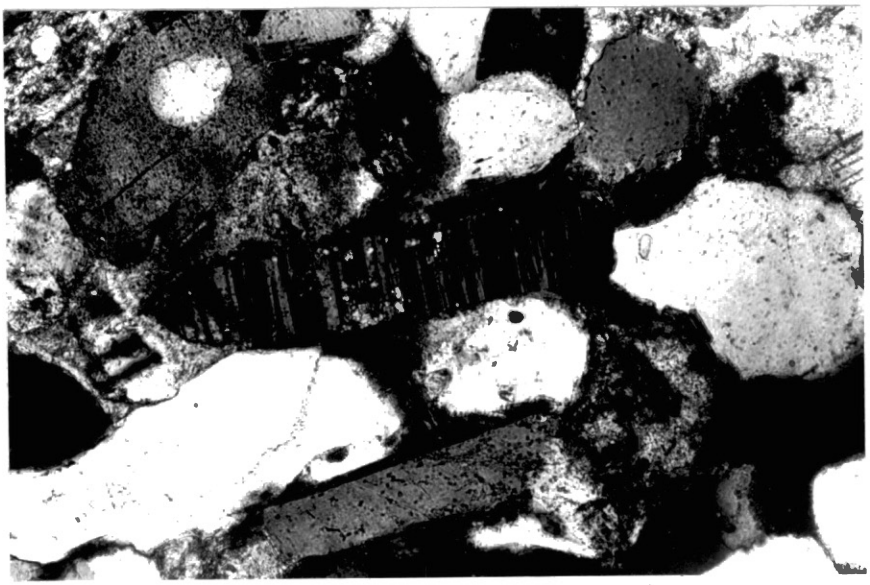

(A)

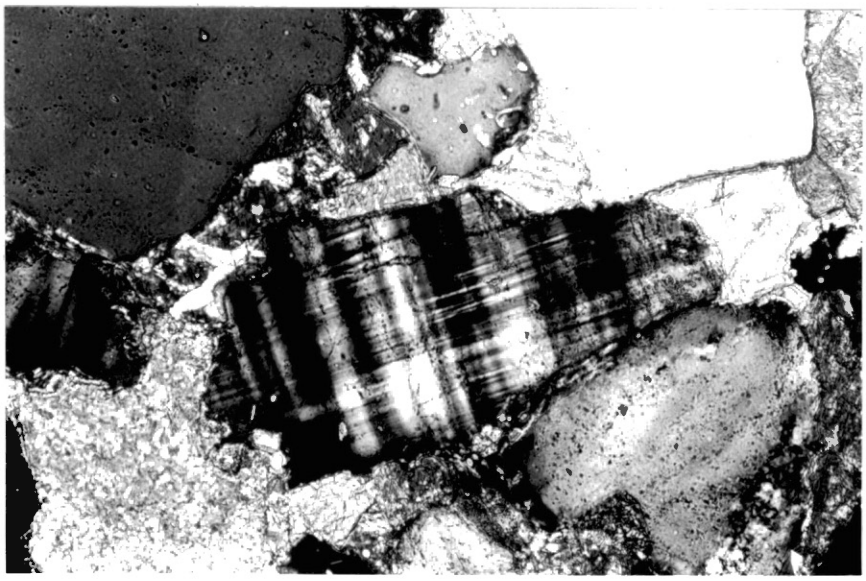

(B)

Figure 61. Photomicrographs of (A) Plagioclase and (B) Microcline (x 200)

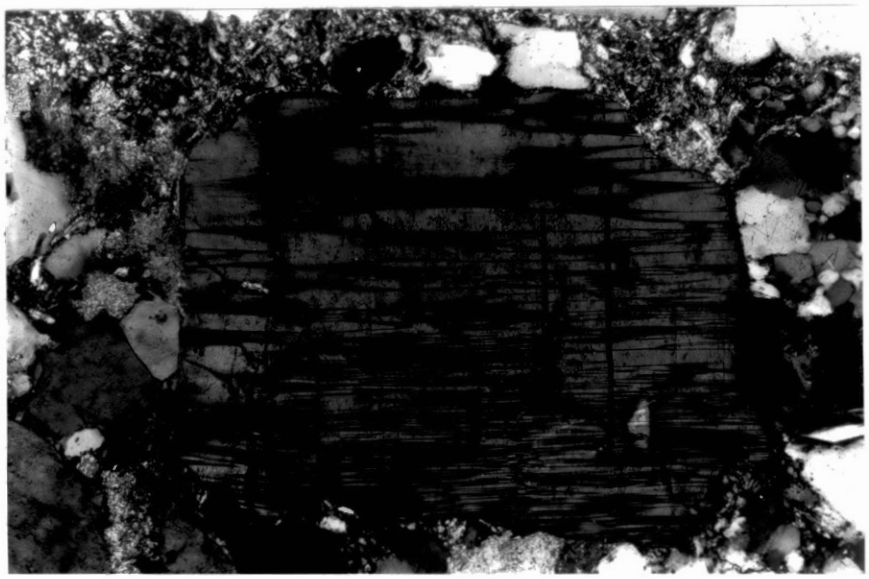

Figure 62. Photomicrograph of Perthite (x 100)

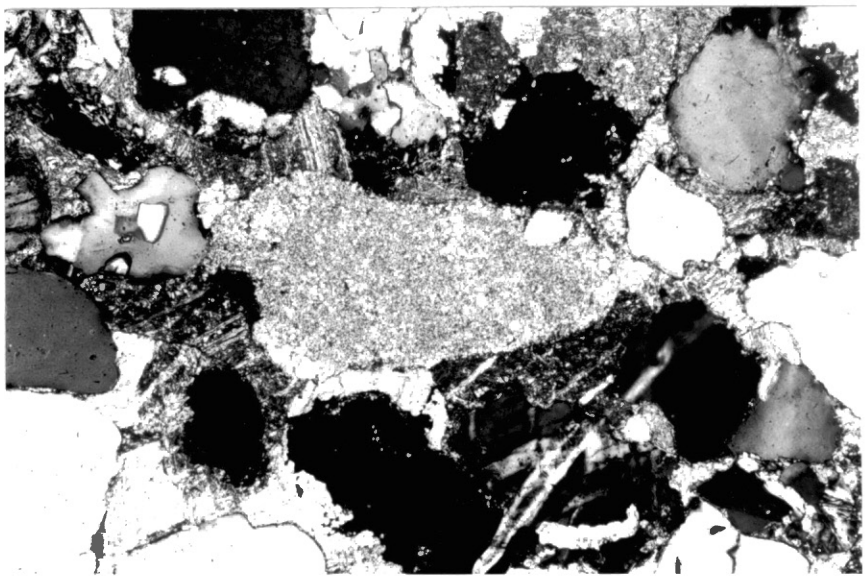

(A)

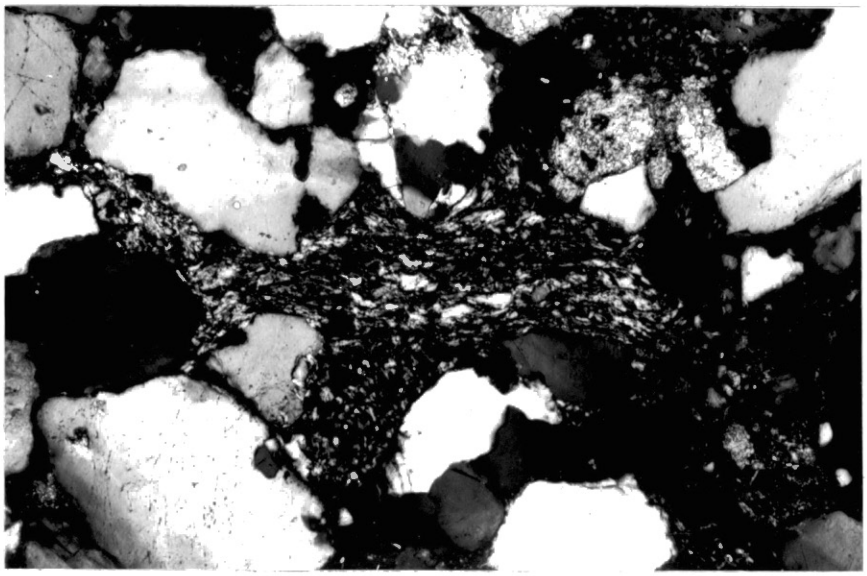

(B)

Figure 63. Photomicrographs of (A) Limestone Lithic Fragment; (B) Compressed Mudstone Lithic Fragment (x 100)

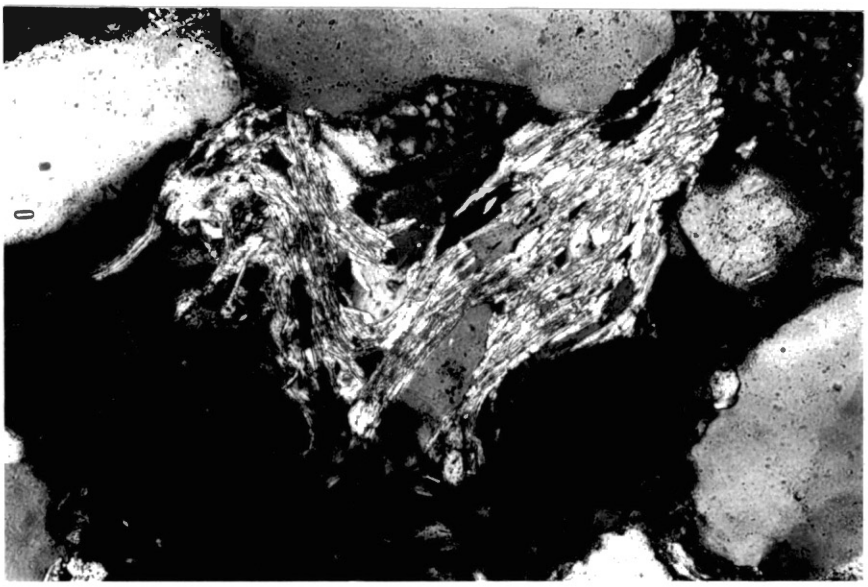

(A)

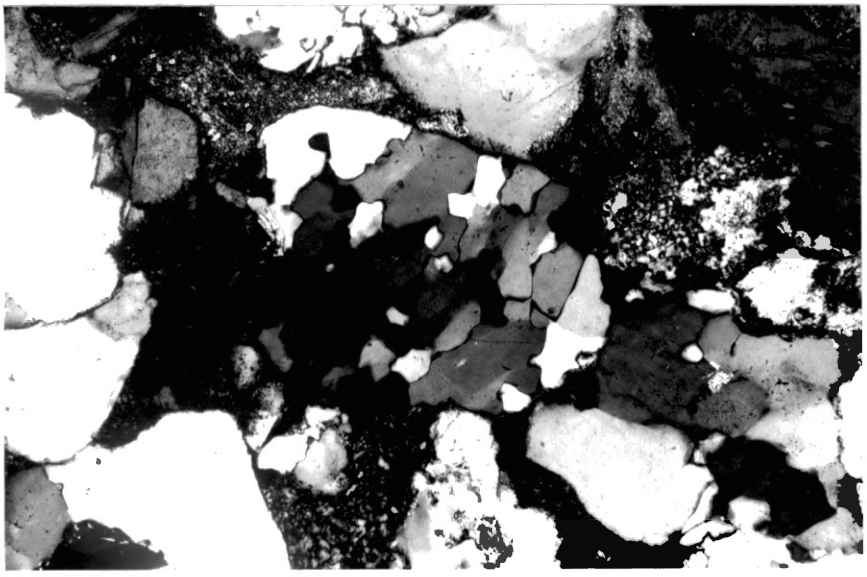

(B)

Figure 64. Photomicrograph of (A) Deformed Gneissic Fragment; (B) Metaquartzite Fragment

Other Constituents

Detrital biotite, muscovite (Figures 65, 66) and heavy minerals (chiefly opaque varieties) (Figure 67) occur in minor to moderate amounts in the M.O.R.S. These minerals are present in concentrations of less than one percent in the U.O.R.S. Heavy minerals and micas present in the M.O.R.S. occur in concentrations of up to five and seven percent, respectively. Both types of concentration are found in very fine-grained sand and silt dominated lithologies (Figures 66, 67). Leucoxene (Figure 67) is the most common heavy mineral type. In oxidized beds, leucoxene is typically altered to hematite. The most abundant translucent heavy mineral is zircon; trace amounts of apatite, hornblende, garnet, and tourmaline are also present. Pyrite was observed in only one instance. Other trace constituents include detrital chlorite, glauconite, and a single occurrence of a silicified oolith clast.

Provenance

Detritus produced during erosion of the Caldonian Orogeny was the principal O.R.S. sediment source. Evidence for a Caledonian source in the Orcadian Basin includes 1) the exposed field relations, particularly in areas of rugged unconformity (Donovan, 1975; Mykura, 1983) where O.R.S. conglomerates contain abundant "Calodenide" fragments; 2) the nature of the drainage system paleocurrent vector analysis (Donovan et al., 1976, and this study); 3) the mineralogy of O.R.S. sediments, both along the Tarbat Peninsula and elsewhere in the Orcadian Basin. The lithic fragments encountered are for the most part compatible with a dissected orogen, e.g., Caledonian granites and Moinian and Dalradian

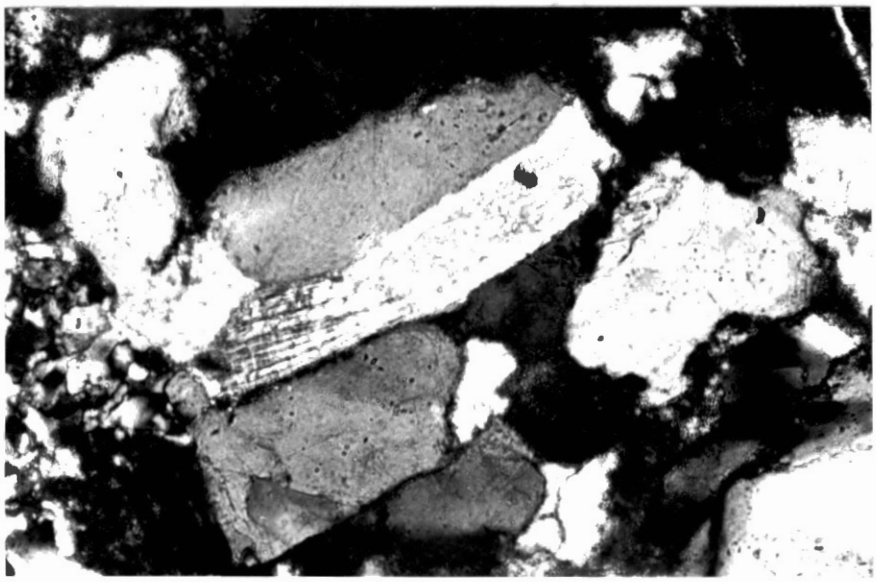

Figure 65. Photomicrograph of Detrital Muscovite (x 100)

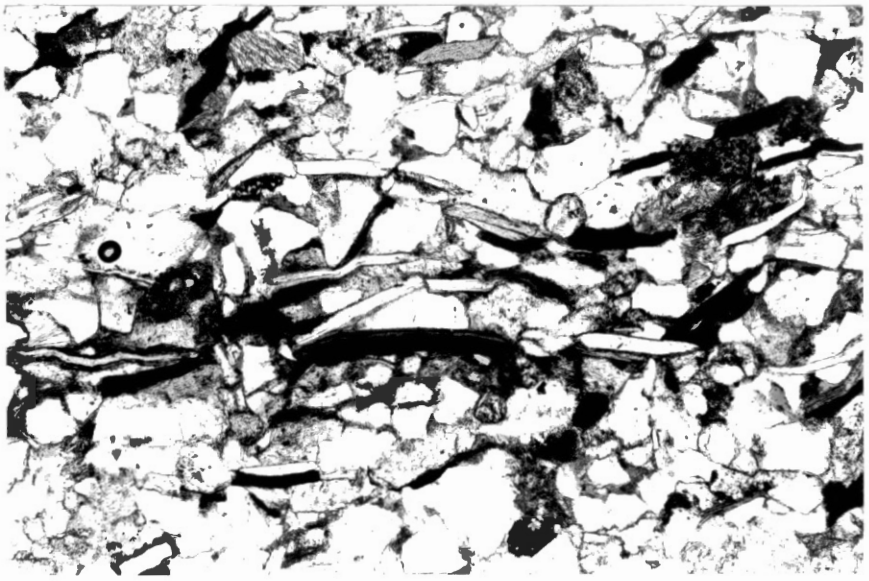

Figure 66. Photomicrograph of Detrital Muscovite and Biotite (x 100). (Biotite fragments are hematized.)

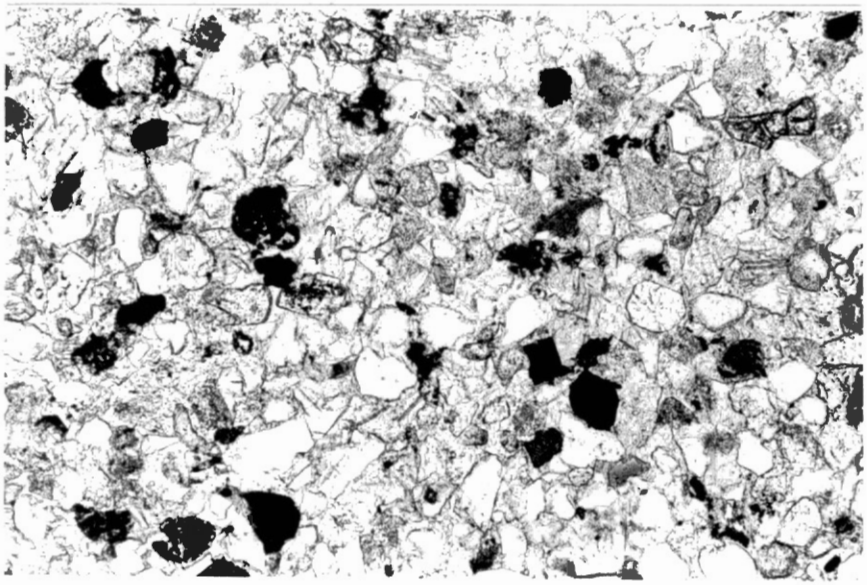

(A)

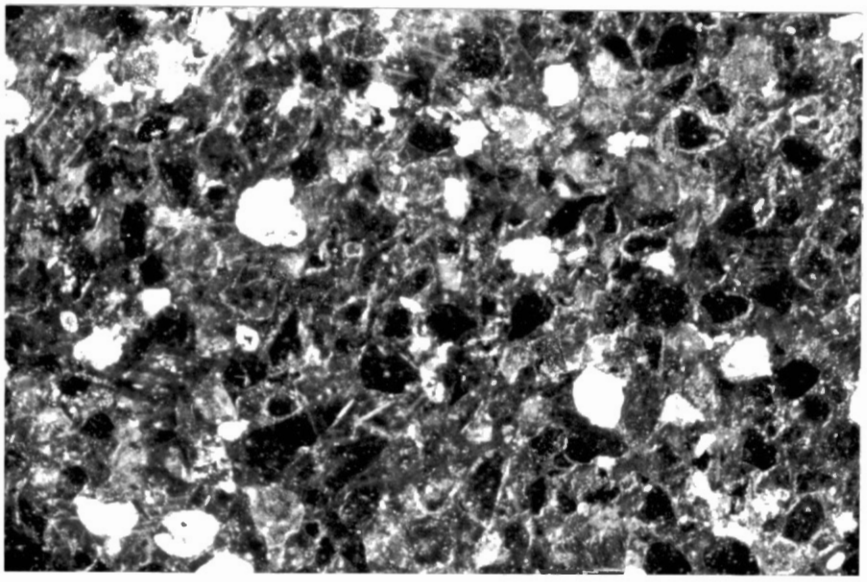

(B)

Figure 67. Photomicrographs of (A) Opaque Heavy Minerals Which are (B) Principally Leucoxene (x 100)

metamorphics (personal communication, R. N. Donovan, 1983). Further evidence of a Caledonian source is suggested by Middle and Upper O.R.S. primary heavy mineral assemblages (leucoxene, biotite, zircon, tourmaline, apatite, garnet, and hornblende). These are indicative of an igneous-metamorphic sourceland (Kerr, 1977). Minor amounts of chert, limestone lithic fragments and glauconite fragments suggest that Cambro-Ordovician carbonates such as the Durness Limestone may have also provided detritus (personal communication, R. N. Donovan, 1983); (Walton, 1970). However, such fragments could also have been provided in part by recycling of M.O.R.S. lacustrine limestones (personal communication, R. N. Donovan, 1983).

While the O.R.S. formed initially as a syntectonic response to the Caledonian Orogeny, recycling of former O.R.S. units may have become more prominent as deposition proceeded. Recycling of the Devonian aged Old Red Sandstone and the Permo-Triassic aged New Red Sandstone (N.R.S.) is the subject of a study by Donovan and Ferraro (1982). The conclusions of this study are 1) the younger rocks are more mature (sp. they contain less feldspar); 2) the younger rocks are mechanically more mature (sp. they contain more quartz showing straight extinction); 3) the younger rocks contain less detrital clay matrix; 4) five stages of recycling are possible (Figure 68); 5) recycling during the Middle and Upper Devonian was interrupted periodically by tectonic and epeirogenic uplift of the Caledonian sourceland (Figure 69).

The M.O.R.S.-U.O.R.S. section along the Tarbat Peninsula is consistent with the O.R.S.-N.R.S. relationship outlined above. Although the section is not extensive, the mineralogical and textural relationships present are consistent with the recycling model. The following arguments are

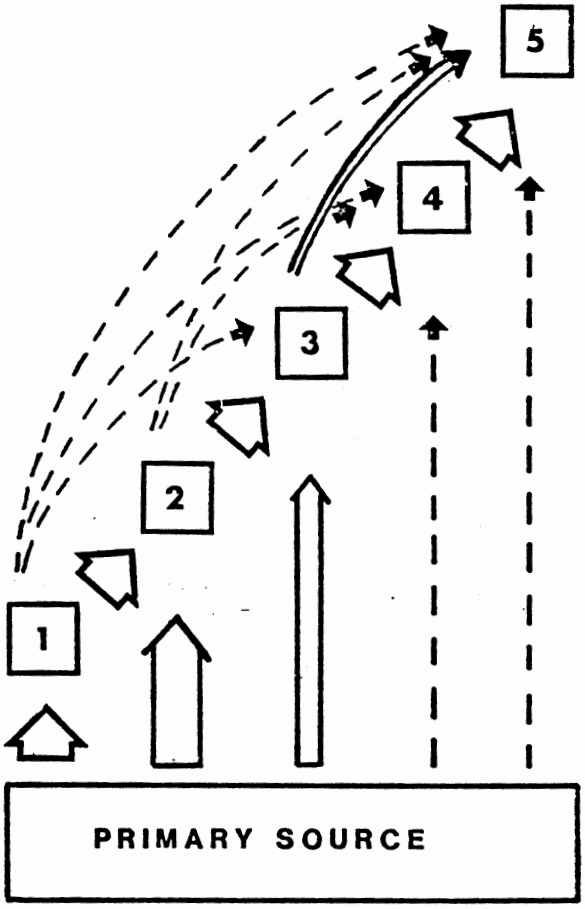

Figure 68. Recycling Possibilities in Moray Firth Sandstones. 1) Lower Old Red Sandstone; 2) Middle Old Red Sandstone; 3) Upper Old Red Sandstone; 4) Lower Triassic; 5) Upper Triassic. (From Donovan and Ferraro, 1982.)

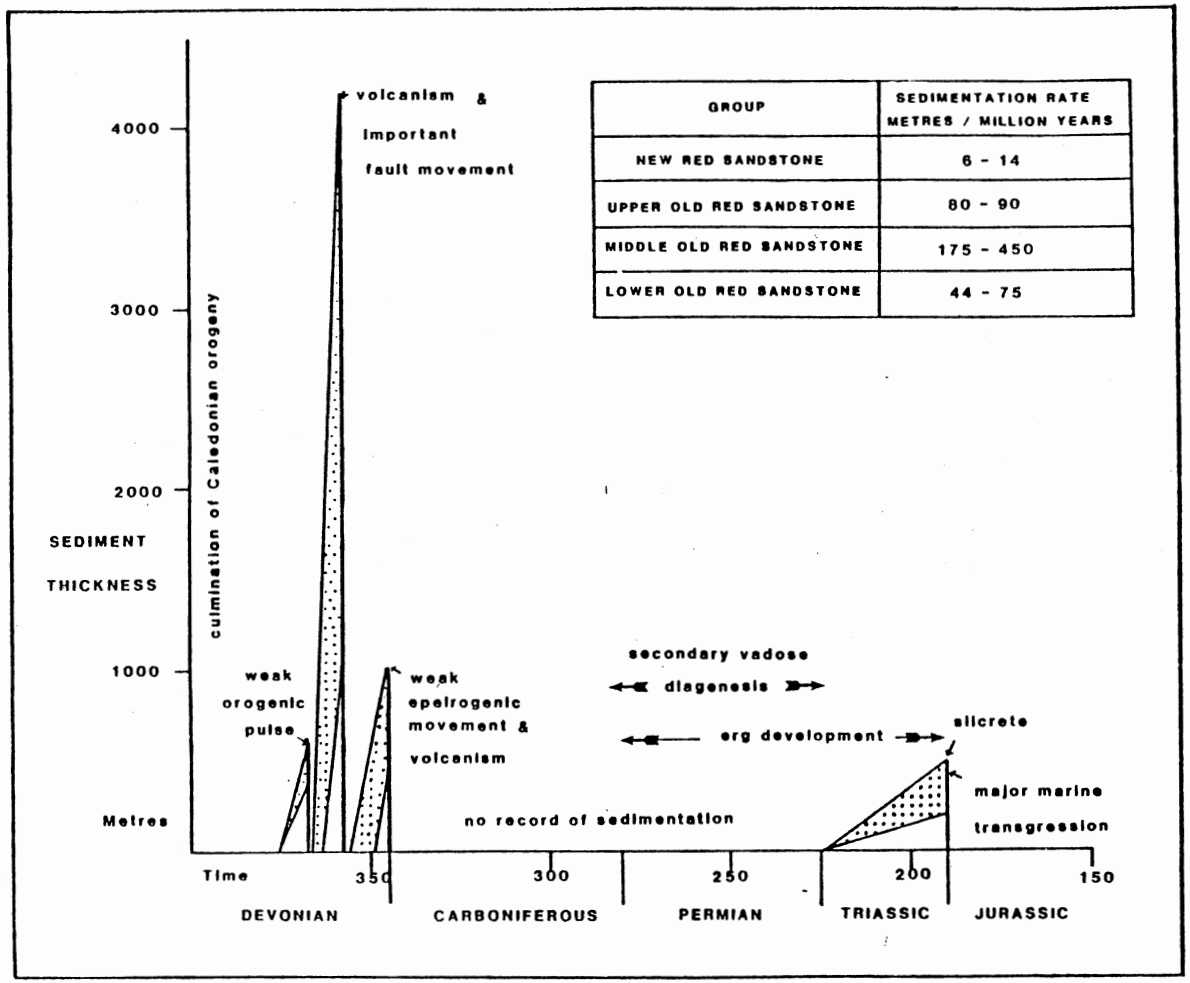

Figure 69. Parameters in Basin Development in Inner Moray Firth from Devonian to end Triassic Times. (From Donovan and Ferraro, 1982.)

pertinent: 1) quartz to feldspar ratios tend to increase upsection in both the M.O.R.S. and the U.O.R.S. (Figures 70, 71), indicating an increase in mineralogic maturity which may, in part, have been inherited from recycling of older O.R.S. deposits; 2) an increase in quartz to feldspar ratios which occurs in conjunction with a M.O.R.S. paleocurrent change from northeast to northwest at meter 140, suggests that a different Caledonian sourceland may have become prominent in the late Middle Devonian (Figure 70); 3) both the Middle and Upper O.R.S. contain high percentages of metamorphic lithic fragments relative to their sedimentary and igneous counterparts (Figure 72). However, metamorphic lithic fragments are about twice as common in the U.O.R.S. as they are in the M.O.R.S. This factor allied with the poorly-sorted nature of the U.O.R.S., the previously noted quartz to feldspar ratios in both the M.O.R.S. and the U.O.R.S. and the change in paleocurrent direction in the upper portion of the M.O.R.S. suggests that a renewed period of Caledonian uplift became prominent in late Middle through early Upper Devonian times; 4) minor amounts of arkosic, matrix-supported lithic fragments in the U.O.R.S. are perhaps recycled from previous O.R.S. deposits.

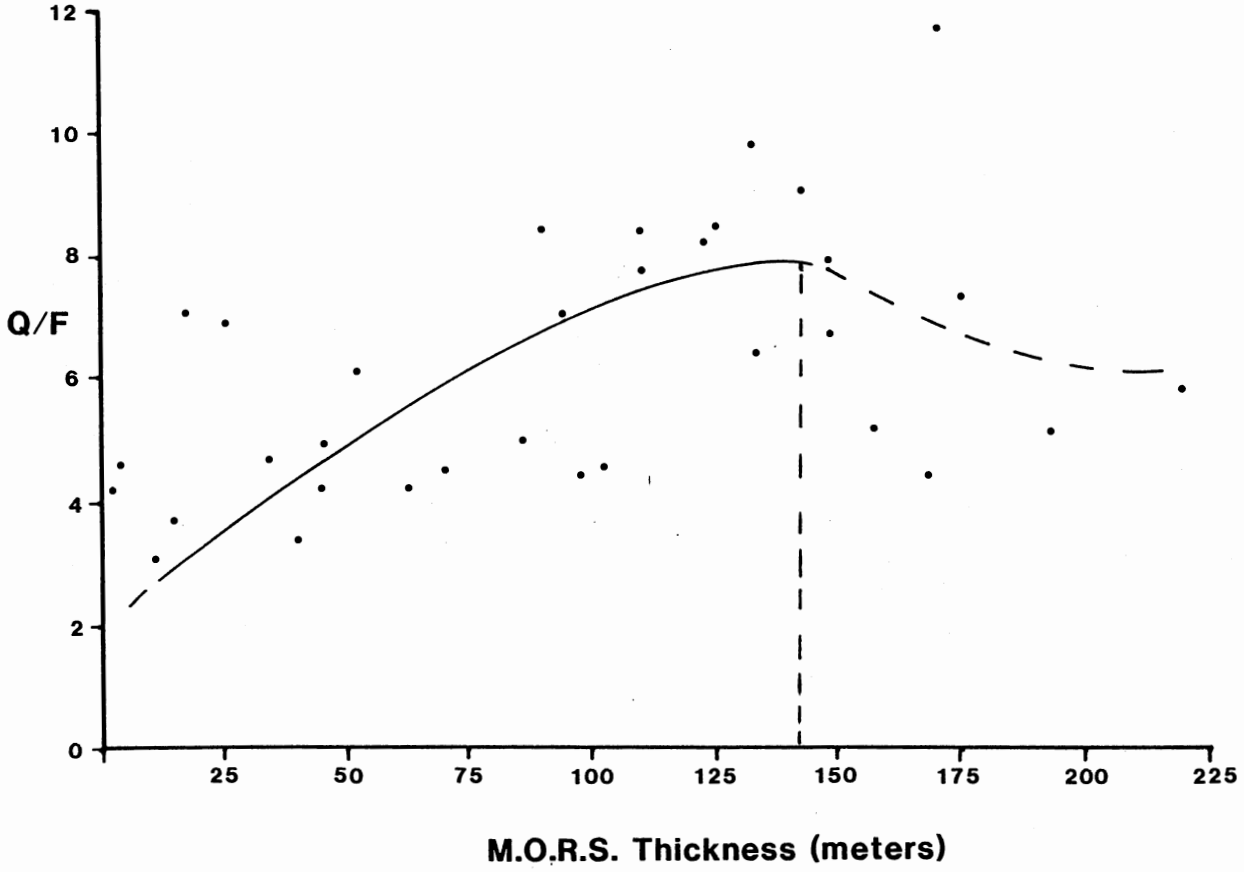

Figure 70. Approximate Relationship for M.O.R.S. Quartz to Feldspar Ratios

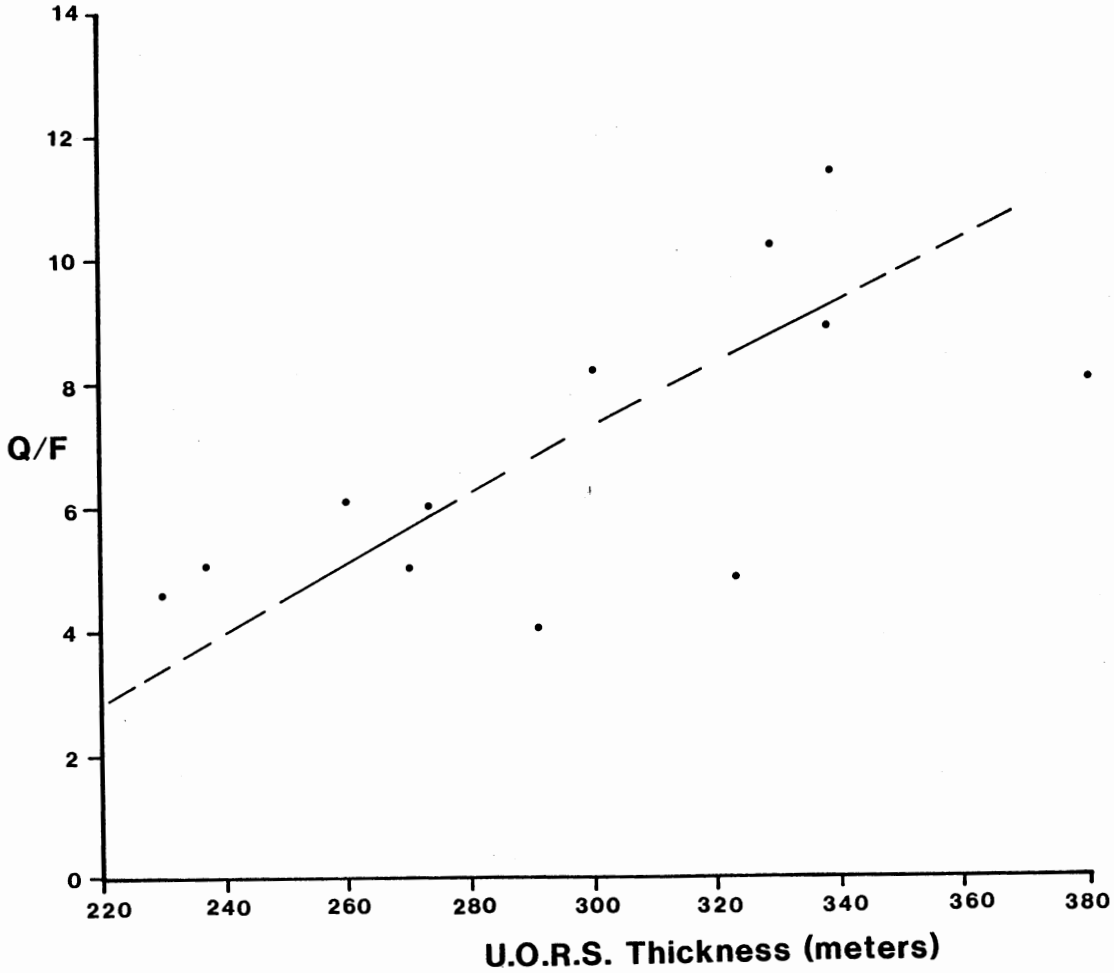

Figure 71. Approximate Relationship for U.O.R.S. Quartz to Feldspar Ratios

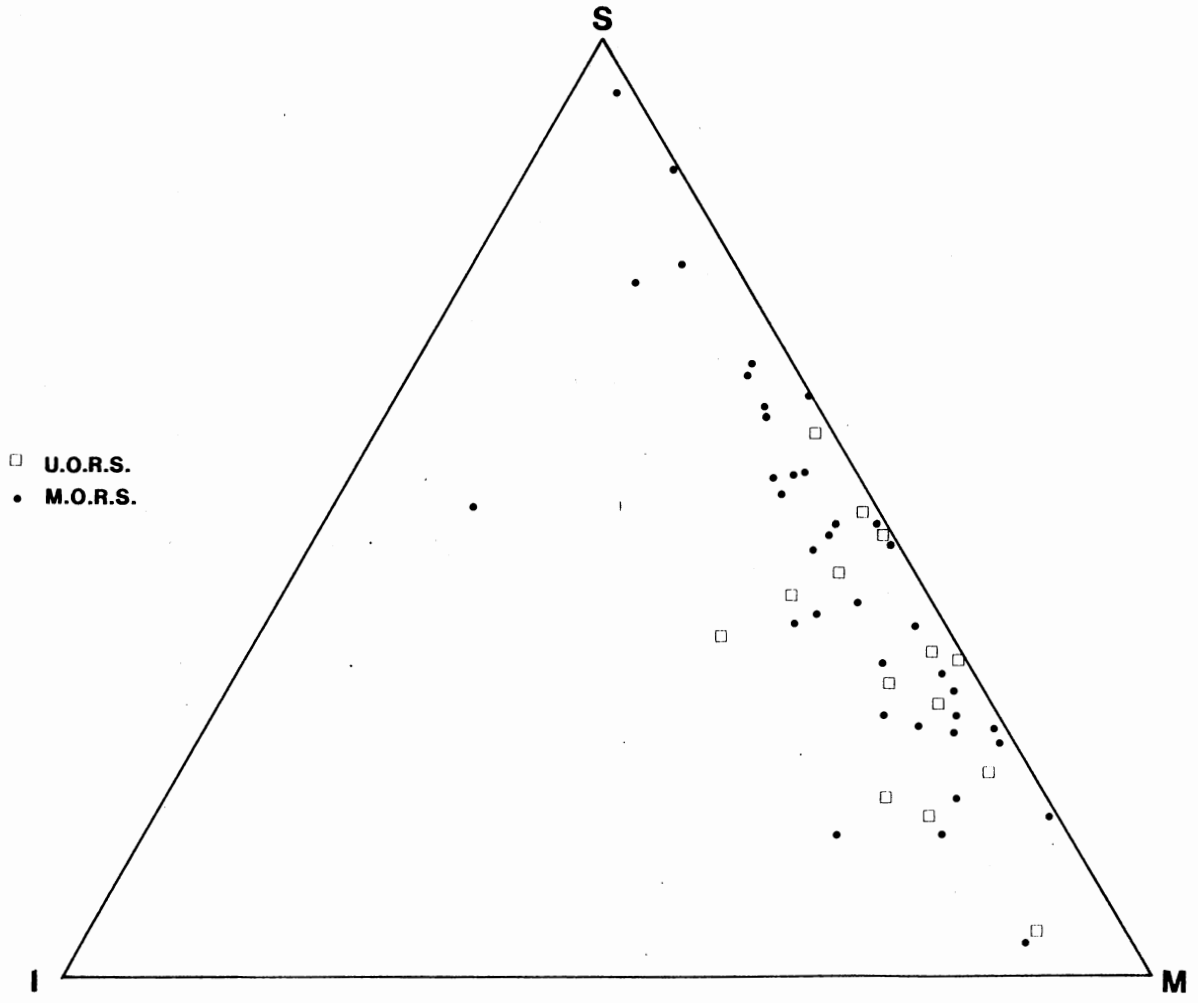

Figure 72. Triangular Diagram of Sedimentary, Metamorphic and Igneous Lithic Fragments from Samples in the Study Area

CHAPTER IX

RED BED FORMATION

Introduction

Physical and chemical parameters of climates which enhance the development of red hematite pigment in clastic rock sequences have been debated over the last 20 years. Even before the present red bed controversy developed, past discussion of red bed genesis was significant. In 1848, Daws observed that drab colored lithologies in red beds of Nova Scotia were usually characterized by high amounts of organic matter (Tomlinson, 1916). While working in red beds of Wyoming and Idaho, Tomlinson (1916) concluded that "coloring matter of red rocks (in this region) was transported and deposited as mechanical sediments." Barrell (1908) suggested that the dehydration of iron oxides was important in the generation of red beds. Robb (1949) emphasized the importance of hematization of biotite to develop red coloring in the Pennsylvanian-Permian Maroon Formation of western Colorado. Perhaps the most significant study that generated debate concerning the origin of red beds was by Krynine (1949). While studying red, hematite stained upland laterite soils in the Tabasco region of southern Mexico, Krynine suggested that the erosion and deposition of these soils produced a dominant red color in stream alluvium which, upon lithification, resulted in red beds. Based on sedimentological and stratigraphic evidence of red colored clastic sequences, Van Houten (1964) recognized that red

beds have both humid-tropical and warm-arid affinities. Walker (1967a), while studying Recent, Pliestocene, and Pliocene red beds in the Sonoran desert of Baja California and northeastern Mexico, indicated that red bed formation is favored by hot and arid climatic conditions. Furthermore, Walker (1967b) examined the field area of Krynine's 1949 study and found that all modern alluvium in the Tabasco region that originated from the erosion of upland laterite soils was drab rather than red. Because Krynine's observations were incorrect and because at that time no recent red bed deposits had been documented, Walker implied that red bed formation is favored by arid climates and that their presence in ancient rocks is a paleoclimatic indicator. Since then, Walker (1974) has conducted research in the Orinoco Basin of Venezuela and has concluded that red beds can form in moist-tropical climates by *in situ* diagenetic alteration of iron-bearing minerals.

Geochemistry

Red coloration, the primary attribute of all red beds, results from the presence of hematite. Free iron in the ferric state is essential to the development of hematite. The source of ferric ions, which results from the release and oxidation of ferrous ions, may have a primary or secondary origin (Van Houten, 1964). Primary origin of ferric ions results from the weathering and erosion of iron-bearing minerals such as amphiboles, pyroxenes, iron-rich phyllosilicates, and lithic fragments from igneous and metamorphic terranes. Examples of these minerals altering to hematite are numerous. Hematite derived from magnetite-ilemite or leucoxene has been documented by 1) Miller and Folk (1955) in samples collected from the Silurian system of West Virginia and from the

Permo-Triassic Pierce Canyon Formation of West Texas, and 2) Van Houten (1968) by comprehensive sample collection in Pennsylvania, Virginia, Nevada, Central America, and Mexico. Pseudomorphs of biotite that have altered to hematite have been cited by Turner and Archer (1977) in the Devonian Old Red Sandstone of northern Scotland. In the red beds of the Baja region of California and Mexico, predominant hematite stained montmorillonite matrix has resulted from intratratal hornblende alteration (Walker, et al. 1967). Secondary origin of hematite results from reworking of sedimentary lithic fragments. In the Upper Ordovician Juniata Formation of central Pennsylvania, Thompson (1970) has cited the significance of hematite genesis from the reworking of sedimentary lithic fragments in floodplain environments.

Another important source of free iron is clay minerals. Kaolinite, with platelet coatings of geothite and hematite, may be transported by rivers to sites of deposition. Oxidation and removal of ferric iron in crystal lattice sites from chlorite, nontronite, vermiculite, glauconite, and chamosite is also significant (Carroll, 1958; Van Houten, 1968). Whether primary or secondary in origin, initial ferrous ions must be oxidized to a ferric state to form hematite.

Large amounts of field evidence and petrographic data suggest that red beds can form in humid-tropical or warm-arid environments. Total iron content in sediments, which is ultimately controlled by the source-land, may also be a significant indicator of the potential for hematite formation. In a comparison of recent red bed development in the seasonally humid tropical savanna of northern Columbia to the arid Sonoran desert, Van Houten (1968) reported that the total iron content ranges between 3.1-7.6 percent and 0.7-7.7 percent, respectively. While field

relations, petrographic studies and total iron content provide significant support for a multiple climate origin of red beds, the geochemistry of hematite should also lend credence to the development of red beds in different climatic regimes.

Ferric oxyhydroxides that are found in the natural environment are listed in Table XIII. Akaganeite, a rare mineral, is commonly associated with oxidation of lunar rocks. Maghemite, which results from the oxidation of magnetite or lepidocrocite is also rare. Neither akaganeite, lepidocrocite, or maghemite are significant in the formation of red beds. Amorphous ferric oxyhydroxide and geothite form as a non-crystalline yellow to brown ferric oxyhydroxide called limonite (Turner, 1980). Limonite may be transported to the site of deposition or precipitated from interstital waters during diagenesis (Turner, 1980). Upon dehydration, limonite alters to hematite (Berner, 1969). Typical chemical paths of limonite dehydration to form hematite are listed in the following reactions (Schmalz, 1968):

$$2Fe(OH)_3 \longrightarrow Fe_2O_3 + 3H_2O \qquad (9.1)$$

$$2Fe(OH)_3 \longrightarrow 2HFeO_2 \longrightarrow Fe_2O_3 + 3H_2O \qquad (9.2)$$

$$2HFeO_2 \longrightarrow Fe_2O_3 + H_2O \qquad (9.3)$$

Negative values for the free energy of formation (ΔG) are critical if limonite will dehydrate to hematite in the presence of water. Schmalz (1968) and Berner (1969) have determined different ΔG values for reaction (9.3) and have, as a result, implied entirely different climatic controls concerning the origin of red beds. A discussion of the

specifics of their research follows.

TABLE XIII

VARIOUS FORMS OF FERRIC OXYHYDROXIDE WHICH OCCUR IN NATURE (from Turner, 1980)

Ferric Oxyhydroxide	Ideal Formula
Amorphous	indefinite $Fe(OH)_3$
Geothite	FeOOH
Akaganeite	FeOOH
Lepidocrocite	FeOOH
Hematite	Fe_2O_3
Maghemite	Fe_2O_3

Schmalz (1968) calculated that the ΔG of hematite and water from limonite at STP ranges between 0.2 and 2.2 kcal/mole; hence, hematite is not stable in the presence of water. At increased temperatures, approximately 130°C, hematite formation will be favored. However, temperatures as high as 130°C are too great to enhance hematite genesis in normal subsurface conditions. Schmalz suggested that an environment exposed to low humidity and moderately high temperatures for long periods of time would be favorable to limonite dehydration and hematite formation. He concluded that red beds are favored by hot and arid climates, and therefore their presence is a meaningful paleoenvironmental indicator.

Using data for the standard enthalapy change as 0.94 kcal/mole from Barany (1965) and for the standard entropy change as 3.65 kcal/mole from

Adamick (1963), Berner (1969) calculated the ΔG of hematite and water from geothite as -0.15 kcal/mole. To attempt to derive more credible evidence concerning the ΔG of hematite, Berner conducted his own experiment. Using differential solubilities of hematite and geothite at 85°C in 0.1 M HCl, geothite was much less stable and more soluble than hematite. Direct experiments at temperatures lower than this were infeasible; i.e., at 25°C, hematite had not crystallized from geothite after 200 days. However, by using ΔG values for 85°C and specific concentrations of ferric iron, Berner calculated that the ΔG of hematite at 25°C and 0°C were -0.33 kcal/mole and -0.20 kcal/mole, respectively. Berner concluded that geothite is relatively unstable in the presence of hematite and water (even though the reaction may be exceedingly slow) "under virtually all geologic conditions." Moreover, upon burial and resultant increasing temperature, hematite will stabilize. Based on these conclusions, Berner implies that geothite, if not reduced, will ultimately dehydrate to form hematite. Hence, the accuracy of red beds as a climatic indicator is in doubt.

Recent opinions from other red bed specialists and geochemists tend to support Berner's conclusions and discredit the conclusions proposed by Schmalz (Turner, 1980; Al-Shaieb, personal communication, 1982). Field and petrographic evidence which indicates that red beds occur in humid-tropical climates are also supportive of Berner's conclusions. However, because temperature is higher and humidity is lower, it is suggested that red bed formation in arid climates is enhanced.

Diagenetic Relations to Environments of Red Bed Formation

Most depositional environments, particularly those characterized

by mollasse and flysch sedimentation, have ample iron to result in red hematite pigment. Red beds, however, are not characteristic of all depositional environments. Clastic sequences resulting from marine and eutrophic lake environments are often drab, whereas oligotrophic lakes and continental alluvial and eolian sequences tend to be brightly pigmented. The ultimate coloration of a clastic sequence is controlled by diagenetic variables such as mineralogy, Eh-pH, levels of organic production, and resulting bacterial activity and climate.

Clastic lithologies in marine sequences often have ample iron to form hematite. Marine environments, particularly slopes and deep basins, are usually characterized by low Eh values and are consequently reducing (Figure 73). While red beds occur in near shore environments, they are not the dominant mode of coloration. Much of the iron in the marine environment is involved in bacterial sulfate reduction which occurs just below the sediment-water interface (Turner, 1980). Goldhabler and Kaplan (1975) have demonstrated that H_2S, HS^-, and Fe^{+2} combine to form machinwite and greigite, which are subsequently transformed to pyrite. In near shore environments, iron reduction by bacterial sulfate is further enhanced by rapid sedimentation rates which results in higher bottom temperatures (Figure 74). Based on the fact that sediments in deep and shallow marine environments are often subject to initial anaerobic conditions or bacterial reduction processes that result in anaerobic conditions, it is concluded that marine environments are not conducive to red bed formation (Turner, 1980). Red bed development during secondary telodiagenesis might result in hematite formation of near shore sediments. This conclusion is supported by the Reagan Sandstone of southern Oklahoma which contains multiple stages of alteration of

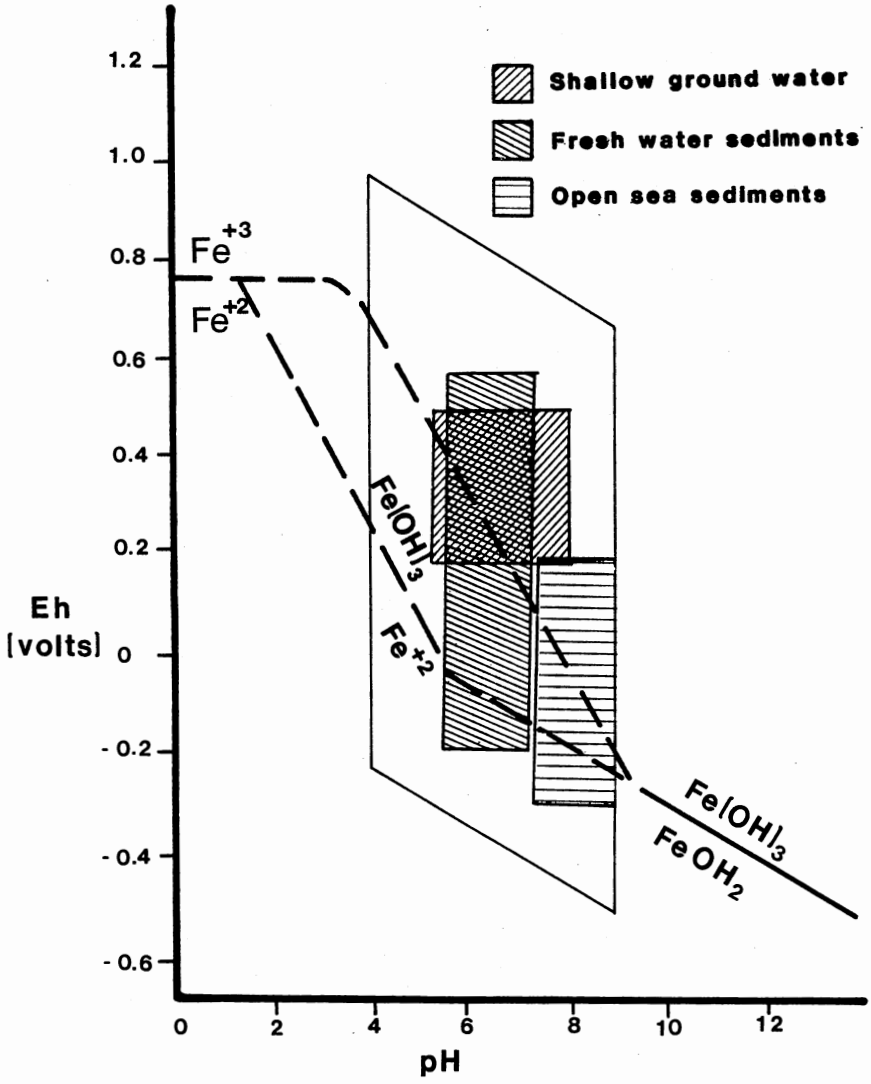

Figure 73. Eh and pH Plots of Shallow Ground Water, Fresh Water Sediments, and Open Sea Sediments. (After Bass et al., 1960, and Krauskopf, 1980.)

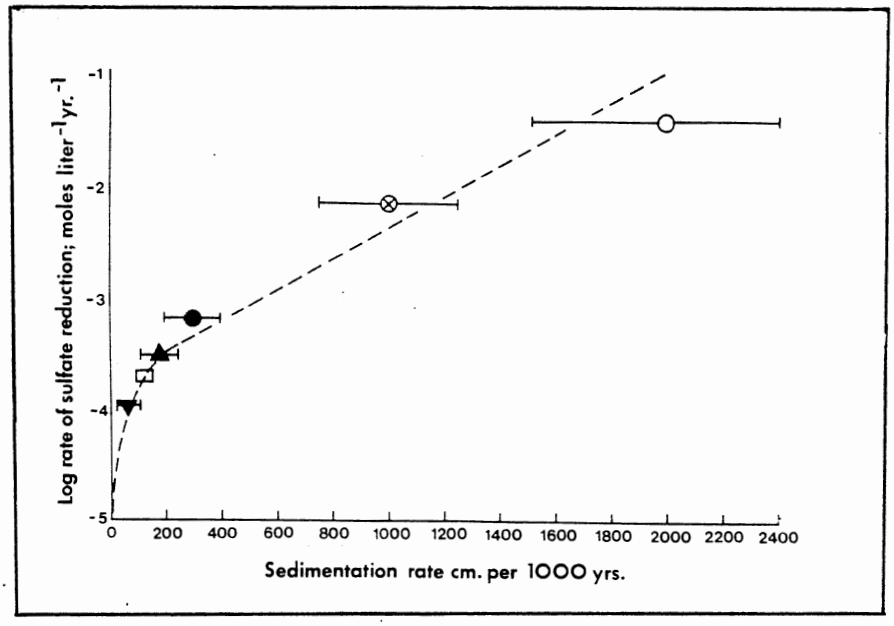

Figure 74. Comparison of Sulfate Reduction to Sedimentation Rate. (Increased sulfate reduction in near shore environments results from increased sedimentation rates.)

○ = Somes Sound Marine
⊗ = Long Island Sound
● = Santa Barbara Basin
△ = Carmen Basin
▽ = Pescadero Basin
□ = Cariaco Trench
(after Turner, 1980)

glauconite to hematite.

Continental red beds form dominantly in eolian and fluvial sequences, and to a lesser extent, in lacustrine sequences. Red bed development in lacustrine sequences is a complex process controlled by mineralogical transformations, organic productivity and redox potentials. The following review of coloration in lacustrine sequences is adapted from Turner (1980).

Coloration of sediments in eutrophic lakes is generally drab. Within the hypolimnon, ferrous ions diffuse from sediments and will precipitage as iron sulfides or will co-precipitate with manganese if pH values are greater than six or seven. Manganese also precipitates as manganese carbonates, manganese hydroxides, and manganese sulfates. Highly productive lakes that are characterized by low redox potentials favor bacterial decomposition, and result in concentrations of sulfide, hydrogen sulfide, and sulfuric acid. Ferrous ions, which are released during periods of lower organic productivity, will precipitate sulfur compounds and form various metal sulfides. Hence, iron remains reduced and sediment color is drab. Highly pigmented lithologies can result from oligotropic lakes. If waters remain oxygenated, bacterial activity remains low and ferric oxyhydroxides form early in diagenesis. Unstable ferric oxyhydroxides will subsequently react to form hematite. In summary, coloration in eutrophic lakes is drab, and oligotrophic lakes are generally highly pigmented.

Generation of color in eolian and fluvial sequences results from *in situ* diagenesis of iron-bearing minerals in the vadose zone and oxygenated levels of the fresh water phreatic zone. This conclusion is supported by the presence of hematite halos surrounding partially

dissolved detrital hornblende and magnetite-illmenite fragments, and pseudomorphed biotite after hematite in red pigmented fluvial and eolian sequences (Walker et al., 1967; Hubert and Reed, 1978; Turner, 1974; Turner and Archer, 1976). In the Upper Ordovician Juniata and Bald Eagle formations in central Pennsylvania, Thompson (1970) identified a 700 foot vertical color change that cuts across lithofacies boundaries of fluvial sandstones. The red pigmented Juniata formation contains high contents of opaque oxide grains, whereas low contents of opaque grains were present in the drab to white Bald Eagle formation. Thompson concluded that following initial diagenesis, the entire succession was red. The Juniata, the stratigraphically higher unit, was at or above the oxygenated water table; hence, it retained its red coloration. Drab coloration in the stratigraphically lower Bald Eagle resulted from its position below the oxygenated water table. Two factors support the mode of coloration in the Juniata-Bald Eagle sequence: 1) the contact between the red Juniata and the drab Bald Eagle cuts across lithofacies boundaries; 2) opaque iron oxides are much higher in the Juniata. This implies that opaque oxides in both the Juniata and Bald Eagle were originally equivalent. Opaque oxides in the Bald Eagle were reduced to chlorite and pyrite.

Fluvial and eolian deposits that result from hot and arid climates are often red pigmented. Ancient examples of such deposits are the Permo-Triassic Rotligendes of western Europe and the New Red Sandstone of Britain. Generation of red pigmentation in these deposits results from extremely low groundwater tables which enhance dehydration and *in situ* alteration of ferric oxyhydroxides to hematite (Tarling et al., 1976). In Cenozoic aged desert alluvium of the southwestern United States,

Walker et al. (1978) have documented *in situ* alteration of detrital quartz, clay, amphibole, pyroxenes, and Ca-plagioclase as a first cycle diagenetic process (Figure 75). Stable minerals which resulted from this alteration are authegenic clays such as kaolinite and montmorillinite, calcite cements, and hematite.

Magenetism

Studies of paleomagnetism in sedimentary rocks have made little lasting contribution to Continental Drift studies but have made considerable contribution to red bed diagenesis studies (Turner, 1980). Hematite is a non-collinear ferromagnet that carries bulk remanance of paleomagnetism at the time of deposition or initial hematite genesis. However, in many studies, a great deal of variation exists between known paleomagnetic orientations and measured paleomagnetic orientations of hematite (Turner, 1980). In studies of remnant magnetism in the Devonian O.R.S. along the northeast coast of Scotland, Tarling, et al. (1976) found considerable variation in the orientation of known Devonian poles to poles resulting from hematite in the O.R.S. A large number of poles were similar to known Permo-Triassic paleomagnetic readings. Hence, it was concluded that the variation in poles resulted from hematite recrystallization during the Permian and Triassic periods. Secondary vadose diagenesis caused by desert conditions in the Permian and Triassic resulted in deep penetration of oxygen and consequent hematite recrystallization. Ground water table elevations of 2000 feet below the surface of the present day Sahara desert lends credence to the possibility of hematite recrystallization during arid conditions (R. N. Donovan, personal communication, 1982).

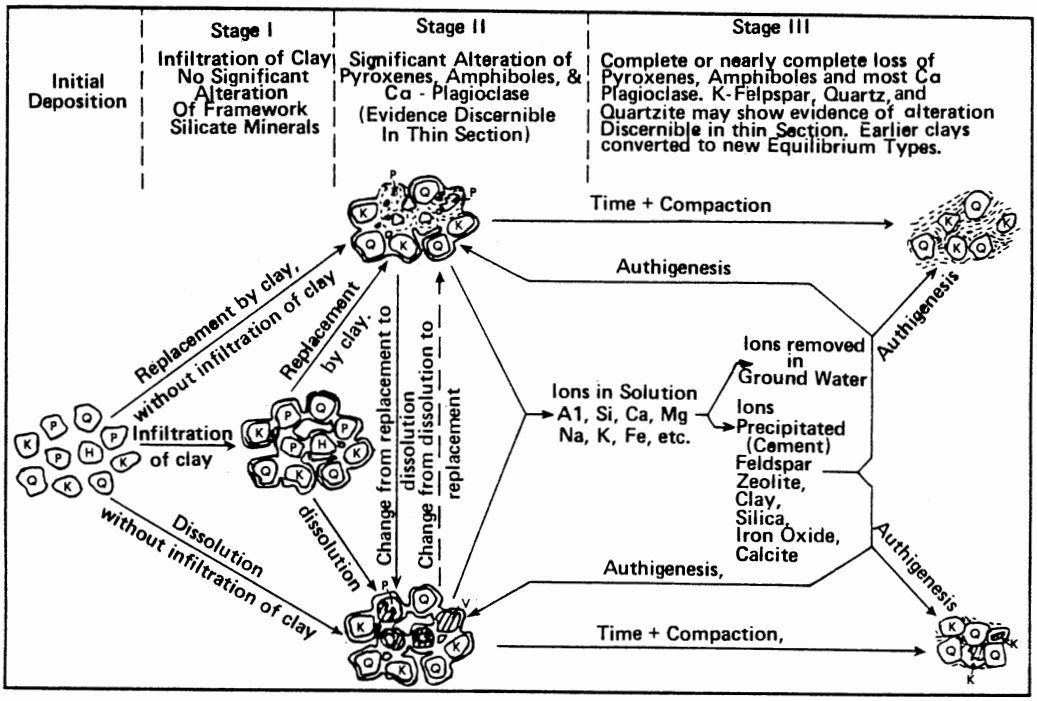

Figure 75. Typical Diagenetic Stages of First Cycle Desert Alluvium (from Walker et al., 1978)

In studies of arid red beds in the Baja region of California, Larson and Walker (1976) found considerable discrepancies in known paleo-magnetic poles to those obtained from hematite in the Baja red beds. They concluded that paleomagnetic poles as determined from hematite in the Baja region were the result of complex stages of chemical remnant magnetism during diagenesis and were therefore invalid. Based on work conducted by Tarling et al. (1976) and Larson and Walker (1976), it is concluded that 1) the use of detrital hematite to determine paleomagnetic poles is in many cases invalid and should be used only when in agreement with known paleomagnetic poles, and 2) seemingly incorrect paleomagnetic readings reflect hematite recrystallization during multiple stages of diagenesis.

Examples of Humid and Arid Red Bed Formation

The central question concerning the genesis of red beds is: What type climate, if any, enhances the development of red hematite pigment and the consequent genesis of red beds? Analysis of Gibbs free energy values for the transformation of geothite to hematite in the presence of water suggests that red beds can form in either humid-tropical or hot-arid climates. Based on sedimentological, stratigraphic, and pertrographic examination of red pigmented clastic sequences, numerous examples of red beds forming in both moist and arid climates have been documented (Van Houten, 1968: Walker, 1967a; Walker and Harms, 1971). Within the context of this discussion, two examples of red bed genesis in different climates--one humid and one arid--will be examined: 1) coloration of red beds in the Catskill Clastic Wedge of central Pennsylvania and eastern West Virginia (Walker and Harms, 1971); 2) red bed genesis in the Sonoran

Desert of Baja California and northeastern Mexico (Walker, 1967a).

The Catskill Clastic Wedge

During the Devonian period, the collision of a series of micro-continents or part of Europe with North America resulted in the uplift of the Acadian Mountains in the northern Appalachians (Cook et al., 1980). In the central and southern Appalachians, Acadian deformation was absent. Mollasse, known as the Catskill Clastic Wedge, was shed to the southwest in a sheet-like fashion into the area of the present states of New York, Pennsylvania, Virginia, and West Virginia. In Pennsylvania, the main facies of the Catskill Clastic Wedge have been identified as 1) marine turbidites; 2) continental shelf deposits; 3) prograding muddy shoreline; 4) alluvial point bar sequences. The lateral or vertical presence of any facies within the sequence reflects the rates of sediment progradation and basin subsidence and the resulting position of the Acadian Sea to the west (Figure 76). The absence of evaporites and calcretes suggests that the Catskill Clastic Wedge formed in a humid climate. Coloration of marine sequences is gray to green; however, point bar alluvial cycles are red. Studies of the same sequence in West Virginia support Walker's conclusions in Pennsylvania. In West Virginia, continental shelf and turbidite facies were drab. However, with the first appearance of point bar sequences, signifying non-marine sedimentation, the dominant mode of coloring changes from drab to red (Cruickshank and Ferraro, 1980).

The Sonoran Desert

In the Sonoran Desert, located in the Baja region of southern

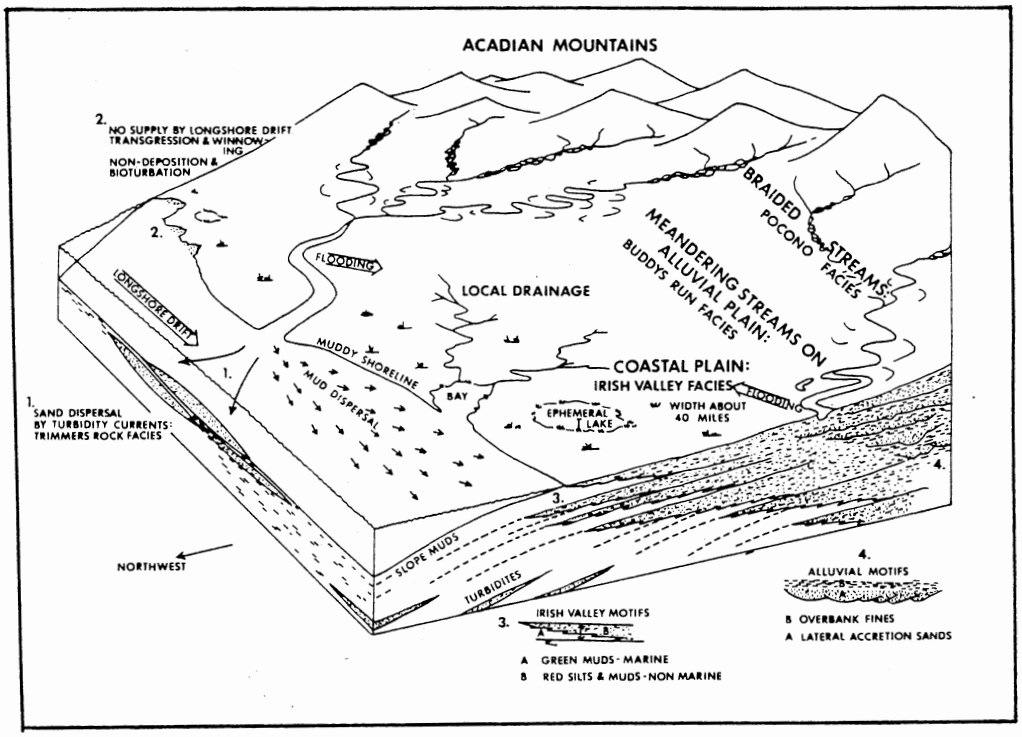

Figure 76. Major Facies of the Catskill Clastic Wedge in Pennsylvania. (Marine sediments are drab; non-marine sediments are red. From Walker and Harms, 1971.)

California and northeastern Mexico, hematite pigmentation and consequent development of red beds has resulted from *in situ* alteration of iron minerals in a desert environment. The presence of altered detrital fragments which consist of hematite halos surrounding hornblende, pseudomorphed biotite and hematized limonite-magnetite indicates that the source of iron was from the crystalline highlands of the Peninsular range to the east. Common authigenic mineral suites that result from dissolution or replacement of iron-bearing minerals, detrital clays, feldspars and quartz are authigenic clays, calcite cement and hematite. The tendency for progressively older sediments to have increasing amounts of red pigmentation and greater dissolution of detrital minerals suggests that the original color of the sediments was drab and with time became red. Typical sedimentary facies consist of 1) Pleistocene evaporites; 2) Recent and Pleistocene alluvium; 3) Pleistocene soils; 4) Pliocene fanglomerates; 5) Recent, Pleistocene, and Pliocene intertidal deposits. Recent alluvium and intertidal deposits are drab. Pleistocene alluvium show some degree of reddening. Pleistocene intertidal deposits are generally yellow to brown and contain limonite halos which are precursors of hematite halos. In Pliocene intertidal deposits, reddening is uneven and is concentrated in sand lenses. This suggests that higher permeabilities in the sands favor iron mobilization. The tendency toward increased reddening in progressively older sediments and hematite halos that surround detrital iron minerals indicates that red pigment was developed diagenetically by *in situ* intrastratal dissolution and replacement. This interpretation of hematite genesis precludes the possibility that laterite soils in humid-tropical climates could be transported to the depositional basin and constitute

immediate formation of red beds. Rather, once laterite soils are transported to the depositional basin, their red color is usually masked (Walker, 1967b).

Tectonic Environments and Red Bed Formation

Examination of sourcelands of past and present red beds indicates that hematite pigment in clastic lithologies is best developed in continent-continent collisions and plate rifting environments. Ancient examples of the former tectonic regimes include the Catskill Clastic Wedge and the Old Red Sandstone. Ancient and Recent examples of red beds forming in plate rifting environments are the Triassic Basins of eastern North America and the Baja Region of California, respectively. Because continental sedimentation is common in these environments, high Eh values persist and hence, hematite formation is enhanced. Sufficient iron is present in basic and intermediate rocks that are typical of island arc and Andean plate environments to enhance red coloration. High sedimentation rates and rapid basin subsidence favors deep burial of flysch in marine environments and results in consequent reduction by bacterial activity and anaerobic conditions. Consequently, flysch or even mollasse which results from Andean and island arc collisions is drab in coloration.

CHAPTER X

DIAGENESIS

Results

The paragenesis and principal diagenetic relationships of the Tarbat Peninsula section (Appendix E, Figure 77) are as follows:

1. Most diagenesis in both the Middle and Upper O.R.S. occurred shortly after deposition. A distinctive diagenetic imprint was imparted to each lithotype in the M.O.R.S. Subsequent diagenesis may have resulted from large-scale fluctuations in the lake level of the Orcadian Basin. Early diagenesis in the U.O.R.S. was controlled principally by semi-arid climatic conditions which persisted during the Upper Devonian.

2. The first diagenetic mineral to precipitate throughout the study area was hematite (Figure 78). In the M.O.R.S., hematite formed in very fine-grained sand to silt-sized floodplain sequences. The principal source of iron in these M.O.R.S. facies resulted from the interstratal alteration of biotite and leucoxene (Figures 66 and 79). Hematite in the U.O.R.S. is concentrated in facies which contain mud fragments or a detrital matrix. Although most hematite formed at an early diagenetic stage, textural evidence suggests that hematite continued to develop sporadically throughout diagenesis.

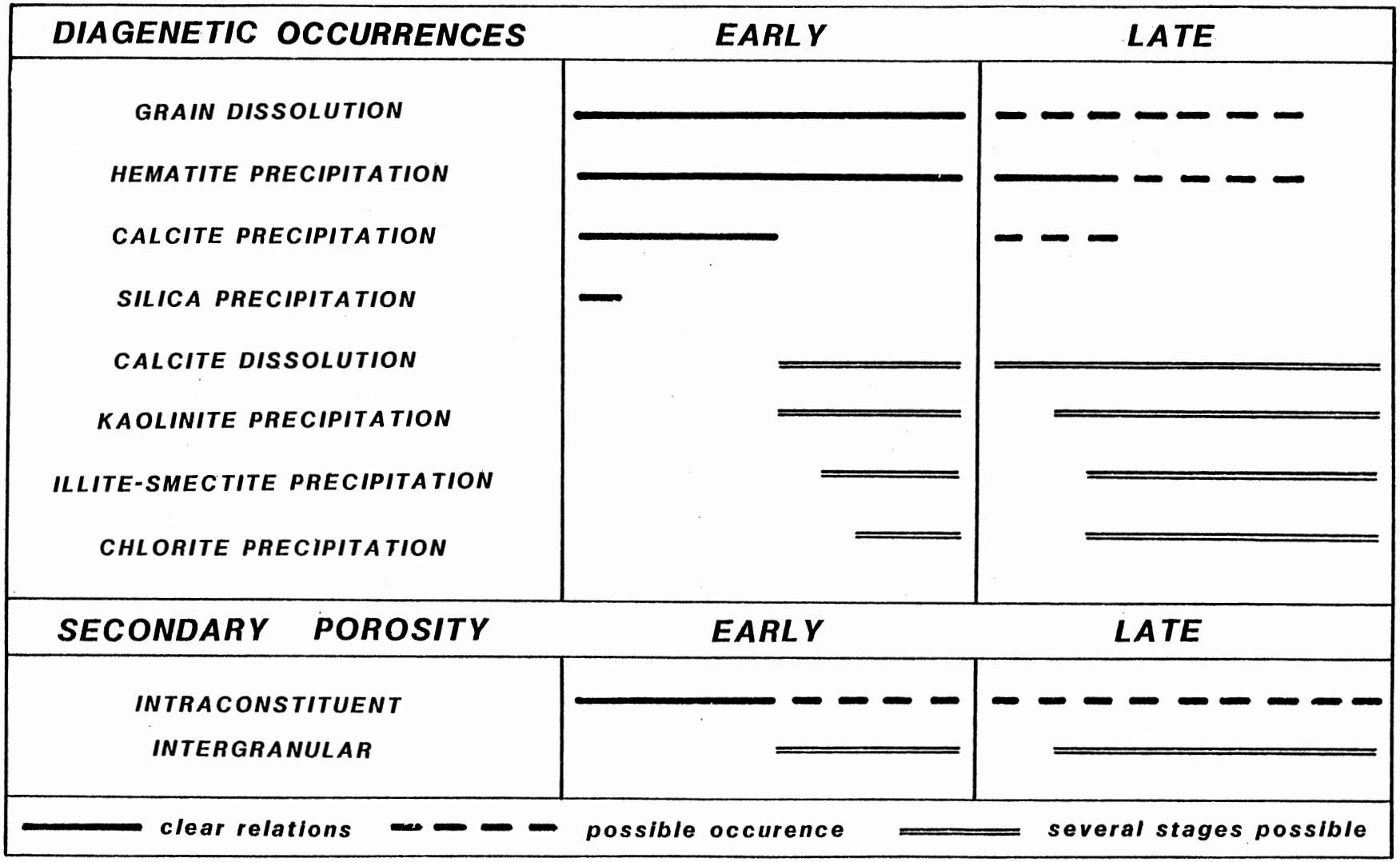

Figure 77. Paragenesis of the Tarbat Peninsula Section

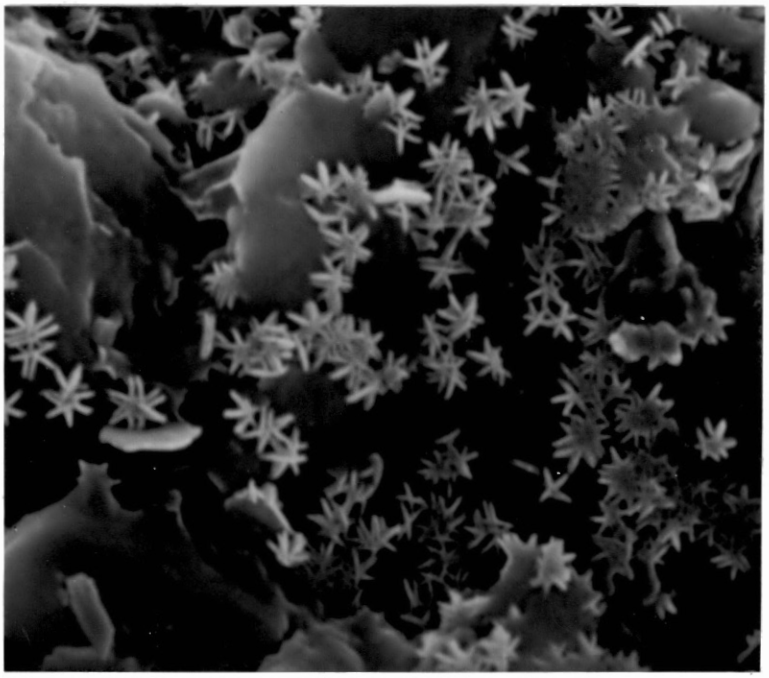

Figure 78. SEM Photograph of Authigenic Hematite Growth on Surface of a Quartz Grain (x 9000)

Figure 79. Photomicrograph of Opaque Hematite After Leucoxene (x 200)

3. Calcite precipitation, which began shortly after initial hematite precipitation, resulted primarily from shallow burial of M.O.R.S.-U.O.R.S. sediments (Figure 80). In the lacustrine facies of the M.O.R.S., a slightly earlier period of calcite precipitation is postulated.

4. Alkaline ground waters which were present during calcite precipitation caused the most significant dissolution of detrital silicates; sp. quartz, feldspar, and lithic fragments (Figure 81). Very minor amounts of authigenic quartz (Figure 82), chert, and chalcedony were subsequently precipitated in local zones of reduced alkalinity.

5. Intra-constituent secondary porosity, most prominent in the M.O.R.S., resulted from internal dissolution of feldspars, sp. plagioclase (Figure 81).

6. The final diagenetic events involve the dissolution of calcite, development of intergranular secondary porosity (Figure 83), and the precipitation of authigenic kaolinite (Figures 83 and 84), illite-smectite (Figure 85), and chlorite.

Discussion

Geologic Parameters Which may Have Influenced M.O.R.S.-U.O.R.S. Diagenesis

The geologic parameters which could have affected the diagenetic evolution of Tarbat Peninsula section are 1) the climatic, sedimentologic and tectonic factors which controlled deposition of the M.O.R.S. and the U.O.R.S.; 2) the subsequent history of the Orcadian Basin in the

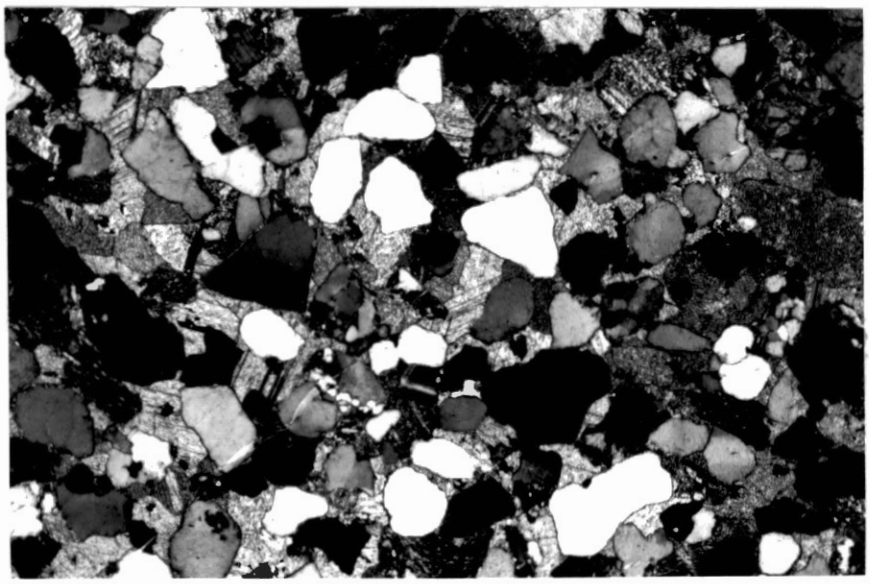

Figure 80. Photomicrograph of Poikilotopic Calcite Cement, Buff Sample, U.O.R.S. (x 40)

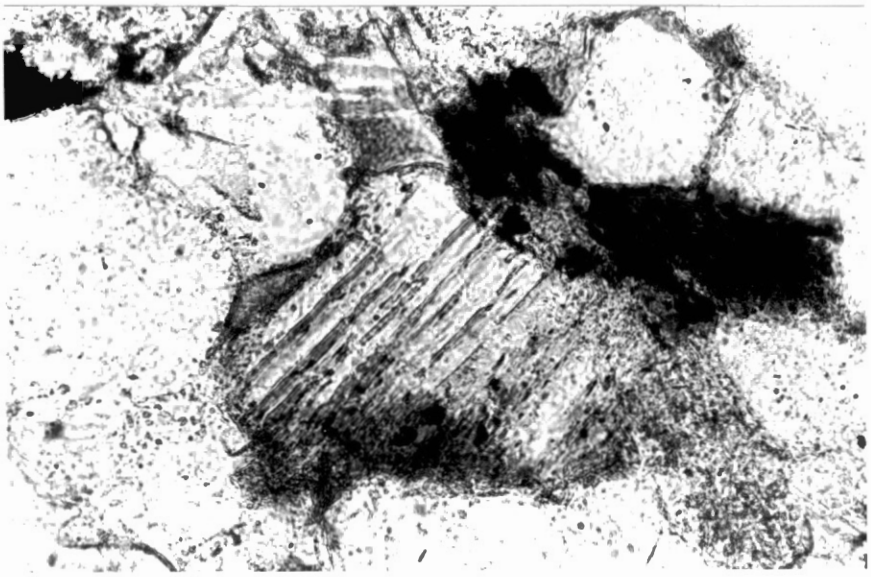

(A)

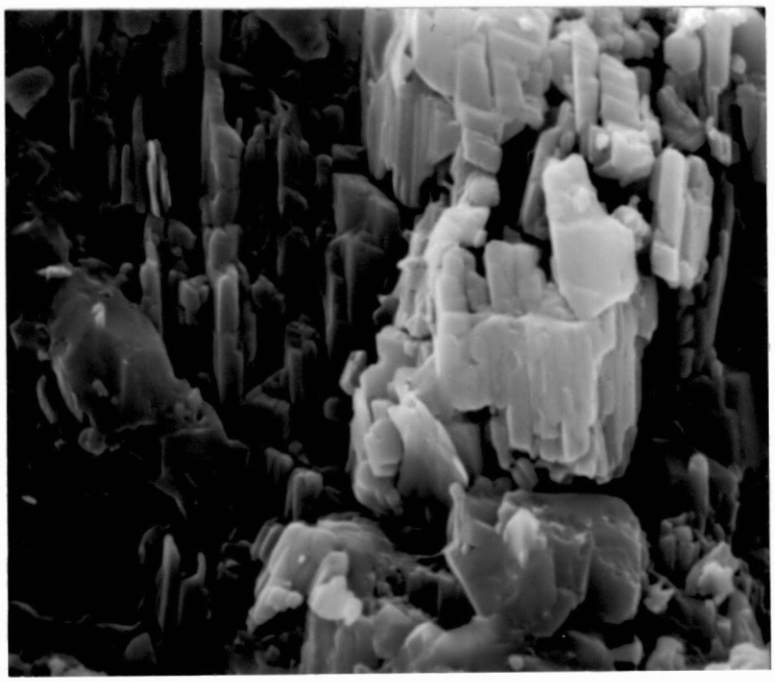

(B)

Figure 81. (A) Photomicrograph of Internal Plagioclase Dissolution (x 400); (B) SEM Photograph of Plagioclase Dissolution (x 6000)

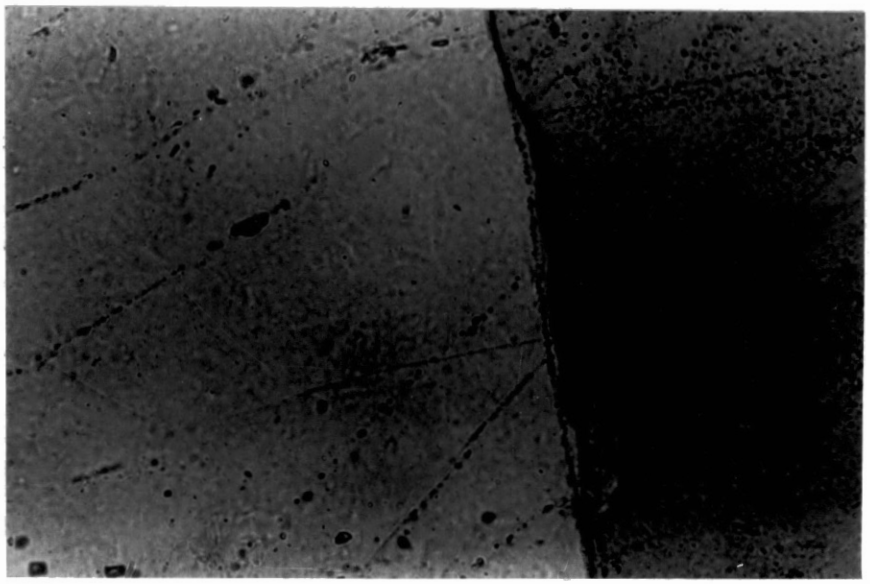

Figure 82. Photomicrograph of Authigenic Quartz Overgrowths. Finely Crystalline Dust rim is Hematite (x 400)

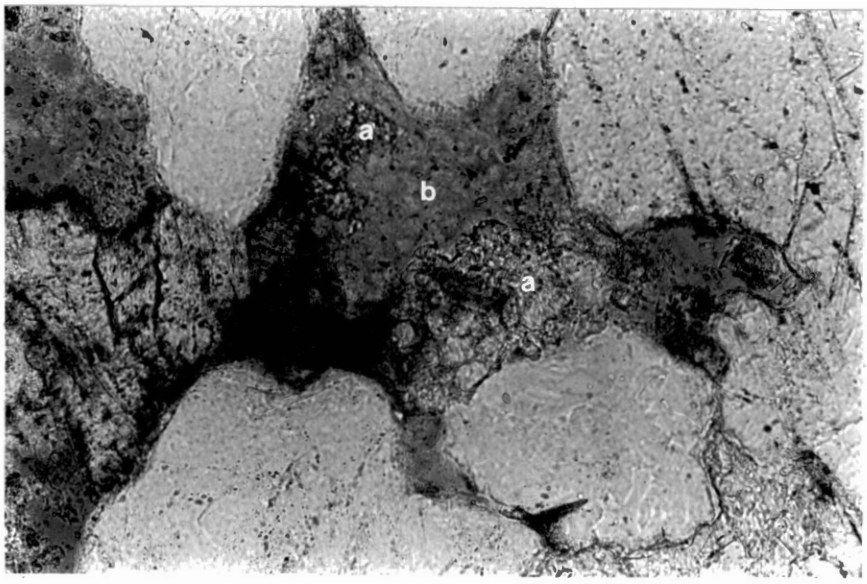

Figure 83. Photomicrograph of Calcite Dissolution (a) Followed by Kaolinite Precipitation (b) (x 200)

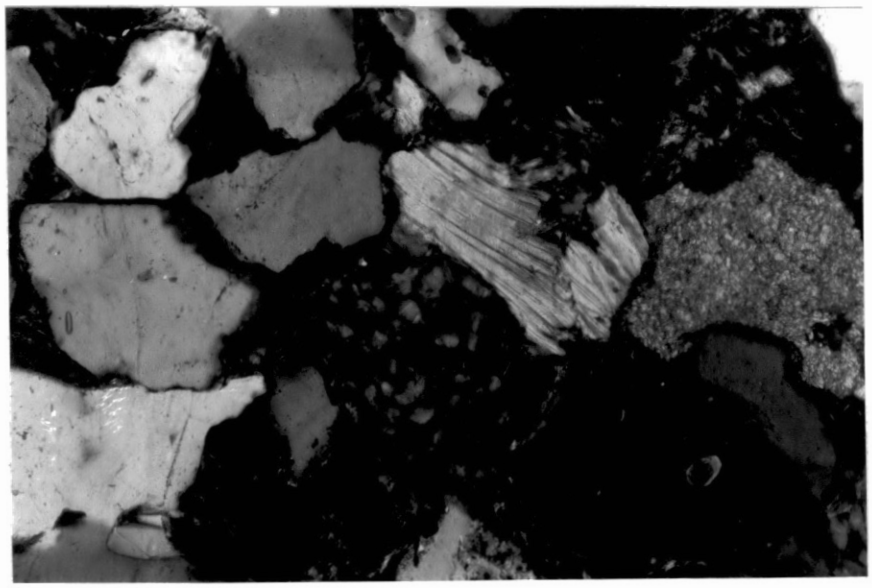

(A)

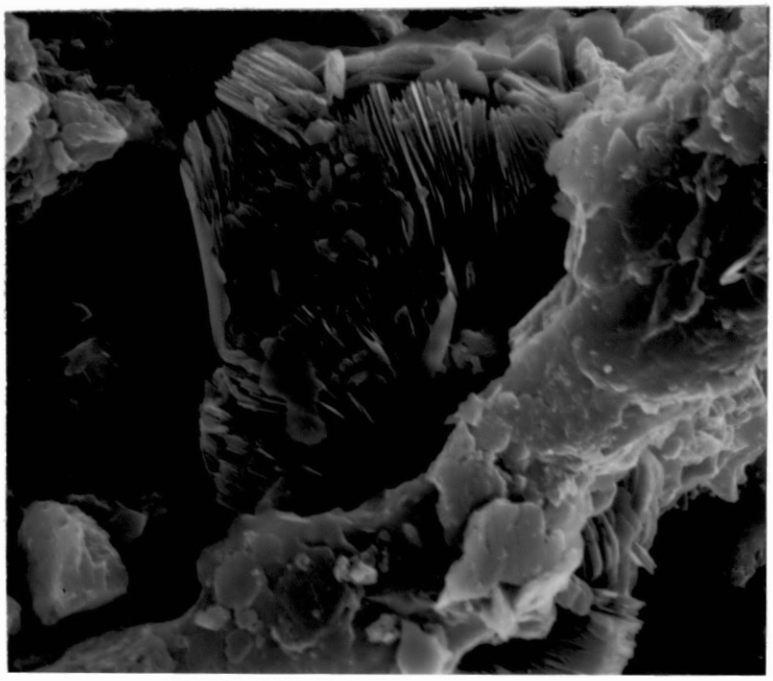

(B)

Figure 84. (A) Photomicrograph of Pore Filling Kaolinite (x 200); (B) SEM Photo of Pore Filling Kaolinite (x 3000)

(A)

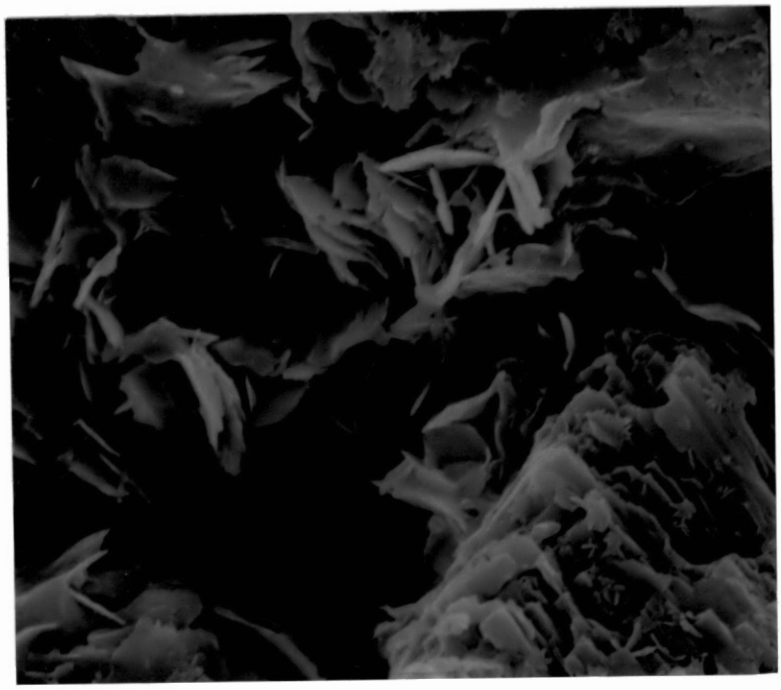

(B)

Figure 85. (A) Photomicrograph of Pore Lining Illite-Smectite (x 400); (B) SEM Photo of Pore Lining Illite-Smectite (x 4200)

late Paleozoic and Mesozoic Eras, and 3) the activity of the Great Glen fault during this period.

Early diagenesis of the M.O.R.S. sediments were probably partially controlled by the variation in Eh-pH which existed in each facies at the time of deposition. In addition, medium-grained sand deposits were subjected to diagenesis as a result of the transgression of Orcadian lakes. These transgressions resulted in stagnant ground waters and led to the development of shallower levels of reduced acidic pore fluids which affected all the Middle O.R.S. facies. Orcadian Basin lake level highs formed in response to moist climatic conditions which persisted periodically throughout the Middle Devonian (Donovan, 1975).

During the Upper Devonian, semi-arid climatic conditions persisted throughout the Orcadian Basin (Donovan, 1981). The presence of calcretes in the U.O.R.S. section at meters 277 and 280 (Figure 86) attests to the semi-arid nature of the climate. Early diagenesis took place in an oxidative environment with significantly lowered water tables throughout the U.O.R.S. section.

The post-Devonian depositional history of the Orcadian Basin is difficult to ascertain because post-Devonian exposures are scanty. Carboniferous units are absent in the Orcadian Basin; however, because of the lack of biostratigraphic control near the top of the U.O.R.S., various workers have suggested that the uppermost U.O.R.S. may actually be of a lower carboniferous vintage (personal communication, R. N. Donovan, 1983).

Arid conditions persisted throughout Great Britain in Permo-Triassic times (Anderson et al., 1979). In the area of the Orcadian Basin, Permo-Triassic arid conditions are indicated by aeolian

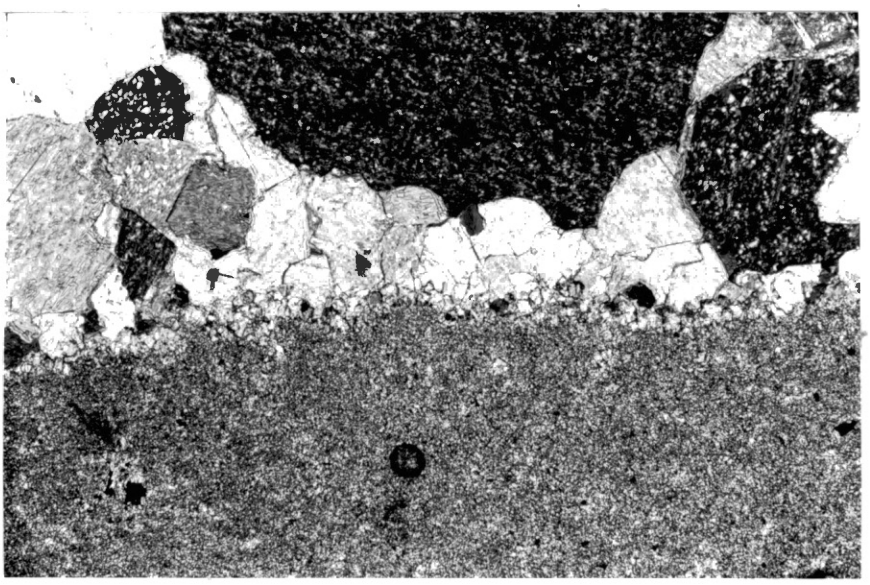

Figure 86. Photomicrograph of Calcrete With Subsequent Aggrading Neomorphism (x 100)

sandstones, a conspicuous silcrete, and recrystallization of hematite which formed initially during the Devonian Period (Tarling et al., 1976).

Conclusive evidence for the Jurassic and Cretaceous marine transgressions, which are present throughout much of southern Great Britain, is lacking in the Orcadian Basin. However, faulted exposures and glacial erratics of Jurassic and Cretaceous strata, which are presently exposed around the shores of the Moray Firth, suggest that such transgressions did affect the O.R.S. deposits. Jurassic strata, present on the downthrown side of the Great Glen fault directly offshore of the Tarbat Peninsula, are marine black shales, mudstones and limestones of variable thicknesses; i.e., between 600 and 2000 meters.

During the Mesozoic Era, the Great Glen fault was the locus of large-scale vertical and minor right-lateral movements which contributed to the evolution of the Inner Moray Firth (McQuillin et al., 1982). The Tarbat Peninsula which is presently on the upthrown block of the Great Glen fault, can be considered as a transitional zone which may have been periodically covered by Jurassic and Cretaceous seas (Appendix F).

Paragenetic History

Three distinct early diagenetic imprints were imparted to the M.O.R.S. sequence. These include very fine-grained sandstones and siltstones of red or gray coloration, and fine to medium-grained sandstones of buff coloration. The factors which influenced early diagenesis were the grain size of individual deposits and the local Eh-pH conditions that existed shortly after deposition.

Very fine-grained sands and silts were deposited on flood plains

or in shallow lakes which were laterally adjacent to the active braid tract. These facies commonly contain accumulations of up to five percent leucoxene (an ilmenite alteration product) and biotite. Floodplain deposits were subjected to oxygen-rich early burial conditions and were subsequently reddened by the alteration of biotite and leucoxene to hematite. At present, this is evidenced by hematite pseudomorphs after biotite and leucoxene which are predominant in reddened deposits (Figures 66 and 79). By contrast, lake sequences were subjected to reducing conditions; hence, biotite and leucoxene remained stable.

Buff sandstones are most prominent within the area identified as the active braid tract. Minor amounts of leucoxene and biotite present in these sandstones show only slight reddening. The buff pigmentation of these sandstones was strongly influenced by 1) the paucity of iron-bearing minerals present (less than one percent), and 2) the relatively low Eh values which are thought to have been characteristic of these channel sands. Alternatively, the amount of biotite and leucoxene in buff beds may have been decreased by a previous period of oxidation. However, the paucity of muscovite and translucent heavy minerals in buff beds indicates that micas and heavy minerals were insignificant accessory grains in these deposits. Similar conclusions are postulated by Turner (1974) to account for the drab coloration of channel sands in the Silurian Ringerlike Group of Norway.

Two modes of calcite precipitation are possible in the M.O.R.S. The predominant type, which is most prevalent in red and buff beds, resulted during shallow burial (personal communication, Z. Al-Shaieb, 1983). In lacustrine beds, calcite precipitation wich occurred immediately after deposition was the result of increased carbonate

production by photo-synthesizing algae. Silicate grains in these lacustrine sequences commonly show intense displacive and replacive dissolution fabrics (Figure 87). Similar relationships have been recognized elsewhere in the Orcadian Basin (Donovan, 1975) and in numerous modern lakes (Kelts and Hsu, 1978).

Subsequent diagenesis in the M.O.R.S. has mostly affected the coarse-grained buff beds. Migration of acidic ground water through red and gray beds was inhibited by their finer grain sizes. This condition is best exemplified in heterolithic (fine to medium sand and silt) beds where sandy zones have suffered secondary reduction, but silty zones have remained (Figure 88).

Early paragenesis in the U.O.R.S. is dominated (as previously noted in the M.O.R.S.) by the precipitation of hematite and calcite. Minor amounts of authegenic silica also precipited as quartz overgrwoths, chert, and chalcedony.

Hematite genesis in the U.O.R.S. is controlled principally by the presence or absence of mudstone intraclasts or a detrital mud matrix. Samples which are comprised of two percent or greater of either constituent are generally red. Mudstone intraclasts were probably reworked from U.O.R.S. floodplains (personal communication, R. N. Donovan, 1983). Detrital clays may have been infiltrated into coarser frameworks by aeolian or fluvial processes. Biotite and leucoxene, which occur in very minor amounts throughout the sequence, generally did not provide significant amounts of iron for hematite formation.

Calcite precipitation and silicate dissolution took place during shallow burial. Subsequent diagenesis, which was dominated by calcite dissolution and authigenic clay precipitation, occurred in both red and

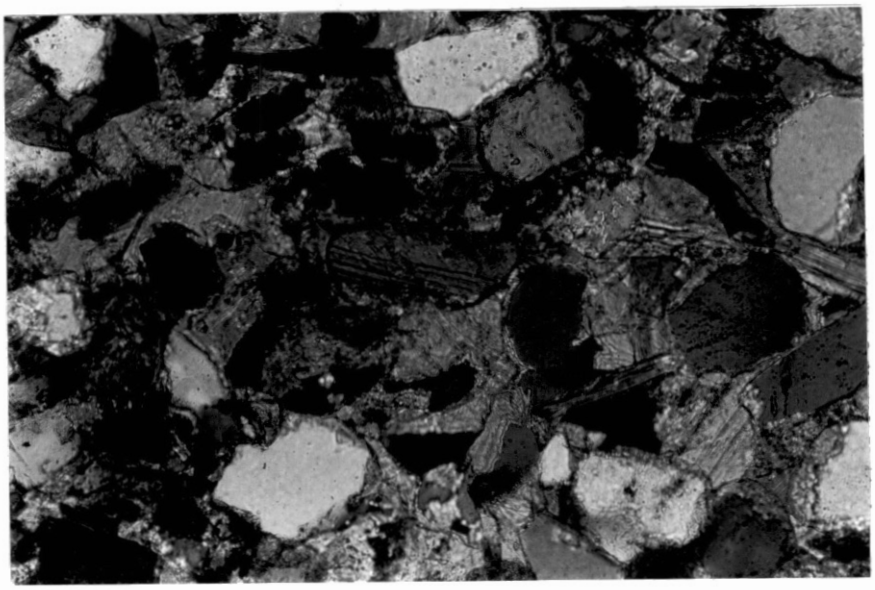

Figure 87. Photomicrograph of Displacive and Replacive Calcite Cement Which is Typical in Lacustrine Sequences

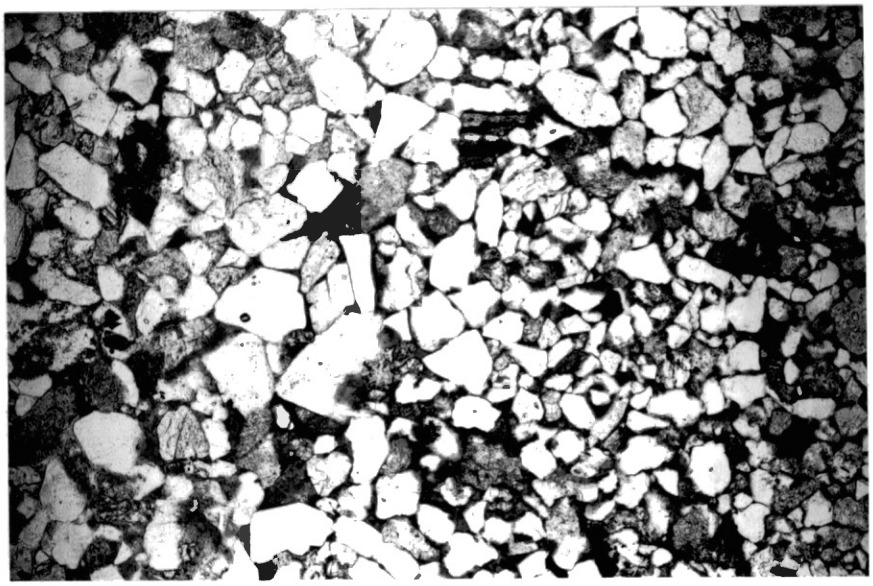

Figure 88. Grain Size Control of Late-Stage Diagenesis in the M.O.R.S. (Coarser-grained fraction [left] has been subsequently reduced while finer-grained fraction [right] has remained [x 40] .)

buff pigmented lithologies.

Late diagenesis in both the M.O.R.S. and in the U.O.R.S. involved primarily the dissolution of calcite, followed by the precipitation of authigenic kaolinite, illite, and chlorite. Kaolinite, which forms most commonly in intergranular pores which were previously occupied by calcite, averages 4.4 percent in the U.O.R.S. and 0.91 percent in the M.O.R.S. Individual kaolinite booklets of up to 0.30 millimeters were noted in the U.O.R.S. Illite-smectite forms predominately as pore lining textures; however, pore filling and pseudomorphic (after lithic fragments and feldspars) textures are also common. Illite-smectite may comprise up to 2.5 percent of buff samples in the M.O.R.S. Authigenic chlorite occurs in trace amounts throughout the study area. Its most common textural form is as surface coats on kaolinite crystals and mud fragments.

X-ray diffraction analysis confirms the previously discussed petrographic observations. In the U.O.R.S., kaolinite (Figures 89 and 90) is more abundant than illite-smectite. In the M.O.R.S., illite-smectite (Figures 91 and 92) becomes more prominent while the abundance of kaolinite decreases relative to the U.O.R.S. The occurrence of mixed-layer illite-smectite (Figures 91 and 92) indicates that original detrital matrices may have been recrystallized. Chlorite (Figure 92) is a very minor authigenic constituent in both the M.O.R.S. and the U.O.R.S.

The physical conditions which were necessary to facilitate the late stage paragenesis in the M.O.R.S. and the U.O.R.S. are as follows: 1) slightly acidic pH values of pore waters will favor the dissolution of calcite and precipitation of kaolinite in the near surface environment (personal communication, Al-Shaieb, 1983; Blatt, 1979).

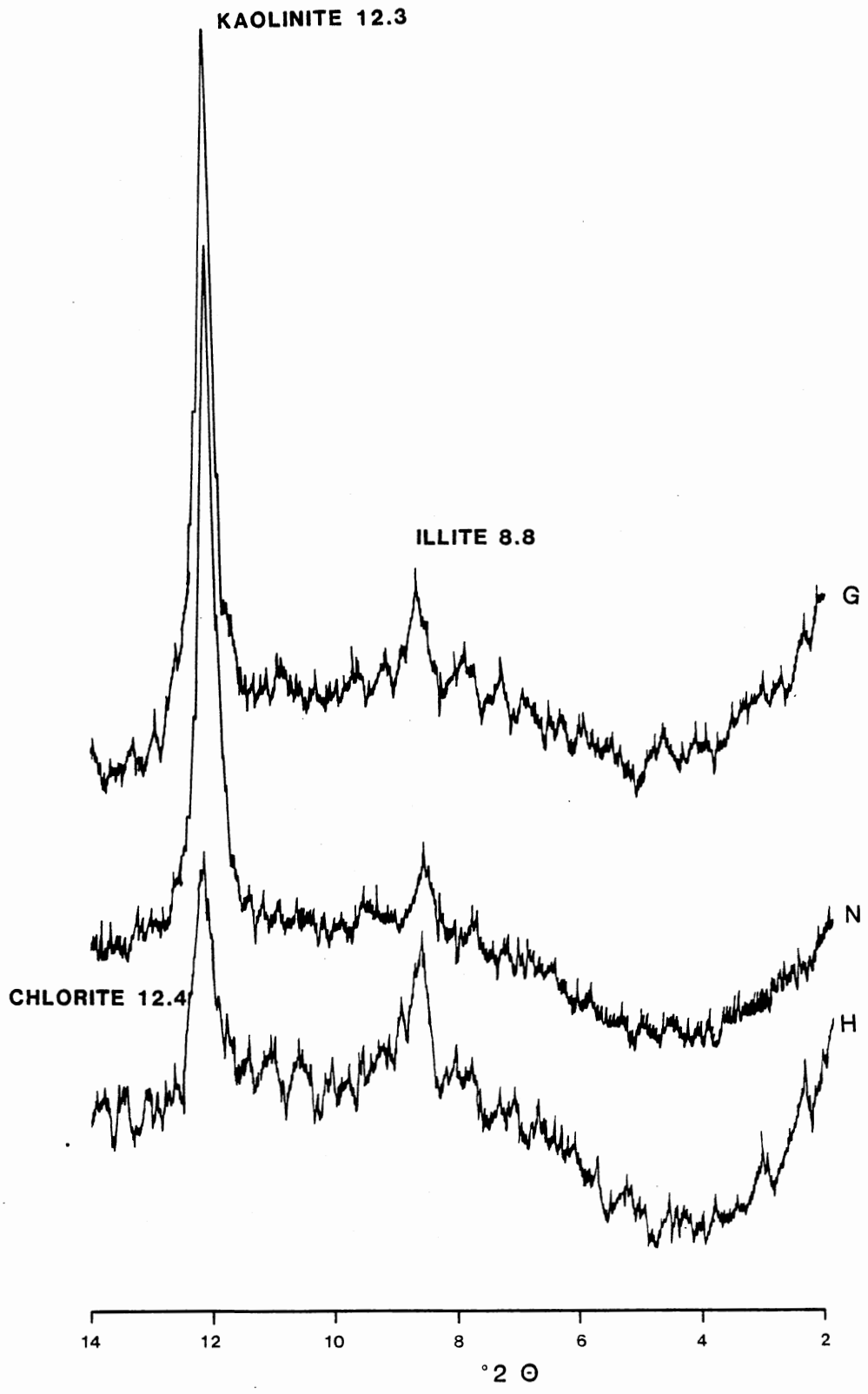

Figure 89. X-ray Diffraction Diagram of a Buff U.O.R.S. Sample

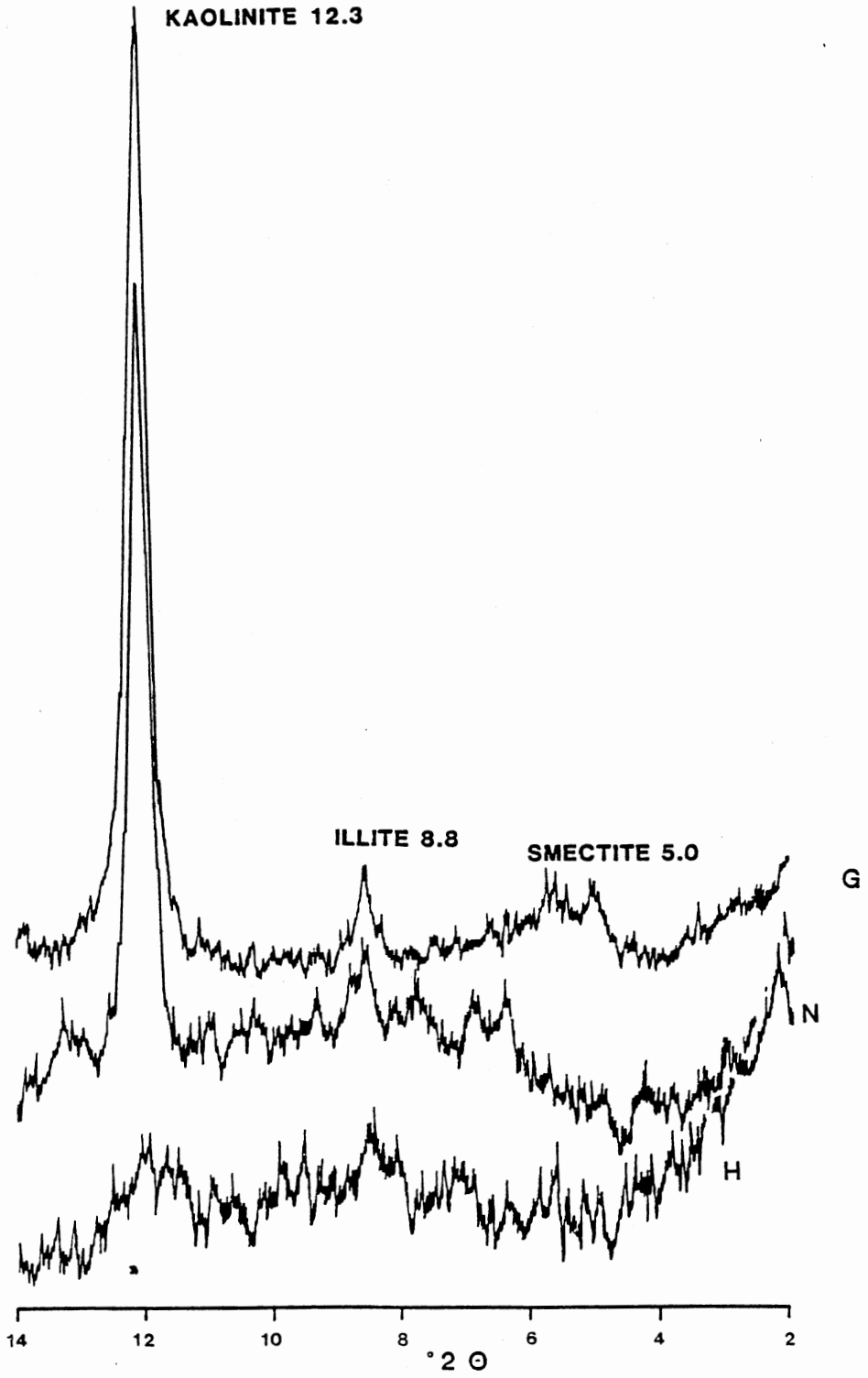

Figure 90. X-ray Diffraction Diagram of a Red U.O.R.S. Sample

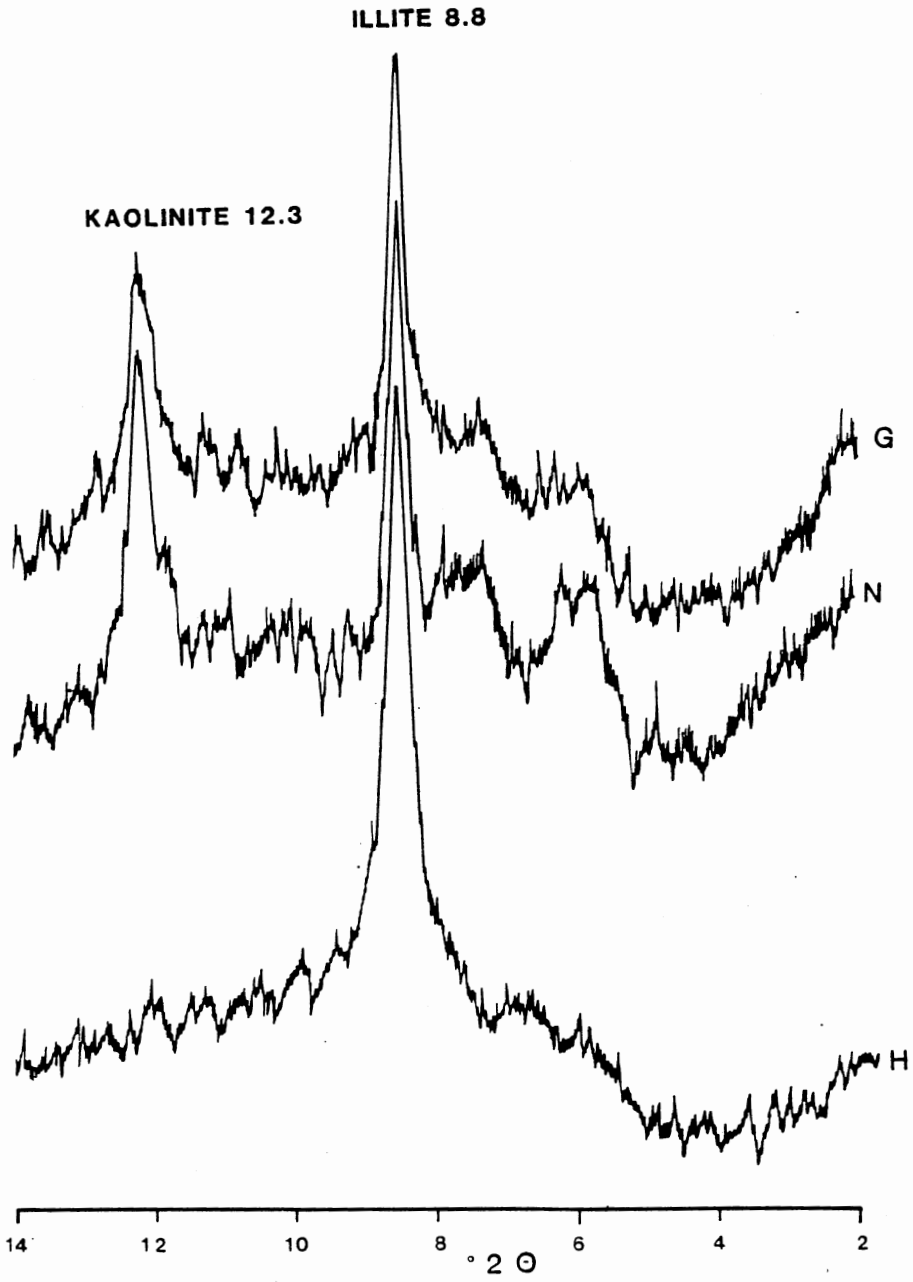

Figure 91. X-ray Diffraction Diagram of a M.O.R.S. Buff Sample

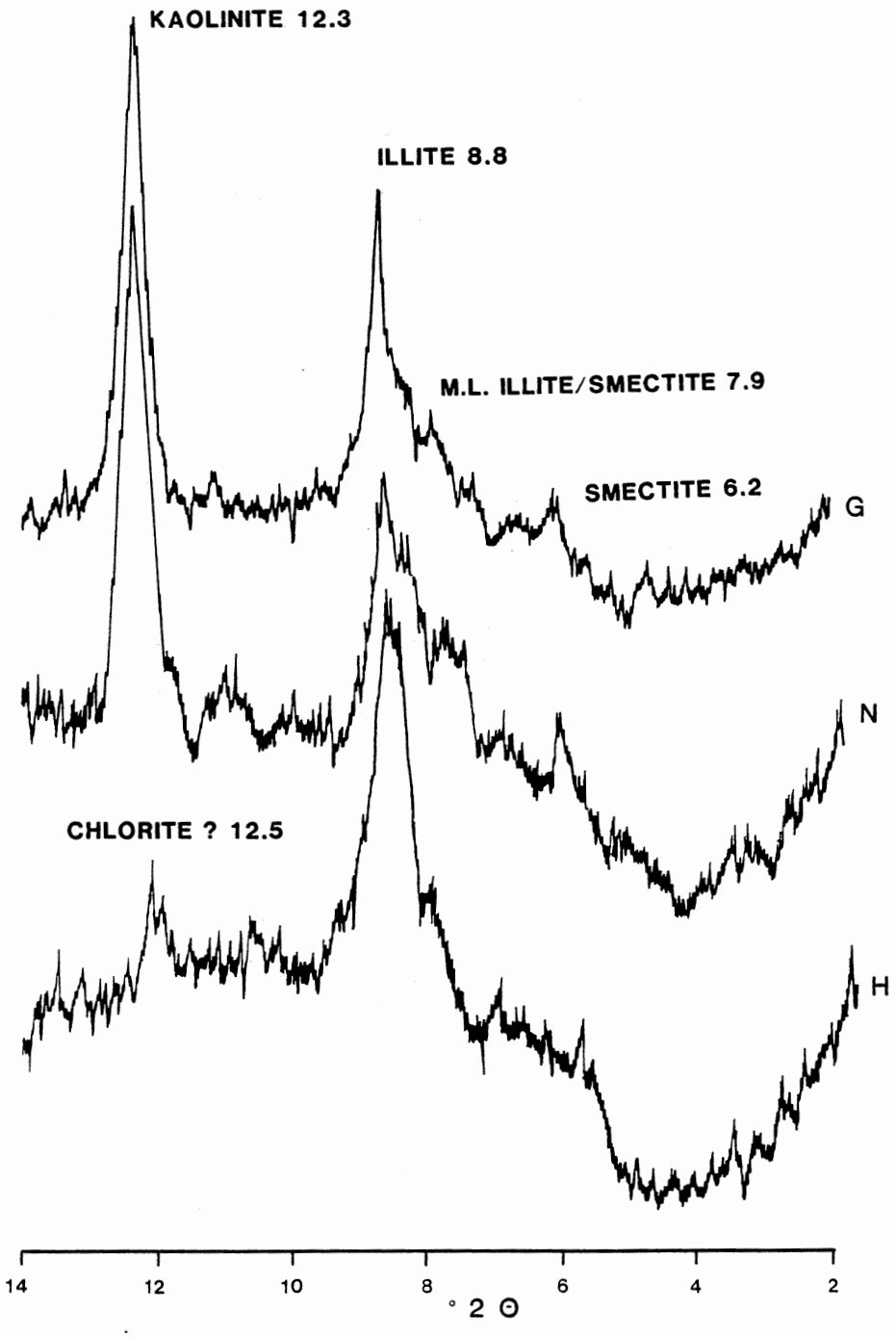

Figure 92. X-ray Diffraction Diagram of M.O.R.S. Gray Sample Which Contains a Recrystallized Detrital Matrix

Specifically, kaolinite will be stable in the pH range between 5.1 and 8.3 (Shelton, 1964); 2) illite and smectite and chlorite will commonly form in the subsurface as a result of elevated temperatures during burial. With increasing burial of Gulf Coast Wilcox Sandstones, Boles and Franks (1978) reported that authegenic illite-smectite and the chlorite became more prominent; 3) pore waters which contain sufficient amounts of silica, alumina, potassium, iron, magnesium, and calcium are essential to promote authigenic clay precipitation.

It is obvious that a diagenetic model to account for the late-stage paragenesis of the Tarbat Peninsula section involves consideration of both near surface and subsurface conditions. Examination of depositional and tectonic parameters which may have existed within the study area suggests that late-stage paragenesis may have occurred in 1) the Devonian Period; 2) Permo-Triassic through early Jurassic time, or 3) late Jurassic through early Cretaceous time.

During the Devonian Period, calcite dissolution in the M.O.R.S. could have resulted from large-scale lake transgressions which would have produced reduced and slightly acidic ground waters in M.O.R.S. deposits. The migration of slightly acidic meteoric waters may have also caused calcite dissolution in the U.O.R.S. Sufficient alumina and silica would have been present from the initial dissolution of detrital constituents to promote kaolinite precipitation. As deposition proceeded, burial of sediment to depths of up to 1300 meters (Armstrong, 1977) would have provided the necessary increase in temperature to precipitate illite-smectite and minor amounts of chlorite.

In Permo-Triassic times, a long period of continental weathering and drastically lowered ground water tables could have caused calcite

dissolution and kaolinite precipitation. A subsequent marine incursion during the Jurassic period could have provided the necessary burial depths and sufficient chemical and thermal gradients to promote the precipitation of illite-smectite and chlorite in the subsurface.

Based on the fact that Upper Jurassic to Lower Cretaceous spores have been identified in the M.O.R.S. (Appendix F), there is a distinct possibility that O.R.S. sediments in the study area were at or near the surface at this time. If a Cretaceous transgression did cover the study area, the same late-stage paragenetic sequence could have resulted.

A difficulty with the generation of late-stage paragenesis in any time other than the Devonian is the ultimate destination of ground waters rich in silica, alumina, etc. which resulted from early dissolution of detrital grains. In the U.O.R.S., sufficient depositional gradients may have existed to promote large-scale groundwater migration toward the center of the Orcadian Basin (personal communication, R. N. Donovan, 1983). During the middle Devonian, large-scale transgressions and regressions of Orcadian lakes may have periodically flushed the M.O.R.S. chemical system. Ultimately, late-stage paragenesis in the study area may have been subjected to several periods of diagenetic modification.

CHAPTER XI

SUMMARY AND CONCLUSIONS

The objectives of this study which investigates the Middle and Upper O.R.S. located along the Tarbat Peninsula in northern Scotland are 1) the interpretation of depositional environments and depositional facies; 2) the interpretation of allocyclic controls on sedimentation; 3) petrographic studies of provenance, red bed genesis and paragenesis, and 4) description of minor structures and interpretation of their relationship to the Great Glen fault.

The results of this study are as follows:

1. Facies relationships indicate that M.O.R.S. and U.O.R.S. sediments were deposited in braided river systms. Prominent features in the M.O.R.S. fluvial system included channel bases, dunes, transverse bars, megaripples, flood deposits, floodplain sequences and lacustrine sequences. The U.O.R.S. fluvial system was dominated by channel bases and dunes.

2. Fluctuations in the lake level of the Orcadian Basin are the allocyclic controls which influenced the pattern of M.O.R.S. deposition. Periods of high lake level (i.e., high base level) led to alluviation and the development of lacustrine and low energy floodplain deposits. Periods of low lake level (i.e., low base level) resulted in widespread fluvial channel incision marked by erosive bases, large-scale bedforms, poorly developed fine sequences

and moderately cyclic fluvial sequences.

Stream floods occurred in equal amounts during periods of high and low lake levels. Rapid runoff rates in upland areas (which were scantily vegetated in the Devonian Period) enhanced the development of stream flooding.

3. U.O.R.S. deposits record a marked increase in the magnitude of fluvial processes over their M.O.R.S. counterparts. This relationship is best evidenced by a) bed thicknesses which average between one and two meters; b) a predominance of coarse-grained sandstones, and c) the ubiquity of large-scale trough cross-bedding. Furthermore, U.O.R.S. deposits show little evidence for reduced discharge rates; i.e., small-scale bedforms and planar-tabular cross-bedding are poorly developed throughout the U.O.R.S. section. The evidence of more vigorous stream behavior in the U.O.R.S. fluvial system when compared with the M.O.R.S. fluvial system may reflect a maximum lowering of base level and renewed uplift of the Caledonian orogen during the Upper Devonian.

4. Paleocurrent analysis indicates that the M.O.R.S. river system flowed toward the northeast and the U.O.R.S. fluvial system flowed toward the northwest. However, a northwest paleocurrent orientation also became prominent in the M.O.R.S. during the late Middle Denovian.

5. The primary sediment source of the Middle and Upper O.R.S. was the dissected Caledonian orogen. However, an upsection increase in quartz to feldspar ratios in both the M.O.R.S. and in the U.O.R.S. suggests that recycling of former O.R.S. deposits may have become prominent as deposition proceeded. At meter 140 of the M.O.R.S.

quartz to feldspar ratios decrease in conjunction with a M.O.R.S. paleocurrent change from northeast to northwest. This relationship suggests that renewed uplift of the present day Grampian Highlands may have occurred in the late Middle Devonian.

6. Early diagenesis in both the M.O.R.S. and the U.O.R.S. involved the dissolution of detrital silicate grains, the precipitation of hematite and calcite, and the minor precipitation of silica. Reddening of the M.O.R.S. occurred in oxygenated floodplain deposits which contained an abundance of iron-bearing accessory minerals; sp. biotite and leucoxene. In the U.O.R.S., reddening occurred in beds which contained mudstone intraclasts and primary detrital matrices.

Late stage diagenesis which involved the dissolution of calcite and the precipitation of authigenic kaolinite, illite-smectite and chlorite may have occurred in a) the Devonian Period, b) Permo-Triassic through early Jurassic times, or c) late Jurassic through early Cretaceous times.

7. Structural analysis of the study area suggests that the Great Glen fault was subjected to modest right-lateral dislocation in post-Devonian times. The plunge of small-scale en echelon folds to the south and southwest, and the means of Reidel fractures (052) and conjugate Reidel fractures (316) are compatible with right lateral dislocation.

8. The M.O.R.S.-U.O.R.S. contact has been interpreted to be obscured by a minor fault located 0.5 kilometers south of Wilkhaven Pier (Armstrong, 1973). This interpretation is problematical; sequences on both sides of the fault show a predominance of large-

scale trough cross-bedding, and are mostly medium-grained sandstones. However, there is a predominance of red coloration in the U.O.R.S. as opposed to buff coloration in the M.O.R.S., and furthermore, there is a significant difference in quartz to feldspar ratios between M.O.R.S. sandstones (5.8) and U.O.R.S. sandstones (12.7) collected near the faulted contact. The U.O.R.S. ratio, however, is atypical. In spite of these local differences, there are regional similarities between the U.O.R.S. section and the upper portion of the M.O.R.S. section. Specifically, both sections show a northwest paleoflow orientation and generally low quartz to feldspar ratios. These relationships imply a similar provenance for the upper portion of the M.O.R.S. and the U.O.R.S. which may have resulted from renewed uplift of the Devonian Grampian Highlands.

Sufficient similarities exist between the U.O.R.S. and the upper portion of the M.O.R.S. to warrant further investigation as to the nature of the M.O.R.S-U.O.R.S. contact. This is significant, as it is the only place in northern Scotland where this type of investigation is possible. Specifically, a detailed petrographic examination is recommended. A possible position for a lithostratigraphic boundary revision could be at meter 231, where the first incoming of conglomerates in the U.O.R.S. was observed.

BIBLIOGRAPHY

Adamack, J. A. 1963. The Water Vapor Content of the Martian Atmosphere as a Problem of Chemical Equilibrium: Plant Space Sci., Vol. 11, pp. 355-359.

Al Shaieb, Z. 1983. Personal Communication, Oklahoma State University.

Allan, D. A. 1940. The Geology of the Highland Border from Glen Almond to Glen Artny: Trans. Roy. Soc. Edinb., Vol. 60, pp. 171-193.

Allen, J. R. L. 1963. The Classification of Cross-stratified Units with Notes on Their Origin: Sedimentology, Vol. 2, pp. 93-114.

_____. 1964. Studies in Fluvatile Sedimentation: Six Cyclothems from the Lower Old Red Sandstone: Vol. 3, pp. 163-198.

_____. 1965c. A Review of the Origin and Characteristics of Recent Alluvial Sediments: Sedimentology, Vol. 5, pp. 89-191.

_____. 1966. On Bedforms and Paleocurrents: Sedimentology, Vol. 6, pp. 153-190.

_____. 1970a. Studies in Fluvatile Sedimentation: A Comparison of Fining Upward Cyclothems with Special Reference to Coarse-Member Composition and Interpretation: J. Sediment. Pet., Vol. 40, pp. 298-323.

_____. 1977. The Possible Mechanics of Convolute Lamination in Graded Sand Beds: J. Geol. Soc. Lond., Vol. 134, pp. 19-31.

Anderton, R., Bridges, P. H., Leeder, P. H., and Sellwood, B. W. 1979. A Dynamic Stratigraphy of the British Isles; A Study in Crustal Evolution: London, England: George Allen and Unwin Publishers.

Armstrong, M., and Harris, A. L. 1973. Institute of Geological Sciences (United Kingdom), Scotland Sheet 94, Solid Edition.

Armstrong, M. 1977. The Old Red Sandstone of Easter Ross and the Black Isle. In The Moray Firth Area Geological Studies. Inverness, Scotland: John G. Eccles Printers, Ltd.

Asquith, G. B., and Cramer, S. L. 1975. Transverse Braid Bars in the Upper Triassic. Trajillo Sandstone of the Texas Panhandle: J. Geol., Vol. 83, pp. 657-661 .

Barany, R. 1965. Heat of Formation of Geothite, Ferrous Vanadate, and Maganese Molybdate: U. S. Bureau of Mines, Report of Investigation 6618, p. 10.

Barrell, J. 1908. Relations Between Climate and Terrestrial Climate: J. Geol., Vol. 16, pp. 255-295.

Bass-Becking, L. G. M., Kaplan, I. R., and Moore D. 1960. Limits of the Natural Environment in Terms of pH and Oxidation-Reduction Potentials: J. Geol., Vol. 68, pp. 243-284.

Berner, R. A. 1969. Geothite Stability and the Origin of Red Beds: Geochemica et Cosmochimica Acta, Vol. 33, pp. 267-273.

Blatt, H. 1967. Original Characteristics of Clastic Quartz Grains: J. Sediment. Pet., Vol. 37, pp. 401-424.

_____. 1979. Diagenetic Processes in Sandstones: In P. A. Scholle and P. R. Schluger (Editors), Aspects of Diagenesis, Soc. Econ. Paleon. Mineral., Spec. Pub., No. 26, pp. 141-157.

Boles, J. R., and Franks, S. G. 1978. Clay Diagenesis in Wilcox Sandstones of Southwest Texas: Implications of Smectite Diagenesis on Sandstone Cementation: J. Sediment. Pet., Vol. 49, pp. 0055-0070.

Bootroyd, J. C., and Ashley, G. M. 1975. Process, Bar Morphology, and Sedimentary Structures on Braided Outwash Fans, Northeastern Gulf of Alaska: In A. V. Jopling and B. C. McDonald (Editors), Glaciofluvial and Glaciolacustrine Sedimentation, Soc. Econ. Paleon. Minerl., Spec. Pub., No. 23, pp. 193-222.

Bull, W. B. 1972. Recognition of Alluvial Fan Deposits in the Stratigraphic Record: In K. J. Rigby and W. K. Hamblin (Editors), Recognition of Ancient Sedimentary Environments, Soc. Econ. Paleon. Mineral., Spec. Pub., No. 16, pp. 68-83.

Cant, D. J., and Walker R. G. 1976. Development of a Braided Fluvial Facies Model for the Devonian Battery Point Sandstone, Quebec: Can. J. E. Sci., Vol. 13, pp. 102-119.

_____. 1978. Fluvial Processes and Facies Sequences in the Sandy Braided South Saskatchewan River, Canada: Sedimentology, Vol. 25, pp. 625-648.

Carroll, D. 1958. Role of Clay Minerals in the Transportation of Iron: Geochemica et Cosmochimica Acta, Vol. 14, pp. 1-27.

Chein, N. 1951. The Braided Stream of the Lower Yellow River: Scientia Sinica, Vol. 10, pp. 734-754.

Coleman, J. M. 1969. Brahmaputra River: Channel Processes and Sedimentation: Sediment. Geol., Vol. 3, pp. 129-239.

Collinson, J. D. 1980. Alluvial Sediments: In H. G. Reading (Editor) Sedimentary Environments and Facies: New York, N. Y.: Elsevier North-Hubbard, Inc.

Cooke, F. A., Brown, L. D., and Oliver, J. E. 1980. The Southern Appalachians and the Growth of Continents: Scientific American, October, pp. 157-168.

Crampton, C. B., and Carruthers, R. G. 1914. The Geology of Caithness: Mem. Geol. Surv. Scotl.

Cruickshank, G., and Ferraro, T. E. 1980. Paleoenvironments of the Chemung Formation near Elkins, West Virginia: Unpublished, pp. 1-14.

Daws, J. W. 1948. On the Coloring Matter of Red Sandstones and of Grayish and White Beds Associated with Them: Quar. J. Geol. Soc. Lond., pp. 25-30.

Donovan, R. M., Foster, R. J., and Westoll, T. S. 1974. A Stratigraphical Revision of the Old Red Sandstone of Northeastern Caithness: Trans. Roy. Soc. Edinb., Vol. 69, pp. 171-205.

Donovan, R. N. 1975. Middle Devonian Limestones Developed at the Margin of the Orcadian Basin, Caithness: J. Geol. Soc. Lond., Vol. 131, pp. 489-510.

Donovan, R. N., Archer, R., Turner, P., and Tarling, D. H. 1976. Devonian Paleogeography of the Orcadian Basin and the Great Glen Fault: Nature, Vol. 259, pp. 550-551.

Donovan, R. N., and Collins, A. 1977. The Age of Two Old Red Sandstone Sequences in Southern Caithness, Scotland: Scot. Jour. Geol., Vol. 12, pp. 53-57.

_____. 1978. Mound Structures From the Caithness Flagstones (Middle Devonian), Northern Scotland: J. Sediment. Pet., Vol. 48, pp. 171-174.

Donovan, R. N. 1979. Georoots, Scotland: A.A.P.G. Pub., Tulsa, Oklahoma.

_____. 1980. Lacustrine Cycles, Fish Ecology and Stratigraphic Zonation in the Middle Devonian of Caithness: Scot. Jour. Geol., Vol. 16, pp. 35-50.

_____. 1981. Devonian Calcretes (Cornstones) Near Tain: Scot. Jour. Geol., Vol. 18, pp. 125-129.

Donovan, R. N., and Meyerhoff, A. A. 1982. Comments and Reply on "Paleomagnetic Evidence for a Large (~2000 km) Sinistral Offset Along the Great Glen Fault During Carboniferous Time," Geology, Vol. 10, pp. 583-589.

Donovan, R. M., and Ferraro, T. E. 1982. Recycling of Siliclastics in Continental Settings: In R. N. Donovan (Editor), The Selenite Blade, Stillwater: Oklahoma State University, Vol. 1, pp. 83-101.

Donovan, R. N. 1982. Personal Communication, Oklahoma State University.

_____. 1983. Personal Communication, Oklahoma State University.

_____. 1983. Georoots, Scotland: An Examination of the Origins of Geologic Thought. Tulsa, Oklahoma: AAPG, Pub.

Donovan, R. N., and Ferraro, T. E. 1983. Post Devonian Right-Lateral Movement on the Great Glen Fault, Nature (recently submitted).

Dott, R. H. Jr. 1973. Paleocurrent Analysis of Trough Cross-Stratification: J. Sediment. Pet., Vol. 43, pp. 779-783.

Dzulynski, S., and Smith, A. J. 1963. Convolute Lamination, Its Origin, Preservation, and Directional Significance: J. Sediment. Pet., Vol. 33, pp. 616-627.

Fannin, N. G. T. 1969. Stromatolites from the Middle Old Red Sandstone of Western Orkney: Geol. Mag., Vol. 106, pp. 77-88.

Fettes, D. J., and Chesher, J. A. 1977. Institute of Geological Sciences (United Kingdom), Sheet 57N 04W.

Flinn, D. 1961. Continuation of the Great Glen Fault Beyond the Moray Firth: Nature, Vol. 191, pp. 589-591.

Folk, R. L. 1974. Petrology of Sedimentary Rocks. Austin, Texas: Hemphill Publishing Company.

Goddard, E. N., Trask, P. D., DeFord, R. K., Rove, O. N., Singewald, J. F. Jr., and Overbeck, M. 1963. The Rock Color Chart. Netherlands: Huyskes-Enschede.

Habicht, T. K. A. 1979. Paleoclimate, Paleomagnetism, and Continental Drift: A.A.P.G. Studies in Geol., No. 9.

Harbaugh, J. W., and Bonham-Carter, G. 1970. Computer Simulation in Geology. New York: Wiley-Interscience.

Harms, J. C, MacKenzie, D. B., and McCubbin, D. G. 1963. Stratification in Modern Sands of the Red River, Louisiana: Jour. Geol. Vol. 71, pp. 566-580.

Harms, J. C., Southard, J. B., Spearing, D. R., and Walker, R. G. 1975. Depositional Environments as Interpreted from Primary Structures and Stratification Sequences. Dallas, Texas: Soc. Econ. Paleon. Minerl., Short Course 2.

Hendry, H. E., and Stauffer, M. R. 1975. Penecontemporaneous Recumbent Folds in Trough Cross-Bedding of Pleistocene Sands in Saskatchewan, Canada: J. Sediment. Pet., Vol. 45, pp. 932-943.

Heward, A. P. 1978. Alluvial Fan Sequence and Megasequence Models: With Examples From Westphalian D-Stephanian B. Coalfields, Northern Spain: In A. D. Miali (Editor), Fluvial Sedimentology, Can. Soc. Petrol. Geol., Mem. 5, pp. 669-702.

Hooke, R. Le B. 1967. Processes on Arid Region Alluvial Fans: Jour. Geol., Vol. 75, pp. 438-460.

Hubert, J. F., and Reed, A. A. 1978. Red-Bed Diagenesis in the East Berlin Formation, Neward Group, Connecticut Valley: Vol. 48, pp. 175-184.

House, M. R., Richardson, J. B., Chaloner, W. G., Allen, J. R. L., Holland, C. H., and Westoll, T. S. 1977. A Correlation of Devonian Rocks in the British Isles: Geol. Soc. Lond., Special Report No. 7.

Kelts, K., and Hsu, K. J. 1978. Freshwater Carbonate Precipitation. In Lerman, A. (Editor), Lakes, Chemistry, Geology, Physics. New York: Springer Verlag.

Kerr, P. F. 1977. Optical Mineralogy. New York, N. Y.: McGraw-Hill Book Company.

Krauskopf, K. B. 1979. Introduction to Geochemistry. New York: McGraw-Hill Book Company.

Krumbein, W. C. 1967. Fortran IV Computer Programs for Markov Chain Experiments in Geology: Computer Contr. Geol. Surv. Kansas, Vol. 13.

Krynine, P. D. 1949. Origin of Red Beds: Trans. New York Acad. Sci., Ser. II, Vol. 2, pp. 60-68.

Larson, E. E., and Walker, T. R. 1976. Development of Chemical Remanent Magnetism in Late Cenozoic Sediments, Baja, California: Geol. Soc. Am. Bull, Vol. 86, pp. 639-650.

Leeder, M. R. 1982. Upper Paleozoic Basins of the British Isles-Caledonide Inheritance versus Hercynian Plate Margin Processes: Jour. Geol. Soc. Lond., Vol. 139, pp. 479-491.

Leopold, L. B., and Wilman, M. G. 1957. River Channel Patterns, Braided, Meandering and Straight: U. S. Geol. Surv., Prof. Pap. 282-B.

Mardia, K. V. 1972. Statistics of Directional Data. New York: Academic Press.

McGregor, D. C. 1983. Personal Communication, Oklahoma State University.

McKee, E. D., Crosby, E. J., and Berryhill, H. L. 1967. Flood Deposits Bijou Creek, Colorado: J. Sediment. Pet., Vol. 37, pp. 829-851.

McQuillin, R., Donato, J. A., and Tulstrup, J. 1982. Development of Basins in the Inner Moray Firth and the North Sea by Crustal Extension and Dextral Displacement of the Great Glen Fault: Earth and Plan. Sci. Lett., Vol. 60, pp. 127-139.

Miall, A. D. 1973. Markov Chain Analysis Applied to an Ancient Alluvial Plain Succession: Sedimentology, Vol. 20, pp. 347-364.

_____. 1974. Paleocurrent Analysis of Alluvial Sediments - A Discussion of Directional Variance and Vector Magnitude: J. Sediment. Pet., Vol. 44, pp. 1174-1185.

_____. 1977. A Review of the Braided River Depositional Environment: Eart Sci. Reviews, Vol. 13, pp. 1-62.

_____. 1978a. Lithofacies Types and Vertical Profile Models in Braided Rivers: A Summary: In A. D. Miall (Editor), Fluvial Sedimentology, Can. Soc. Petrol. Geol., Mem. 5, pp. 597-604.

_____. 1982. Analysis of Fluvial Depositional Systems: A.A.P.G. Bookstore, Tulsa, Oklahoma.

Miles, R. S., and Westoll, T. S. 1963. Two New Genera of Coccosteid Arthrodira From the Middle Old Red Sandstone of Scotland, and Their Stratigraphical Distribution: Trans. R. Soc. Edinb., Vol. 65, pp. 179-210.

_____. 1968. The Placoderm Fish Coccosteus Cuspidatus Miller ex Agassiz From the Middle Old Red Sandstone of Scotland. Part 1: Trans. R. Soc. Edinb., Vol. 67, pp. 179-210.

Miller, D. M., and Folk, R. L. 1955. Occurrence of Detrital Magnetite and Illmenite in Red Sediments: New Approach to the Significance of Red Beds: A.A.P.G. Bull., Vol. 39, pp. 338-345.

Miller, H. Jr. 1889. Institute for Geological Sciences (United Kingdom), Scotland Sheet 94; Ross, Cromarty and Surtherland.

Mykura, W. 1976. Orkney and Shetland: Brit. Reg. Geol., H.M.S.O., London, England.

_____. 1983. The Old Red Sandstone East of Loch Ness, Inverness-shire: Ins. Geol. Sci., No. 82/13, pp. 1-26.

Potter, P. E., and Pettijohn, F. J. 1977. Paleocurrents and Basin Analysis: New York: Springer-Verlag.

Reading, H. G. 1980. Facies: In H. G. Reading (Editor), Sedimentary Environments and Facies: New York: Elsevier North-Hubbard, Inc.

Reineck, H. E., and Singh, I. B. Depositional Sedimentary Environments: New York: Springer-Verlag.

Richardson, J. B. 1965. Middle Old Red Sandstone Spore Assemblages From the Orcadian Basin, Northeast Scotland: Paleotology, Vol. 7, pp. 559-605.

Robb, G. L. 1949. Red Bed Coloration: J. Sediment. Pet., Vol. 19, pp. 99-103.

Rust, B. R. 1968. Deformed Cross-Bedding in Tertiary-Cretaceous Sandstone, Arctic Canada: J. Sediment. Pet., Vol. 38, pp. 87-91.

_____. 1972. Structure and Process in a Braided River: Sedimentology, Vol. 18, pp. 221-246.

_____. 1975. Fabric and Structure in Glaciofluvial Gravels: In A. V. Jopling and B. C. McDonald (Editors), Glaciofluvial and Glaciolacustrine Sedimentation, Soc. Econ. Paleon. Mineral., Spec. Pub., Vol. 23, pp. 238-248.

_____. 1978b. Depositional Models for Braided Alluvium: In A. D. Miall (Editor), Fluvial Sedimentology, Can. Soc. Petrol. Geol., Mem. 5, pp. 605-625.

Sanderson, D. J. 1973. Some Inference Problems in Paleocurrent Studies: J. Sediment. Pet., Vol. 43, pp. 1096-1100.

Schmalz, R. F. 1968. Formation of Red Beds in Modern and Ancient Deserts: Geol. Soc. Am. Bull., Vol. 79, pp. 277-280.

Schumm, S. A. 1963a. A Tentative Classification of Alluvial River Channels: U. S. Geol. Surv., Circ. 477.

_____. 1968a. Speculations Concerning Paleohydrologic Controls of Terrestrial Sedimentation: Geol. Soc. Am. Bull., Vol. 79, pp. 1573-1588.

Sedwick, W., and Murchinson, R. 1829. On the Old Conglomerates and Other Secondary Deposits of the North Coast of Scotland: Proc. Geol. Soc. Lond., Vol. 1, pp. 1-77.

Selley, R. C. 1969. Torridonian Alluvium and Quicksand: Scot. Jour. Geol., Vol. 5, pp. 328-346.

Shelton, J. W. 1964. Authigenic Kaolinite in Sandstone: J. Sediment. Pet., Vol. 34, pp. 102-111.

Simon, J. B., and Bluck, B. J. 1982. Paleodrainage of the Southern Margin of the Caledonian Mountain Chain in the Northern British Isles: Trans. Roy. Soc. Edinb., Vol. 73, pp. 11-15.

Simpson, C. 1983. Personal Communication, Oklahoma State University.

Smith, N. D. 1970. The Braided Stream Depositional Environment: Comparison of the Platte River With Some Silurian Clastic Rocks, North-Central Appalachians: Geol. Soc. Am. Bull, Vol. 81, pp. 2993-3014.

_____. 1971a. Transverse Bars and Braiding in the Lower Platte River, Nebraska: Geol. Soc. Am. Bull, Vol. 82, pp. 3407-3420.

_____. 1971b. Pseudo-Planar Stratification Produced by Very Low Amplitude Sand Waves: J. Sediment. Pet., Vol. 41, pp. 69-73.

_____. 1972a. Some Sedimentological Aspects of Planar Cross-Stratification in a Sandy Braided River: J. Sediment. Pet., Vol. 42, pp. 624-634.

_____. 1974. Sedimentology and Bar Formation in the Upper Kicking Horse River, A Braided Outwash Stream: Jour. Geol., Vol. 82, pp. 205-224.

Sorby, H. C. 1859. On the structures Produced by the Current Present During the Deposition of Stratified Rocks: The Geologist, Vol. 2, pp. 137-147.

Speight, J. M., and Mitchell, J. G. 1979. The Permo-Carboniferous Dyke-Swarm of Northern Argyll and its Bearing on Dextral Displacement on the Great Glen Fault: Jour. Geol. Soc. Lond., Vol. 136, pp. 3-11.

Stephenson, D. 1977. Intermontane Basin Deposits Associated With an Early Great Glen Feature in the Old Red Sandstone of Inverness-Shire: In The Moray Firth Area Geological Studies: Inverness, Scotland: John C. Eccles Printers Ltd.

Tarling, D. H., Donovan, R. N., Abou-Deeb, J. M., and El-Batrouk, S. I. 1976. Paleomagnetic Dating of Hematite Genesis in Orcadian Basin Sediments: Scot. Jour. Geol., Vol. 12, pp. 125-134.

Tchalenko, J. S., and Ambraseys, N. N. 1970. Structural Analysis of the Dasht-e Bayaz (Iran) Earthquake Fractures: Geol. Soc. Am. Bull, Vol. 81, pp. 41-60.

Thompson, A. H. 1970. Geochemistry of Color Genesis in Red Bed Sequence, Juniata and Bald Eagle Formations, Pennsylvania: J. Sediment. Pet., Vol. 40, pp. 599-615.

Tomlinson, C. W. 1916. The Origin of Red Beds: Jour. Geol., Vol. 24, pp. 153-179.

Turnbridge, I. P. 1981. Sandy High Energy Flood Sedimentation - Some Criteria for Recognition, With an Example From the Devonian of Southwest England: Sediment. Geol., Vol. 28, pp. 79-95.

Turner, P., and Archer, R. 1977. The Role of Biotite in the Diagenesis of Red Beds From the Devonian of Northern Scotland: Sediment. Geol., Vol. 19, pp. 241-251.

Turner, P. 1974. Origin of Red Beds in the Ringerlike Group (Silurian) of Norway: Sediment. Geol., Vol. 12, pp. 215-235.

_____. 1980. Developments in Sedimentology, Continental Red Beds. ElSevier Scientific Publishing Co., Vol. 29.

Van Houten, F. B. 1964. Origins of Red Beds; Some Unsolved Problems in Paleoclimatology: New York: John Wiley and Sons, Ltd.

_____. 1968. Iron Oxides in Red Beds: Geol. Soc. Am. Bull., Vol. 79, pp. 399-416.

Van der Voo, R., and Scotese, C. 1981. Paleomagnetic Evidence for a Large (~2000 km) Sinistral Offset Along the Great Glen Fault During Carboniferous Times: Geology, Vol. 9, pp. 583-589.

Von Mises, R. 1918. Über die "Ganzzahligkeit" der Atomgewicht und Verwandre Fragen: Physikal Ziet., Vol. 19, pp. 490-500.

Walker, R. G., and Harms, J. C. 1971. The "Catskill Delta": A Prograding Muddy Shoreline in Central Pennsylvania: Jour. Geol. Vol. 79, pp. 381-399.

Walker, T. R. 1967a, Formation of Red Beds in Modern and Ancient Deserts: Geol. Soc. Am. Bull., Vol. 78, pp. 353-368.

_____. 1967b. Color of Recent Sediments in Tropical Mexicos: A Contribution to the Origin of Red Beds: Geol. Soc. Am. Bull, Vol. 78, pp. 917-920.

Walker, T. R., Ribbe, P. H., and Honea, R. M. 1967. Geochemistry of Hornblende Alteration in Pliocene Red Beds, Baja, California and Mexico: Geol. Soc. Am. Bull., Vol. 78, pp. 1055-1060.

Walker, T. R. 1974. Formation of Red Beds in Moist Tropical Climates: A Hypothesis: Geol. Soc. Am. Bull, Vol. 85, pp. 623-638.

Walker, T. R., Waugh, B., and Crone, A. J. 1978. Diagenesis in First Cycle Desert Alluvium of Cenozoic Age, Southwestern United States and Northwestern Mexico: Geol. Soc. Am. Bull, Vol. 89, pp. 19-32.

Walton, E. K. 1970. Lower Paleozoic Rocks - Stratigraphy: In G. Y. Craig (Editor). The Geology of Scotland: Edinburgh, Scotland: Oliver and Boyd.

Wasson, R. J. 1977. Last Glacial Alluvial Fan Sedimentation in the Lower Dervent Valley, Tasmania: Sedimentology, Vol. 24, pp. 781-799.

Waterson, C. D. 1970. Old Red Sandstone: In G. Y. Craig (Editor) The Geology of Scotland, Oliver and Boyd, Edinburgh, Scotland.

Westoll, T. S. 1977. A Correlation of the Devonian Rocks in the British Isles: M. R. House (Editor), Geol. Soc. Lond., Special Report No. 7.

Wilcox, R. E., Harding, T. P., and Seely, D. R. 1973. Basic Wrench Tectonics: A.A.P.G. Bull, Vol. 57, pp. 74-96.

Williams, P. F., and Rust, B. R. 1969. The Sedimentology of a Braided River: J. Sediment. Pet., Vol. 39, pp. 649-679.

Wilson, G. V., Edwards, W., Knox, J., Jones, R. C. B., and Stephens, J. 1935. The Geology of the Orkneys: Mem. Geol. Surv., Great Britain.

Woodrow, D. L., Fletcher, F. W., and Ahrnsbrak, W. F. 1973. Paleogeography and Paleoclimate at the Deposition Sites of the Devonian Catskill and Old Red Facies: Geol. Soc. Am. Bull., Vol. 84, pp. 3051-3064.

APPENDIX A

POST DEVONIAN RIGHT-LATERAL MOVEMENT ON THE GREAT GLEN FAULT

Two distinct schools of thought exist as to the nature of post-Devonian movement on the Great Glen Fault. The sinistral school, often invoking movements of considerable magnitude, offers as evidence either interpretations of various paleomagnetic data from the Devonian Old Red Sandstone[1-6] or tectonic analysis of offshore seismic and well data[7].

A more conservative school involves vertical movement coupled to modest dextral movement. Proponents of this view offer as evidence: (1) alternative explanations of the paleomagnetic data noted above,[8,9]; (2) matches of miscellaneous Devonian and post-Devonian entities (dykes, drainage patterns, Devonian facies) across the fault[10-18]; (3) tectonic analysis of offshore seismic and well data from the Inner Moray Firth [19-21].

The equally disputed history of pre-Devonian fault movement is not considered here. However, we note the danger of using pre-Devonian evidence in support of post-Devonian argument.

North of Inverness the line of the Great Glen Fault has controlled erosion of the eastern coasts of the Black Isle and Tarbat Ness peninsulas (Fig. 1). In several places a fault trace on the foreshore juxtaposes Jurassic and Middle Devonian (Old Red Sandstone) or Precambrian (Moine) rocks. Along the foreshore of Tarbat Ness Devonian rocks strike northeast and dip gently northwest to southeast, although at the seaward margin (closest to the fault) they may be chaotically shattered. More extensive areas of disturbance are a fold belt at Ballone Castle and a fault complex 1 km north of Geanies.

At the latter location an open anticline plunging at c. 20° to c. 028 has been cut by several small vertical faults which parallel the main fault (Fig. 2). Slight stratigraphic displacement of lacustrine limestone

in the Middle Devonian Strath Rory Group[15] was most likely due to small dextral movements, as horizontal slickensides occur at two fault planes and the sense of displacement is the same on both limbs of the fold.

Folds at Ballone Castle are developed in well-bedded sandstones in the upper part of the Strath Rory Group[15]. The folds are open, upright chevrons with limb dips less than 60°. Fold wave lengths are less than 10 m and the structures, which are en echelon, generally plunge gently to between 180 and 210 (Fig. 3). Fractures, which post-date the folds, show a distinct major mode with a mean oriented 047 (Fig. 4).

Analysis of the fold belt indicates two phases of folding. An early large-scale upright fold plunged at c. 10° to 210. This fold, the trend of which parallels the Great Glen Fault, is interpreted as having formed under a stress field which led to a vertical component of displacement on the fault.

The smaller-scale folds described above record a late reorientation of stress across the fault. The orientation, style and sequence of these later folds and of the fracture patterns is compatible with wrench tectonic theory[22-25]. Thus the right-handed arrangment of folds is compatible with dextral movement on the Great Glen Fault. Similarly, the fractures can be interpreted as dextral Riedel shears.

The information presented there is the first onshore small-scale data intimately related to the Great Glen Fault. It is all compatible with post-Devonian dextral movement on this structure.

We are grateful to Carol Simpson for her helpful review.

R. N. Donovan & T. E. Ferraro
Department of Geology
Oklahoma State University
Stillwater, OK 74078

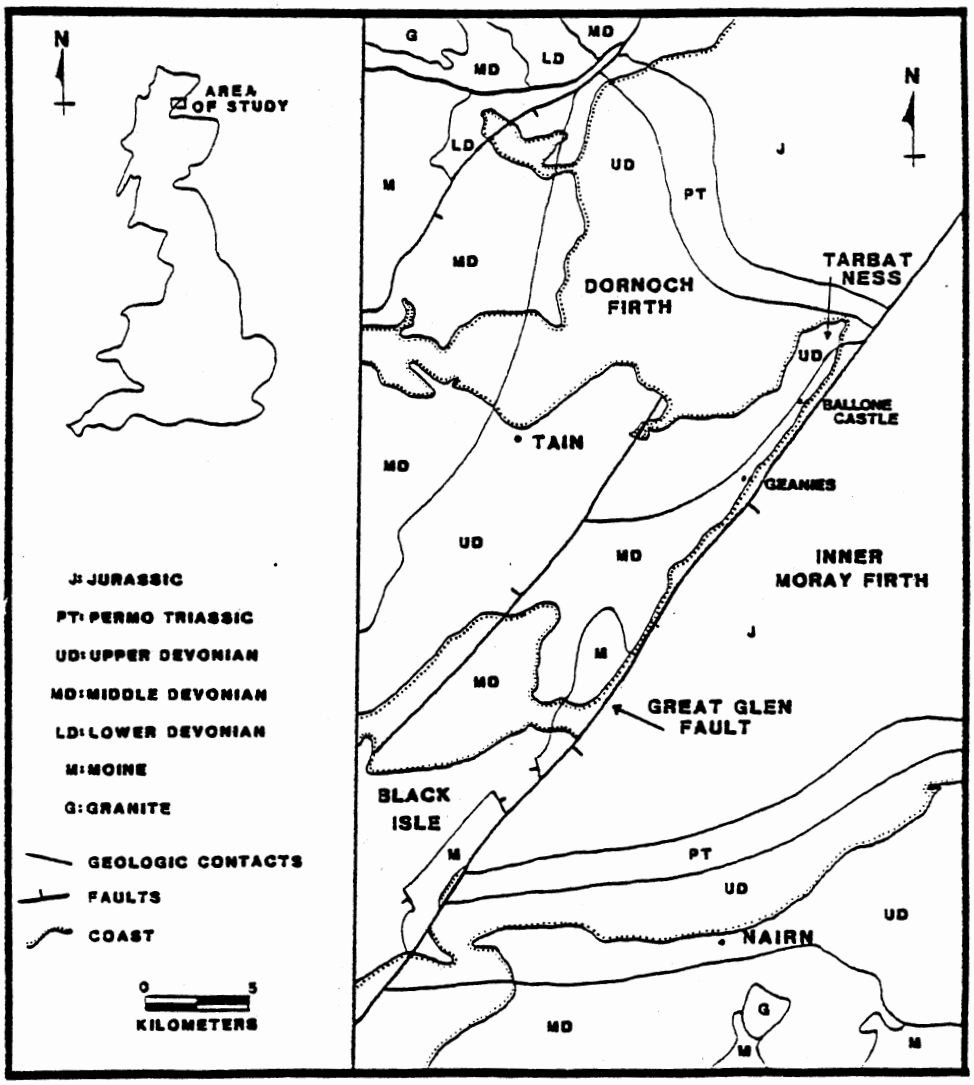

Figure 1. Locality map of the Inner Moray Firth region. Geology redrawn from[26]

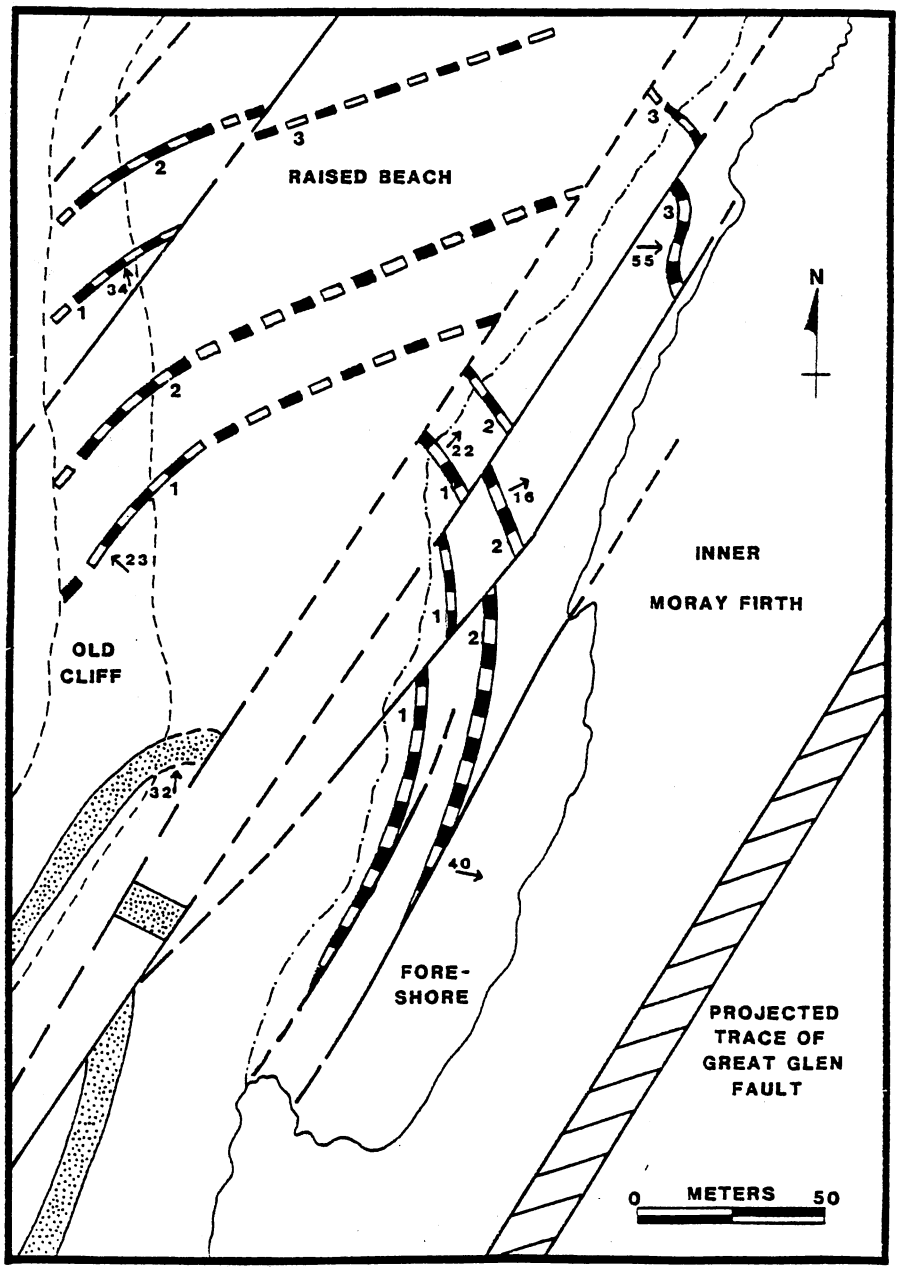

Figure 2. The fault and fold complex north of Geanies
Stipple: sandstone marker; 1, 2, 3, lacustine limestones used as stratigraphic markers

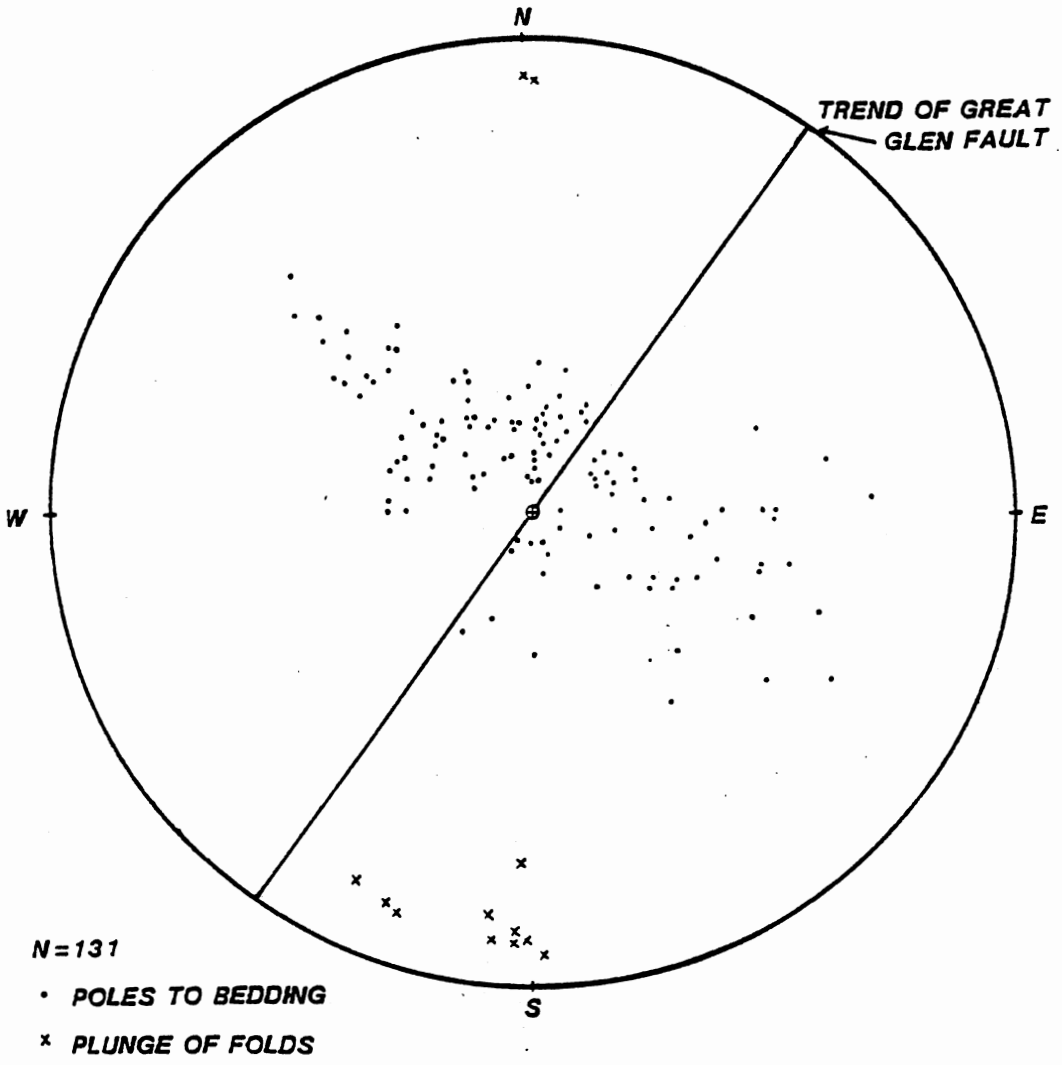

Figure 3. Ballone Castle fold belt: (A) poles to bedding, (B) contoured analysis. (Readings were taken as a series of east-west transverses.)

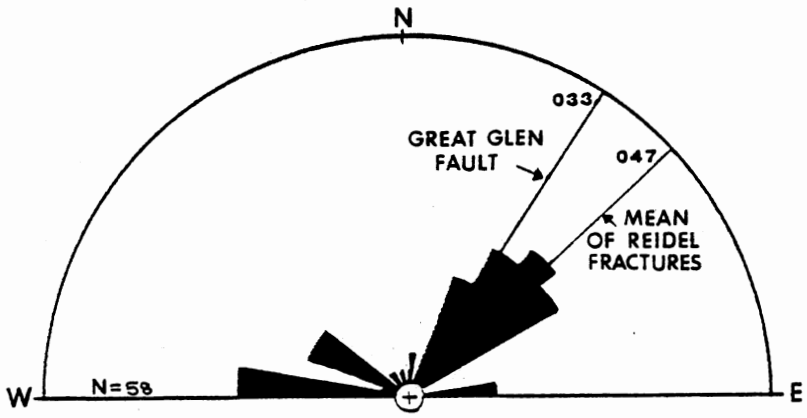

Figure 4. Fracture pattern distribution at Ballone Castle

REFERENCES

1. Storevedt, K. M., Geol. Mag., 111, 23-30 (1974).
2. Storevedt, K. M., Geol. Mag., 112, 94-96 (1975).
3. Ziegler, P. A., Petroleum geology of the continental shelf of North-west Europe, 3-39 (1981).
4. Van der Voo, R. and Scotese, C., Geology, 9, 583-589 (1981).
5. Van der Voo, R. and Scotese, C., Geology, 10, 487-488 (1982).
6. Van der Voo, R. and Scotese, C., Geology, 10, 604-607 (1982).
7. Threlfall, W. F., Petroleum geology of the continental shelf of North-west Europe, 98-103 (1981).
8. Turner, P., Tarling, D. H., Donovan, R. N. and Archer, R. A., Geol. Mag. 113, 365-370 (1976).
9. Winchester, J. A., Geology, 10, 487-488 (1982).
10. Holgate, N., Scott, J. Geol., 5, 97-139 (1969).
11. Garson, M. S. and Plant, J., Nature, 240, 31-35 (1972).
12. Flinn, D., Geol. J. Vol. 6, 279-292 (1969).
13. Mykura, W., Geol. Mag., 112, 91-94 (1975).
14. Donovan, R. N., Archer, T., Turner, P., and Tarling, D. H., Nature, 259, 550-551 (1976).
15. Armstrong, M., Moray Firth Area Geological Studies, 25-34 (1977).
16. Speight, J. M. and Mitchell, J. G., J. Geol. Soc. London, 136, 3-11 (1979).
17. Donovan, R. N. and Meyerhoff, A. A., Geology, 10, 604-607 (1982).
18. Parnell, J., Geology, 10, 604-607 (1982).
19. Bacon, M. and Chesher, J. A., Scott. J. Geol., 11, 79-82 (1975).
20. Linsley, P. N., Potter, H. C., McNab, G. and Racher, D., in Am. Assoc. Pet. Geol. Mem. 30, 117-129 (1980).

21. McQuillin, R., Donato, J. A. and Tulstrap, J., Earth Plan. Sci. Letters, 60, 127-139 (1982).

22. Wilcox, R. E., Harding, T. P., and Seely, D. R., Bull. Am. Assoc. Pet. Geol., 57, 74-96 (1973).

23. Tchalenko, J. S. and Ambraseys, N. N., Geol. Soc. Am. Bull., 81, 41-60 (1970).

24. Tchalenko, J. S., Geol. Soc. Am. Bull., 81, 1625-1640 (1970).

25. Bartlett, W. L., Friedman, M. and Logan, J. M., Tectonophysics, 79, 255-277 (1981).

26. Fettes, D. J. and Chesher, J. A., Institute of Geological Sciences (U.K.), Sheet 57N 04W (1977).

APPENDIX B

M.O.R.S.--U.O.R.S. MEASURED SECTION

EXPLANATION

SEDIMENTARY STRUCTURES

Large


large-scale trough cross beds


large-scale planar-tabular cross-beds


medium-scale trough cross-beds

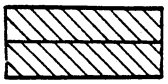
medium-scale planar-tabular cross-beds

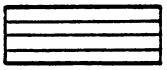
horizontal laminations in sandstone


horizontal laminations in siltstone, mudstone, and limestone

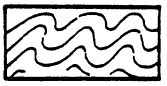
convolute bedding

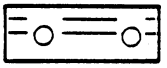
pillow and ball

Small

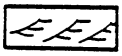
small-scale trough cross-beds

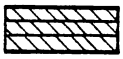
small-scale planar-tabular cross-beds


small-scale ripples

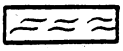
climbing ripples

OTHER

M micaceous

trough axes orientation

* * * 3 or more readings

parting lineations

mudcracks

E-3 position of sample collection

LITHOTYPES

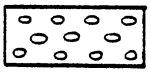
conglomerate

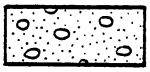
matrix supported conglomerate

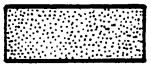
sandstone

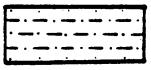
siltstone

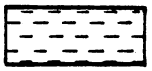
mudstone

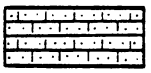
sandy limestone

CONTACTS

abrupt

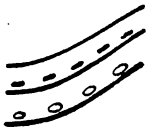
intraclast lags

pebble lags

erosional

GRAIN SIZE

Md	mud	m	med. sand
Sl	silt	c	coarse sand
f	fine sand	Gr	gravel

COLOR

R	red	Gr	gray
B	buff	M	mottled
Gn	green		

Section is measured in meters.

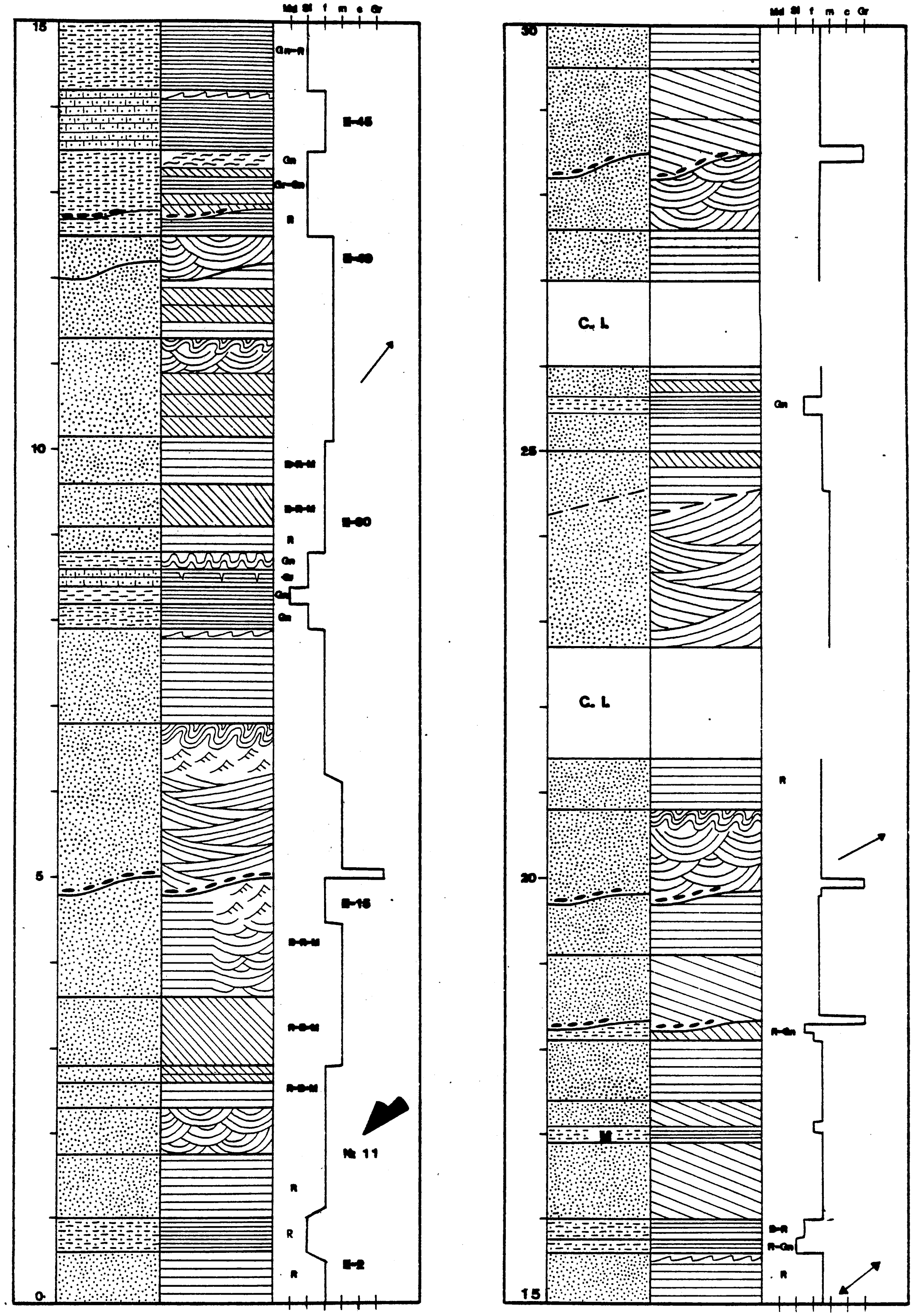
15
10
5
0
30
C. L.
25
C. L.
20
15

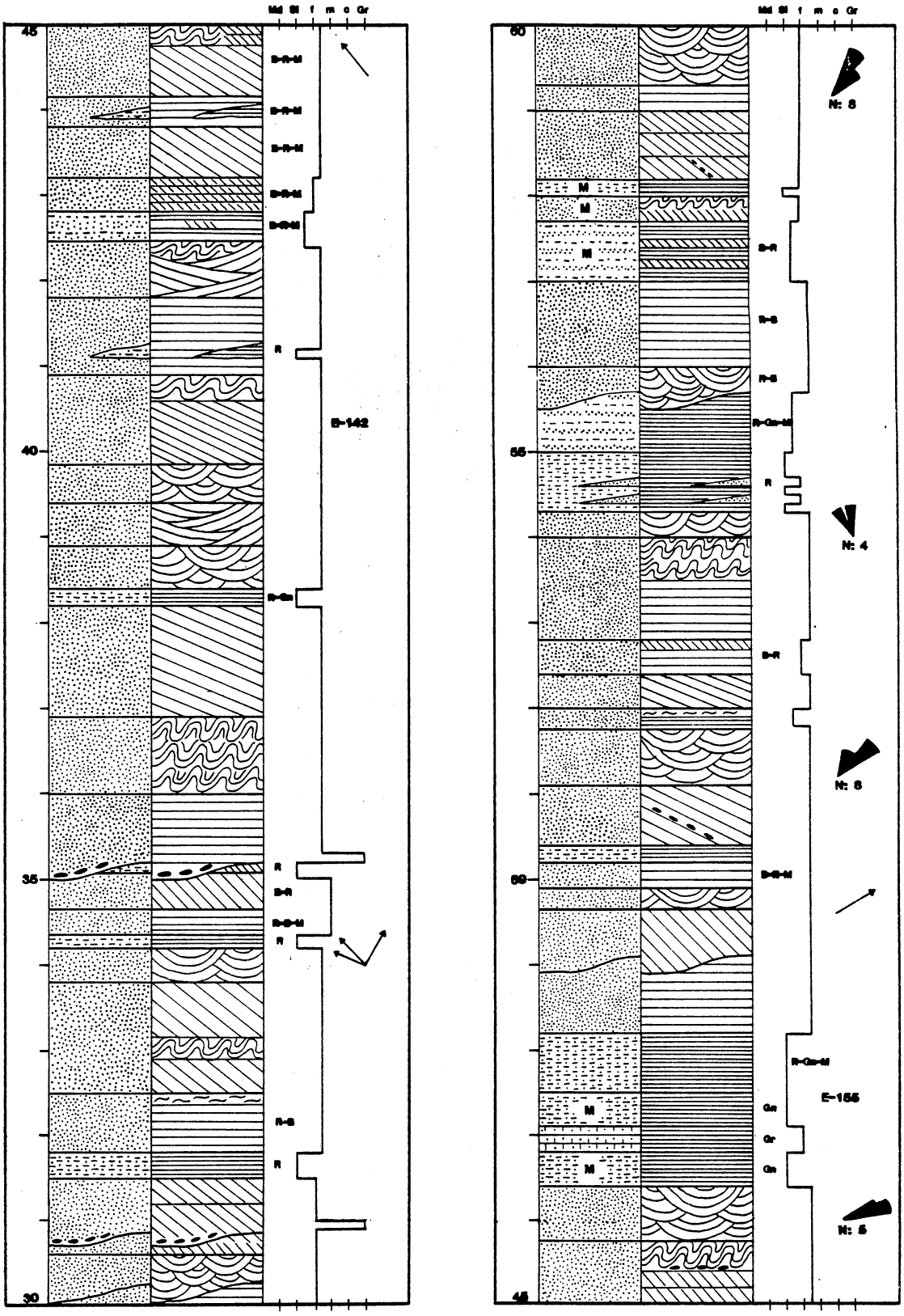
Md
Sl
f
m
c
Gr
45
40
35
30
B-142
N: 8
N: 4
N: 6
N: 5
E-155
60
55
50
45

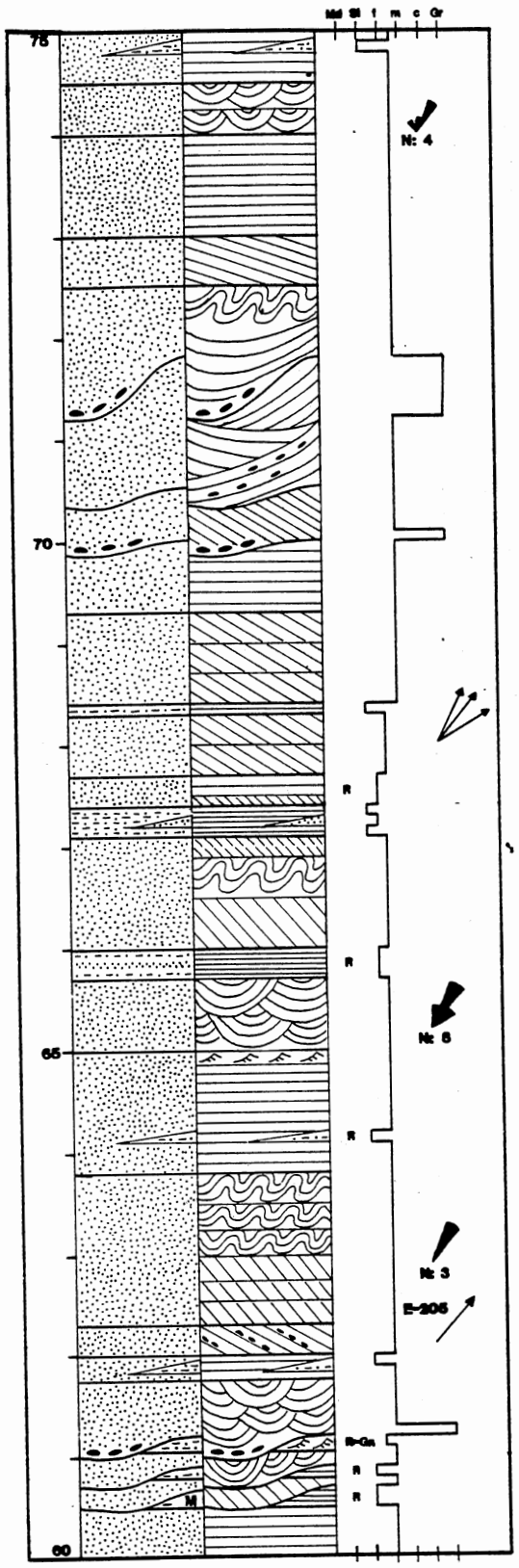
Md Sl f m c Gr
75
70
65
60
N: 4
N: 5
N: 3
E-205
R
M
R-Gn

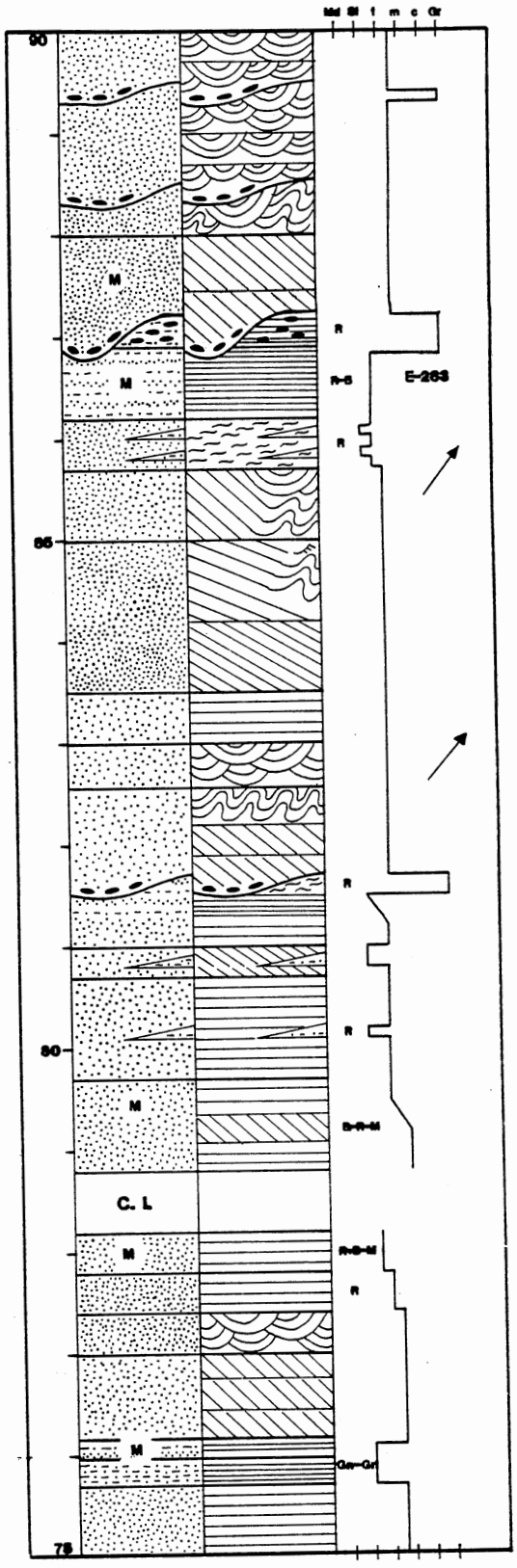
Md Sl f m c Gr
90
85
80
75
M
R
R-S
E-263
C. L
R-S-M
Gn-Gr

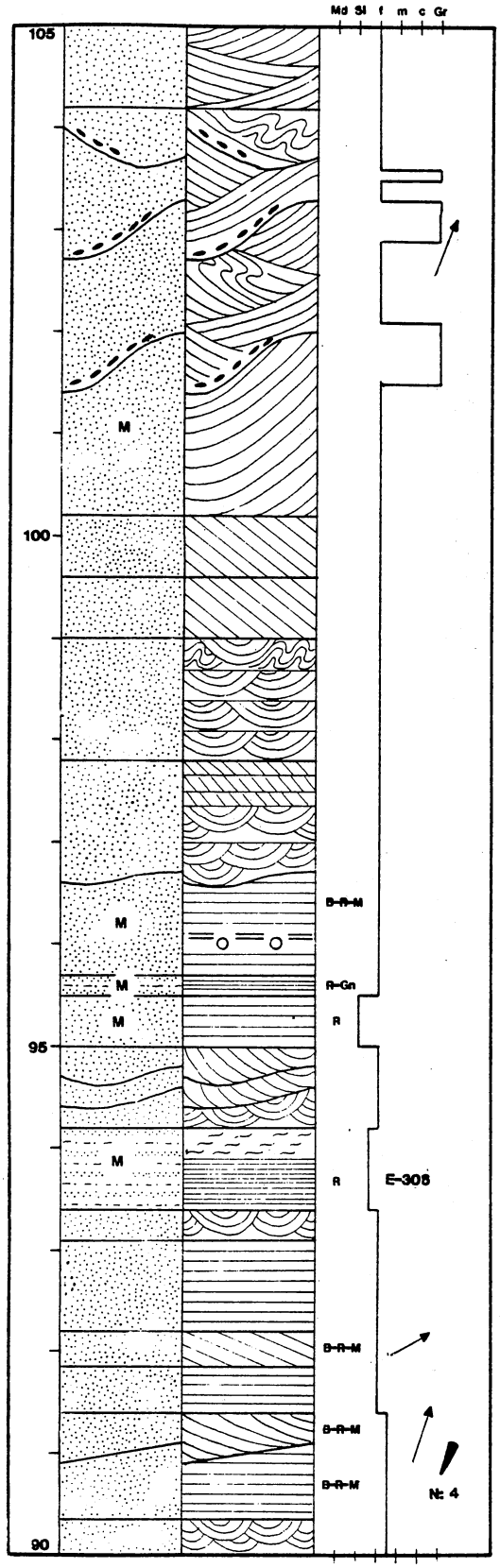
Md Si f m c Gr
105
100
95
90
M
M
M
M
M
B-R-M
R-Gn
R
R
E-305
B-R-M
B-R-M
B-R-M
N: 4

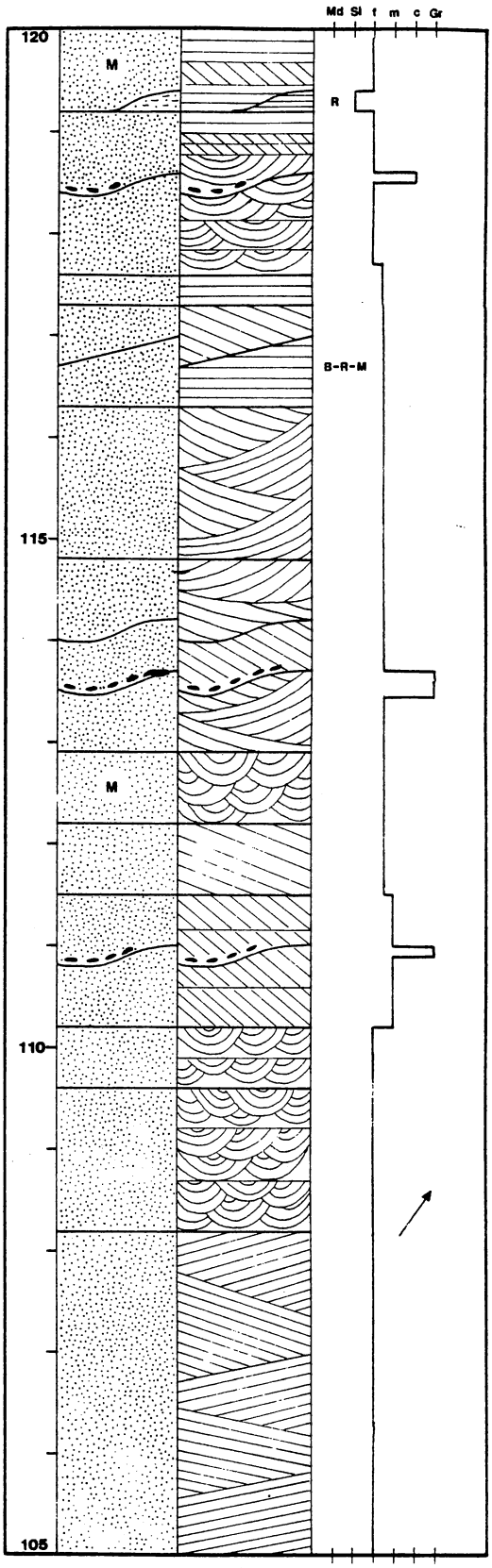
Md Si f m c Gr
120
115
110
105
M
R
B-R-M
M

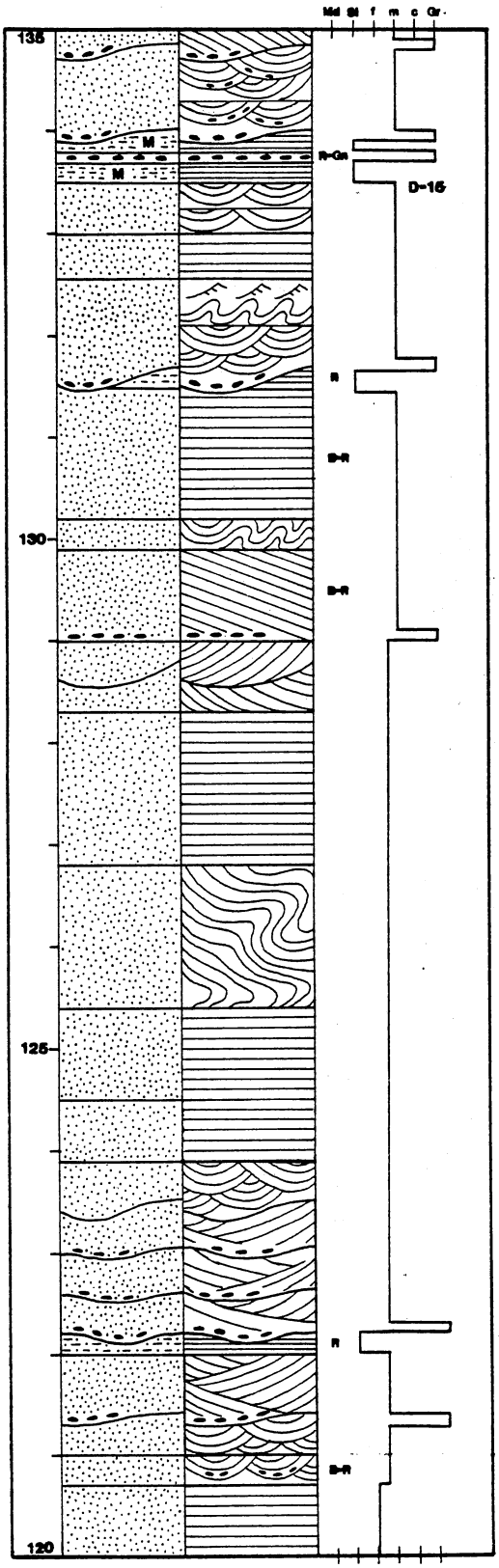
Mud Sil f m c Gr
135
M
M
R-Gn
D-15
R
B-R
130
B-R
125
R
B-R
120

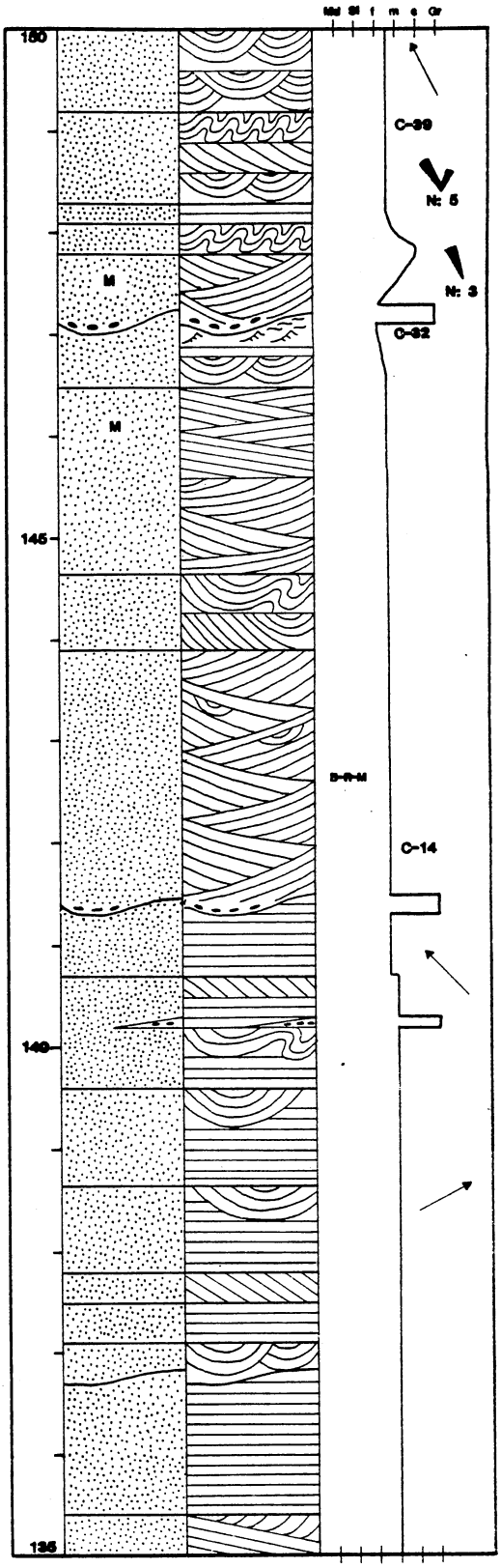
Mud Sil f m c Gr
150
R
C-39
N: 5
N: 3
M
C-32
M
145
B-R-M
C-14
140
135

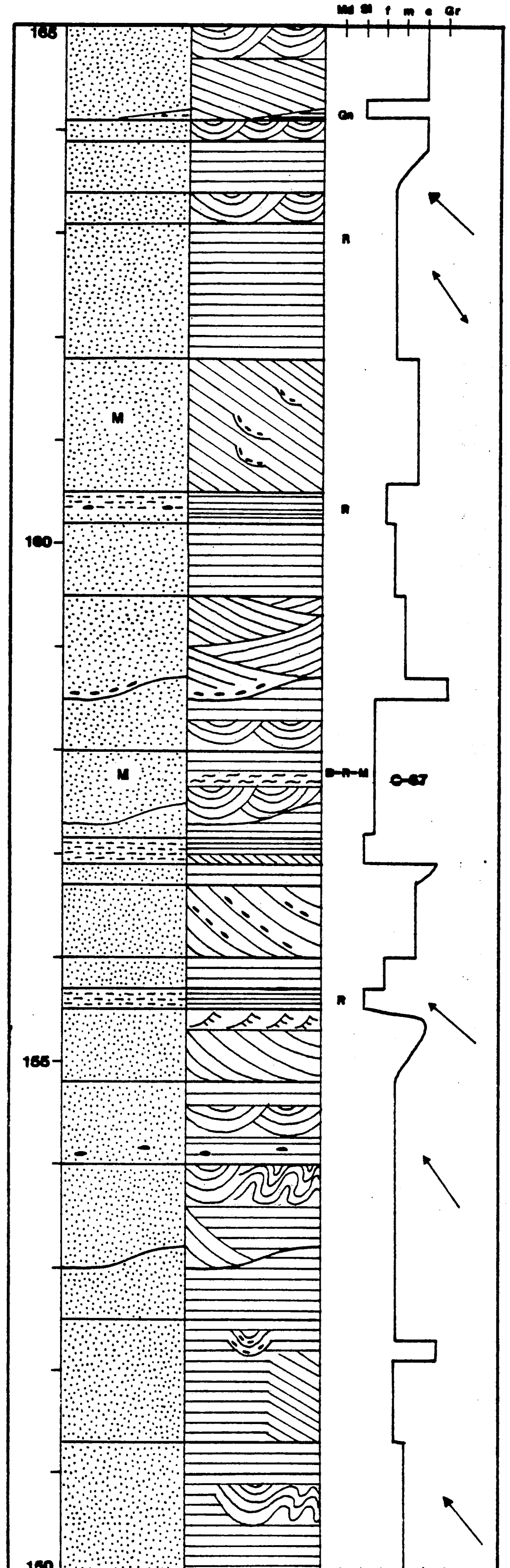
Md Sl f m c Gr
165
160
155
150
Gn
R
M
R
B-R-M
C-87
R

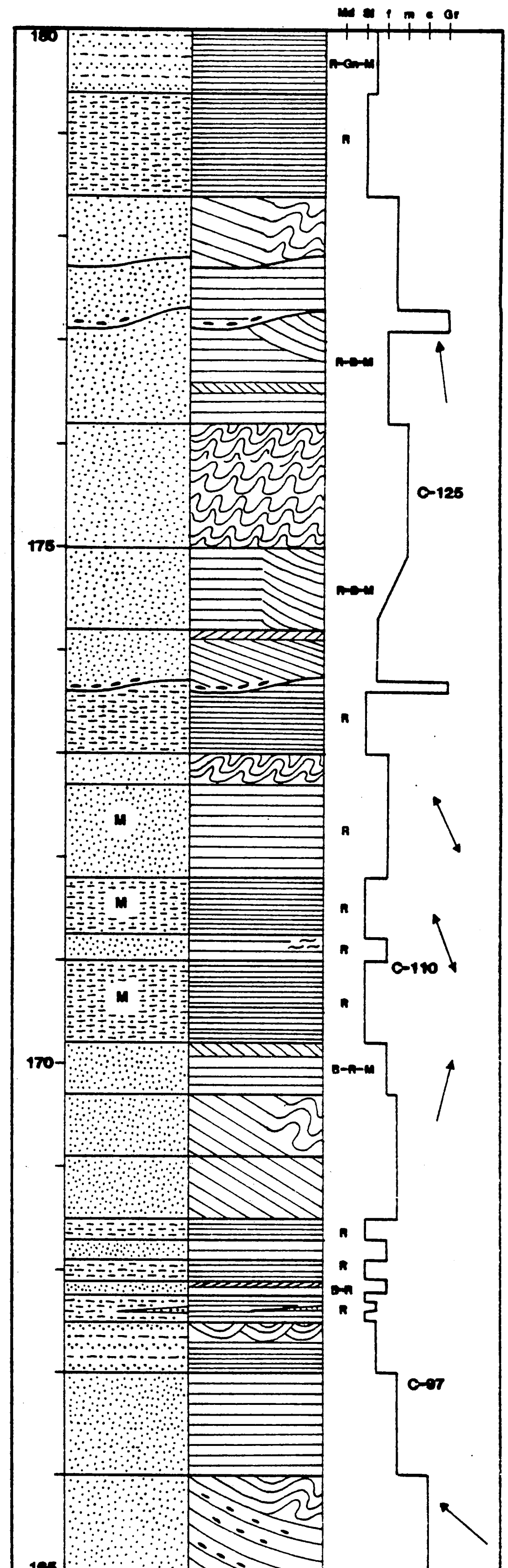
Md Sl f m c Gr
180
175
170
165
R-Gn-M
R
R-B-M
C-125
R-B-M
R
M
R
M
R
R
C-110
M
R
B-R-M
R
R
B-R
R
C-97

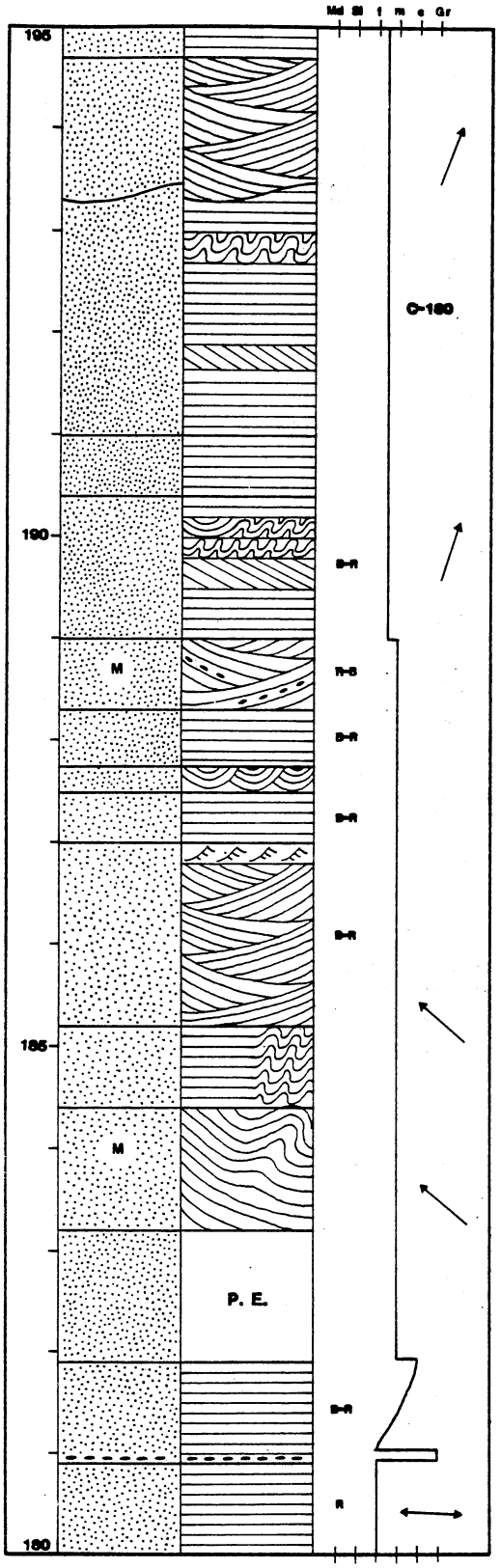
Md Si f m c Gr
195
190
185
180
C~180
M
M
P. E.
B-R
R-B
B-R
B-R
B-R
R

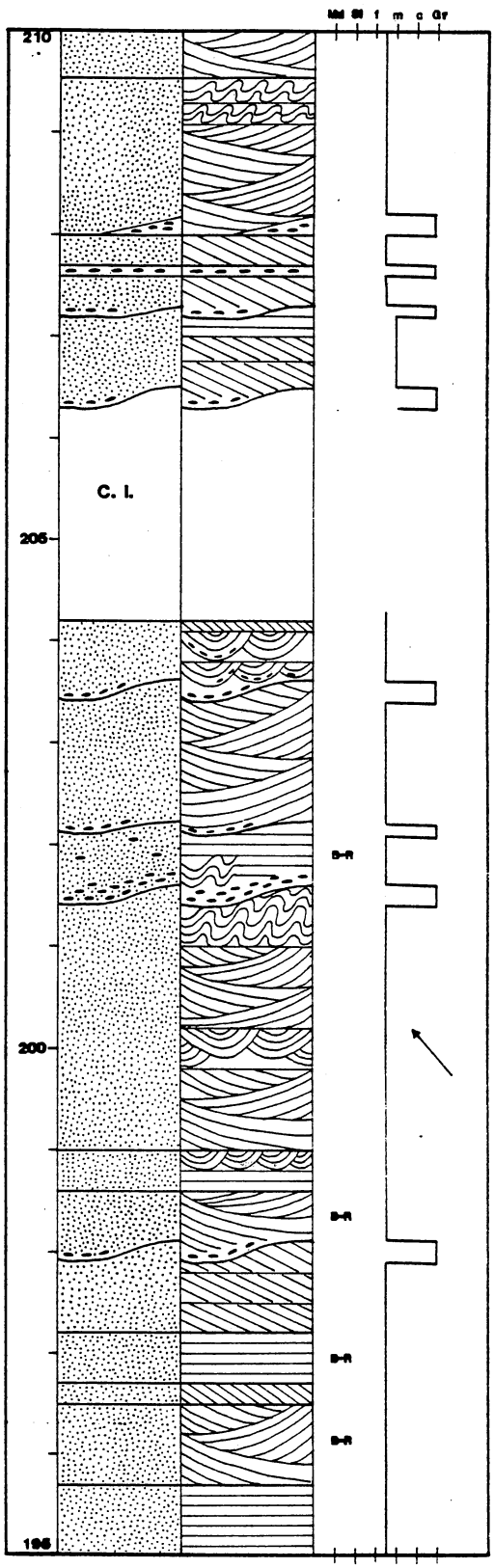
Md Si f m c Gr
210
205
200
195
C. I.
B-R
B-R
B-R
B-R

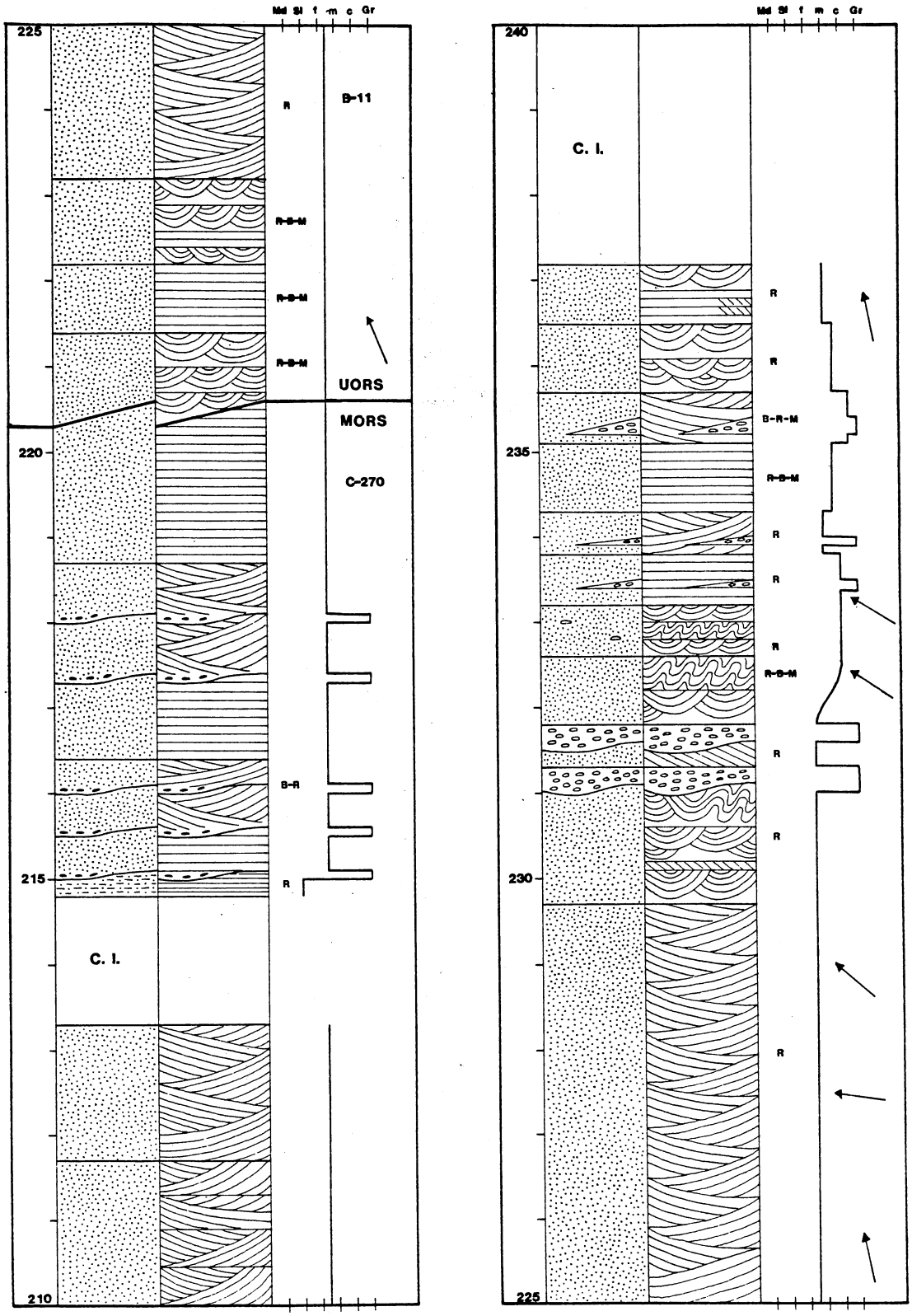
Md Sl f m c Gr
225
220
215
210
R
R-S-M
R-S-M
R-S-M
B-11
UORS
MORS
C-270
B-R
R
C. I.
Md Sl f m c Gr
240
235
230
225
C. I.
R
R
B-R-M
R-S-M
R
R
R
R-S-M
R
R
R

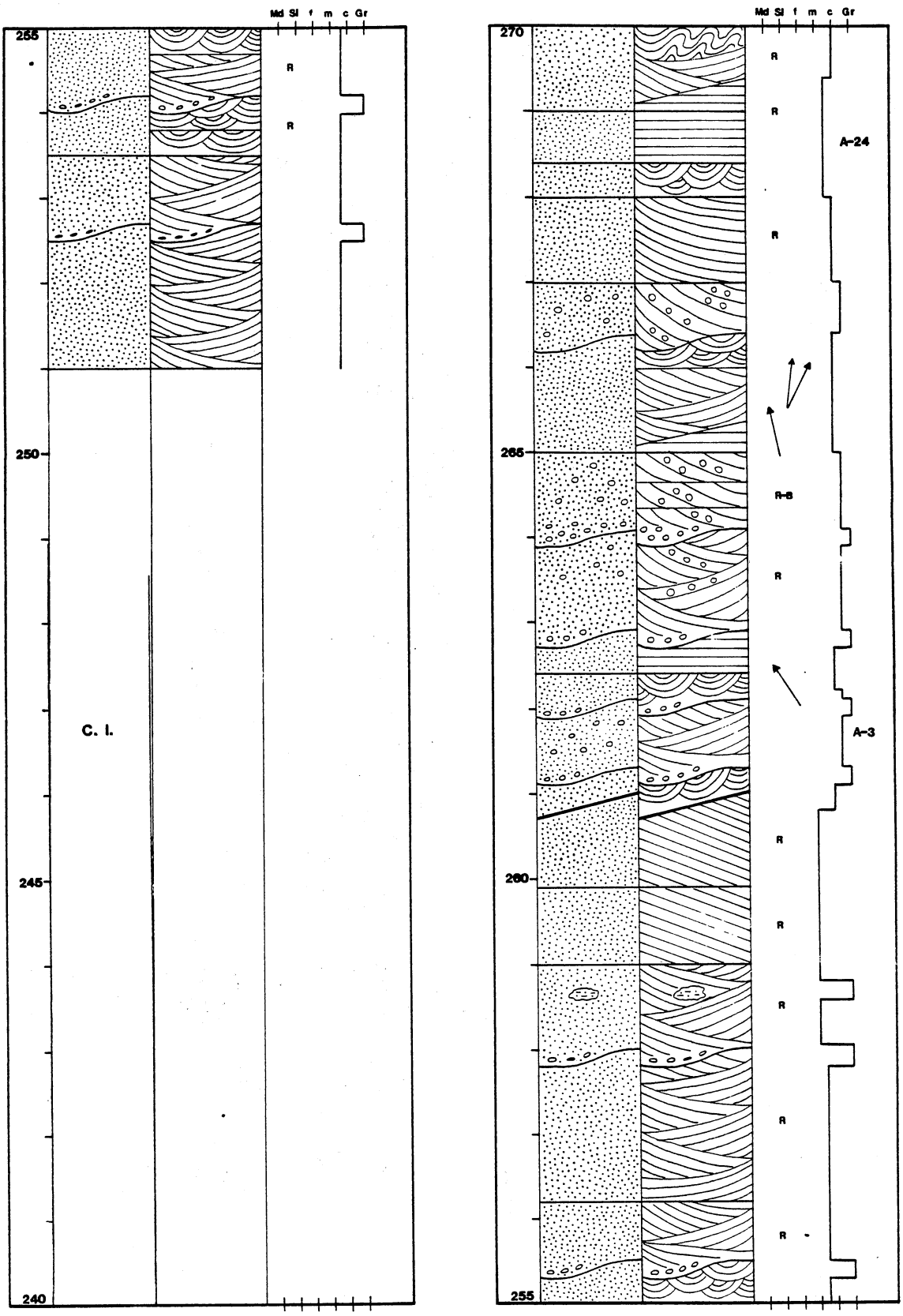
Md Sl f m c Gr
255
250
245
240
C. I.
R
R
Md Sl f m c Gr
270
265
260
255
R
R
R
R-8
R
R
R
R
R
R
A-24
A-3

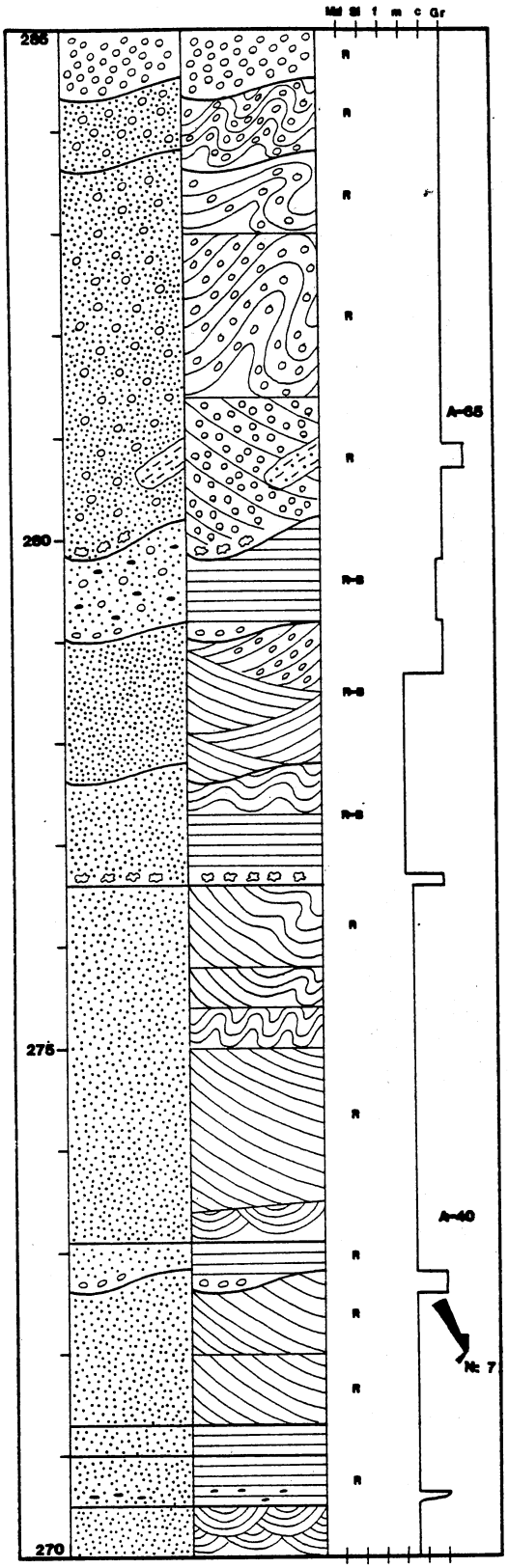
Md Si f m c Gr
285
280
275
270
R
R-S
A-65
A-40
№ 7

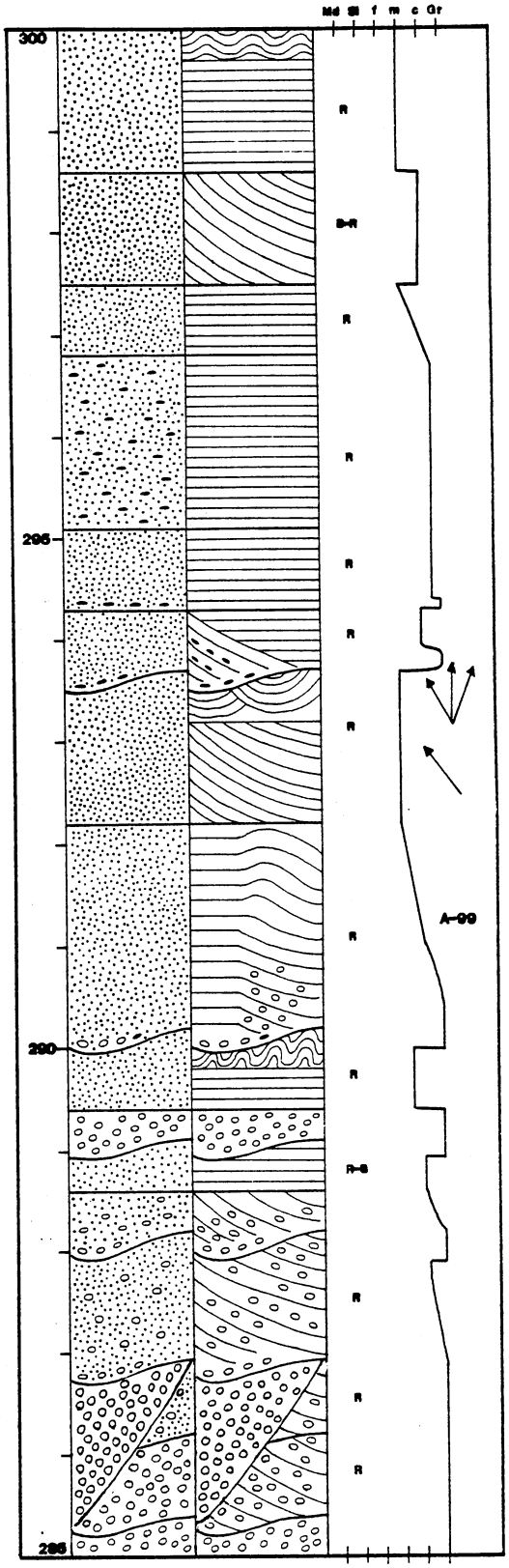
Md Si f m c Gr
300
295
290
285
R
S-R
R-S
A-99

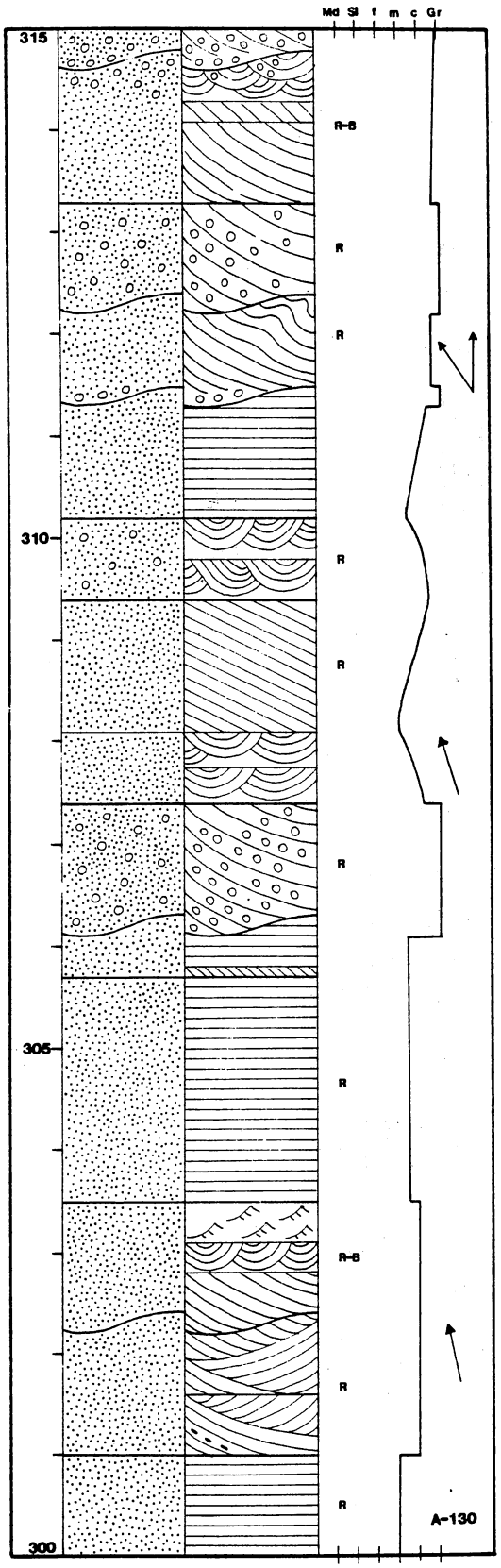
Md Si f m c Gr
315
310
305
300
R-B
R
R
R
R
R
R
R-B
R
R
A-130

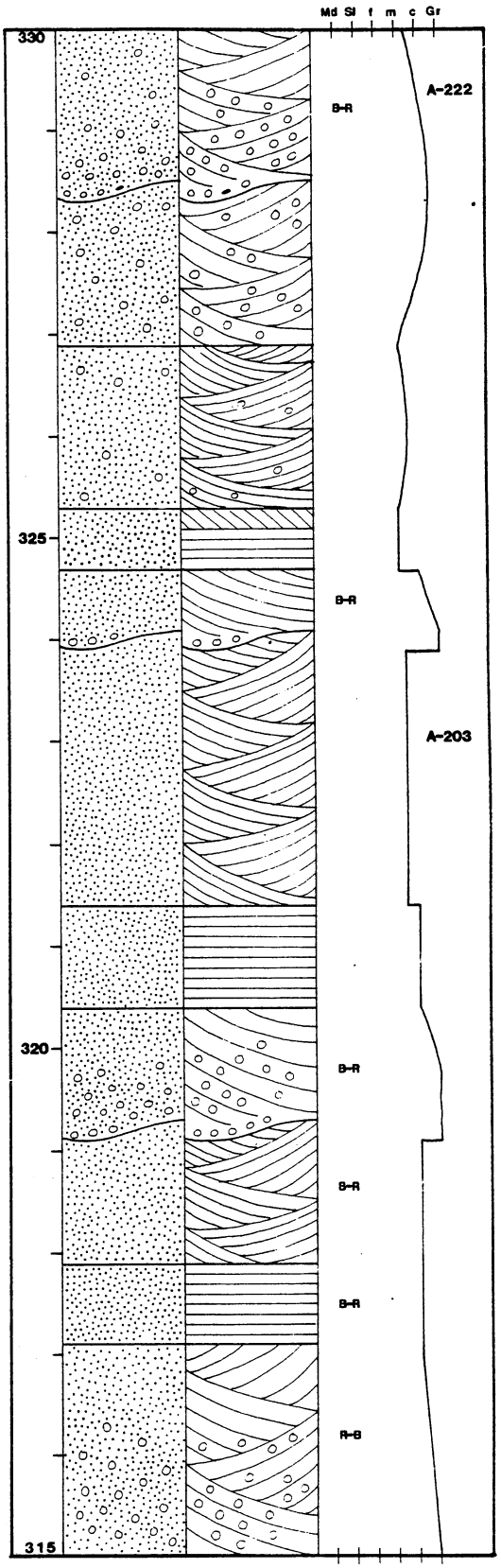
Md Si f m c Gr
330
325
320
315
A-222
B-R
B-R
A-203
B-R
B-R
B-R
R-B

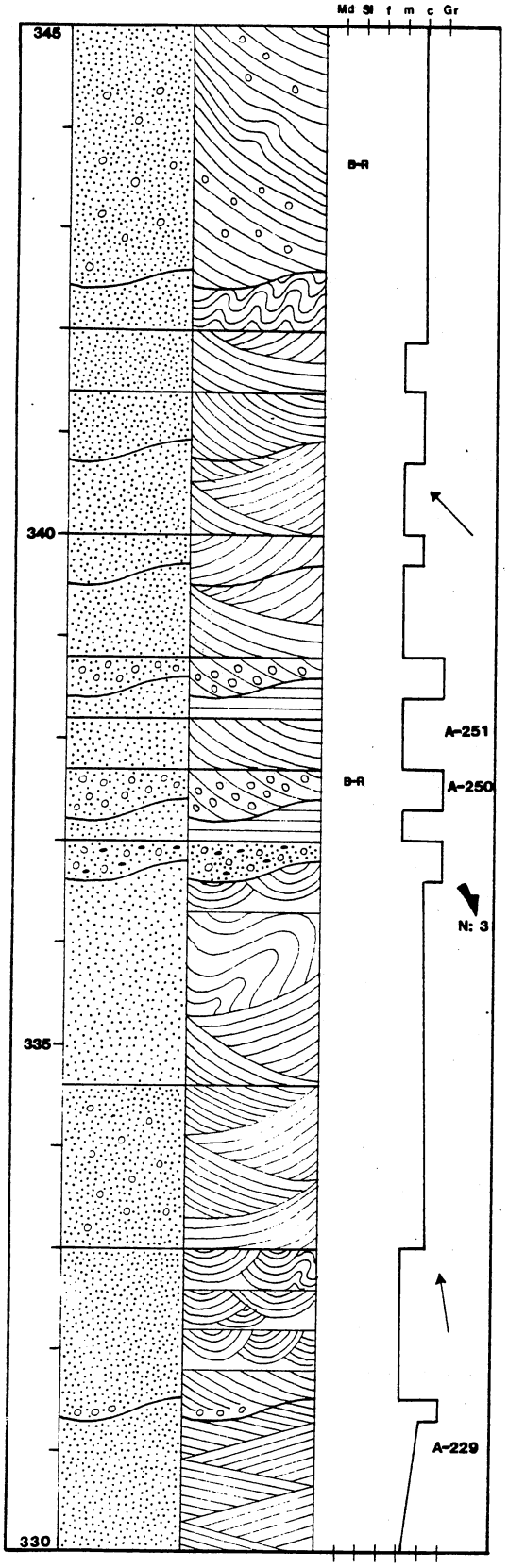
Md Sl f m c Gr
345
340
335
330
B-R
B-R
A-251
A-250
N: 3
A-229

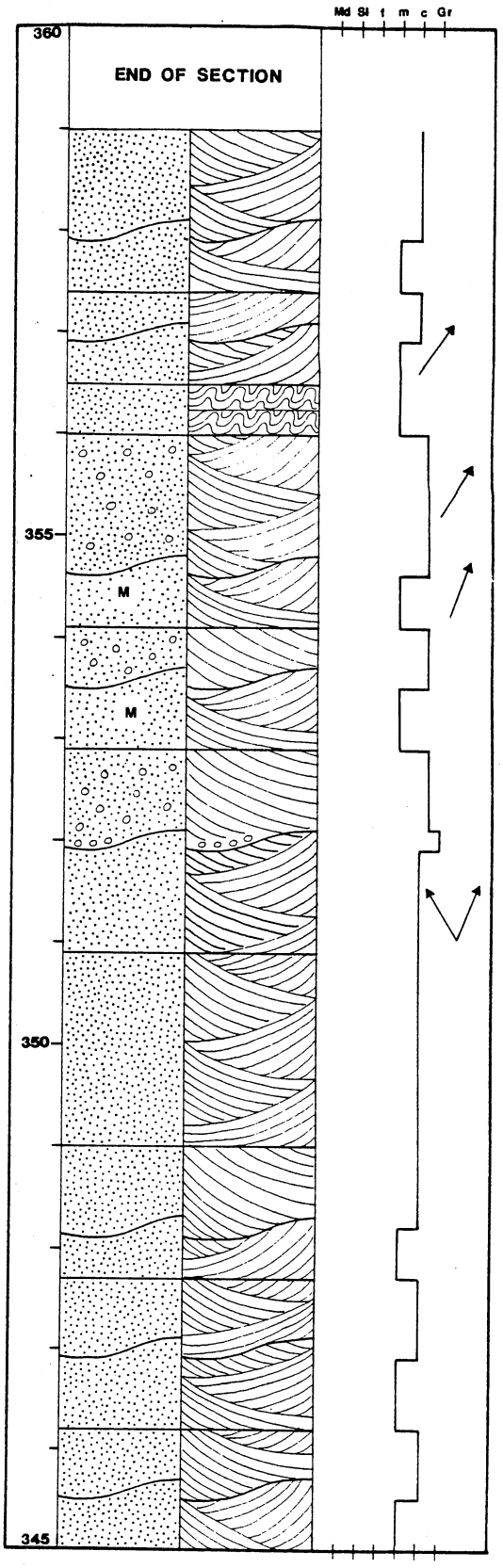
Md Sl f m c Gr
360
END OF SECTION
355
350
345
M
M

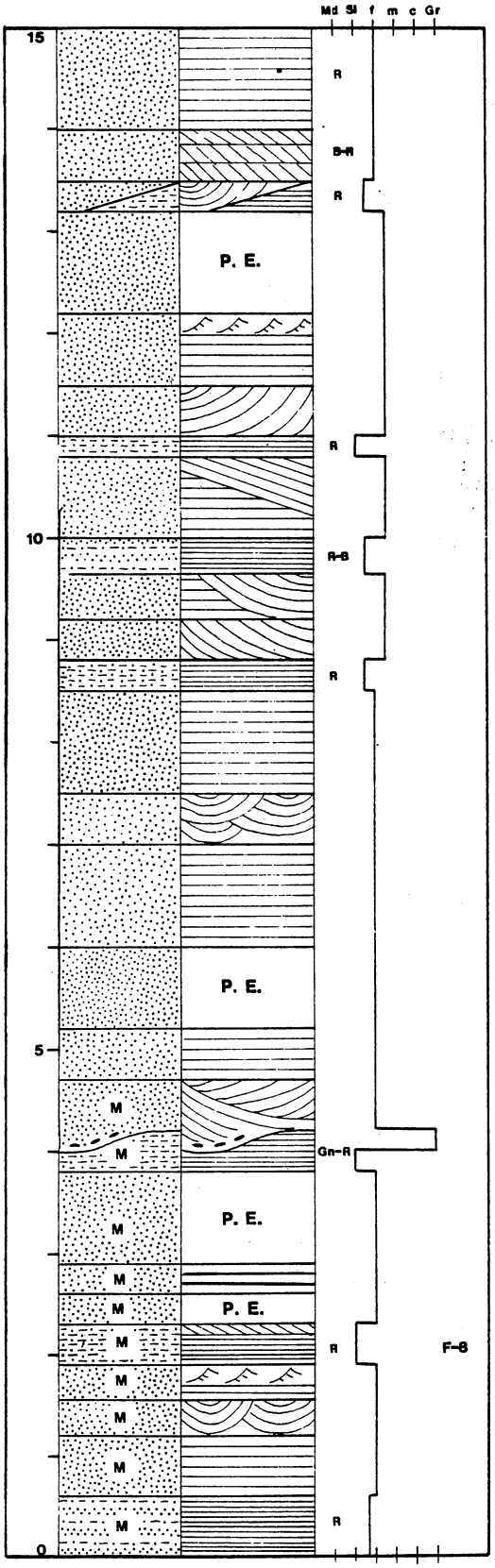
Md Si f m c Gr
15
10
5
0
R
B-R
R
P. E.
R
R-B
R
P. E.
M
M
Gm-R
P. E.
M
M
M
P. E.
M
M
M
M
M
R
R
F-8

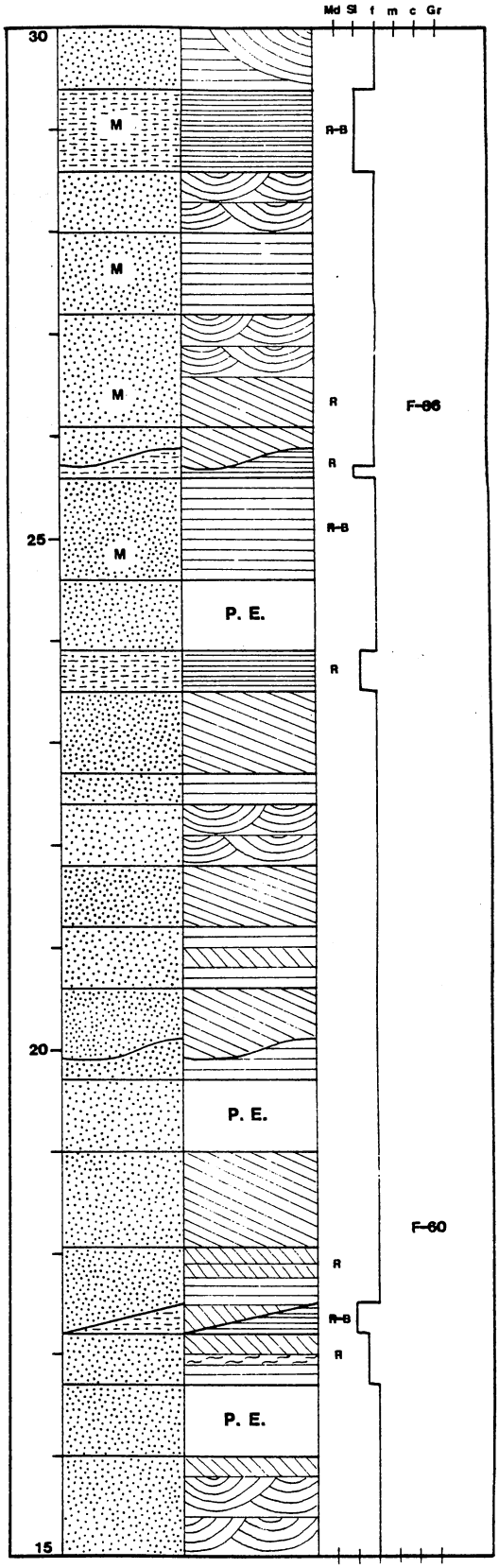
Md Si f m c Gr
30
25
20
15
M
M
M
M
P. E.
P. E.
P. E.
R-B
R
R
R-B
R
R
R-B
R
F-66
F-60

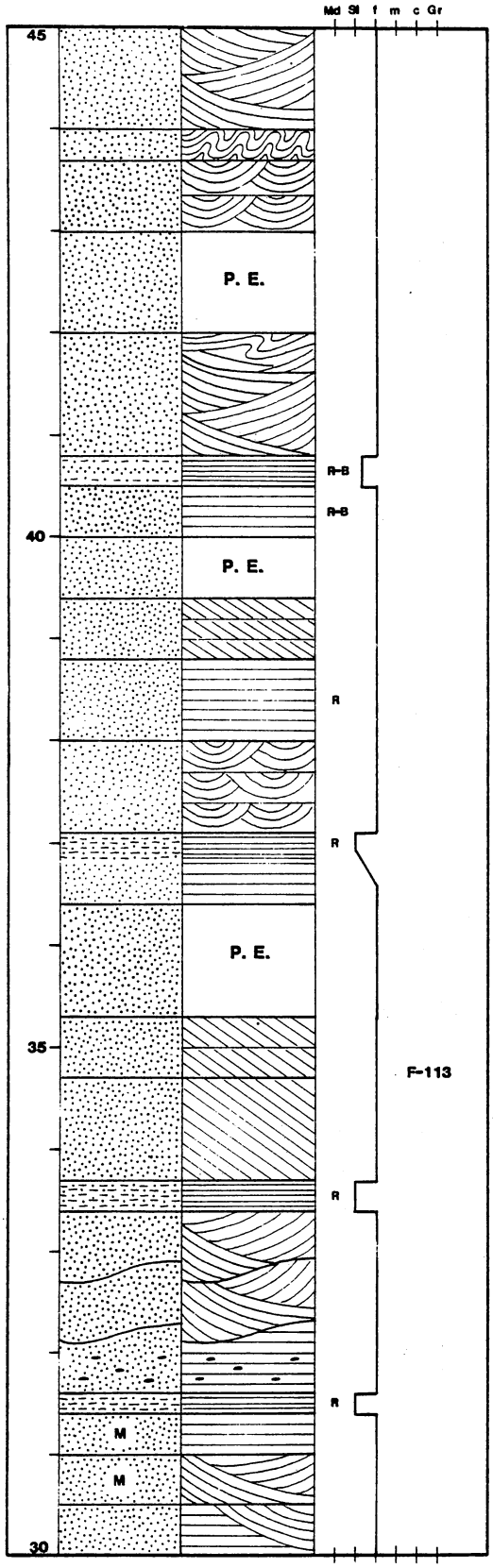
Md St f m c Gr
45
P. E.
R-S
R-S
40
P. E.
R
R
P. E.
35
F-113
R
R
M
M
30

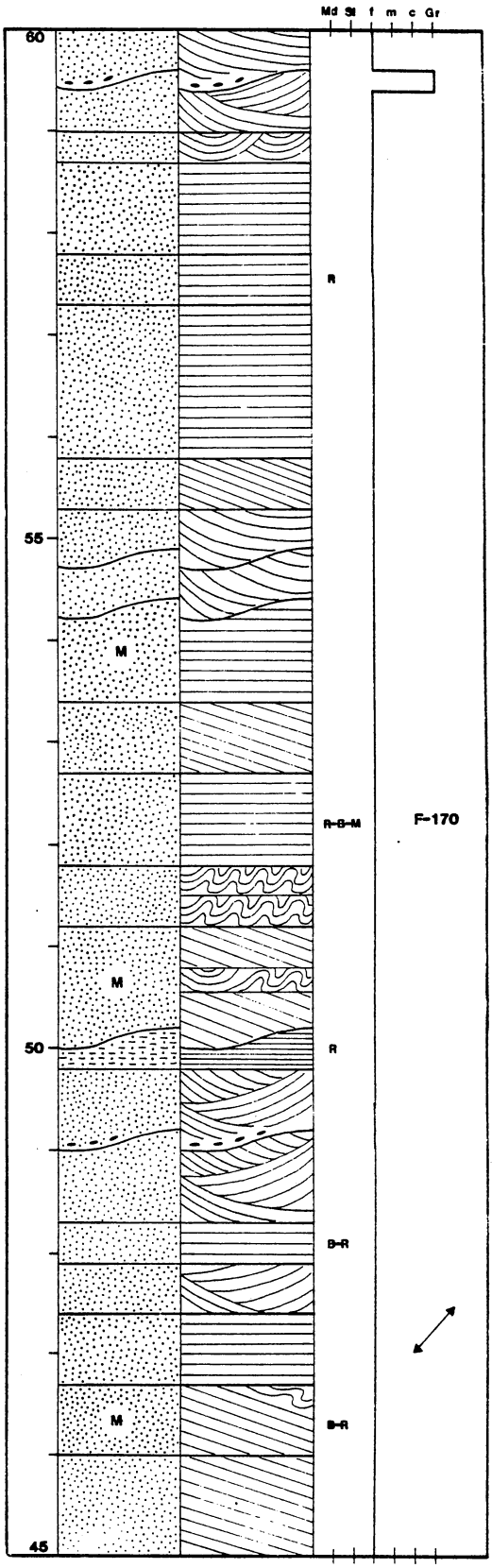
Md St f m c Gr
60
R
55
M
R-S-M
F-170
M
50
R
S-R
M
S-R
45

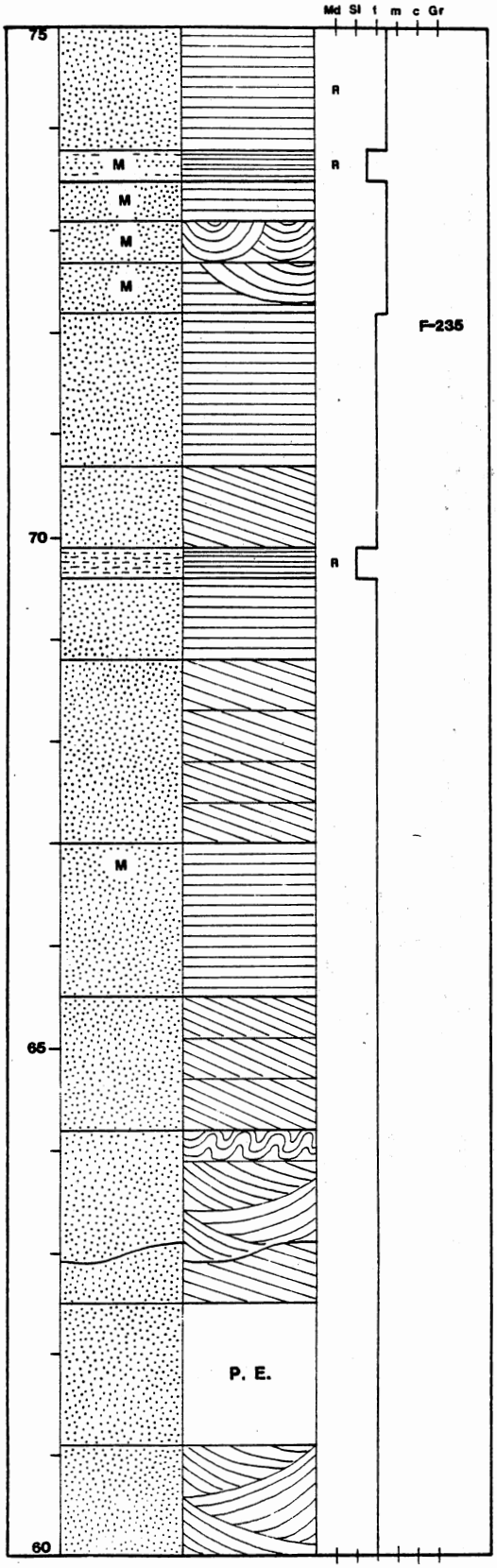
Md Si f m c Gr
75
70
65
60
M
M
M
M
M
P. E.
R
R
R
F-235

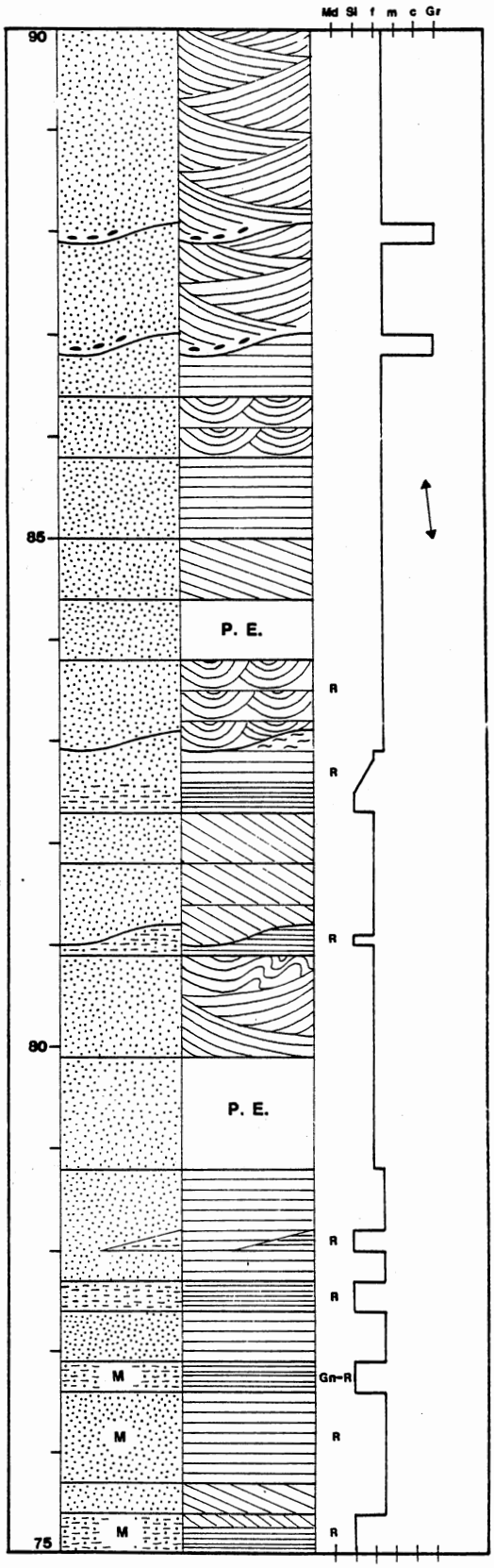
Md Si f m c Gr
90
85
80
75
P. E.
P. E.
M
M
M
R
R
R
R
R
R
R
Gn-R

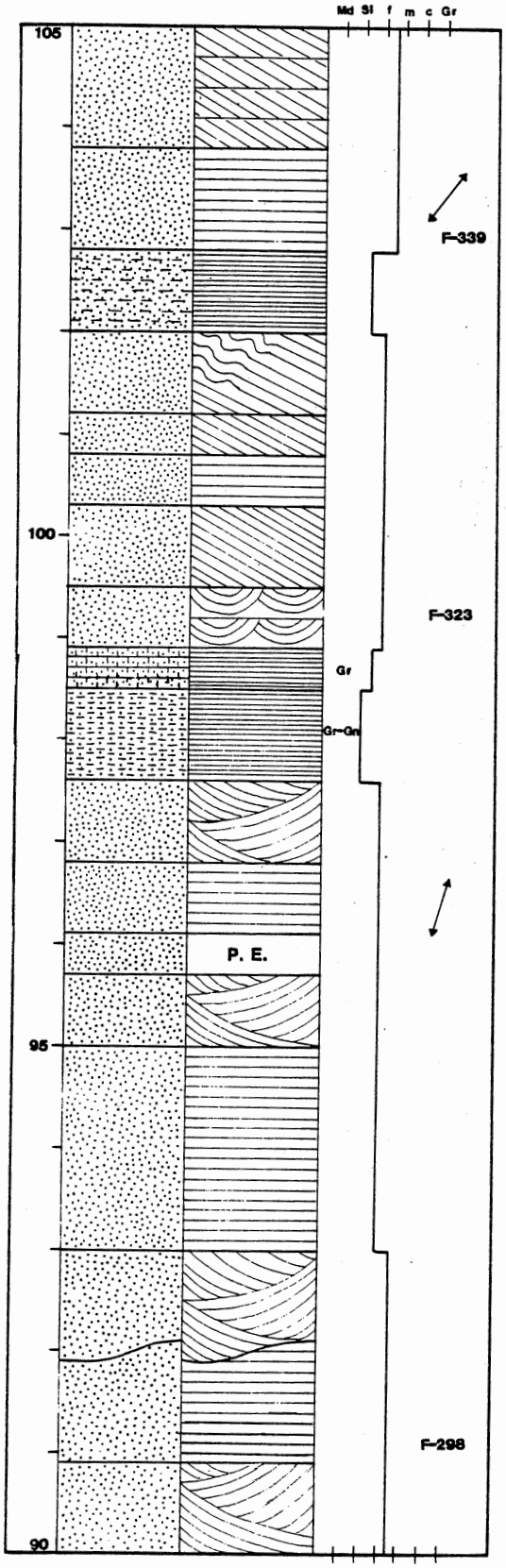
Md Sl f m c Gr
105
100
95
90
F-339
F-323
Gr
Gr-Gn
P. E.
F-298

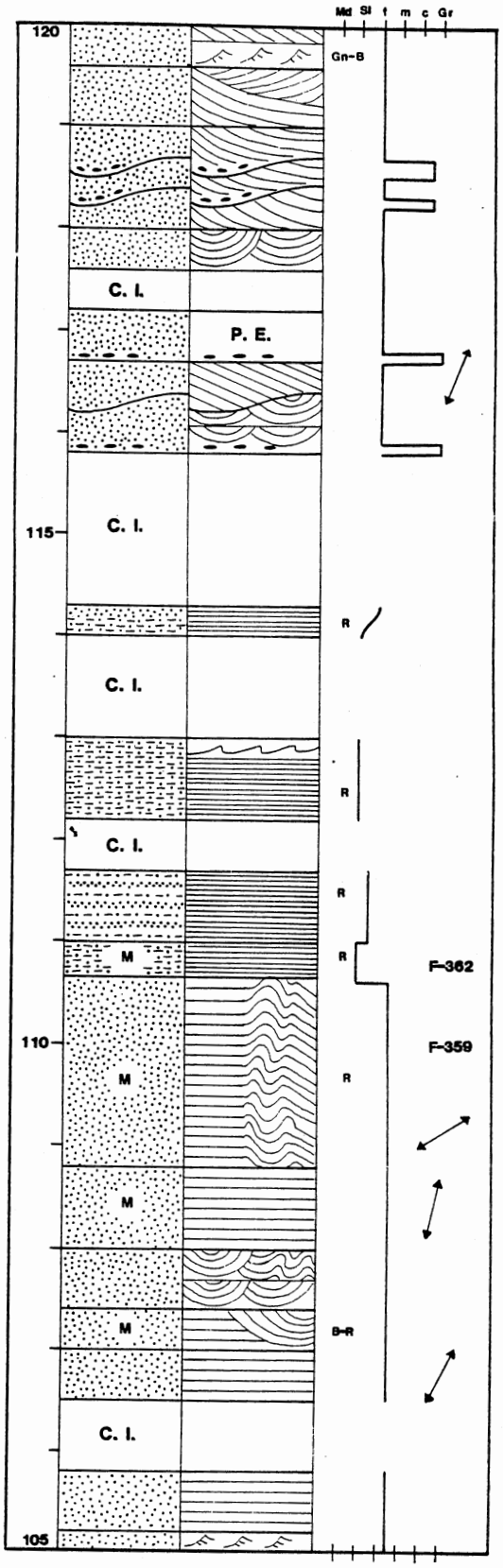
Md Sl f m c Gr
120
115
110
105
Gn-B
C. I.
P. E.
C. I.
R
C. I.
R
C. I.
R
M
R
F-362
M
R
F-359
M
M
B-R
C. I.

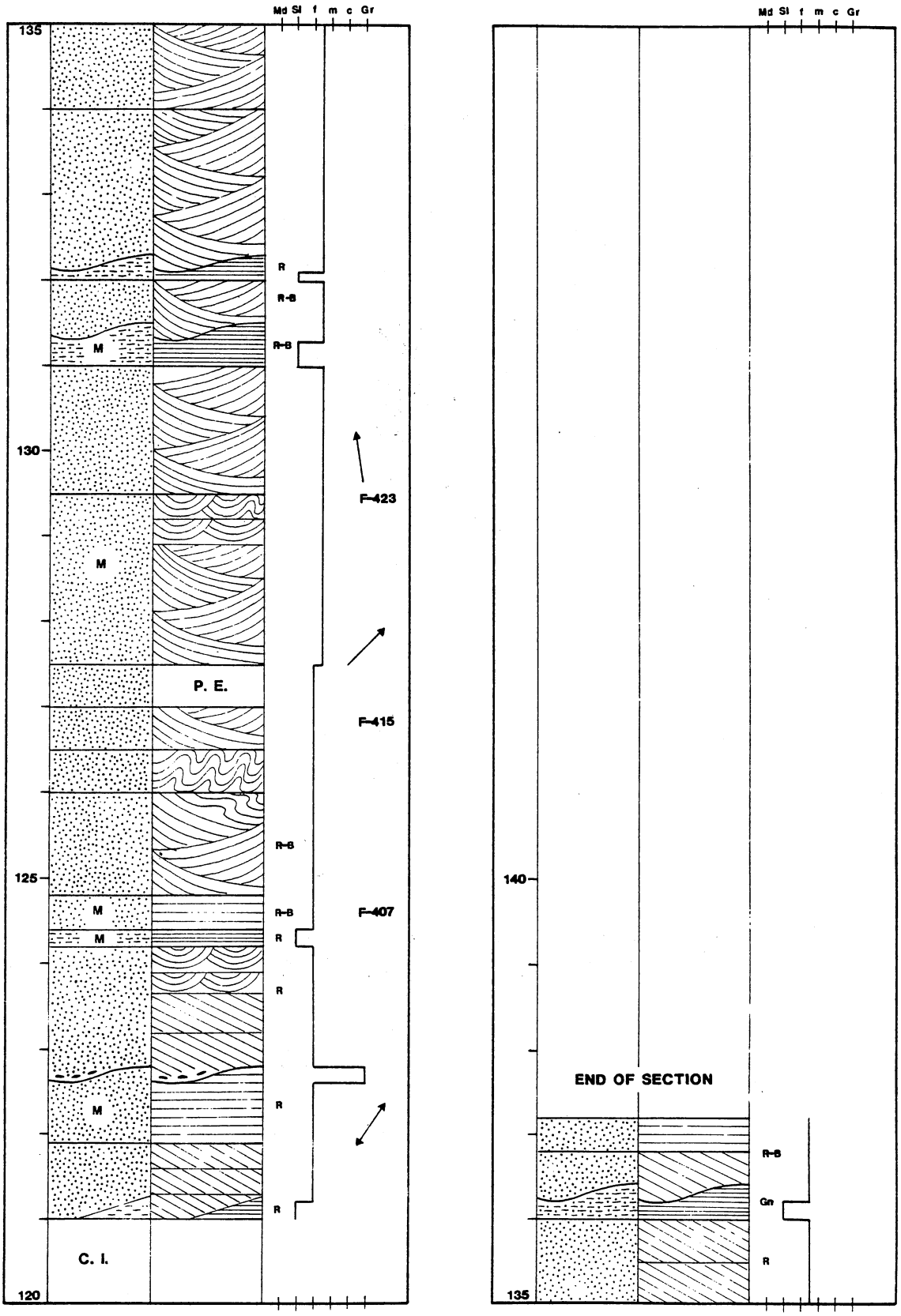
Md Sl f m c Gr
135
130
125
120
M
M
M
M
P. E.
C. I.
R
R-S
R-S
R-S
R-S
R
R
R
R
F-423
F-415
F-407
Md Sl f m c Gr
140
135
END OF SECTION
R-S
Gn
R

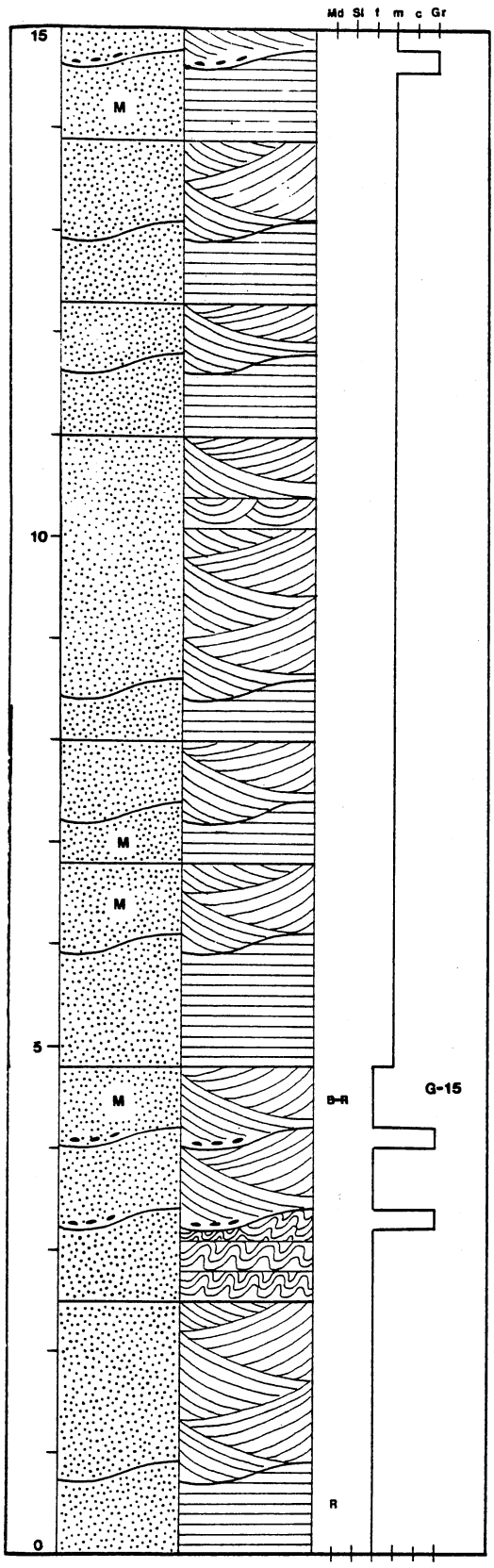
Md Si f m c Gr
15
10
5
0
M
M
M
M
B-R
R
G-15

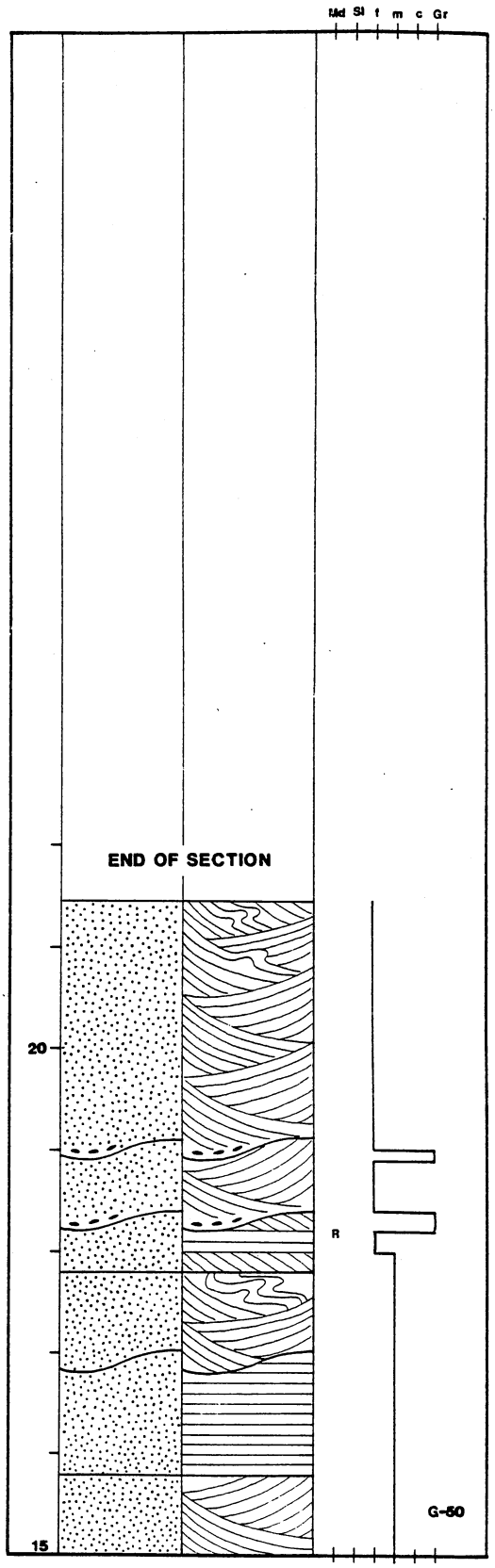
Md Si f m c Gr
END OF SECTION
20
15
R
G-50

APPENDIX C

MARKOV ANALYSIS

Introduction

A process exhibits the Markov property if "the preceding events have some influence on succeeding events" (Krumbein, 1967). With respect to sedimentary processes, a former depositional event (i.e., a stream flood) influences the following depositional event (i.e., flood-plain accretion).

The computer program used in this portion of the study was written by Krumbein (1967). Subsequently it was adapted for use on an Apple II computer by Bradley S. Huffman, a computer analyst for the Department of Geology at Oklahoma State University. This program appears on pages 248-253, Appendix C. The Markov tests which were completed on the various sequences in the Tarbat Peninsula section appear on pages 254-261, Appendix C.

Discussion

Miall (1973) provided an excellent review of the use of Markov analysis on alluvial plain successions. The following discussion is adapted chiefly from this work.

The first step in a Markov analysis is to develop a frequency matrix, a two-dimensional array which records the number of vertical transitions of each transition couplet. The lower and upper beds of each transition are represented by the row and column numbers, respectively. The symbol for transitions in the frequency matrix is f_{ij} where i is the row number, and j is the column number.

Two methods exist to tally the transitions which occur in a stratigraphic section. Method one records the transitions which occur at a fixed interval. Multi-storied units are not recognized in method one

analysis. Hence, positions in the frequency matrix where i equals j are arbitrarily assigned the value zero. Method one analysis was used in this study.

The number of transitions used in a Markov analysis is largely dependent on the number of major facies which occur in a stratigraphic succession. However, the use of too many transitions can result in needless complexity; usually, four to seven work best. In this study, four transitions were used in the U.O.R.S. and six transitions were used in the M.O.R.S.

The observed probability matrix and predicted probability matrix are derived from the frequency matrix. The observed probability matrix predicts the actual probability for a given transition to occur. Its formula is

$$P_{ij} = f_{ij}/S_i \qquad \text{(C-1)}$$

where P_{ij} equals the probability of the transition, and S_i equals the sum of the row. The predicted probability matrix predicts the probability of any transition occurring randomly. It is derived by the formula

$$r_{ij} = S_j/(t - S_i) \qquad \text{(C-2)}$$

Where r_{ij} equals the probability of a transition occurring randomly, S_j equals the sum of the row, and t equals the total number of transitions.

While strong transitions in the observed probability matrix denote the potential for a transition to occur, they do not indicate the presence of the Markov property. A difference matrix is necessay

to emphasize the presence of the Markov property for each transition. It is derived by the formula

$$d_{ij} = P_{ij} - r_{ij} \qquad \text{(C-3)}$$

where d_{ij} represents the presence or absence of the Markov property for each transition. Positive entries in the difference matrix are considered non-random, and thus emphasize the presence of the Markov property. Negative entries in the difference matrix are considered random, and thus are non-Markovian.

Ultimately, a chi-square test is necessary to determine if the stratigraphic succession exhibits the Markov property. For this study, the chi-square formula that was used is

$$X^2 = 2 \sum_{ij}^{n} f_{ij} \cdot \log_e\left(P_{ij}\left[S_j/f_{ij}\right]\right) \qquad \text{(C-4)}$$

where n equals the total number of rows or columns. The resulting statistic is then compared to a chi-square distribution table where the limiting value is derived from

$$(n - 1)^2 \qquad \text{(C-5)}$$

degrees of freedom. If the chi-square statistic exceeds the limiting value, the tested succession exhibits the Markov property. If the chi-square statistic is less than the limiting value, the tested succession is considered to be random and hence non-Markovian. All sequences subjected to Markov analysis in this study exhibit the Markov property to a 0.95 confidence level.

Application

When analyzing a stratigraphic sequence, it is customary to generate idealized vertical profiles from the subjective interpretation of a Markov analysis. This type of interpretation is very precise if the sequence is dominated by a cyclic process. However, if two or more processes interact, the strict application of a Markov analysis might result in an inaccurate representation of the stratigraphic sequence.

In such a sequence, transitions with high and low frequencies might produce difference matrix values which are negative and positive, respectively. An example of each is as follows: 1) in a total of sixteen possible transitions, the U.O.R.S. transition of facies Slt, Sglt, and Gm to erosional scours was observed in 29 of 140 instances, and has an observed probability of 0.52. The difference matrix value is zero and indicates a random transition; 2) between meter 0-70 of the M.O.R.S. section facies Slt is preceded by an erosive scour in two instances, and has an observed probability of 0.14. However, the resulting difference value of 0.12 indicates a non-random transition. The strict use of these transitions would not be representative of the sequence in which they occur.

Although atypical transitions may occur in complex stratigraphic sections, Markov analysis remains a viable interpretive tool to determine both obvious and subtle facies relations. However, each transition must be carefully scrutinized and interpreted subjectively before reasonable models can be developed.

```
]LOAD MATRIX
]LIST

1  REM            PROGRAM:   MATRIX
2  REM
3  REM            ORIGINAL ROUTINES BY
4  REM                W.C. KRUMBEIN
5  REM                     AND
6  REM                BETTY BENSON
7  REM                    1967
8  REM
9  REM            MODIFIED BY
10  REM                 BRADLEY S. HUFFMAN
11  REM                 OSU GEOLOGY DEPARTMENT
12  REM                 STILLWATER, OK 74078
13  REM                       1983
14  REM
15  REM
19  DIM F(10,10),P(10,10),R(10,10),SI(10),SJ(10)
20  CALL  - 936
30  PRINT : PRINT : PRINT
40  PRINT "****************************************"
50  PRINT "*             MARKOV    CHAINS         *"
60  PRINT "****************************************"
70  PRINT : PRINT
71  FOR I = 1 TO 10
72  FOR J = 1 TO 10
73 F(I,J) = 0
74 P(I,J) = 0
75 R(I,J) = 0
76 SJ(J) = 0
77  NEXT J
78 SI(I) = 0
79  NEXT I
80  PRINT "TITLE FOR THIS RUN?"
90  INPUT ") ";TS$
100  PRINT : PRINT
110  INPUT "NUMBER OF STATES (MAXIMUN OF 10)? ";M
120  IF M ) 10 THEN  GOTO 110
130  GOSUB 330
140  GOSUB 550
150  GOSUB 640
160  GOSUB 740
170  CALL  - 936
180  INPUT "POSTION PAPER AND PRESS RETURN";J$
190  PRINT  CHR$ (4);"PR#1"
200  PRINT  CHR$ (9) + "80N"
210  GOSUB 830
220  PRINT  CHR$ (4);"PR#0"
230  PRINT
240  PRINT
250  PRINT "DO YOU WISH TO SAVE THESE MATRICES?"
260  INPUT "ANSWER Y-YES, N-NO ) ";A$
270  IF A$ = "Y" THEN  GOSUB 1490
275  PRINT : PRINT : PRINT
280 A$ = "N"
290  PRINT "ENTER ANOTHER FREQUENCY MATRIX"
300  INPUT "ANSWER Y-YES , N-NO ) ";A$
310  IF A$ = "Y" THEN  GOTO 20
320  END
330  REM      **********************************
340  REM      *     INPUT FREQUENCY MATRIX     *
350  REM      **********************************
360  REM
370  CALL  - 936
380  PRINT "INPUT FREQUENCY MATRIX"
390  PRINT "=====================
```

```
400  PRINT
410 SM = 0.0
420  FOR I = 1 TO M
430  PRINT
440  PRINT "ROW ";I
450  PRINT "-------"
460  FOR J = 1 TO M
470  PRINT "COLUMN ";J;
480  INPUT ") ";F(I,J)
490 SM = SM + F(I,J)
500 SI(I) = SI(I) + F(I,J)
510 SJ(J) = SJ(J) + F(I,J)
520  NEXT J
530  NEXT I
540  RETURN
550  REM      ************************************
560  REM      *     CREATE PROBABILITY MATRIX     *
570  REM      ************************************
580  FOR I = 1 TO M
590  FOR J = 1 TO M
600  IF SI(I) ) 0.0 THEN P(I,J) = F(I,J) / SI(I)
610  NEXT J
620  NEXT I
630  RETURN
640  REM      ***********************************
650  REM      *     CREATE PREDICTED MATRIX     *
660  REM      ***********************************
670  FOR I = 1 TO M
680  FOR J = 1 TO M
690 SS = (SM + 1) - SI(I)
700  IF SS <  ) 0.0 THEN R(I,J) = SJ(J) / SS
710  NEXT J
720  NEXT I
730  RETURN
740  REM      ************************************
750  REM      *     CREATE DIFFERENCE MATRIX     *
760  REM      ************************************
770  FOR I = 1 TO M
780  FOR J = 1 TO M
790 D(I,J) = P(I,J) - R(I,J)
800  NEXT J
810  NEXT I
820  RETURN
830  REM      ***********************************
840  REM      *     PRINT FREQUENCY MATRIX     *
850  REM      ***********************************
860  PRINT "PROJECT: ";TS$
870  PRINT : PRINT
880  PRINT "FREQUENCY MATRIX"
890  PRINT
900  FOR I = 1 TO M
910  FOR J = 1 TO M
920  PRINT  RIGHT$ ("     " +  STR$ (F(I,J)),5);
930  NEXT J
940  PRINT " I "; LEFT$ ( STR$ (SI(I)) + "     ",5)
950  NEXT I
960  PRINT " ";
970  FOR J = 1 TO M
980  PRINT "-----";
990  NEXT J
1000  PRINT
1010  FOR J = 1 TO M
1020  PRINT  RIGHT$ ("     " +  STR$ (SJ(J)),5);
1030  NEXT J
1040  PRINT "   ";SM
1050  PRINT : PRINT
1060  REM      ***********************************
1070  REM      *     PRINT PROBABLITY MATRIX     *
1080  REM      ***********************************
```

```
1090  PRINT "OBSERVED PROBABILITY MATRIX"
1100  PRINT
1110  FOR I = 1 TO M
1120  FOR J = 1 TO M
1130 RR = P(I,J) + .005
1140 RR =  INT (100 * RR) / 100
1150  PRINT  RIGHT$ ("     " +  STR$ (RR),5);
1160  NEXT J
1170  PRINT
1180  NEXT I
1190  PRINT : PRINT
1200  REM      ***********************************
1210  REM      *     PRINT PREDICTED MATRIX      *
1220  REM      ***********************************
1230  PRINT "PREDICTED PROBABILITY MATRIX"
1240  PRINT
1250  FOR I = 1 TO M
1260  FOR J = 1 TO M
1270 RR = R(I,J) + .005
1280 RR =  INT (100 * RR) / 100
1290  PRINT  RIGHT$ ("     " +  STR$ (RR),5);
1300  NEXT J
1310  PRINT
1320  NEXT I
1330  PRINT : PRINT
1340  REM      ***********************************
1350  REM      *     PRINT DIFFERENCE MATRIX     *
1360  REM      ***********************************
1370  PRINT "DIFFERENCE MATRIX"
1380  PRINT
1390  FOR I = 1 TO M
1400  FOR J = 1 TO M
1410 RR = D(I,J) + .005
1420 RR =  INT (100 * RR) / 100
1430  PRINT  RIGHT$ ("     " +  STR$ (RR),5);
1440  NEXT J
1450  PRINT
1460  NEXT I
1470  RETURN
1480  RETURN
1490  REM      ***********************************
1500  REM      *     SAVE MATRICES IN A FILE     *
1510  REM      ***********************************
1520  PRINT : PRINT
1530  PRINT "ENTER A NAME FOR THE FILE"
1540  PRINT "  (NAME MUST BEGIN WITH A LETTER)"
1550  INPUT ") ";F$
1560  PRINT  CHR$ (4);"OPEN " + F$
1570  PRINT  CHR$ (4);"WRITE " + F$
1580  PRINT TS$
1590  PRINT M
1600  FOR I = 1 TO M
1610  FOR J = 1 TO M
1620  PRINT F(I,J)
1630  PRINT P(I,J)
1640  PRINT R(I,J)
1650  PRINT D(I,J)
1660  NEXT J
1670  NEXT I
1680  PRINT  CHR$ (4);"CLOSE " + F$
1690  RETURN
```

```
]LOAD TESTMARK
]LIST

1  REM             PROGRAM:   TESTMARK
2  REM
3  REM            ORIGINAL ROUTINES BY
4  REM                W.C. KRUMBEIN
5  REM                     AND
6  REM                BETTY BENSON
7  REM                    1967
8  REM
9  REM            MODIFIED BY
10  REM                 BRADLEY S. HUFFMAN
11  REM                 OSU GEOLOGY DEPARTMENT
12  REM                 STILLWATER, OK 74078
13  REM                       1983
14  REM
15  REM
19  DIM F(10,10),P(10,10),R(10,10),SI(10),SJ(10),PV(10),L(10,10)
20  CALL  - 936
30  PRINT "*********************************"
40  PRINT "*     TEST MARKOV PROPERTY      *"
49  PRINT "*********************************"
50  FOR I = 1 TO 10
51  FOR J = 1 TO 10
52 F(I,J) = 0
53 P(I,J) = 0
54 R(I,J) = 0
55 SJ(J) = 0
56  NEXT J
57 SI(I) = 0
58  NEXT I
60  GOSUB 910
70  GOSUB 1140
80  PRINT : PRINT
90  PRINT "PRINT INPUT MATRICES?"
100  INPUT "ANSWER Y-YES , N-NO ) ";A$
110  PRINT  CHR$ (4);"PR#1"
120  PRINT  CHR$ (9) + "80N"
130  PRINT "PROJECT: ";TS$
140  PRINT "DATA LOADED FROM FILE) ";F$
150  IF A$ = "Y" THEN  GOSUB 240
160  GOSUB 1340
170  PRINT  CHR$ (4);"PR#0"
180  PRINT
190  PRINT
200  PRINT "DO YOU WANT TO TEST ANOTHER FILE?"
210  INPUT "ANSWER Y-YES , N-NO ) ";A$
220  IF A$ = "Y" THEN  GOTO 20
230  END
240  REM       *************************
250  REM       *     PRINT MATRICES    *
260  REM       *************************
270  REM
280  REM
290  REM       PRINT FREQUENCY MATRIX
300  REM
310  PRINT "FREQUENCY MATRIX"
320  PRINT
330  FOR I = 1 TO M
340  FOR J = 1 TO M
350  PRINT  RIGHT$ ("     " +  STR$ (F(I,J)),5);
360  NEXT J
370  PRINT " I "; LEFT$ ( STR$ (SI(I)) + "     ",5)
380  NEXT I
390  PRINT " ";
400  FOR J = 1 TO M
```

```
410  PRINT "-----";
420  NEXT J
430  PRINT
440  FOR J = 1 TO M
450  PRINT  RIGHT$ ("     " +  STR$ (SJ(J)),5);
460  NEXT J
470  PRINT "   ";SM
480  PRINT : PRINT
490  REM
500  REM       PRINT PROBABLITY MATRIX
510  REM
520  PRINT "OBSERVED PROBABILITY MATRIX"
530  PRINT
540  FOR I = 1 TO M
550  FOR J = 1 TO M
560 RR = P(I,J) + .005
570 RR =  INT (100 * RR) / 100
580  PRINT  RIGHT$ ("     " +  STR$ (RR),5);
590  NEXT J
600  PRINT
610  NEXT I
620  PRINT : PRINT
630  REM
640  REM       PRINT PREDICTED MATRIX
650  REM
660  PRINT "PREDICTED PROBABILITY MATRIX"
670  PRINT
680  FOR I = 1 TO M
690  FOR J = 1 TO M
700 RR = R(I,J) + .005
710 RR =  INT (100 * RR) / 100
720  PRINT  RIGHT$ ("     " +  STR$ (RR),5);
730  NEXT J
740  PRINT
750  NEXT I
760  PRINT : PRINT
770  REM
780  REM       PRINT DIFFERENCE MATRIX
790  REM
800  PRINT "DIFFERENCE MATRIX"
810  PRINT
820  FOR I = 1 TO M
830  FOR J = 1 TO M
840 RR = D(I,J) + .005
850 RR =  INT (100 * RR) / 100
860  PRINT  RIGHT$ ("     " +  STR$ (RR),5);
870  NEXT J
880  PRINT
890  NEXT I
900  RETURN
910  REM       ************************************
920  REM       *     LOAD MATRICES FROM A FILE     *
930  REM       ************************************
940  REM
950  PRINT : PRINT
960  PRINT "ENTER NAME OF THE FILE"
970  INPUT ") ";F$
980  PRINT
990  PRINT "LOADING MATRICES"
1000  PRINT  CHR$ (4);"OPEN " + F$
1010  PRINT  CHR$ (4);"READ " + F$
1020  INPUT TS$
1030  INPUT M
1040  FOR I = 1 TO M
1050  FOR J = 1 TO M
1060  INPUT F(I,J),P(I,J),R(I,J),D(I,J)
1070 SM = SM + F(I,J)
1080 SI(I) = SI(I) + F(I,J)
```

```
1090 SJ(J) = SJ(J) + F(I,J)
1100  NEXT J
1110  NEXT I
1120  PRINT  CHR$ (4);"CLOSE " + F$
1130  RETURN
1140  REM       **********************************
1150  REM       *      CREATE N LOG P MATRIX     *
1160  REM       **********************************
1170  REM
1180  PRINT
1190  PRINT "CALCULATING P(J) ROW VECTOR"
1200  FOR J = 1 TO M
1210  IF SM ) 0.0 THEN PV(J) = SJ(J) / SM
1220  NEXT J
1230  PRINT
1240  PRINT "CALCULATING N LOG P MATRIX"
1250 TT = 0.0
1260  FOR I = 1 TO M
1270  FOR J = 1 TO M
1280  IF PV(J) (  ) 0.0 AND P(I,J) (  ) 0.0 THEN L(I,J) = F(I,J) *  LOG (P(I,J) / PV(J))
1290 TT = TT + L(I,J)
1300  NEXT J
1310  NEXT I
1320 TT = 2.0 * TT
1330  RETURN
1340  REM       ************************************
1350  REM       *     PRINT   P(J) ROW VECTOR      *
1360  REM       *        AND  N LOG P MATRIX       *
1370  REM       ************************************
1380  REM
1390  PRINT : PRINT
1400  PRINT "P(J) ROW VECTOR"
1410  PRINT
1420  FOR J = 1 TO M
1430 RR = PV(J) + .005
1440 RR =  INT (100 * RR) / 100
1450  PRINT  RIGHT$ ("     " +  STR$ (RR),5);
1460  NEXT J
1470  PRINT : PRINT
1480  PRINT "N LOG P MATRIX"
1490  PRINT
1500  FOR I = 1 TO M
1510  FOR J = 1 TO M
1520 RR = L(I,J) + .005
1530 RR =  INT (100 * RR) / 100
1540  PRINT  RIGHT$ ("       " +  STR$ (RR),7);
1550  NEXT J
1560  PRINT
1570  NEXT I
1580  PRINT : PRINT
1590  PRINT "2(SUM OF N LOG P MATRIX)= ";TT
1600  RETURN
```

PROJECT: MORS TOTAL
DATA LOADED FROM FILE) MORS TOTAL
FREQUENCY MATRIX

0	49	21	21	3	0	I	94
23	0	7	8	29	9	I	76
2	2	0	17	24	12	I	57
13	10	7	0	54	17	I	101
33	15	15	41	0	32	I	136
20	4	9	16	22	0	I	71
91	80	59	103	132	70		535

OBSERVED PROBABILITY MATRIX

0	.52	.22	.22	.03	0
.3	0	.09	.11	.38	.12
.04	.04	0	.3	.42	.21
.13	.1	.07	0	.53	.17
.24	.11	.11	.3	0	.24
.28	.06	.13	.23	.31	0

PREDICTED PROBABILITY MATRIX

.21	.18	.13	.23	.3	.16
.2	.17	.13	.22	.29	.15
.19	.17	.12	.22	.28	.15
.21	.18	.14	.24	.3	.16
.23	.2	.15	.26	.33	.17
.2	.17	.13	.22	.28	.15

DIFFERENCE MATRIX

-.21	.34	.09	-.01	-.27	-.16
.1	-.17	-.04	-.12	.09	-.03
-.15	-.13	-.12	.08	.15	.06
-.08	-.08	-.07	-.24	.23	.01
.02	-.09	-.04	.04	-.33	.06
.09	-.12	0	0	.03	-.15

P(J) ROW VECTOR

.17	.15	.11	.19	.25	.13

N LOG P MATRIX

0	61.19	14.83	3.12	-6.14	0
13.25	0	-1.26	-4.83	12.64	-.9
-3.16	-2.9	0	7.44	12.83	5.71
-3.62	-4.12	-3.25	0	41.76	4.28
11.72	-4.57	0	18.39	0	18.78
10.09	-3.9	1.25	2.52	5.01	0

2(SUM OF N LOG P MATRIX)= 412.338384

PROJECT: MORS M 0-70
DATA LOADED FROM FILE) MORS M 0-70
FREQUENCY MATRIX

0	2	5	7	0	0 I	14
0	0	0	0	0	2 I	2
0	0	0	3	7	5 I	15
2	0	1	0	9	10 I	22
5	0	5	6	0	9 I	25
7	0	5	6	8	0 I	26
14	2	16	22	24	26	104

OBSERVED PROBABILITY MATRIX

0	.14	.36	.5	0	0
0	0	0	0	0	1
0	0	0	.2	.47	.33
.09	0	.05	0	.41	.45
.2	0	.2	.24	0	.36
.27	0	.19	.23	.31	0

PREDICTED PROBABILITY MATRIX

.15	.02	.18	.24	.26	.29
.14	.02	.16	.21	.23	.25
.16	.02	.18	.24	.27	.29
.17	.02	.19	.27	.29	.31
.17	.02	.2	.28	.3	.32
.18	.03	.2	.28	.3	.33

DIFFERENCE MATRIX

-.15	.12	.18	.26	-.26	-.29
-.14	-.02	-.16	-.21	-.23	.75
-.16	-.02	-.18	-.04	.2	.04
-.08	-.02	-.15	-.27	.12	.14
.02	-.03	0	-.04	-.3	.04
.09	-.03	-.01	-.05	0	-.33

P(J) ROW VECTOR

.13	.02	.15	.21	.23	.25

N LOG P MATRIX

0	4.01	4.21	6.02	0	0
0	0	0	0	0	2.77
0	0	0	-.17	4.93	1.44
-.79	0	-1.22	0	5.15	5.98
1.98	0	1.31	.76	0	3.28
4.85	0	1.12	.52	2.3	0

2(SUM OF N LOG P MATRIX)= 96.9270635

PROJECT: MORS M 70-153
DATA LOADED FROM FILE) MORS M 70-153
FREQUENCY MATRIX

0	12	5	11	0	0	I	28
8	0	3	1	4	1	I	17
2	1	0	6	4	1	I	14
7	2	3	0	19	2	I	33
5	2	2	13	0	7	I	29
5	0	0	4	2	0	I	11
27	17	13	35	29	11		132

OBSERVED PROBABILITY MATRIX

0	.43	.18	.39	0	0
.47	0	.18	.06	.24	.06
.14	.07	0	.43	.29	.07
.21	.06	.09	0	.58	.06
.17	.07	.07	.45	0	.24
.45	0	0	.36	.18	0

PREDICTED PROBABILITY MATRIX

.26	.16	.12	.33	.28	.1
.23	.15	.11	.3	.25	.09
.23	.14	.11	.29	.24	.09
.27	.17	.13	.35	.29	.11
.26	.16	.13	.34	.28	.11
.22	.14	.11	.29	.24	.09

DIFFERENCE MATRIX

-.26	.27	.05	.06	-.28	-.1
.24	-.15	.06	-.24	-.01	-.04
-.08	-.07	-.11	.13	.04	-.02
-.06	-.11	-.04	-.35	.29	-.05
-.09	-.09	-.06	.11	-.28	.14
.23	-.14	-.11	.08	-.06	-.09

P(J) ROW VECTOR

.2	.13	.1	.27	.22	.08

N LOG P MATRIX

0	14.43	2.98	4.32	0	0
6.67	0	1.75	-1.51	.27	-.35
-.72	-.59	0	2.88	1.05	-.15
.25	-1.51	-.24	0	18.31	-.64
-.85	-1.25	-.71	6.83	0	7.44
3.99	0	0	1.26	-.38	0

2(SUM OF N LOG P MATRIX)= 127.082261

PROJECT: MORS M 153-180
DATA LOADED FROM FILE) MORS M 153-180
FREQUENCY MATRIX

0	3	1	1	1	0 I	6
0	0	0	0	5	1 I	6
0	0	0	2	3	1 I	6
0	1	1	0	5	1 I	8
4	2	1	5	0	5 I	17
1	0	3	0	3	0 I	7
5	6	6	8	17	8	50

OBSERVED PROBABILITY MATRIX

0	.5	.17	.17	.17	0
0	0	0	0	.83	.17
0	0	0	.33	.5	.17
0	.13	.13	0	.62	.13
.24	.12	.06	.29	0	.29
.14	0	.43	0	.43	0

PREDICTED PROBABILITY MATRIX

.11	.13	.13	.18	.38	.18
.11	.13	.13	.18	.38	.18
.11	.13	.13	.18	.38	.18
.12	.14	.14	.19	.4	.19
.15	.18	.18	.24	.5	.24
.11	.14	.14	.18	.39	.18

DIFFERENCE MATRIX

-.11	.37	.03	-.01	-.21	-.18
-.11	-.13	-.13	-.18	.46	-.01
-.11	-.13	-.13	.16	.12	-.01
-.12	-.01	-.01	-.19	.23	-.06
.09	-.06	-.12	.06	-.5	.06
.03	-.14	.29	-.18	.04	-.18

P(J) ROW VECTOR

.1	.12	.12	.16	.34	.16

N LOG P MATRIX

0	4.28	.33	.04	-.71	0
0	0	0	0	4.48	.04
0	0	0	1.47	1.16	.04
0	.04	.04	0	3.04	-.25
3.42	-.04	-.71	3.04	0	3.04
.36	0	3.82	0	.69	0

2(SUM OF N LOG P MATRIX)= 55.2676536

PROJECT: MORS M 180-220
DATA LOADED FROM FILE) MORS M 180-220
FREQUENCY MATRIX

0	5	2	1	2	0	10
3	0	0	3	6	1	13
0	1	0	1	0	0	2
2	1	0	0	5	0	8
4	3	0	4	0	0	11
1	0	0	0	0	0	1
10	10	2	9	13	1	45

OBSERVED PROBABILITY MATRIX

0	.5	.2	.1	.2	0
.23	0	0	.23	.46	.08
0	.5	0	.5	0	0
.25	.13	0	0	.62	0
.36	.27	0	.36	0	0
1	0	0	0	.0	0

PREDICTED PROBABILITY MATRIX

.28	.28	.06	.25	.36	.03
.3	.3	.06	.27	.39	.03
.23	.23	.05	.2	.3	.02
.26	.26	.05	.24	.34	.03
.29	.29	.06	.26	.37	.03
.22	.22	.04	.2	.29	.02

DIFFERENCE MATRIX

-.28	.22	.14	-.15	-.16	-.03
-.07	-.3	-.06	-.04	.07	.05
-.23	.27	-.05	.3	-.3	-.02
-.01	-.14	-.05	-.24	.28	-.03
.08	-.01	-.06	.11	-.37	-.03
.78	-.22	-.04	-.2	-.29	-.02

P(J) ROW VECTOR

.22	.22	.04	.2	.29	.02

N LOG P MATRIX

0	4.05	3.01	-.69	-.74	0
.11	0	0	.43	2.81	1.24
0	.81	0	.92	0	0
.24	-.58	0	0	3.86	0
1.97	.61	0	2.39	0	0
1.5	0	0	0	0	0

2(SUM OF N LOG P MATRIX)= 43.9105405

PROJECT: MORS LATERAL BC M 0-70
DATA LOADED FROM FILE) MORS LATERAL BC M 0-70
FREQUENCY MATRIX

0	8	3	0	0	0	I	11
5	0	3	0	5	2	I	15
0	0	0	4	6	3	I	13
0	2	1	0	9	2	I	14
3	4	6	8	0	6	I	27
2	3	1	3	3	0	I	12
10	17	14	15	23	13		92

OBSERVED PROBABILITY MATRIX

0	.73	.27	0	0	0
.33	0	.2	0	.33	.13
0	0	0	.31	.46	.23
0	.14	.07	0	.64	.14
.11	.15	.22	.3	0	.22
.17	.25	.08	.25	.25	0

PREDICTED PROBABILITY MATRIX

.12	.21	.17	.18	.28	.16
.13	.22	.18	.19	.29	.17
.13	.21	.17	.19	.29	.16
.13	.22	.18	.19	.29	.16
.15	.26	.21	.23	.35	.2
.12	.21	.17	.19	.28	.16

DIFFERENCE MATRIX

-.12	.52	.1	-.18	-.28	-.16
.21	-.22	.02	-.19	.04	-.03
-.12	-.21	-.17	.12	.17	.07
-.13	-.07	-.11	-.19	.35	-.02
-.04	-.11	.01	.07	-.35	.03
.04	.04	-.09	.06	-.03	-.16

P(J) ROW VECTOR

.11	.18	.15	.16	.25	.14

N LOG P MATRIX

0	10.96	1.75	0	0	0
5.6	0	.82	0	1.44	-.12
0	0	0	2.54	3.68	1.47
0	-.51	-.76	0	8.5	.02
.07	-.88	2.27	4.78	0	2.72
.85	.91	-.6	1.28	0	0

2(SUM OF N LOG P MATRIX)= 93.5782249

PROJECT: MORS LATERAL BC M 70-137 MORS R
DATA LOADED FROM FILE) MORS LATERAL BC M 70-137 MORS R
FREQUENCY MATRIX

0	19	5	1	0	0 I	25
7	0	1	4	9	2 I	23
0	0	0	1	4	2 I	7
2	4	1	0	7	2 I	16
12	4	1	5	0	5 I	27
4	1	0	3	6	0 I	14
25	28	8	14	26	11	112

OBSERVED PROBABILITY MATRIX

0	.76	.2	.04	0	0
.3	0	.04	.17	.39	.09
0	0	0	.14	.57	.29
.13	.25	.06	0	.44	.13
.44	.15	.04	.19	0	.19
.29	.07	0	.21	.43	0

PREDICTED PROBABILITY MATRIX

.28	.32	.09	.16	.3	.13
.28	.31	.09	.16	.29	.12
.24	.26	.08	.13	.25	.1
.26	.29	.08	.14	.27	.11
.29	.33	.09	.16	.3	.13
.25	.28	.08	.14	.26	.11

DIFFERENCE MATRIX

-.28	.44	.11	-.12	-.3	-.12
.03	-.31	-.05	.02	.1	-.04
-.24	-.26	-.08	.01	.33	.18
-.13	-.04	-.02	-.14	.17	.01
.15	-.18	-.06	.02	-.3	.06
.03	-.21	-.08	.07	.17	-.11

P(J) ROW VECTOR

.22	.25	.07	.13	.23	.1

N LOG P MATRIX

0	21.13	5.15	-1.14	0	0
2.17	0	-.5	1.32	4.7	-.24
0	0	0	.13	3.6	2.14
-1.16	0	-.13	0	4.44	.48
8.26	-2.09	-.66	1.97	0	3.17
.99	-1.25	0	1.62	3.68	0

2(SUM OF N LOG P MATRIX)= 115.526236

PROJECT: UORS TOTAL
DATA LOADED FROM FILE) UORS TOTAL
FREQUENCY MATRIX

0	41	1	3 I	45
29	0	14	12 I	55
7	5	0	7 I	19
9	10	2	0 I	21
45	56	17	22	140

OBSERVED PROBABILITY MATRIX

0	.91	.02	.07
.53	0	.25	.22
.37	.26	0	.37
.43	.48	.1	0

PREDICTED PROBABILITY MATRIX

.47	.58	.18	.23
.52	.65	.2	.26
.37	.46	.14	.18
.38	.47	.14	.18

DIFFERENCE MATRIX

-.47	.33	-.15	-.16
0	-.65	.06	-.04
0	-.2	-.14	.19
.05	.01	-.05	-.18

P(J) ROW VECTOR

.32	.4	.12	.16

N LOG P MATRIX

0	33.75	-1.7	-2.57
14.35	0	10.36	3.94
.96	-2.09	0	5.96
2.59	1.74	-.49	0

Σ(SUM OF N LOG P MATRIX)= 133.614148

APPENDIX D

VON MISES PROGRAM AND PALEOCURRENT READINGS

```
]LIST

1  REM      VON MISES
2  REM
3  REM      ORIGINAL AUTHOR: D.J. SANDERSON
4  REM      MODIFIED BY:     BRADLEY S. HUFFMAN
5  REM                       GEOLOGY DEPARTMENT
6  REM                       OKLAHOMA STATE UNIVERSITY
7  REM                       STILLWATER, OK 74074
10  DIM TD(2000),TW(2000)
20  CALL  - 936
30  PRINT "****************************************"
40  PRINT "*      2-D ORIENTATION STATISTICS      *"
50  PRINT "****************************************"
60  PRINT : PRINT
70  PRINT "SELECT FROM :"
80  PRINT
90  PRINT
100  PRINT "1: BASIC VON MISES STATS"
110  PRINT
120  PRINT "2: 2-SAMPLE 'F' TEST"
130  PRINT
140  PRINT "Q: QUIT PROGRAM"
150  PRINT
160  INPUT "WHICH ONE? ";C$
170  IF C$ = "Q" THEN  END
180  IF C$ = "1" THEN  GOSUB 210
190  IF C$ = "2" THEN  GOSUB 1130
200  GOTO 20
210  CALL  - 936
220  PRINT "**     VON MISES STATISTICS     **"
230  PRINT : PRINT
240  PRINT "TERMINATE DATA WITH (-9999)"
250  PRINT
260 SS = 0
270 SC = 0
280 N = 0
290 DR = 3.14159265 / 180
300 I$ = "2"
310 D$ = "N"
320 W$ = "N"
330 N = 0
340 DD = 1
350 CN = 1
360  PRINT
370  PRINT "WHERE IS THE DATA?"
380  PRINT
390  PRINT "     1: INPUT FROM A TEXT FILE"
400  PRINT
410  PRINT "     2: INPUT FROM THE KEYBROAD"
420  PRINT
```

```
430  INPUT "WHICH ONE? ";I$
431  IF I$ <  > "1" AND I$ <  > "2" THEN  GOTO 210
432  IF I$ = "1" THEN  GOSUB 880
433  IF I$ = "2" THEN  GOSUB 740
460  FOR I = 1 TO CN
470 D = TD(I) * DD * DR
480 SS = SS +  SIN (D) * TW(I)
490 SC = SC +  COS (D) * TW(I)
500 N = N + TW(I)
510  NEXT I
515 A$ = "N"
530  IF I$ <  > "1" THEN  INPUT "DO YOU WANT TO SAVE THE DATA (Y/N)? ";A$
540  IF A$ = "Y" THEN  GOSUB 1000
550 MD =  ATN (SS / SC) / DR
555  IF SC < 0 THEN MD = 180 + MD
560  IF SC = 0 THEN MD =  SGN (SS) * 90
580  IF MD < 0 THEN MD = 360 + MD
590 R =  SQR (SS * SS + SC * SC)
600 RN = R / N
610  CALL  - 936
620  PRINT : PRINT
630  IF DD = 2 THEN  THEN  PRINT "DATA DOUBLED"
640  PRINT
650  PRINT "VECTOR MEAN = ";MD
660  PRINT "RESULTANT = ";R
670  PRINT "R/N = ";RN
680  PRINT "N = ";N
690  PRINT "Z STATISTIC = ";R * R / N
710  PRINT : PRINT : PRINT
720  INPUT "PRESS RETURN TO CONTINUE...";J$
730  RETURN
731  REM
732  REM
733  REM
740  PRINT
750  INPUT "DOUBLING OF THE DATA (Y/N)? ";D$
760  IF D$ = "Y" THEN DD = 2
770  PRINT
780  PRINT
790  INPUT "DO YOU WANT LENGTH WEIGHTING (Y/N)? ";W$
800  PRINT
810  PRINT "*** INPUT DATA ***"
820  PRINT
840  IF W$ = "Y" THEN  INPUT TD(CN),TW(CN)
850  IF W$ <  > "Y" THEN  INPUT TD(CN):TW(CN) = 1
860  IF TD(CN) =  - 9999 THEN  RETURN
870 CN = CN + 1
875  GOTO 840
876  REM
877  REM
878  REM
880  PRINT "NAME OF TEXT FILE?"
```

```
890  INPUT ") ";F$
900  PRINT  CHR$ (4);"OPEN " + F$
910  PRINT  CHR$ (4);"READ " + F$
920  INPUT D$
930  INPUT W$
940  INPUT CN
950  FOR I = 1 TO CN
960  INPUT TD(I)
961  INPUT TW(I)
970  NEXT I
980  PRINT  CHR$ (4);"CLOSE " + F$
990  RETURN
991  REM
992  REM
993  REM
1000  PRINT "NAME FOR TEXT FILE?"
1010  INPUT ") ";F$
1020  PRINT  CHR$ (4);"OPEN " + F$
1030  PRINT  CHR$ (4);"WRITE " + F$
1040  PRINT D$
1050  PRINT W$
1060  PRINT CN
1070  FOR I = 1 TO CN
1080  PRINT TD(I)
1085  PRINT TW(I)
1100  NEXT I
1105  PRINT
1110  PRINT  CHR$ (4);"CLOSE " + F$
1120  RETURN
1130  CALL  - 936
1140  PRINT "**   2-SAMPLE 'F' TEST    **"
1150  PRINT : PRINT
1160  PRINT "SAMPLE A"
1170  INPUT "N = ";NA
1180  INPUT "MEAN = ";MA
1190  INPUT "R/N = ";RA
1200  PRINT
1210  PRINT "SAMPLE B"
1220  INPUT "N = ";NB
1230  INPUT "MEAN = ";MB
1240  INPUT "R/N = ";RB
1250 RB = RB * NB
1260 RA = RA * NA
1270 PH = (MA - MB) * 3.1415927 / 180
1280 R =  SQR (RA * RA + RB * RB + 2 * RA * RB *  COS (PH))
1290 F = (NA + NB - 2) * (RA + RB - R) / (NA + NB - RA - RB)
1300  PRINT : PRINT
1310  PRINT "F = ";F
1320  PRINT "WITH 1, ";NA + NB - 2;" DEG. FREEDOM"
1330  PRINT : PRINT
1340  INPUT "PRESS RETURN TO CONTINUE...";J$
1350  RETURN
```

Trough Axis Readings collected from M.O.R.S. units within the study area. Data collected by R. N. Donovan and the author.

065	035	025	065	290	017	315
080	055	038	075	318		016
070	085	020	070	030	050	320
050	080	095	065	320		310
065	035	020	035	069	022	
070	055	060	045	045	035	
060	085	070	036	055	065	
065	080	075	041	065	315	
070	065	080	034	079	339	
060	080	075	041	052	335	
065	065	075	034	040	342	
070	080	050	042	044	010	
055	080	055	065	025	030	
065	035	065	045	040	330	
070	005	090	058	040	340	
080	015	070	045	023	320	
075	055	070	058	013	326	
075	065	065	045	036	313	
085	040	100	059	036	310	
075	030	070	039	040	310	
055	050	080	062	035	015	
050	070	110		022	338	
085	110	075		027	358	
080	045	070		026	274	

Trough Axis Readings collected from M.O.R.S units south of the study area.

058	038	035	065
055	052	065	078
015	060	028	060
050	052	052	055
052	060	036	060
055	060	064	075
058	058	038	045
070	052	039	052
042	035	058	065
038	040	072	052
035	037	010	058
055	048	058	067
040	055	063	082
052	042	084	060
037	046	070	040
065	050	057	030
015	060	059	050

Parting Lineation Readings collected from M.O.R.S. units within the study area. Data collected by R. N. Donovan and the author.

025	080	153	145	022
030	085	085	068	045
050	125	065	068	045
105	055	045	068	
040	078	065	068	
045	085	030	070	
030	065	000	044	
070	160	065	135	
045	065	090	016	
050	160	044	048	
100	093	045	026	
045	060		010	

Small-scale Trough Axis Readings from M.O.R.S. units within the the study area. Data collected by R. N. Donovan and the author.

070	065	048
065	110	060
070	105	045
065	105	095
050	115	090

Trough Axis Readings collected from U.O.R.S. units within the study area. Data collected by the author.

335	024	332	002	014
350	024	222	315	022
270	007	335	352	314
310	306	024	323	348
305	334	355	327	334
300	336	330	359	339
350	336	347	020	345
346	348	345	036	355
328	329	320	042	

APPENDIX E

TEXTURAL, DETRITAL AND DIAGENETIC DESCRIPTIONS OF SAMPLES COLLECTED WITHIN THE STUDY AREA

Explanation:

Textures

R - range
A - average
} grain size in millimeters, unless indicated otherwise

Detrital constituents

Quartz

st - straight extinction
un - undulose extinction
px - polycrystalline extinction

Feldspars

or - orthoclase
mc - microcline
pl - plagioclase
pt - perthite

Lithic fragments

SRF - sedimentary
md - mudstone
sl - siltstone
ch - chert
ls - limestone
ss - sandstone
MRF - metamorphic
qz - metaquartzite
gn - gneissic
sh - schistose
IRF - igneous
gr - granitic
rh - rhyolite

Others

bt - biotite
mu - muscovite
hhm - opaque heavy minerals, principally hematite
lhm - opaque heavy minerals, principally leucoxene
thm - translucent heavy minerals, principally zircon; others include garnet, hornblende, epidote, and apatite
gl - glauconite
dtmx - detrital matrix
auch - authigenic chert

Explanation (Continued)

Diagenetic constituents*

Cement

qtz - quartz overgrowths
? - possible but very minor
✓ - probable but very minor
- - absent

Authigenic clays

K - kaolinite
I - illite-smectite
Chl - chlorite

Secondary porosity

irg - regular intergranular
ingr - intragranular
inrp - intrareplacement
incm - intracement
inmx - intramatrix
fg - fractured grains
mn - minor
md - moderate
dm - dominant

*Percentage of samples include both detrital and diagenetic constituents.

TABLE XIV

TEXTURAL DESCRIPTIONS OF SAMPLES COLLECTED WITHIN THE STUDY AREA

Sample Number	Section Location	Grain Size	Rounding	Sphericity	Packing	Fabric	Textural Maturity
A'- 25	U.O.R.S.	R: .06 - .50 A: .31	subangular	low	moderate	floating	submature
A'- 56	U.O.R.S.	R: .05 - .70 A: .30	subangular	moderate	loose	floating	submature
A- 3	U.O.R.S. 262 m	R: .05 -1.75 A: .90	subangular	low	moderate	long	submature
A- 24	U.O.R.S. 269	R: .07 -1.75 A: .50	subangular subrounded	moderate	moderate	long	submature
A- 40	U.O.R.S. 273 m	R: .05 - .75 A: .40	subrounded	moderate	loose	floating	submature
A- 65	U.O.R.S. 281 m	R:2.5mμ-2.5mm A: 5mμ	-	-	-	-	-
A- 99	U.O.R.S. 291 m	R: .1 - .70 A: .50	subrounded	moderate	moderate	long	submature
A-130	U.O.R.S. 300 m	R: .07-1 A: .30	subangular subrounded	moderate		long	submature
A-203	U.O.R.S. 323 m	R: .07-1 A: .35	subangular	moderate		long	submature
A-222	U.O.R.S. 329 m	R: .04-15 A: .45	subrounded	moderate	moderate	moderate	submature
A-229	U.O.R.S. 331 m	R: .10-1.1 A: .45	subrounded	moderate	moderate	point	submature
A-250	U.O.R.S. 338 m	R: .07-2.5 A: .6	subangular	moderate	loose	floating	submature
A-251	U.O.R.S. 338 m	R: .05-.8 A: .30	subrounded	moderate	moderate	point	submature

TABLE XIV (Continued)

Sample Number	Section Location	Grain Size	Rounding	Sphericity	Packing	Fabric	Textural Maturity
A- ab	U.O.R.S.	R: .05 - .8 A: .30	subrounded	low	loose moderate	floating	submature
B- 11	U.O.R.S 224 m	R: .06 - .45	subrounded	moderate	moderate	point	submature
E- 2	M.O.R.S. 1 m	R: .02 - .19 A: .11	subangular	low	loose	floating	submature
E- 15	M.O.R.S. 5 m	R: .05 - .48 A: .15-A2:.22	subangular subrounded	low moderate	moderate	point floating	submature
E- 30	M.O.R.S. 9 m	R: .03 - .44 A: .15	subangular	low moderate	loose	point floating	submature
E- 40	M.O.R.S. 12 m	R: .05 - .31 A: .15	angular subangular	moderate	loose	floating	submature
E- 45	M.O.R.S.$_1$ 14 m	R: .05 - .30 A: .15	angular subangular	low	loose	floating	submature
E-142	M.O.R.S.$_1$ 40 m	R: .03 - .42 A: .22	subrounded	moderate	moderate	point floating	submature
E-155	M.O.R.S.$_1$ 47 m	R: .03 - .27 A: .14	subangular	low	loose	point floating	submature
E-205	M.O.R.S.$_1$ 62 m	R: .06 - .11 A: .22	subrounded	moderate	moderate	point floating	submature
E-283	M.O.R.S.$_1$ 87 m	R: 5mμ -.22mm A: .12	subangular	low	moderate light	point long	immature
E-306	M.O.R.S.$_1$ 94 m	R: .06 - .6 A: .22	subrounded	moderate	moderate	point floating	submature
E-362	M.O.R.S.$_2$ 111 m	R: .03 - .50 A: .12-A2:.2	subangular subrounded	moderate high	moderate	point floating	submature
D- 15	M.O.R.S.$_1$ 134 m	R: .09 - .51 A:	subrounded	moderate high	moderate	point floating	submature

TABLE XIV (Continued)

Sample Number	Section Location	Grain Size	Rounding	Sphericity	Packing	Fabric	Textural Maturity
C- 14	M.O.R.S.$_1$ 142 m	R: .05 - .72 A: .32	subrounded	moderate	moderate	point floating	submature
C- 32	M.O.R.S.$_1$ 147 m	R: .02 - .35 A: .10	subangular	low moderate	tight	long	submature
C- 39	M.O.R.S.$_1$ 149 m	R: .05 - .35 A: .20	subrounded	moderate	moderate	long	submature
C- 67	M.O.R.S.$_1$ 158 m	R: - .22 A: .12-A2-.18	subrounded	low moderate	moderate	long	mature
C- 97	M.O.R.S.$_1$ 167 m	R: .02 - .25 A: .15	subangular	low moderate	loose	floating	submature
C-110	M.O.R.S.$_1$ 171 m	R: .02 - .20 A: .10	subangular	moderate	loose	floating	submature
C-125	M.O.R.S.$_1$ 175 m	R: .05 - .42 A: .20	subrounded	moderate	moderate	point floating	submature
C-180	M.O.R.S.$_1$ 192 m	R: .05 - .30 A: .19	subangular subrounded	moderate	moderate	floating	sumbature
C-270	M.O.R.S.$_1$ 220 m	R: .05 - .42 A: .22	subrounded	moderate	loose	floating	submature
F- 8	M.O.R.S.$_2$ 2 m	R: .03 - .45 A: .18	subrounded	moderate	loose	point floating	submature
F- 60	M.O.R.S.$_2$ 18 m	R: .03 - .37 A: .15	subangular	moderate low	loose	point floating	submature
F- 86	M.O.R.S.$_2$ 26 m	R: .02 - .35 A: .16	subangular	moderate	moderate	long	submature
F-113	M.O.R.S.$_2$ 35 m	R: .05 - .30 A: .21	subrounded	moderate	moderate	point floating	submature
F-170	M.O.R.S.$_2$ 52 m	R: .05 - .48 A: .20	subrounded	moderate	point moderate	point floating	submature
F-235	M.O.R.S.$_2$ 72 m	R: .03 - .52 A: .17	subangular	low	moderate	point floating	submature

TABLE XIV (Continued)

Sample Number	Section Location	Grain Size	Rounding	Sphericity	Packing	Fabric	Textural Maturity
F-298	M.O.R.S.$_2$ 91 m	R: .04 - .7 A: .23	subrounded	moderate	moderate	point floating	submature
F-323	M.O.R.S.$_2$ 99 m	R: 5mμ-.25mm A: .08	angular subangular	low	loose	floating	immature
F-339	M.O.R.S.$_2$ 103 m	R: .03 - .65 A_1:.20-A_2.30	subrounded	moderate high	moderate light	point floating	submature
F-359	M.O.R.S.$_2$ 110 m	R: .05 - .53 Ai:.21-A_2.10	subrounded	moderate	moderate	point floating	submature
F-407	M.O.R.S.$_2$ 125 m	R: .03 - .42 A: .19	subrounded	moderate high	moderate	point floating	submature
F-415	M.O.R.S.$_2$ 127 m	R: .05 - .52 A: .18	subrounded	moderate	moderate	point floating	submature
F-423	M.O.R.S.$_2$ 129 m	R: .03 - .70 A_1:.2-A_2:.12	subrounded	moderate	moderate	point floating	submature
G- 15	M.O.R.S.$_3$ 5 m	R: .07 - .60 A_1:.32 A_2:.15	subrounded rounded	high	loose	point floating	submature
G- 50	M.O.R.S.3 15 m	R: .02 - .87 A_1:.15-A_2-.35	subrounded rounded	high	moderate	point floating	submature

TABLE XV

DETRITAL DESCRIPTIONS OF SAMPLES COLLECTED WITHIN THE STUDY AREA

Sample Number	Quartz, %			Feldspars, %				Q/F ratio	Lithic Fragments, %			Other Detrital Constituents
	st	un	px	or	mc	pl	pt		SRF	MRF	IRF	
A'- 25	20.75	18.50	10.5	3.0	2.50	2.75	1.0	4.6	md-1.25 si-1.25 ch- .5 ch-1.75	qz-2.25 gn-0.75 qz-3.75	gr-0.75 gr-1.75	bt-0.50 mu-0.75 ohm-1.0 mu-1.75
A'- 56	25.0	14.0	12.0	6.75	1.50	1.0	0.75	5.1	sl-1.25 md-0.75 ch-1.0	qz-18.-	gr-1.5	ohm-1.75 thm-0.5 bt-0.25 au.ch-0.75
A - 3	13.0	23.25	15.75	3.75	1.75	2.0	1.0	6.1	md-1.5 ss-1.25	sh-0.5		mu-0.5 ohm-0.5 dt mx-1.0
A - 24	14.25	28.25	12.25	7.0	2.25	1.25	0.5	5.0	md-1.0 ch-1.25 ls-1.0	qz-7.25 sh-0.5	gr-1.0	mu-0.25 ohm-0.25 thm-0.25
A - 40	25.0	25.25	10.25	5.5	3.0	1.25	0.25	6.0	ch-2.5 md-1.0 ls-1.0	qz-4.75 gn-0.25	-	-
A - 65	-	-	-	-	-	-	-	-	-	-	-	-
A - 99	10.25	25.75	11.5	6.75	2.5	2.0	0.50	4.0	md-6.0 ch-0.5	qz-7.5 gn-1.0	gr-0.25	mu-trace thm-0.25 dt mx-3.0
A -130	26.25	24.25	9.0	3.75	1.25	1.5	0.75	8.2	md-225 sl-0.75 ch-0.25	qz-275	gr-0.5	bt-trace mu-0.75 ohm-0.50 dt mx-2.0
A -203	19.75	17.0	7.25	5.0	2.5	1.0	-	5.1	md-2.25 ch-0.25 sl-0.25	qz-7.25 gn-0.25	gr-0.5	bt-trace mu-0.75 ohm-0.50 dt mx-2.0
A -222	17.0	18.5	1.75	2.75	1.0	3.5	-	5.1	sl-6.75 ch-1.25 ls-1.25	qz-6.26	gr-0.75	bt-trace mu-0.25 dt mx-1.60

TABLE XV (Continued)

Sample Number	Quartz, % st	un	px	Feldspars, % or	mc	pl	pt	Q/F ratio	Lithic Fragments, % SRF	MRF	IRF	Other Detrital Constituents
									md-4.25	qz-9.0	gr-0.50	bt-0.25
A -229	14.0	24.5	12.5	1.5	2.0	1.25	0.25	10.2	ls-0.50	gn-0.25	rh-0.25	mu-0.25
									ch-0.25			dt mx-5.0
									md-1.25	qz-9.0	gr-2.0	bt-0.25
A -250	18.25	24.25	9.75	2.5	1.5	1.5	-	9.6	sl-1.25			mu-0.25
									ls-1.0			dt mx-20
									md-2.5	qz-6.25	gr-0.25	bt-0.25
A -251	20.25	34.0	5.75	2.5	1.75	1.0	-	11.4	ch-1.75	gr-0.50		mu-0.25
									ls-0.25			ohm-0.25
									md-0.75	qz-9.75	gr-1.0	bt-trace
A - ab	20.75	26.5	8.0	3.75	1.75	1.0	0.50	7.9	ch-0.50	gn-0.50		mu-trace
									md-2.25	qz-4.0	-	bt-0.25, mu-1.5
B - 11	30.0	23.0	4.0	3.0	0.75	0.50	0.25	12.7	ls-0.25			ohm-2.50,thm-0.5
									md-2.25	qz-1.5	-	bt-2.25
E - 2	28.0	7.0	1.25	1.5	0.25	1.0	0.25	1.21	ls-2.0			mu-1.75,thm-0.50
									sl-9.25			hhm-2.75
									md-1.5	qz-5.5	gr-1.0	bt-0.5
E - 15	33.25	12.25	4.75	7.5	0.5	2.75	0.25	4.6	ls-1.0			mx hm-2.0
									ch-0.5			thm-0.5
									md-0.5	qz-2.0	gr-0.25	bt-1.5
E - 30	28.25	6.75	4.75	11.75	1.0	2.0	0.25	2.6	ch-0.5			mu-1.5
												hhm-1.0 thm-0.25
									ls-0.75	qz-1.75	gr-0.25	bt-0.5
E - 40	25.75	6.5	0.75	4.25	1.75	4.25	0.25	3.1	md-0.5			mu-trace
									sl-0.25			lhm-4.0 thm-1.0
									ch-0.75	qz-3.5	gr-0.25	bt-0.25
E - 45	34.0	5.0	4.0	7.25	2.0	1.75	0.25	3.8	md-0.5			mu-1.0
									ls-0.5			lhm-1.0
									md-2.25	qz=3.25	gr-0.25	bt-0.25
E -142	29.5	18.25	4.0	10.0	2.5	2.5	0.25	3.4	ls-0.5		rh-0.25	mu-0.25
									ch-0.25			mx hm-1.5 thm-trace

TABLE XV (Continued)

Sample Number	Quartz, % st	un	px	Feldspars, % or	mc	pl	pt	Q/F ratio	Lithic Fragments, % SRF	MRF	IRF	Other Detrital Constituents
									md-1.75	qz-1.75	gr-0.25	bt-0.7t
E -155	36.5	8.25	3.25	7.0	2.25	2.25	0.25	4.1	ls-0.5	gn-0.25		mu-0.5
												mx hm-1.25 thm-0.25
									md-2.75	qz-4.25		bt-0.25
E -205	25.25	19.5	8.0	7.75	1.5	3.75	-	4.1				mu-0.75
									md-2.0	qz-2.25	gr-0.5	bt-6.75 hhm-0.5
E -283	31.0	9.5	2.25	4.0	1.0	3.75	-	7.0				mu-3.0
												dt mt-7.0
									md-1.25	qz-1.5	gr-0.25	bt-0.25
E -306	34.75	22.5	3.75	6.0	1.0	1.75	-	7.0	ch-1.5			mu-trace
									ls-0.25			lhm-1.0
									md-2.0	qz-3.25	gr-1.25	br-1.25
E -362	49.75	8.0	4.25	3.75	1.0	1.5	0.75	7.7	sl-1.0	gr-0.25	mu-1.25	
									ch-0.25			thm-0.25 dt mx-1.25
									md-3.5	qz-8.5	gr-0.75	bt-0.25
D - 15	35.75	19.0	4.75	6.75	1.75	0.75	0.25	6.3	ls-1.0	gn-0.25		mu-trace
									ch-0.25			hhm-trace
									md-1.0	qz-1.5	rh-0.25	bt-0.50
C - 14	35.25	19.75	4.25	4.0	1.0	1.0	0.5	9.1	ch-0.75			mu-trace
									sl-0.5			lhm-0.50 thm-trace
									md-2.25	qz-1.5	gn-0.25	bt-0.50
C - 32	31.75	14.75	5.00	3.75	1.5	1.25	-	7.9	ls-1.0			mu-trace
									sl-0.25			hhm-2.75
									md-1.75	qz-3.0	-	bt-1.0
C - 39	36.0	13.0	6.5	4.75	1.5	1.75	0.25	6.7	ls-1.0			mu-0.5
									ch-0.25			lhm-0.25 thm-0.25
									md-2.25	qz-0.5	-	bt-3.0
C - 67	29.5	11.5	3.5	5.5	1.75	0.75	0.5	5.2	sl-1.0			mu-2.75
												lhm-0.5 dt mt-10.0
									md-1.0	qz-1.0	gr-0.25	bt-1.5
C - 97	28.5	7.0	4.5	6	2.25	0.5	0.25	4.4	ls-0.85	gn-0.25		mu-0.5
												hhm-4.5 thm-0.25

TABLE XV (Continued)

Sample Number	Quartz, %			Feldspars, %				Q/F	Lithic Fragments, %			Other Detrital Constituents
	st	un	px	or	mc	pl	pt	ratio	SRF	MRF	IRF	
C -110	30.5	11.5	2.0	1.0	0.5	2.0	11.7	11.7	md-0.5	qz-3.75 gn-0.5	gr-0.25	bt-0.25 mu-trace lhm-1.0 thm-0.75
C -125	34.5	16.0	6.0	5.0	1.5	0.75	0.5	7.3	md-2.75 sl-0.75	qz-2.25	gr-0.25	bt-2.5 mu-1.0
C -180	34.75	16.75	3.5	7.25	2.25	1.00	0.25	5.1	md-3.75 ls-0.5 ch-0.25	qz-2.25 gn-0.25	- mu-1.0	bt-0.25 lhm-1.0
C -270	24.0	21.75	5.25	4.0	2.25	2.5	-	5.8	md-3.25 ls-0.25 ch-0.25	qz-8.75	gr-0.25	bt-0.25 mu-0.50 hhm-0.75
F - 8	30.75	14.0	3.0	6.25	2.5	2.75	0.25	4.1	md-0.75 ls-0.25	qz-2.5 gn-0.25	gr-0.25	mu-0.25 lhm-0.75 thm-0.25
F - 60	25.5	14.0	10.5	4.0	1.0	3.00	0.25	6.9	md-0.25	qz-2.25	gr-0.25	bt-1.0 mu-0.25 hhm-1.75
F - 86	34.25	9.75	5.0	4.0	1.25	2.0	-	6.8	md-0.5 ls-0.25	qz=1.5 gn-0.25	-	bt-1.75 mu-2.25 hhm-2.5 thm-0.25
F -113	45.25	17.0	4.75	6.5	2.25	3.75	0.25	5.2	md-2.0	qz-0.5	gr-1.0 rh-0.25	bt-trace mu-trace lhm-0.5
F -170	40.00	11.25	8.0	5.0	1.5	3.0	0.25	6.1	md-0.5 ch-0.5	qz-3.25	gn-0.5	bt-trace mu-trace lhm-0.25 thm-0.25
F -235	37.75	9.5	5.0	6.75	2.25	3.0	0.25	4.3	md-0.50 ch-0.25	qz-0.5	-	bt-2.0 mu-2.25 hhm-0.5

TABLE XV (Continued)

Sample Number	Quartz, % st	un	px	Feldspars, % or	mc	pl	pt	Q/F ratio	Lithic Fragments,% SRF	MRF	IRF	Other Detrital Constituents
F -298	42.5	12.5	6.0	4.0	2.0	1.0	0.25	8.4	md-0.75 ch-0.50 ls-0.50	qz-3.75	gr-0.25	bt-0.25 mu-1.0 lhm-0.25
F -298	42.5	12.5	6.0	4.0	2.0	1.0	0.25	8.4	md-0.75 ch-0.50 ls-0.50	qz-3.75	gr-0.25	bt-0.25 mu-1.0 lhm-0.25
F -323	25.75	4.0	1.25	4.5	1.0	1.0	0.50	4.4	md-0.25	qz-0.75	gr-0.25	bt-1.75 mu-2.25 lhm-1.5 dt mt-1.5
F -339	43.75	7.0	5.5	7.0	2.75	1.5	1.25	4.5	md-3.0 ch-0.5	qz-4.5 gn-0.25	gr-0.25	br-0.25 mu-0.5 lhm-0.25 thmm-0.25
F -359	41.25	8.0	5.75	3.0	1.0	1.75	0.75	8.4	md-0.5 ch-0.25	qz-2.5	-	mu-0.5 hhm-1.25
F -407	41.5	11.5	1.5	3.0	1.5	1.25	0.75	8.4	md-2.5	qz-4.0 gn-0.25	gr-0.25	bt-2.0 mu-1.0 hhm-0.5
F -415	46.25	13.5	2.5	4.0	2.0	0.75	0.25	8.9	md-1.25 sl-1.0 ch-0.25	qz-3.75	gr-0.5	bt-2.0 mu-0.5 lhm-1.25 thm-05
F -423	42.25	1.30	2.25	0.75	1.0	0.75	-	23	md-3.75 ch-0.5	qz-4.0	-	bt-1.25 mu-0.25 hhm-1.0 gl-trace
G - 15	32.5	22.5	1.75	3.75	1.25	2.0	0.25	7.8	md-2.75 ch-1.0 sl-1.0	qz-8.5	gn-0.25	bt-0.25 mu-0.75
G - 50	27.0	20.25	5.75	2.25	1.25	2.0	1.0	8.1	md-5.5 sl-0.75 ls-0.5	qz-10.0	gr-1.5	bt-0.75 mu-0.25 lhm-0.75

TABLE XVI

DIAGENETIC DESCRIPTIONS OF SAMPLES COLLECTED WITHIN THE STUDY AREA

Sample Number	Color	Cement, % Calcite	Cement, % Qtz	Hematite %	Authigenic Clays, % K	Authigenic Clays, % I	Authigenic Clays, % Chl	Porosity, Secondary %	Porosity, Secondary Types
A' - 25	pale reddish brown 10 R 5/4	19.75	-	3.75	2.5	0.75	tr	5.25	ingr-d inrp-m
A' - 56	pale reddish brown 10 R 5/4	19.25	-	3.75	2.0	0.25	-	0.5	irg-d ingr-m inrp-m
A - 3	dark reddish brown 10 R 3/4	7.75	-	1.75	6.0	1.0	-	6.26	inrp-d inrp-md icm-mn
A - 24	very pale orange 10 YR 8/2	5.75	-	1.0	6.25	1.25	tr	7.25	ingr-d inrp-d
A - 40	very pale orange 10 YR 8/2	16.75	-	0.25	9.75	0.75	-	0.50	ingr-mn
A - 65	very light gray N 8	100.0	-	-	-	-	-	-	-
A - 99	pale red 10 R 6/2	9.0	?	2.5	3.25	0.5	-	7.0	ingr-d inrp-md incm-mn
A -130	dark reddish brown 10 R 3/4	3.25	?	5.75	7.0	1.0	tr	6.5	irg-d ingr-md inrp-mn
A -203	light brown 5 YR 5/6	15.5	-	0.5	4.0	0.25	-	5.25	ingr-d inrp-md irg-mn
A -222	light brown 5 YR 5/6	15.50	?	0.25	4.25	tr	-	3.0	ingr-d inrp-md irg-m
A -229	pale yellowish brown 10 YR 8/6	8.50	?	1.25	6.00	tr	-	7.25	ingr-d inrp-md irg-mn

TABLE XVI (Continued)

Sample Number	Color	Cement, % Calcite	Cement, % Qtz	Hematite %	Authigenic Clays, % K	Authigenic Clays, % I	Authigenic Clays, % Chl	Porosity, Secondary %	Porosity, Secondary Types
A -250	dark reddish brown 10 R 3/4	5.75	✓	-	1.25	0.25	-	-	-
A -251	grayish orange 10 YR 7/4	1.5	?	0.25	8.25	0.75	-	11.75	irg-d ingr-md inrp-m
A - ab	grayish orange 10 YR 7.4	11.0	?	1.0	7.50	0.25	0.5	5.0	irg-d ingr-md
B - 11	dark reddish brown 10 YR 3/4	6.25	-	9.25	2.0	0.50	-	9.25	irg-d ingr-md inrp-mm
E - 2	pale brown 5 YR 5/2	42.5	-	4.5	tr	0.25	-	0.25	ingr-mn
E - 15	very pale orange dark reddish brown	5.0	-	8.5	0.75	0.5	-	11.5	irg-d ingr-md
E - 30	pale reddish brown 10 R 5/4	31.0	-	2.0	tr	-	-	4.75	inrp-mn
E - 40	medium light gray N-6	47.0	-	0.5	-	-	-	-	
E - 45	light gray N 7	36.75	-	-	0.25	0.25	0.25	0.5	ingr-mn
E -142	dark reddish brown very pale orange	19.5	-	1.0	0.25	-	-	3.5	
E -155	light gray N 7	32.75	-	-	-	-	-	0.25	ingr-mn
E -205	very pale orange 10 YR 8/2	4.25		-	tr	0.25	-	21.75	
E -283	moderate reddish brown 10 R 4/6	6.5	-	6.75	1.25	1.75	-	10.25	inmx-dm ingr-md irg-md

TABLE XVI (Continued)

Sample Number	Color	Cement, % Calcite	Cement, % Qtz	Hematite %	Authigenic Clays, % K	Authigenic Clays, % I	Authigenic Clays, % Chl	Porosity, Secondary %	Porosity, Secondary Type
F - 60	light gray N 7	29.75	-	3.0	0.75	0.25	0.25	2.0	ingr-mn ingr-md
F - 86	moderate reddish brown 10 R 6/6	20.0	-	8.75	0.5	-.25	-	5.0	irg-mn ingr-md
F -113	very pale orange 10 YR 8/2	8.00	-	-	1.25	0.5	-	6.25	inrp-md irg-mn ingr-d
F -170	very pale orange 10 YR 8/2	12.25	-	-	1.5	0.5	-	11.5	inrp-md irg-mn inmx-d
F -235	very pale orange dark reddish brown	9.25	-	2.25	2.25	1.5	-	14.25	ingr-md inrp-mn ingr-d
F -298	very pale orange 10 YR 8/2	11.5	-	-	1.5	2.75	-	8.75	inrp-d irg-mn ingr-md
F -323	light gray N 7	42.0	-	1.0	1.5	2.0	0.5	6.75	inmx-md inrp-mn ingr-d
F -339	yellowish gray 5 Y 7/2	10.5	-	0.25	0.5	0.5	-	9.75	irp-me ingr-dm
F -359	dark reddish brown 10 R 3/4	17.75-hm	-	8.5	0.75	0.5	-	6.0	inrp-md ingr-md
F -407	very pale orange 10 YR 8/2	17.75	-	-	2.0	9.75	-	7.0	inrp-md inmx-mn ingr-d
F -415	very pale orange 10 YR 8/2	10.0	-	0.25	2.25	1.0	-	6.25	inrp-md irg-mn

TABLE XVI (Continued)

Sample Number	Color	Cement, % Calcite	Cement, % Qtz	Hematite %	Authigenic Clays, % K	Authigenic Clays, % I	Authigenic Clays, % Chl	Porosity, Secondary %	Porosity, Secondary
	very pale orange								ingr-d
E -306	10 YR 8/2	10.75	-	-	1.5	1.0	-	11.0	irg-md
									fg-mn
	very pale orange								ingr-md
E -362	10 YR 8/2	9.5	-	1.5	1.5	1.25	-	4.25	inrp-mn
	grayish orange								irg-dm
D - 15	10 YR 7/4	3.0	-	-	0.25	0.25	-	13.0	ingr-md
	very pale orange								irg-dm
C - 14	10 YR 8/2	11.0	?	-	0.25	1.0	0.25	16.75	ingr-md
									inrp-mn
	dark reddish brown								ingr-md
C - 32	10 R 3 4	5.25	-	21.25	3.0	0.50	-	3.5	inrp-mn
	very pale orange								ir-d
C - 39	10 YR 8/2	13.0	?	0.25	0.5	0.50	-	14.0	ingr-d
									inrp-md
	very pale orange								inmt-d
C - 67	10 YR 8/2	11.5	-	0.5	1.5	1.5	-	12.0	irg-md
	dark reddish brown								
C - 97	10 R 3/4	35.25	-	4.75	0.25	tr	-	0.75	ingr-mn
	dark reddish brown								
C -110	10 R 3/4	37.25	-	6.5	0.5	0.5	-	-	
	very pale orange								irg-d
C -125	10 YR 8/2	14.75	-	1.75	0.25	0.5	tr	9.0	ingr-md
	very pale orange								irg-d
C -180	10 YR 8/2	10.0	-	-	0.25	0.75	0.25	13.75	ingr-d
	dark reddish brown								
C -270	10 R 3/4	19.75	-	4.5	0.5	0.25	-	1.0	ingr-mn
	very light gray								ingr-d
F - 8	N 8	24.50	-	0.25	0.25	0.5	-	9.75	irg-d

TABLE XVI (Continued)

Sample Number	Color	Cement, % Calcite	Cement, % Qtz	Hematite %	Authigenic Clays, % K	Authigenic Clays, % I	Authigenic Clays, % Chl	Porosity, Secondary %	Porosity, Secondary Type
	very pale orange								ingr-md
F -423	10 YR 8/2	20.75	-	2.25	0.75	1.25	-	4.26	inrp-md
	pale yellowish orange								ingr-d
G - 15	10 YR 8/6	4.25	-	-	3.0	1.0	-	13.25	inrp-md
	very pale orange								ingr-d
G - 30	10 YR	7.75	-	-	2.25	0.75	0.5	9.25	inrp-md

APPENDIX F

RESULTS OF SPORE ANALYSIS

Spores extracted from samples collected by the author in a flood-plain sequence of the M.O.R.S. and which have been examined by D. C. McGregor (1983), have yielded an age close to the Jurassic-Cretaceous boundary. This age is greatly at variance with that indicated by the fish faunas collected in U.O.R.S. deposits at Portmahomack and in M.O.R.S. deposits south of Rockfield. The age of these fish faunas is consistent with the M.O.R.S. and U.O.R.S. divisions used throughout this study (personal communication, R. N. Donovan, 1983). Moreover, no tectonic evidence exists to suggest the presence of a faulted inlier of Jurassic or Cretaceous strata anywhere within the study area. The most obvious explanation to account for this spore anomaly is M.O.R.S.-U.O.R.S. deposits were at or near the Jurassic-Cretaceous paleosurface and that Mesozoic spores infiltrated this surface. Further work has been undertaken to study this anamoly.

VITA

Thomas Edward Ferraro

Candidate for the Degree of

Master of Science

Thesis: THE GEOLOGY OF THE COASTAL TRACT BETWEEN TARBAT NESS AND ROCKFIELD, CROMARTY DISTRICT, SCOTLAND

Major Field: Geology

Biographical:

Personal Data: Born in Brookville, Pennsylvania, September 21, 1953, the son of Mr. and Mrs. L. E. Ferraro.

Education: Graduated from Brookville Area High School, Brookville, Pennsylvania, in May, 1972; received Bachelor of Science degree in Earth Science Education from Slippery Rock State College, Slippery Rock, Pennsylvania, in 1976; received Bachelor of Science degree in Geology from James Madison University, Harrisonburg, Virginia, in 1981; completed requirements for the Master of Science degree at Oklahoma State University, Stillwater, in December, 1983.

Professional Experience: Undergraduate teaching assistant, Department of Geology, Slippery Rock State College, 1974-1976; Earth Science instructor, Gar-Field High School, Woodbridge, Virginia, 1977-1980; undergraduate teaching assistant, Department of Geology, James Madison University, 1981; graduate teaching assistant, Oklahoma State University, 1981-1983; professional geologist, Exxon Company of America, 1983.